The Role of Norrie Disease Pseudoglioma (Ndp) in Cerebellar Development/Tumorigenesis and its Relationship with the Sonic Hedgehog Pathway.

Nicholas Tokarew

A Thesis Submitted to the

Faculty of Graduate and Postdoctoral Studies

In Partial Fulfillment of the Requirements for the

PhD degree in Biochemistry

Department of Biochemistry, Microbiology and Immunology

Faculty of Medicine

University of Ottawa

Abstract

Medulloblastoma (MB), a cancer of the cerebellum, is the most common solid tumor affecting children. In the cerebellum, Sonic Hedgehog (Shh) drives the proliferative expansion of granule neuron progenitors (GNP). These cells are located in the external granule layer (EGL) and are the cells of origin of Shh-MB. We recently identified Norrie Disease Pseudoglioma (Ndp) as a novel downstream target of Hh signaling in the developing retina. Ndp encodes an X-linked cysteine-rich secreted protein called Norrin, which is best known for its role in angiogenesis and blood brain barrier (BBB) maintenance in the developing retina and cerebellum, respectively. Norrin mediates this effect by binding to its receptor Frizzled4 (Fzd4) and co-receptors LRP5/6 and Tpsan12 to activate the canonical, β-catenin-dependent Wnt signaling pathway in endothelial cells (ECs). We detected the expression of Ndp and all required receptors in mouse GNPs and MB samples. To investigate a potential role for Ndp in Hh-driven MB, we genetically and pharmacologically inactivated Ndp/Fzd4 signaling in $Ptch^{+/-}$ mice (a mouse model for human Gorlin syndrome), which dramatically increased the incidence and reduced the latency of MB. This accelerated rate of tumorigenesis was caused by an increase in the number of preneoplastic lesions (PNLs), the precursor lesions to MB, and a faster conversion of these lesions to MB. We showed that Ndp mediates this increase in tumorigenesis by signaling through endothelial cell receptor Fzd4 to alter the GNP stroma, which is characterised by 5 major alterations: 1) activated angiogenic program, 2) open BBB, 3) aberrant deposition of extracellular matrix, 4) aberrant lymphocyte recruitment and 5) reduction in meningeal lymphatic vasculature. We propose that these stromal alterations are associated with a pro-tumor microenvironment that promotes DNA damage in GNPs and leads to enhanced lesion formation and progression towards MB. This research highlights 1) an unanticipated role for Ndp/Fzd4 signaling in Shh-MB initiation and

progression, 2) a role for stromal signaling in the regulation of MB development and 3) a previously undescribed role for Ndp signaling in maintaining meningeal cerebellum lymphatic vessels.

Table of Contents

Table of figures

Table of Tables

List of Abbreviations

MB, Medulloblastoma

Shh, Sonic hedgehog

GNP, Granule neuron progenitor

EGL, External granule neuron

IGL, Internal granule neuron

Ndp, Norrie Disease Pseudoglioma

BBB, blood brain barrier

Fzd4, Frizzled4

LRP5, Low-density lipoprotein receptor-related protein 5

BMP, Bone morphogenetic protein

FGF, Fibroblast growth factors

MAPK, mitogen-activated protein kinase

Wnt, Wingless/Int

Ptch, Patched

Smo, Smoothened

Gli, Glioma-associated oncogene

Gli-A, Activator Glioma-associated oncogene

Gli-R, Repressor Glioma-associated oncogene

Sufu, Suppressor of fused

PDD, processing determining domain

EC, Endothelial cell

LEC, Lymphatic ECs

PKA, Protein kinase A

GSK3β, Glycogen synthase kinase 3 beta

CK1, Casein kinase 1

IFT, intraflagellar transport

PNL, Preneoplastic lesion

CAF, cancer associated fibroblasts

MMPs, matrix metalloproteinases

ECM, extracellular matrix

VEGF, vascular endothelial growth factor

VEGF-A, vascular endothelial growth factor-A

VEGFR-1, vascular endothelial growth factor receptor 1

AIDS, acquired immunodeficiency syndrome

PC, Purkinje cells

PCL, Purkinje cell layer

GN, Granule Neurons

IGL, inner granule layer

ML, molecular layer

CNS, central nervous system

PCP, Planar Cell Polarity pathway

CRD, cysteine-rich domain

GPCR, G-coupled proteins receptors

DVL, Dishevelled

APC, adenomatous polyposis coli

PP2A, phosphatase 2A

TCF, transcription factors

LEF, Lymphoid enhancer-binding factor

HDAC, histone deacetylase

HAT, histone acetyltransferase

TGF-β, Transforming Growth Factor- β

FEVR, familial exudative vitreoretinopathy

ND, Norrie disease

vSMC, vascular smooth muscle cells

HIF, hypoxia-inducible factor

VPF, vascular permeability factor

PGF, placenta growth factor

PKC, Protein kinase C

PKD, Polycystin-1

PI3K, Phosphatidylinositol-4,5-bisphosphate 3-kinase

Ang2, angiopoietin-2

TIE-2, tyrosine kinase with immunoglobulin-like and EGF-like domains 2

PDGF- β, platelet-derived growth factor β

PDGFR-β, platelet-derived growth receptor-β

Angpt-1, angiopoeitin-1

ISF, interstitial fluid

CNS-Endo, central nervous system ECs

TJ, tight junctions

TAMPs, tight junctions-associated MARVEL proteins

JAM, Junctional adhesion molecule

TEER, transendothelial electric resistance

NVU, neurovascular unit

Glut1, glucose transporter 1

Tnfrsf19, tumor necrosis factor receptor superfamily member 19 (or Troy)

Dr6, death receptors 6

Plvap, plasmalemma vesicle-associated protein (or Meca32)

TEM5, tumor endothelial marker 5 (also known as GPR124)

VR, Virchow-Robin

CSF, cerebrospinal fluid

ISF, interstitial fluid

AQP4, Aquaporin-4

CV, cardinal vein

ISV, intersomitic vein

COUP-TFII, COUP transcription factor 2

Prox-1, prospero homeobox protein 1

PDPN, Podoplanin

Ccne1, Cyclin E1

SmoA1, Neurod2-SmoA1

$Ptch^{+/-}$, Patched1 heterogeneous (haploinsufficiency)

Acknowledgment

I would like to first and foremost thank Dr. Valerie A. Wallace for her continued guidance and support throughout my PhD studies. Valerie was the single most influential person in my scientific and personal development over the last 7 years. Her mentorship was indispensable and she was an incredible source of new ideas and motivation for me.

I would also like to thank Dr. Erin Bassett, my mentor during my early years as a Masters and Ph.D. student, she allowed me to grow as a person and scientist, enabling me to spread my wings and fly to Toronto with confidence and independence.
In addition I want to thank my TAC members Dr. Rashmi Kothary and Dr. Steffany Bennett for being incredible advisors and for all the continued support and ideas they have provided me with.

My sincere appreciation goes to my wife Dr. Kristin Dauner for all the love, support and inspiration she has provided me with over the years. For always being a strong shoulder to lean on and her loving smile which has kept me motivated and focused all these years. She has been an incredible influence in my life, without which I would not be the same person. I also want to thank her for being a supportive and encouraging source of motivation and guidance. Furthermore, I would also like to thank her for looking over my thesis and providing me with some valuable insight into figure design and thesis redaction.

To my family for all their love and support. Additional thanks go to Dr. Yuriy Baglaenko, with whom I shared a lot of the ups and downs of being a PhD student. I owe a very special gratitude to my entire lab, especially for making Thursday after work beers a thing! Finally, I would like to dedicate this thesis to my 8 month old daughter Leonie Mila Dauner-Tokarew, with whom I shared countless sleepless nights and, without whom I would have finished my thesis 3 months earlier and without whom I would be lost.

Additional thanks to:

- Dr. Phil Nickerson (data analysis), Fig 6F and for proofreading my thesis
- Dr. Yuriy Baglaenko for the training on flow cytometry and for being a great person to bounce ideas off of. Also with the conception of several flow experiments.
- Neno Pokrajac for picking up and continuing the lymphatic project
- Dr. A. Prat and JI Alvarez (immunostaining of acetone-fixed tissue)
- Dr. Arturo Ortín for teaching me Neurosurgery and retina flatmounts preparations, Fig22A

Chapter 1. Introduction

1.0 Cancer

Cancer is one of the leading causes of morbidity and mortality worldwide [1]. It is the result of genetic mutations, sporadic or inherited, which either inactivate or activate a tumor suppressor or oncogene, respectively [2]. Many of these oncogenes and tumor suppressors are components or targets of signaling pathways such as Bone morphogenetic protein (BMP), Fibroblast growth factors (FGF), mitogen-activated protein kinase (MAPK), Wingless/Int (Wnt) and Hedgehog (Hh) [3, 4]. A classic example of an aberrantly activated signaling pathway that can promote carcinogenesis is the Hh pathway.

1.1 The Sonic Hedgehog (Shh) Pathway and tumorigenesis

The Hedgehog (Hh) signaling pathway regulates several fundamental embryonic and postnatal processes, such as stem cell maintenance [5-7], differentiation [8], patterning [9], proliferation [10], wound healing [11], and the establishment and maintenance of the blood brain barrier (BBB) [12]. The Hh pathway is evolutionarily conserved from *Drosophila melanogaster* to *Homo sapiens*. Although the framework of the pathway is conserved in humans, it is more complex due to duplications (homologues) and divergences (specialization, e.g. primary cilium) [13, 14]. The core Hh signaling pathway components are composed of the secreted ligand, Hedgehog (Hh), the receptor, Patched (Ptch), the downstream effector, Smoothened (Smo) and the glioma-associated oncogene (Gli) protein transcriptional effectors. In mammals, there are 3 Hh homologues (Indian hedgehog, Desert hedgehog and Sonic Hedgehog (Shh)), two Ptch receptor (Ptch1 and 2) homologues and 3 Gli homologues (Gli1-3). Interestingly, Gli2 and Gli3 are multifunctional, as they contain a transcriptional activator and repressor domain at their C- and N-termini, respectively. In contrast, Gli1 contains only a transcriptional activation domain [15]. Hh

signaling can be subdivided into canonical, Smo-dependent, and non-canonical, smo-independent, signaling pathways, the former of which will be the focus of the following paragraphs [16].

Mammalian Hh signaling requires the primary cilium (Figure 1A), which is a small specialized, microtubule-based single projection from the surface of the cell [14]. In the absence of ligand, Ptch inhibits entry of Smo into the primary cilium. This causes the Gli proteins, which are associated with the chaperone Suppressor of fused (Sufu) [17], to be sequentially phosphorylated by various kinases. The phosphorylation target the Gli proteins for partial proteasome degradation, and generates a repressor Gli protein (Gli-R). The Sufu-Gli-R complex is shuttled to the nucleus, associates with chromatin Hh consensus binding sites, and represses the transcription of Hh target genes [18]. Gli3 acts as the predominant repressor of Hh signaling, as it is efficiently processed into a repressor transcription factor due to the specific sequence of its processing determining domain (PDD) [19]. The sequence of the PDD in Gli2 is less effective, which results in a higher frequency of complete protein degradation [20]. Gli1 is a direct target of the pathway and is not expressed in the absence of Ptch ligand. Furthermore, it lacks the PDD domain and in the absence of Hh signaling, residual Gli1 is completely degraded [21].

In the presence of the ligand (Figure 1B), Hh binds Ptch and relieves its inhibition on Smo, which in turn allows it to enter the primary cilium. Although not completely characterized, Smo in the primary cilium clusters and activates Hh signaling via the Sufu-Gli complex (Sufu-Gli-A), which transits through the primary cilium [18]. The Sufu-Gli-A complex can then be imported into the nucleus to displace Sufu-Gli-R complexes, ultimately functioning as a transcriptional activator of Hh target genes [18, 22].

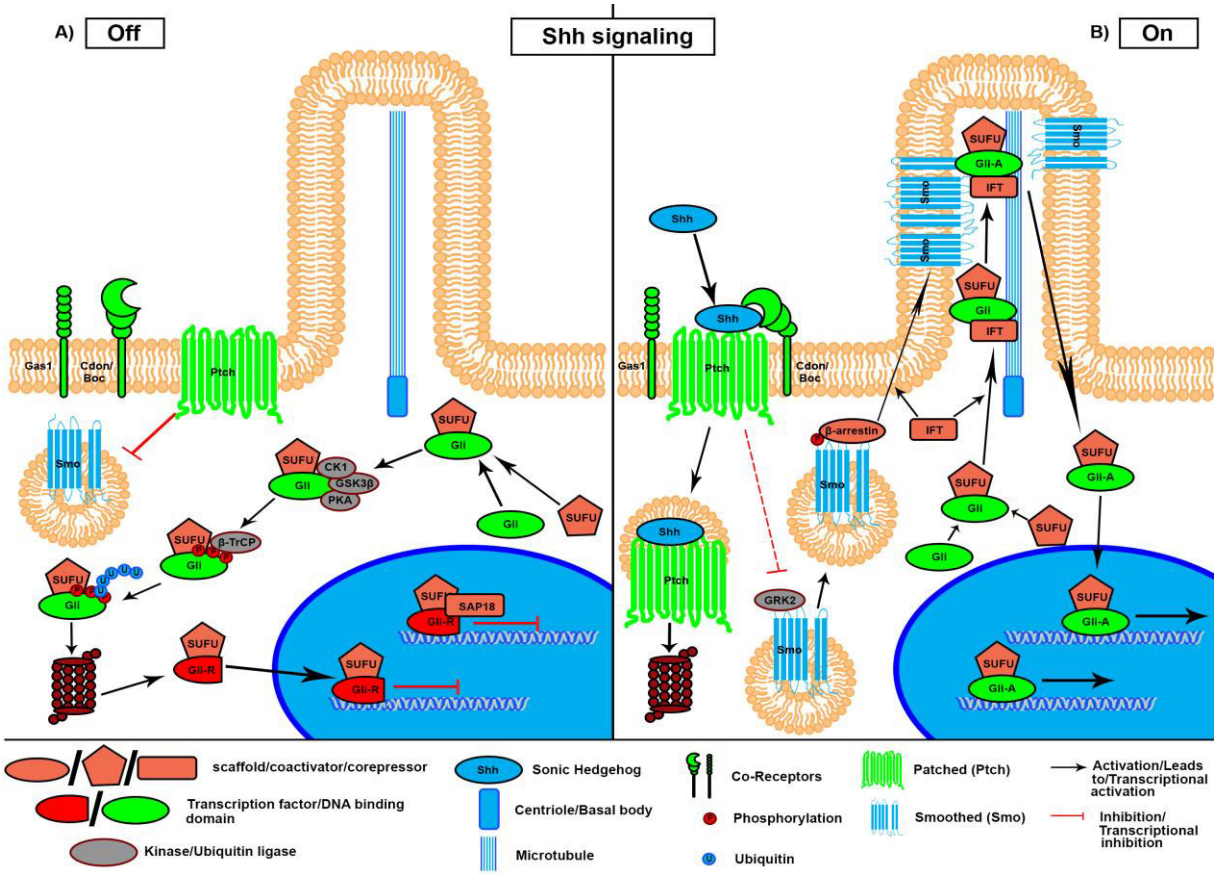

Figure 1. Shh signaling.

(**A**) Mammalian Hh signaling requires the primary cilium, which is a small specialized, microtubule-based single projection from the surface of the cell [9]. In the absence of ligand, Ptch is located at the base of the primary cilium, actively preventing Smo entry. Nascent Gli2 and 3 proteins (Gli1 is a transcriptional target of the Hh pathway), quickly become associated and remain in a complex with the chaperon protein Suppressor of fused (Sufu), which stabilizes them [12]. The Sufu-Gli complex is shuttled to the base of the primary cilium [13] where the Gli protein is sequentially phosphorylated by kinases (PKA, GSK3β and CK1), generating a binding sites for an E3 ubiquitin ligase complex (β-TrCP). The subsequent ubiquitination of the Gli proteins targets them for partial C-terminal degradation by the 26S proteasome, creating repressor Gli proteins (Gli-R). The resulting Sufu-Gli-R complex is shuttled to the nucleus, associates to chromatin Hh consensus binding sites and represses the transcription of Hh target genes [13]. (**B**) Hh binds to Ptch, relieving its inhibition on Smo and the Hh-Ptch complex is internalized in an endosome, destined for lysosomal degradation [13]. Smo, which is found within intracellular vesicles, is phosphorylated at its C-terminus by GRK2, promoting the recruitment of β-arrestins and enabling the Smo-β-arrestins complex to associate with anterograde intraflagellar transport (IFT) kinesin-II machinery. This association shuttles Smo into the primary cilium, where it accumulates and dimerizes. The Sufu-Gli complexes travel through the primary cilium, become activated through a yet incompletely understood mechanism and are able to be imported into the nucleus as a transcriptional activator (Gli-A) [13]. The newly formed Sufu-Gli-A complexes displace Sufu-Gli-R complexes and activate the transcription of Hh target genes [13, 17]. Figure adapted from [13].

Disruption of the Hh through either ligand-dependent or independent pathways, is involved in several malignancies of various organs [23, 24]. In ligand-independent malignancies, there is a requirement for cell autonomous, constitutive Hh pathway activation, which requires activating mutation(s) in activator(s) (e.g. Smo) and/or inactivating mutation(s) in inhibitor(s) (e.g. Ptch) of the Hh pathway. Both basal cell carcinoma and medulloblastoma (MB) can be ligand-independent [9, 21, 25, 26]. However, ligand-dependent Hh malignancies do not harbor mutations in components of the Hh pathway, but rather, require persistent ligand-dependent pathway activation for tumor progression. Examples of these include gastrointestinal tumors, prostate cancer, hematological malignancies, and gliomas [23, 27]. This group can be further stratified into autocrine (the tumor cell produces and responds to the secreted Hh) and paracrine (multicellular signaling involving untransformed cells from the stroma) signaling. This paracrine group can be further sub-divided into 1) Stroma-to-tumor signaling, wherein the tumor stimulates the expression of Hh from stromal cells, which in turn signal back to the tumor cells; and 2) Tumor-to-stroma signaling, whereby tumor cells secrete Hh which signals to neighboring stromal cells, driving the production of pro-growth mitogens [23, 27]. Both examples of paracrine tumor signaling highlight the key participation of stromal cells in creating a clinically relevant, pro-tumor microenvironment [28, 29].

1.2 Tumor microenvironment

The current doctrine for cancer is a tumor-centric model, in which tumor precursor cells acquire mutations that lead to cell autonomous growth via proliferation to form a preneoplastic lesion (PNL) [30-32]. This lesion can grow to 1-2mm^3 before its size exceeds the diffusion limits of nutrients and gases, requiring novel blood vessel supply to sustain its growth [33].

In the established tumor, cancer cells can co-opt or "reprogram" the normal stromal cells through a bidirectional communication (with morphogens and cytokines) to promote the growth of the developing neoplasia [32, 34, 35]. Various stromal cell types, such as fibroblasts termed cancer associated fibroblasts (CAFs), can contribute to tumor growth. CAFs have been shown to secrete various proteins, including matrix metalloproteinases (MMPs), extracellular matrix (ECM), cytokines and growth factors, which can promote the acquisition of almost every single hallmark of cancer [36, 37]. ECs can also be recruited to the tumor by the secretion of angiogenic factors such as VEGF-A, from tumor cells or re-programmed stromal cells [33, 38]. These ECs contribute to the formation of new blood vessels, which nourish the developing tumor. These blood vessels also contribute to the establishment of an immune-suppressive environment within the tumor, as excessive activation of the angiogenic program down-regulates the surface expression of receptors required for leukocyte infiltration [39, 40]. Additional examples of stromal cells that can promote tumor progression include numerous cell types from the immune system. Several studies describe an increased risk of cancer in patients with chronic inflammation [32, 41] or a suppressed immune response, as seen in patients receiving chronic treatment with immunosuppressive agents [32, 42], or patients suffering from acquired immunodeficiency syndrome (AIDS) [32, 43]. Tumors can also selectively recruit certain subtypes of immune cells by altering the secretion of specific chemokines. This can promote the formation of an immune-suppressive environment, and enhance the evation of tumor cells from immune-mediated destruction [44]. The tumor can also alter the gene expression pattern and even increase the genetic instability in normal stromal cells [45]. A growing number of studies demonstrate that activation of the angiogenic program, recruitment of CAF, and immune cell infiltration are markers for poor prognosis for several cancers, further highlighting the importance of stroma/tumor communication

[29]. Although much is known about the importance of stroma in promoting tumor progression and metastasis, little is known about its role in lesion initiation in organs which are difficult to study, such as the central nervous system (CNS).

1.3 The cerebellum and medulloblastoma (MB)

The cerebellum is a posterior brain structure located ventral to the visual cortex, and is predominantly composed of granule neurons and Purkinje cells, surrounded by a diverse array of modulating interneurons [46]. The cerebellum plays essential roles in sensory motor functions, the coordination of balance, the vestibular-ocular reflex, and spatial learning [46, 47].

The cerebellum is organized in a laminar fashion, where the granule neuron progenitors (GNP) occupy the apically located external granular layer (EGL) (Figure 2). During early postnatal life, Purkinje cells (PC), located in the Purkinje cell layer (PCL) secret Shh, which signals to the apically located GNPs, driving Shh signaling. This can be seen by the up-regulation of known Hh target genes and the proliferative expansion of the GNPs [48]. As development ensues, the GNPs gradually become unresponsive to Shh-mediated proliferation due to a combination of asymmetric cell division, ECM composition, and additional inhibitory cues [49, 50]. The GNPs migrate along Bergmann glia radial fibers to terminally differentiate into Granule Neurons (GN) in the inner granule layer (IGL) [51]. Bergmann glial cell bodies are located in the PCL, while their radial fibers span the EGL and molecular layer (ML). As a result of the massive postnatal proliferative expansion of the GNPs, the GNs are the most abundant neurons in the adult human CNS [48, 51-54]. In the mature cerebellum, there are no more GNPs located in the EGL, as they have all migrated inwards towards the IGL. However, if GNPs remain on the apical surface of the cerebellum, developmental accidents can arise and the sustained activation of the Hh pathway, along with additional oncogenic events, can lead to the formation of Shh- medulloblastoma (MB).

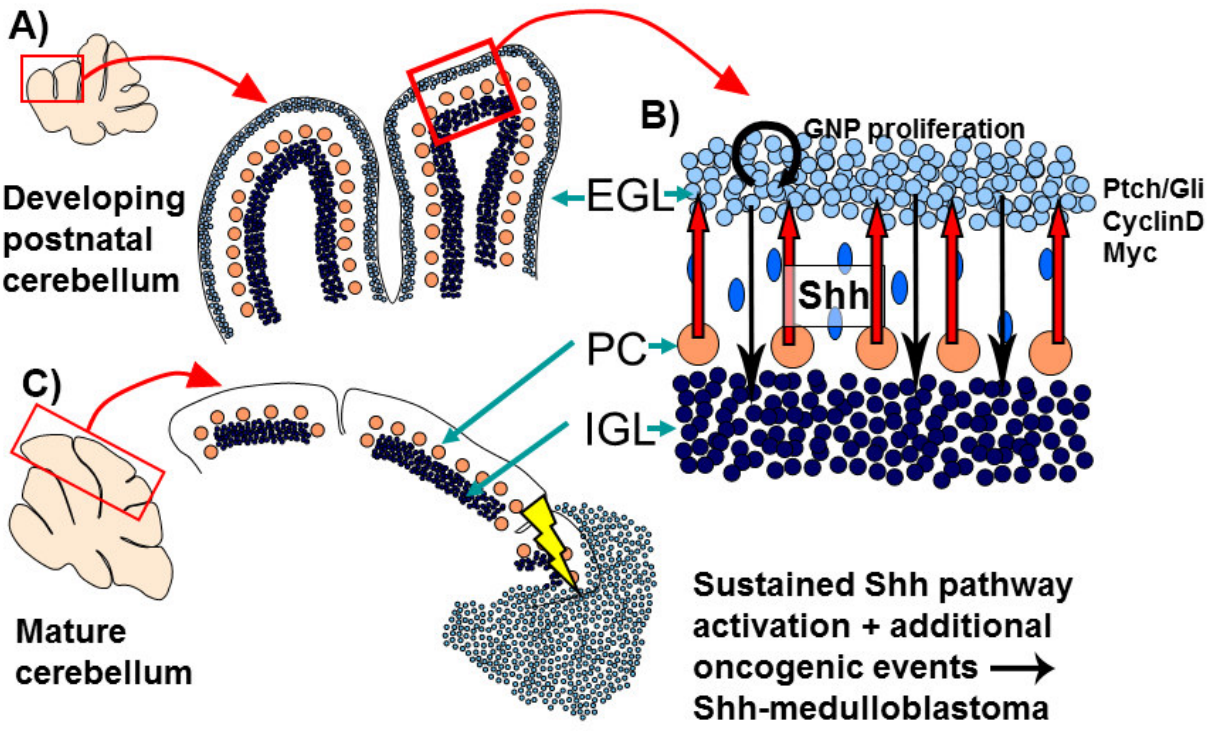

Figure 2. Postnatal Cerebellum development.

(**A**) Schematic diagram of an early postnatal cerebellum, red square denoting area zoomed in for cellular resolution. (**B**) Purkinje cells (PC), located in the Purkinje cell layer (PCL), secrete sonic hedgehog (Shh), which drives the proliferation of Granule neuron progenitors (GNPs) located in the external granule layer. As development ensues, GNPs become unresponsive to the pro-proliferative signal of Shh, due to asymmetrical division, ECM composition and additional inhibitory cues. The differentiating GNPs migrate along Bergmann glia radial fibers, which have their cell body located in the PCL, while their radial fibers span the EGL and molecular layer (ML), to terminally differentiate into Granule Neurons (GN) in the inner granule layer (IGL). (**C**) In the adult cerebellum there are no GNPs left on the apical surface. However, if GNPs remain on the apical surface of the cerebellum and maintain a sustained Hh pathway activation, and if additional oncogenic events occur, this can drive the formation of Shh- medulloblastoma (MB). Figure adapted from [55].

MB is the most common pediatric solid malignancy [56]. Historically, MB was considered a single disease, although recent molecular and genomic analyses have stratified MB into 4 major subgroups: Shh, Wnt, Group3 and Group4 [56-59]. The Shh subgroup represents ≈ 30% of reported cases [56], has a moderate prognosis, and arises from aberrant Hh pathway activation in proliferating GNPs [60, 61]. Group 3 and 4 MBs are associated with moderate to poor prognosis and represent ≈60% of reported cases (Group 3 ≈ 25% and Group 4 ≈35%). Biologically and genetically Group 3 and 4 are not as well defined and the cell of origin is still speculative, but the predominant drivers are thought to be altered chromosomal copy number variation and oncogene amplifications (E.g. MYC and MYCN) [56, 62]. The Wnt MB subgroup represents ≈ 10% of reported cases [56] and has a good prognosis, as the tumor typically responds very well to treatment and has a very low probability of recurrence. The Wnt MB subgroup arises from aberrant Wnt pathway activation that typically involves mutations in β-catenin [63] in cells originating from the Rhombic lip [56, 62, 63].

1.4 Wnt signaling

Wnt signaling is involved in several essential cellular processes, such as cell fate determination, proliferation, survival, differentiation, migration, and polarity [64, 65]. Similar to other developmental pathways such as Hh, the aberrant activation of the Wnt pathway is associated with several different neoplasms [64-66]. The Wnt signaling pathway is evolutionary conserved from *Drosophila melanogaster* to *Homo sapiens* and like the Hh pathway, it contains several examples of divergence and duplications [67]. Wnt signaling can be roughly subdivided into canonical, β-catenin-dependent, and two non-canonical signaling pathways termed the Planar Cell Polarity pathway (PCP) and the Wnt/calcium pathway [68-70]. The core canonical Wnt signaling pathway components are comprised of the secreted ligand Wnt, the receptor Frizzled (Fzd), the

co-receptor Low-Density Lipoprotein Receptor-Related Protein 5 (Lrp5) or 6 (Lrp6), and the transcriptional co-activator ß-catenin. In humans, there are 19 Wnt ligands, which can bind with different affinities to the cysteine-rich domain (CRD) [71] of the G-coupled proteins receptors (GPCR) Fzd, of which there are 10 [70, 72, 73]. The following review will only focus on the canonical Wnt signaling pathway.

In the presence of ligand (Figure 3B), Wnt binds to its respective Fzd receptor and co-receptors (LRP (5/6)), which promote their dimerization and induces a conformational change in Fzd and LRP (5/6) [78]. The conformational change in Fzd promotes the recruitment and dimerization of Dishevelled (DVL), which in turn promotes the recruitment of Axin to the cytoplasmic tail of LRP5, effectively inhibiting the β-catenin destruction complex composed of the scaffold protein adenomatous polyposis coli (APC), the serine threonine kinases, glycogen synthase kinase 3 beta (GSK3β) and Casein Kinase 1 (CKI), the phosphatase 2A (PP2A), the phosphatase 2P (PP2P) and the E3-ubiquitin ligase b-TrCP) [61, 68, 79]. This in turn stabilises cytoplasmic β-catenin, and in association with mandatory DNA binding partner transcription factors (TCF) or Lymphoid enhancer-binding factor (LEF) family of transcription factors [82, 83], allows it to enter the nucleus to activate the transcription of key target genes.

In the absence of Wnt ligand (Figure 3A), newly synthesised β-catenin is quickly bound by the β-catenin destruction complex, which targets it for proteasomal degradation. The lack of β-catenin in the nucleus enables the association of the DNA binding proteins TCF and LEF with transcriptional repressors such as Groucho and histone deacetylases (HDACs) to epigenetically repress Wnt target genes [67].

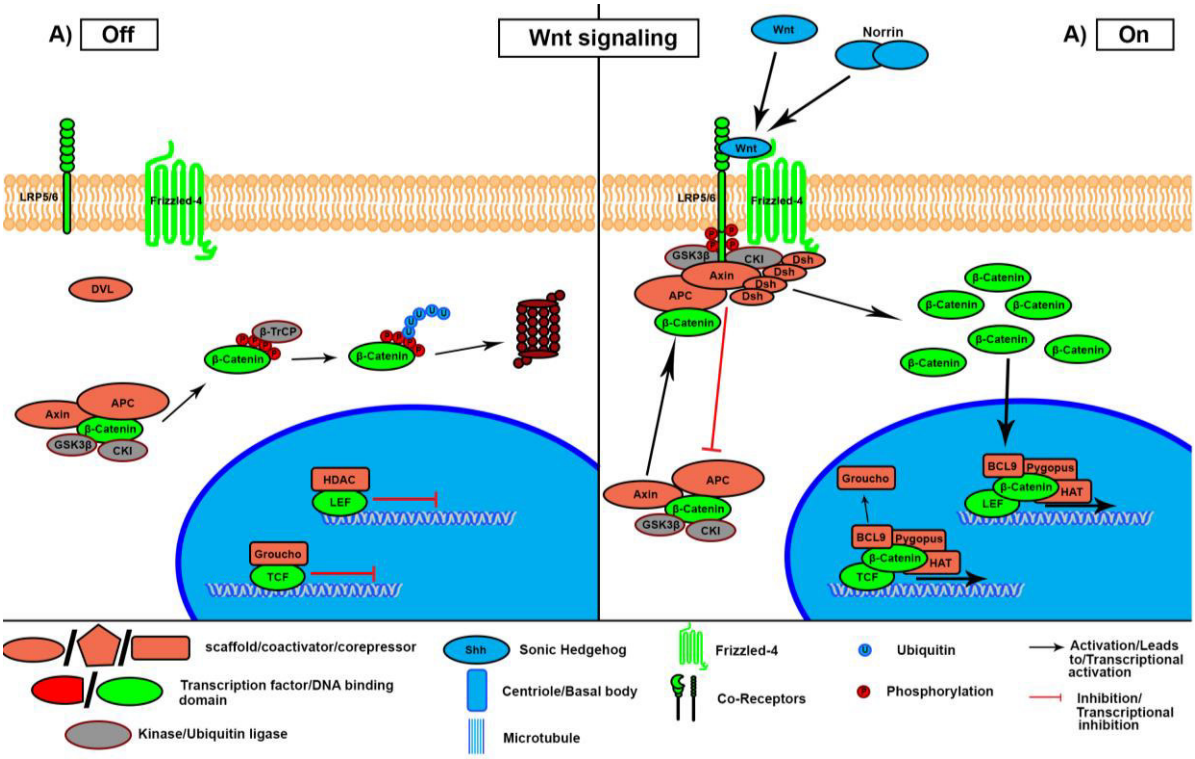

Figure 3. Canonical Wnt signaling.

(**A**) In the absence of Wnt ligand, newly synthesized β-catenin is quickly bound by the β-catenin destruction complex (composed of the scaffold protein adenomatous polyposis coli (APC), the serine threonine kinases, glycogen synthase kinase 3 beta (GSK3β) and Casein Kinase 1 (CKI), the phosphatase 2A (PP2A) the phosphatase PP2P and the E3-ubiquitin ligase b-TrCP), [64, 74] and is sequentially phosphorylated at the amino terminus, creating a docking site for the E3 ubiquitin ligase, β-TrCP. The subsequent ubiquitination of β-catenin targets it for proteasomal degradation [75]. In the nucleus, the mandatory DNA binding partners of β-catenin, TCF/LEF, associate with repressive complexes, such as Groucho and histone deacetylases (HDACs) to repress Wnt target gene transcription [70]. (**B**) In the presence of ligand, Wnt binds Fzd and co-receptors (LRP (5/6)), promoting their dimerization and inducing conformational change in Fzd and LRP (5/6) (Figure 3B). The conformational change in Fzd recruits Dishevelled (DVL) and promotes its polymerization through the DIX domain [71, 76]. The DVL multimer, in turn, is thought to facilitate the recruitment of Axin to the cytoplasmic tail of LRP (5/6). The recruitment of the scaffold protein Axin directs the β-catenin destruction complex to the plasma membrane [64, 71, 74]. In addition, it drives the sequential phosphorylation of LRP (5/6) in a GSK3 and CKI-dependent manner, promoting b-TrCP dissociation and inhibiting the destruction complex by some yet uncharacterized mechanism [66, 69, 70, 75]. Newly synthesized β-catenin can now accumulate, often referred to as "stabilized", in the cytoplasm where it can bind directly to nuclear pore machinery (importin-β/β-karyopherin or other importin-β-factors like transportin) and enter the nucleus in an energy-dependent manner [77]. In the nucleus, β-catenin displaces transcriptional repressors, such as transducin-like enhancer (TLE, also known as Groucho) [70] and associates with transcription factors (TCF) or Lymphoid enhancer-binding factor (LEF) family of transcription factors [78, 79]. The association of β-catenin with TCF/LEF recruits additional transcriptional co-activators BCL9, Pygopus and some histone acetyltransferases (HATs), to drive transcription of key target genes [66, 70, 75, 79]. Figure adapted from [80].

1.5 Norrie disease Pseudoglioma (Ndp)

Recently, a novel Wnt ligand, Norrin, has been characterized, adding to the growing list of known Wnt ligands [81]. Norrin is a small, 133 amino acid, secreted protein encoded by the X-linked gene, Ndp [82]. Norrin is an atypical Wnt, which appears more closely related to the Transforming Growth Factor- β (TGF-β) proteins (protein sequence identity ≤17%), than to all other Wnts [81]. Norrin forms an obligatory homodimer [81, 83] and binds Frizzled 4 (Fzd4), as well as co-receptors Lrp5/6 and Trans-Membrane Spanning Protein 12 (Tspan12) (Fig 2B) [82, 84, 85] with picomolar [83] affinity, to activate canonical β-catenin dependent Wnt signaling in ECs [82, 84, 85]. In humans, autosomal-dominant mutations in Fzd4 [86-88], LRP5 [86, 87] and Tspan12 [86, 89], in addition to autosomal-recessive mutations in LRP5 [86, 90], Tspan12 [86, 91] and Ndp [86, 92, 93] have been implicated in a number of diseases, including X-linked Norrie disease, familial exudative vitreoretinopathy (FEVR), Coat's disease and retinopathy of prematurity, all of which are characterized by hypovascularization in the retina and progressive vision loss [82, 85, 94, 95]. Almost every Norrie disease (ND) patient exhibits a progressive loss of hearing, and over one third of ND patients also exhibit a delay in cognitive development. This is often concomitant with other psychiatric disorders [82, 85, 96], suggesting that Ndp could have additional functions in other parts of the CNS. Norrin is predominantly studied in the context of angiogenesis in several organs including the retina, the endometrium, and more recently, for its role in the blood brain barrier (BBB) maintenance [97].

1.6 Vascular development

The circulatory system (Figure 4) is composed of 1) the blood-vascular network, which transports blood and nutrients to all organs, and 2) the lymphatic vascular network, which returns extravasated lymph and cells back into the vascular network [98]. The blood vascular network is

a highly organized system composed of the heart, blood and the supporting vasculature (Figure 4A), its function is to provide the entire organism with the transport of nutrients, oxygen, hormones, and immune cells, while removing unwanted metabolic by-products and gases (e.g. Carbon Dioxide). The blood vascular tree can roughly be sub-divided into arteries, capillaries and veins. Arteries and veins are composed of a similar basic structure (Figure 4E): an outer layer or tunica externa (composed of connective tissue), a middle layer or tunica media (composed of elastic fibers, connective tissue and vascular smooth muscle cells (vSMC)) and an inner layer or tunica intima (composed of a single endothelial lining or endothelium, surrounded by a basement membrane). Although the arteries and veins are composed of a similar structure, there are some distinctions, e.g. in arteries, the tunica media is the thickest layer, while in veins, the tunica externa is the thickest layer [99]. Initially, the specification of arterial versus venous fate was believed to be due to physiological cues, such as blood flow direction, pressure and oxygen levels. However, recent studies have revealed that this fate decision is determined by gene expression during very early embryonic development (during early vasculogenesis) [99-103].

The vascular network is generated through two key processes, vasculogenesis and angiogenesis. Vasculogenesis is the process by which ECs differentiate from the embryonic mesoderm and organize themselves into a primitive vascular network [104]. Angiogenesis on the other hand (Figure 4B), is the expansion of the pre-existing vasculature by vessel destabilization, sprouting, endothelial cell proliferation, vascular migration, and vessel re-stabilization [105]. It is a tightly regulated process, which involves the integration of several molecular cues. Deregulation can precipitate numerous diseases, including rheumatoid arthritis, infertility, stroke, heart disease, ulcers, retinopathy, scleroderma and psoriasis [105-111]. Currently, there are a plethora of factors

that are known to influence angiogenesis [112]. The following review of angiogenesis will only focus on the contribution of two prominent players, VEGF and the Angiopoietins.

Under physiological conditions, the vasculature is found in a quiescent state and angiogenesis is initiated in response to tissue growth (during development or carcinogenesis), wound healing, or during a state of prolonged increased metabolic demand (physical training) [107]. These events lead to hypoxia, which has been shown to be one of the strongest stimulators of angiogenesis [113]. Under hypoxic conditions the Hypoxia-Inducible Factor (HIF) α subunit is stabilized, enabling it to dimerize with the constitutively expressed β subunit [114, 115] and drive the expression of genes involved in glycolysis (anaerobic respiration) and angiogenesis, such as VEGF-A [116, 117].

VEGF, also known as vascular permeability factor (VPF), is composed of 5 members: placenta growth factor (PGF), VEGF-A, VEGF-B, VEGF-C, VEGF-D. VEGF-A is the most potent angiogenic driver, while VEGF-C and D are essential drivers of lymphangiogenesis, a subject discussed in greater detail below. VEGF-A shows a higher affinity for VEGF receptor 1 (VEGFR-1) as compared to VEGFR-2, however, VEGFR-1 has a weaker kinase activity compared to VEGFR-2, the predominant angiogenic driving receptor [107, 118, 119]. The binding of VEGF-A to VEGFR-2 induces receptor dimerization and autophosphorylation, which drives downstream activation of various kinases (PKC, PKD, PI3K and MAPK) [107, 118], and activates various cellular processes, including transcription [120].

The stromal increase in VEGF-A signals to neighboring ECs, inducing the re-activation of the quiescent vasculature. VEGF-A initiates angiogenesis by specifying a tip cell, which is a non-dividing endothelial cell with multiple dynamic VEGFR2-enriched filopodia, and leads the invading vasculature [121]. The tip cell expresses the Notch ligand Dll4, which induces Notch

signaling in neighboring stalk cells, preventing excessive angiogenic sprouting [107, 122]. VEGF-A signaling through VEGFR-2 also induces the release of Angiopoietin-2 (Ang2) from endothelial cell intracellular granules, called Weibel-Palade bodies. Ang2 functions as a competitive antagonist of Ang-1, which is secreted by pericytes and vSMC. Ang2 binds tyrosine kinase with immunoglobulin-like and EGF-like domains 2 (TIE-2) receptor on ECs and blocks receptor phosphorylation, leading to the disruption of endothelial cell association with the basal lamina, associated pericytes and vSMC [123, 124]. VEGF-A-VEGFR-2 signaling also drives expression of matrix metalloproteinases (MMPs), which degrade the surrounding basal lamina and extracellular matrix (ECM), enabling the tip cells to penetrate and navigate in the surrounding stroma [123]. The migration of the tip cell is driven by the highly proliferative, tightly associated juxtaposed stalk cells [121].

The invading vasculature is a fragile monolayer of ECs, which requires support and stabilization by the normally associated mural cells. Mural cells can be roughly subdivided into vSMC and pericytes; the vSMC are typically associated with the large diameter arteries and veins, while pericytes are predominantly associated with the smaller diameter vasculature such as arterioles, capillaries and venules [125]. The invading vascular tip cell secretes and deposits platelet-derived growth factor β (PDGF-β), with a minor contribution from trailing stalk cells, onto the cell surface and surrounding extracellular matrix [126]. PDGF-β signals through PDGF receptor-beta (PDGFR-β) on mural cells to stabilize the nascent vasculature. In arteries and veins, PDGF-β/PDGFR-β signaling promotes the recruitment and proliferation of vSMC, while in the smaller diameter vasculature PDGF-β - PDGFR-β signaling serves as a chemoattractant for co-migrating pericytes [127]. PDGF-β can also signal to undifferentiated mesenchymal cells within the stroma to induce a mural cell fate, recruiting them to the nascent vasculature [125, 128-130].

The differentiation and maturation of mural cells is not completely understood and involves several other signaling pathways such as Sphingosine-1-Phosphate signaling to endothelial cells and endothelial cell secreted TGF-β [125].

When tip cells of two or more capillary sprouts meet, they fuse and vacuoles within the ECs coalesce to give rise to the lumen [131], which allows oxygenated blood to flow through and reduces stromal hypoxia [107, 118]. The stalk cells and pericytes secrete basal membrane components, such as CollagenIV and Laminin [132], which ensheathes and stabilizes the newly formed vasculature [107, 118, 133]. Furthermore, the associated mural cells actively secrete Ang1, activating Tie2 signaling in ECs, driving vascular stabilization and endothelial cell survival [123, 134-136].

The sequential stepwise process of angiogenesis is fairly ubiquitous throughout an organism, however some organs require the activation of additional signaling pathways, a noteworthy example is Central Nervous system (CNS) angiogenesis, which requires β-catenin-dependent signaling in ECs [137].

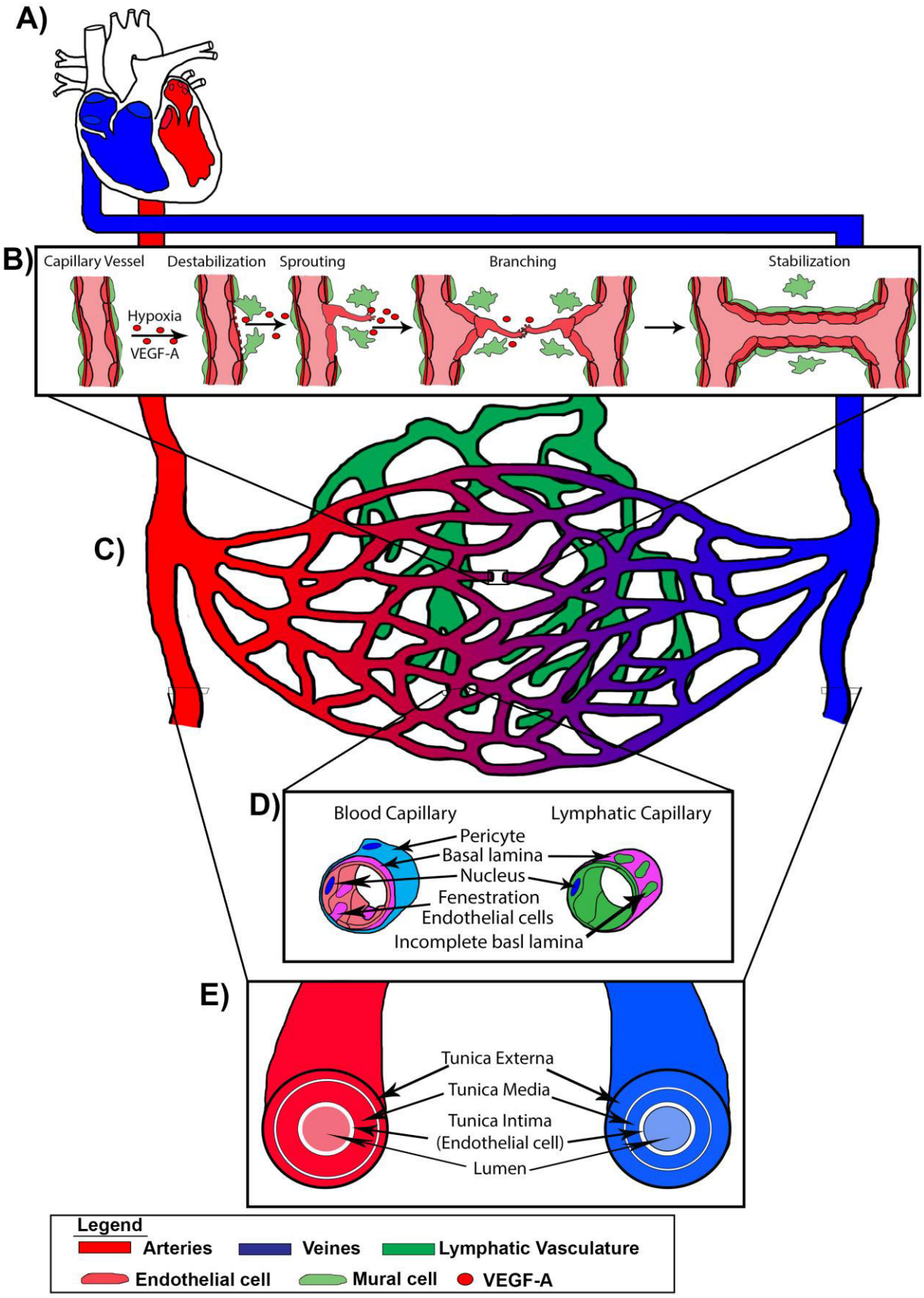
A)
B)
Capillary Vessel
Destabilization
Sprouting
Branching
Stabilization
Hypoxia
VEGF-A
C)
D)
Blood Capillary
Lymphatic Capillary
Pericyte
Basal lamina
Nucleus
Fenestration
Endothelial cells
Incomplete basl lamina
E)
Tunica Externa
Tunica Media
Tunica Intima
(Endothelial cell)
Lumen
Legend
Arteries
Veines
Lymphatic Vasculature
Endothelial cell
Mural cell
VEGF-A

Figure 4. The vascular tree and angiogenesis.
(A) The vasculature tree can roughly be subdivided into the heart, arteries, veins and (C) the capillary bed. (B) Angiogenesis is the process of novel vasculature formation from the expansion of pre-existing vasculature. This process takes place in several sequential steps. Vessel destabilization: Vascular endothelial growth factor A (VEGF-A) activates quiescent ECs and induces the dissociation of the associated mural cells and the degradation of the surrounding basement membrane. Sprouting: the tip cell is specified and extravagates out into the surrounding parenchyma, following the VEGF-A gradient and trailed by the tightly associated stalk cells. Branching: Tip cells from different vessels meet and fuse, while vacuoles within them coalesce to form a lumen, which enables blood flow and starts the vascular stabilization process. Vascular stabilization: ECs recruit mural cells, which secrete various factors such as angiopoeitin-1 (Angpt-1), along with the deposition of extracellular matrix (ECM) proteins, promoting the stabilization and maturation of the newly formed vasculature. (D) Representational diagram illustrating the composition of capillary blood vasculature and capillary lymphatic vasculature. This diagram also highlights the unique features of the two capillaries, such as the presence of pericytes coverage and endothelial fenestration for the blood capillaries. The lymphatic capillaries have an incomplete or absent basement membrane, no pericyte coverage and no fenestration. (E) Representational diagram of the composition of arteries and veins. This diagram also highlights some of the differences between them, e.g. the thicker tunica media in arteries as compared to the veins, while the tunica externa is thicker in veins as compared to arteries. Adapted from [138, 139].

1.7 The Blood brain barrier (BBB)

The functional unit within the vasculature, in terms of nutrient and gas exchange, is the capillary bed. In humans, the capillary bed can roughly be subdivided into 3 groups; sinusoidal (discontinuous), fenestrated and continuous. This classification is based on two predominant features. The first is the presence and size of the openings between and within ECs (called fenestrations). The size of the openings between ECs is a feature which is related to the spacing and distribution of the inter-endothelial cell adhesion junction complexes, which are found ubiquitously throughout the vascular tree. The second feature depends on the completeness of the surrounding basement membrane [140, 141]. These different types of capillary beds are organ-specific and essential for the proper functioning of the designated organ. Notable examples include the fenestrated vasculature within the renal glomerulus of the kidneys [142], and the highly selective virtually impenetrable continuous vasculature of the CNS.

The CNS blood brain barrier (BBB) is essential for the maintenance of the brain interstitial fluid (ISF) homeostasis and for the creation of a specialized environment that is essential for the proper functioning of the brain. The CNS ECs (CNS-Endo) are highly specialized ECs and contain several unique adaptations that contribute to the assembly of the blood brain barrier (BBB). These adaptions include: the high expression and selective localization of influx and efflux transporters, the presence of continuous intercellular tight junctions (TJ) complexes, the lack of fenestration, and a reduced expression of leukocyte adhesion molecules (abrogating the recruitment of infiltrating leukocytes and limiting immune surveillance) [143]. Furthermore, CNS-Endo have a complete and continuous basement membrane. The elevated expression of several tight junction (TJ) proteins (Claudins, TJ-associated MARVEL proteins (TAMPs, which include Occludins) and immunoglobulin superfamily membrane proteins (JAM-A/-B/-C)) are concentrated at the apical side towards the vessel lumen and are often intermingled with adherens junction complexes [135,

144, 145]. The TJ effectively seals the inter-endothelial cell membranes together, giving the luminal surface of the vasculature a smooth continuous appearance. This reduces solute/ion permeability and contributes to the elevated transendothelial electric resistance (TEER) of the CNS, as compared to non-CNS vasculature [146, 147]. The TJ is also essential for the establishment of cell polarity, which enables the apical versus basal localization expression of substrate specific transporters, which enables the ECs to control the directionality of the trans-endothelial influx and efflux of substrates [135, 148]. Furthermore, CNS-Endo also have a low pinocytic activity and an elevated abundance of mitochondria and various metabolic enzymes, which cooperate together to establish a "metabolic barrier" [135, 149]. All together these unique adaptions of the brain ECs form the BBB and enable the creation of a unique brain interstitial fluid (ISF), which is essential for proper brain function. While the brain ISF is comparable to blood plasma, it has a much lower K^+, Ca^{2+}, glutamate and protein concentration and an increased Mg^{2+} concentration [135, 144, 149].

Over recent decades, it has become increasingly clear that the BBB is not a rigid property that is strictly controlled by the brain ECs, but rather is a dynamic property that can be actively modulated by the cell within the neurovascular unit (NVU). Brain ECs, astrocytes, neurons, microglia, pericytes and immune cells all belong to the NVU, and can actively modulate BBB plasticity [150, 151]. The contribution of these different cell types to the formation of the NVU and BBB vary depending on various factors, including inflammatory status and their location either deep in the parenchyma or in the meninges.

1.8 BBB development and maintenance

The ability of ECs (ECs) to adopt BBB properties is not intrinsic to ECs, but rather is an acquired property that is gained from EC interactions with neural cells (astrocyte and their

progenitors) [152, 153]. The development of the BBB is a multistep process that begins with the invasion of ECs into the embryonic neuroectoderm under the guidance of several neural progenitor secreted factors. These early angiogenic sprouts exhibit several features unique to the CNS vasculature, including expression of TJ proteins and nutrient transporters, such as Glucose transporter 1 (Glut1), as well as some general vascular features, such as a large number of transcytotic vesicles and an elevated expression of leukocyte adhesion molecules [143].

Angiogenesis in the CNS require the convergence of the VEGF and Wnt signaling pathways. VEGF is secreted by the neural progenitor cells and is essential for the initiation and guidance of the developing sprout [154]. Canonical β-catenin-dependent Wnt signaling is required for sprout invasion and capillary bed formation [137]. Canonical Wnt signaling also promotes the expression of Tumor necrosis factor receptor superfamily member 19 (Tnfrsf19 also known as Troy) and Death receptor 6 (Dr6) in ECs, which synergize with VEGF signaling to promote downstream JNK activation, providing a potential point of cross talk between both pathways and highlighting the need for both pathways to activate angiogenesis in the CNS [137].

Canonical Wnt signaling is also essential for embryonic and postnatal BBB establishment and maturation. Canonical Wnt increases the expression of TJ proteins (e.g. Claudin-3) [155] and specialized transporters (e.g. Glut1) [155, 156] and inhibits the expression of Plasmalemma vesicle-associated protein (Plvap or Meca32), a marker of fenestrated ECs [94]. Furthermore, canonical Wnt signaling has been shown to directly regulate the expression of PDGF-β, which drives mural cell recruitment and enhances vessel stabilization and quiescence [157]. The regulation of canonical Wnt signaling in ECs of the CNS is regulated by a collection of regionally expressed Wnts, which include Wnt7a and Wnt7b in the developing forebrain and ventral region of the neural tube, Wnt1, Wnt3, Wnt3a and Wnt4 in the developing dorsal, hindbrain and spinal

cord [137, 143] and Norrin, an atypical Wnt, in the cerebellum, retina and olfactory bulb [84, 97]. Recently, a novel receptor, tumor endothelial marker 5 (TEM5 as known as GPR124), has been shown to be essential for forebrain and ventral spinal cord sprout formation, EC survival and BBB formation [158-160]. In the developing forebrain, TEM5 is believed to be involved in angiogenesis and BBB formation, at least in part, by promoting Wnt7-dependent canonical Wnt signaling [161].

Canonical Wnt signaling is essential for BBB formation and maturation, however, it is not sufficient by itself and requires enhancement from several other cell types, predominantly mural cells (mostly pericytes in the capillary beds [162-164]) and astrocytes [165-167] to complete the maturation of the BBB. The maturation of the BBB includes the expansion, redistribution and further elaboration of the TJ complexes, increased expression of specialized influx and efflux transporters, and the decreased expression of transcytosis and leukocyte adhesion molecule expression [143].

Astrocytes are important for the maturation and maintenance of the BBB and their association (direct or indirect) with the vasculature is dependent on the vasculature localization within the CNS. The vasculature within the brain parenchyma is intimately associated with the astrocyte end feet, which almost completely envelop the outer, ECM rich, surface of the vasculature [143]. In contrast, the vasculature confined within the meninges is separated from the astrocyte end feet by a layer of meningeal cells [132].

1.9 The perivascular space

In the brain, at the level of pre-capillary arteriole, post-capillary venule or larger vessels (all predominantly confined within the meninges), there are 4 layers of basement membrane that surround the vasculature. The first layer encapsulates the ECs and separates them from the pericytes, the second surrounds the pericytes and separates them from the meningeal epithelium,

the third envelops meningeal epithelium and separates it from the astrocytes and the fourth layer is produced by the astrocyte end feet and forms the glial limiting membrane [132]. The pericytes are encased between two (the ECs and pericyte) basement membranes, which are often regarded as a composite basement membrane. The pericytes maintain direct contact with the ECs through peg-socket junctions, which are imbedded in and extend through the basement membrane surrounding the ECs [143]. The last two basement membranes that are produced and deposited by the astrocyte end feet and meningeal epithelium are collectively termed the parenchymal basement membrane and are structurally continuous and function to delimit the brain parenchyma [168]. The composite endothelial/pericyte basement membrane together with the parenchymal basement membrane form the inner and outer limits of the Virchow-Robin (VR) space [132, 143, 169, 170] (Figure 5C), a space that is known to have an immune surveillance function [171-173]. As the vasculature travels deeper into the brain parenchyma, the meningeal layer and associated basement membrane is lost, designating the end of the VR space. At the level of the vascular capillary bed a small perivascular space is still present between the glial end feet and the pericyte basement membrane. The VR space and perivascular space are important structures as they have an essential role in metabolite and ISF homeostasis, as illustrated by tracer dye experiments, where tracer dyes injected into the CSF or brain parenchyma could be observed travelling along the perivascular and VR spaces [165, 174].

1.10 The meninges

The meninges is a system of envelops composed of 3 membranes that surrounds the brain and spinal cord, protecting the brain and acting as a cushion by keeping it in suspension. In mammals, the 3 layers relative to the skull are the outer dura mater, the arachnoid mater, and the inner pia mater. The cerebrospinal fluid (CSF) is located in the subarachnoid space between the

arachnoid mater and the pia mater [175]. The pia mater, the innermost layer of the meninges, is directly associated with the astrocyte end feet (forming the glial limiting membranes), surrounding the brain and following its every contour and fold. In the cerebellum it is the pia mater which follows the external granule layer into the deep cerebellar folds [176].

The blood vessels traversing the subarachnoid space are encased by a layer of meningeal cells, which isolates them from the CSF. As the vasculature penetrates the interstitium of the brain, it loses its meningeal and vSMC coverage, and is ensheathed solely by pericytes and astrocyte end feet at the capillary bed level within the brain parenchyma. At the capillary bed level the meninges and associated VR space is absent. However, the VR space and the perivascular space are continuous as the meningeal cells which delimite the VR and perivascular space are fenestratsted, allowing the passage of CSF and ions from one compartment to the other [168]. The presence and continuity of the VR and perivascular spaces has been shown to have an essential role in removing metabolic waste and turning over the interstitial fluid (ISF) in the brain through the glymphatic system [165, 177].

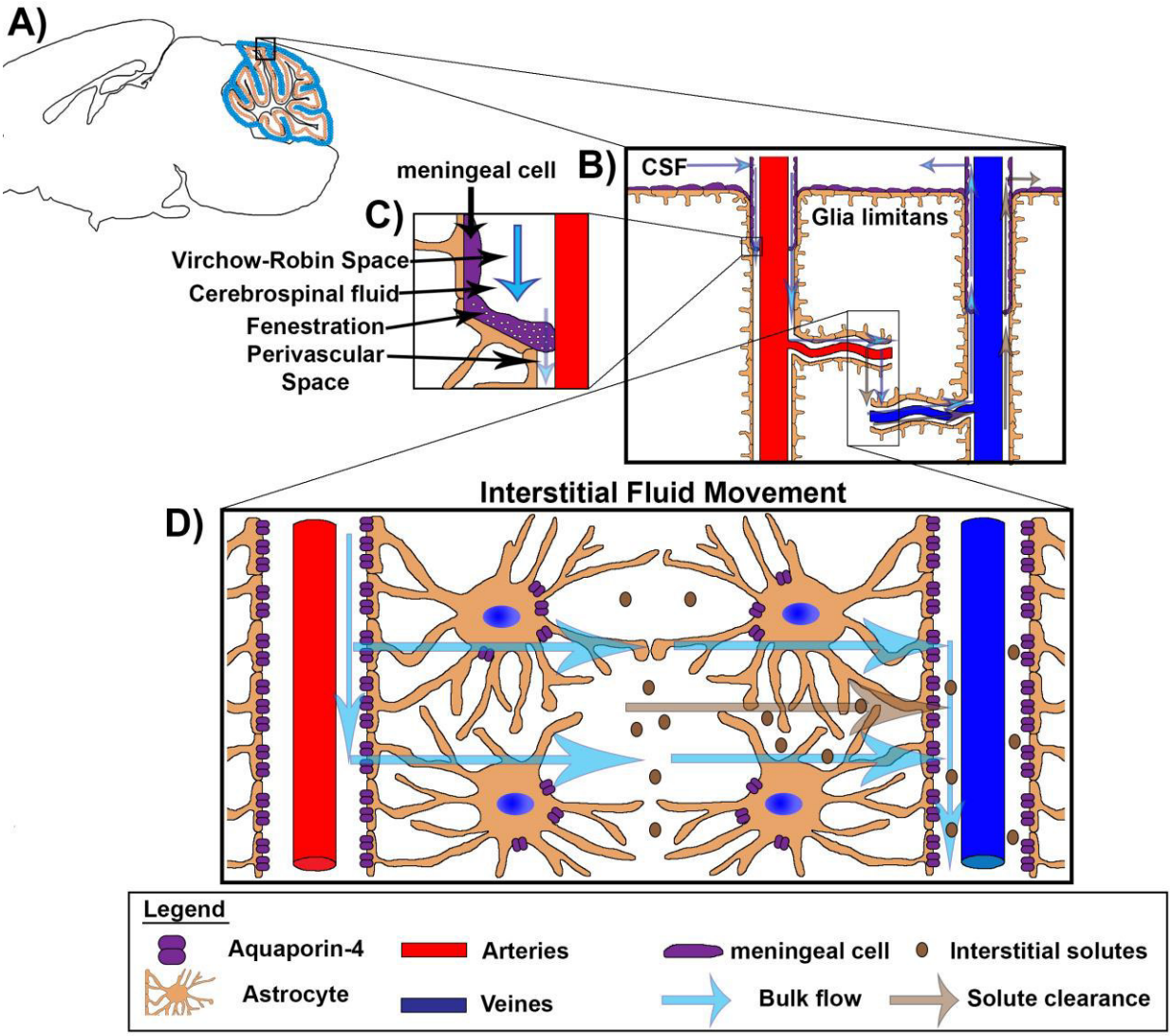

Figure 5. Cerebrospinal fluid movement and the glymphatic system.
(A) Schematic of a sagittally sectioned mouse P14 brain, black box illustrating the zoomed-in section (B). (B) Simplified diagram illustrating the movement of fluid within the central nervous system (CNS) that maintains brain interstitial fluid (ISF) homeostasis. Cerebral spinal fluid (CSF) enters the Virchow-Robin (VR) space by travelling through the meningeal layer in the subarachnoid space and travels along arteries to enter the brain parenchyma (C). At some point the meningeal layer disappears and the CSF from inside the VR space travels through the fenestrated meningeal cells to enter the perivascular space of the arterial vasculature. (B) The CSF continues to travel along the vasculature to enter the brain parenchyma. (D) Water and transportable ions enter the brain's parenchyma in an Aquaporin-4 (AQP4) dependent manner, where it mixes with the interstitial fluid (ISF) and exits the parenchyma of the brain, along with dissolved solutes and macromolecules by bulk flow, draining into the para-venous space. (B) The ISF and dissolved solutes follow the venous vasculature and exit the brain, either by draining back into the CSF in the subarachnoid space, or by re-entering the venous circulation through selective transporters, or by draining into the lymphatic system confined along the sinus veins. Adapted from [178].

1.11 Glymphatics and Lymphatic system

The human brain is a large, dense and highly metabolic organ, which would not be able to eliminate waste and cellular debris through simple diffusion alone. As such, alternative adaptive mechanisms are required to accomplish these roles and upon further investigation the glymphatic system was discovered. Essentially, the CSF in the subarachnoid space enters the VR space of arterioles, travels along the arteriole, propelled by arterial pulsations (Figure 5B) [179]. As the vasculature further ramifies into the capillary bed the pia sheath becomes fenestrated as it disappears and enables the exchange of substance and water in the VR space with the structurally continuous perivascular space (Figure 5C) [174, 180]. At the capillary level (Figure 5D), the CSF enters the brain parenchyma through astrocyte end feet in an Aquporin4-dependent manner to mix with the ISF in the brain interstitium. The CSF-ISF and solutes are propelled out of the brain interstitium by bulk flow (Figure 5B) and travel along the perivascular space of veins to exit the brain [165, 166]. Initially, the glymphatic system was believed to functionally replace traditional lymphatic vasculature. However, recently, functional lymphatic vasculature has been discovered within the meningeal dura layer [181, 182], which contributes to lymphocyte trafficking [181], CSF absorption from the subarachnoid space and ISF removal, presumably by cooperating with the glymphatic system [182]. Currently little is known about the lymphatic development in the CNS, as most scientific insight was gained from studying lymphatic vasculature in non-CNS organs.

The lymphatic vasculature is an essential component of the circulatory system and is essential for maintaining blood volume and protein homeostasis, effectively preventing corporal edema, in addition to accomplishing an essential immunological surveillance function [183]. The fundamental building blocks of the lymphatic network are the lymphatic ECs (LECs), which differentiate embryonically from vein ECs located within the cardinal vein (CV) and the

intersomitic veins (ISVs) [184-186]. These initial embryonic lymphatic progenitor cells proliferate and reorganize themselves to form the lymphatic vasculature network [186-188].

The molecular mechanisms that control lymphatic development and maturation are not completely understood. However, with the development of reporter mice and the discovery of novel lymphatic markers, some insight into the process has been gained. During embryonic development Sox18 is expressed in a subpopulation of vein ECs, which co-operates with COUP-TFII to induce the expression of Prospero homeobox protein 1 (Prox-1), a master transcriptional regulator of lymphatic fate specification, maintenance and development [99, 139, 189-191]. Prox-1 regulates the expression of many essential lymphatic genes, including Podoplanin (PDPN), Cyclin E1 (Ccne1) and VEGFR3. As lymphatic development ensues, Prox-1 expression becomes dependent on a VEGFR3-Prox1 feedback loop [192, 193]. The sustained expression of Prox-1 in LEC during embryonic development and adulthood is highlighted by the observation that the conditional down-regulation or deletion of Prox-1 is sufficient to revert terminally differentiated LECs to vein ECs [193].

The embryonic lymphatic vascular expansion and development was shown to be induced in response to the increase in interstitial pressure (a mechano-induction) [194]. Upon further investigation it was shown that the mechano-induction of lymphatic patterning and development is mediated by canonical Wnt, β-catenin dependent signaling [195]. Furthermore the targeted deletion of β-catenin from the lymphatic vasculature induced aberrant lymphatic vessel patterning and prevented lympho-venous valve specification [195]. The role of canonical Wnt signaling in lymphatic vessel patterning and lympho-venous valve specification is believed to be mediated, at least in part, by the modulation of two of its direct downstream target genes, Prox1 and FOXC2 [189-191, 195]. Furthermore, an additional investigation has highlighted tissue specific Wnts, such

as Wnt5b and Wnt5a, which have been shown to be essential for cardinal vein lymphatic specification [196] and dermal lymphatic maintenance during postnatal life, respectively [197]. The importance of Wnt signaling in lymphatic development and CNS angiogenesis [137], and their common origin, have raised the possibility that some tissue-specific Wnt ligand may be able to modulate the patterning and development of both vasculatures simultaneously.

Rationale and Objectives – Micro-environment in PNL initiation and MB development

The tumor microenvironment is a heterogeneous population predominantly composed of tumor cells and stromal cells. These stromal cells can support tumor growth through various mechanisms, such as the induction of angiogenesis [198], which in turn promotes tumorigenesis by enhancing growth and metastasis and/or by preventing necrosis and apoptosis [33, 199, 200]. It has been shown that there is a positive correlation between the expression level of angiogenic factors and the aggressiveness of the tumor [33]. Furthermore, for some CNS tumors, such as malignant glioma, the activation of the angiogenic program and the opening of the BBB is believed to be essential for driving tumor cell proliferation, growth, invasion and destruction of the normal neighboring brain tissue [201, 202]. The disruption of the BBB was also shown to be a common feature amongst both human and mouse CNS malignancies [201, 203], which makes the vascular component of the microenvironment a candidate of interest in the context of tumor progression. However, the relationship between tumor progression and angiogenesis is not well characterized in the CNS, as the opportunities for studying early stage human CNS tumor samples are very rare. Recently, several lines of research have promoted the concept of a shared mechanism that co-ordinates CNS vascular and neuronal development [204]. This notion was initially inspired by the observation that axonal growth cone and vascular tip cells have several similar anatomical and cellular features [205]. In addition, several CNS injury models showed that angiogenesis enhances neurogenesis through the mobilization of neural progenitor cells to the site of injury. Furthermore, some angiogenic factors, such as VEGF, have neuroprotective properties [206-208]. Interestingly, several axon guidance molecules, such as Slit/Robo, semaphorin/neuropillin, Ephrin/Eph and others, in addition to several mitogens, such as Shh and Wnt, have known roles in directing CNS angiogenesis [137, 205, 209-211]. As some CNS malignancies were associated with

developmental defects (e.g. Wnt and Shh-MB) and CNS angiogenesis is associated with normal CNS development, there could also be a functional relationship between tumor initiation and angiogenesis. Studying the role of angiogenesis in CNS tumor initiation requires an adequate multistage CNS tumor model [212]. An ideal mouse model for such a study is the $Ptch^{+/-}$ MB model [213]. The $Ptch^{+/-}$ mouse model has a LacZ-neo gene construct inserted into one of the *Ptch1* alleles, rendering the mouse haploinsufficient for Ptch1, resulting in a slight gain of function for the Shh pathway [213]. The $Ptch^{+/-}$ mouse model is considered a paradigm for Shh-MB and an ideal mouse to model human Gorlin syndrome [213]. MB development in $Ptch^{+/-}$ mice is well-characterized with a sequential multi step developmental program in which GNPs accumulate on the surface of the cerebellum. Sustained Hh pathway driven-proliferation in these ectopic GNPs creates the formation of a lesion [51, 55]. The additional rounds of replication of GNPs located within the lesion promotes DNA damage [214, 215], thereby increase the chance of acquiring mutations in growth regulation genes (e.g. *Ptch1*), which can lead to cell autonomous growth. In $Ptch^{+/-}$ mice, the inactivation of the remaining *Ptch1* allele is an early event in lesion progression and is associated with elevated levels of P53 oncogene-induced senescence [216, 217]. To circumvent senescence additional mutations in *P53* or epigenetic alterations in cell cycle checkpoint proteins, such as *Cdkn2a*, are required [217] to enable lesions progression towards Shh-MB [212, 216]. Interestingly, it has been shown that the majority of PNLs regress [25] and even Ptch null GNPs can differentiate [218]. This observation highlights the importance of senescence evasion in lesion progression [217]. Furthermore, it has been shown that in established non-CNS tumor the microenvironment can promote DNA damage [45, 219]. These observations create the possibility that the microenvironment could contribute to the early lesion initiation and progression in $Ptch^{+/-}$ mice. To explore the relationship between the stroma and pre-tumor

initiation/progression in Ptch$^{+/-}$ mice, we modulated Norrin/Frizzled4 (Fzd4) signaling, a signaling axis which is involved in neuronal-mediated vascularization and BBB maintenance in the cerebellum [84].

Hypothesis: Modulation or disruption of the endogenous neuronal to endothelial ligand, Ndp, is an important event during early tumorigenesis to drive the establishment of a pro-tumor microenvironment, promoting tumorigenesis through enhanced lesion formation and tumor progression.

Specific aims

1) Characterization of the role of Ndp signaling in cerebellar development and Ndp/Fzd4 signaling in MB initiation and progression.

2) Characterization of stromal alterations as a function of inactivation of endothelial Ndp/Fzd4 signaling.

3) Dissection of the requirement for the stromal alterations in MB development.

Chapter 2. Material and methods

2.1 Mice

All experiments were approved by the University of Ottawa Animal Care Ethics Committee and adhered to the guidelines of the Canadian Council on Animal Care (CCAC).

Ndp-/Y mice

$Ndp^{-/Y}$ mice (RRID:MGI:4414648), generated by disruption of the Ndp locus by a lacZ-containing cassette were obtained from Lexicon Pharmaceuticals [85] and maintained by interbreeding on a mixed background. Ndp is an X-linked gene, therefore we used $Ndp^{-/Y}$ males for the lacZ-based reporter expression analysis in (Figure 6). $Ndp^{-/-}$ females are infertile, therefore the experimental cross to generate $Ndp^{-/Y}$;$Ptch^{+/-}$ compound mutants and littermate controls must be performed by crossing $Ndp^{+/-}$ females with $Ptch^{+/-}$ males. Thus, the $Ndp^{-/Y}$ and $Ndp^{-/Y}$;$Ptch^{+/-}$ genotypes are restricted to male mice carrying the $Ndp^{-/Y}$ allele, whereas additional controls include both sexes.

$Ptch^{+/-}$ Mice

$Ptch^{+/-}$ (RRID:MGI:2177702) mice were obtained from Jackson Laboratories and maintained on a C57BL/6 background.

$Fzd4^{Flox/Flox}$

$Fzd4^{Flox/Flox}$ (RRID:MGI:4412187) mice were obtained from Jackson Laboratories and maintained on a C57BL/6 background.

Atoh1-Cre

Atoh1-Cre (RRID:IMSR_JAX:011104) mice were obtained from Jackson Laboratories and maintained on a C57BL/6 background.

Tie2-Cre

Tie2Cre (RRID:IMSR_JAX:008863) mice were obtained from Jackson Laboratories and maintained on a C57BL/6 background. $Tie2Cre^{+/-};Fzd4^{Flox/Flox}$ females are infertile, therefore $Tie2Cre^{+/-};Fzd4^{Flox/Flox};Ptch^{+/-}$ compound mutants were generated by crossing $Fzd4^{Flox/Flox};Ptch^{+/-}$ females with $Tie2Cre^{+/-};Fzd4^{Flox/Flox}$ males.

Neurod2-SmoA1

Neurod2-SmoA1 (RRID:MGI:3831004) mice [220] were maintained as homozygotes, crossed with $Ndp^{+/-}$ females and tumors were monitored in Neurod2-SmoA1+/−;Ndp-/y and Neurod2-SmoA1+/−;Ndp+/y littermates.

In every experiment, all compound mutants were compared to single mutant or wild-type controls from the same breeding cohort to ensure matched backgrounds. In Kaplan-Meier survival curve studies, mice were continually monitored and sacrificed upon display of advanced tumor symptoms (a domed head, dysmorphic skull, head tilt, hunched posture, ataxia and weight loss) or other adverse health effects as per CCAC endpoint guidelines. All animals were dissected to confirm presence or absence of medulloblastoma.

2.2 Antibodies

The following primary antibodies were used for immunostaining or flow cytometry:

Table 1. List of Antibodies

Antibody	Source	Dilution
rabbit anti-mouse collagen IV	AbD Serotec 2150–1470 RRID:AB_2082660	1:1000
rat anti-mouse CD31	clone MEC13.3, BD Biosciences 550274 RRID:AB_393571	1:200
rabbit anti-pan-Laminin	Abcam ab11575 (AB_298179)	1:500
rabbit anti-NeuN	Millipore ABN78 (AB_10807945)	1:1000
rabbit anti-phospho-histone H3	Millipore 06–570 (AB_310177)	1:500

rabbit anti-phospho-histone H3	Millipore 06–570 (AB_310177)	1:500
rat anti-mouse PLVAP	clone MECA-32, BD Biosciences 553849 (AB_395086)	1:100
rabbit anti-mouse Claudin-5	Thermo Fisher 34–1600 RRID:AB_2533157	1:500
Rat anti-mouse CD45	Stem Cell (Cat#60030.1)	1:300
rat anti-mouse CD45R	clone RA3-6B2, BD Biosciences 550286 RRID:AB_393581	1:100
rabbit anti-active caspase-3	clone C92-605, BD Biosciences 559565 RRID:AB_397274	1:200
rabbit anti-Pax6	Covance PRB-278P RRID:AB_2313780	1:500
rat anti-myelin basic protein AbD	Serotec MCA409S RRID:AB_325004	1:100
mouse anti-β-tubulin isotype III	clone SDL.3D10, Sigma-Aldrich T8660 RRID:AB_477590	1:1000
rabbit anti-GFAP	Sigma-Aldrich G9269 RRID:AB_477035	1:1000
rabbit anti-PDGF receptor beta	Abcam ab32570 RRID:AB_777165	1:100
rat anti-mouse Endomucin	Santa Cruz sc-65495 RRID:AB_2100037	1:250
mouse anti-ZO-1	Thermo Fisher 339100 RRID:AB_2533147	1:300
Rabbit anti-LEF1	Clone C12A5, Cell Signaling 2230 RRID:AB_823558	1:250
Rat anti-Lyve-1	Monoclonal ThermoFisher scientific (Cat# 14-0443-82)	1:300
Mouse aanti-Podoplanin	eBioscience Inc, Mouse IgG, Ref:12-5381-80, Clone #:eBio8.1.1	1:300
Mouse anti-Occludin	Monoclonal BD Bioscicence (Cat# 611090)	1:300
Anti-Prox-1 antibody	AngioBio Co., Rabbit IgG, (Cat# 11-002P)	1:300
Mouse anti-NeuroD1	Abcam (Cat# AB60704)	1:300
Isolectin GS-IB4 Alexa Fluor 594 Conjugate	Life Technologies I21413	1:100 – 1:300
488 anti-mouse CD11c	clone N418, BD Biosciences 117313	1:100
488 anti-mouse CD3ε	clone 145-2c11, BD Biosciences 100321	1:100
647 anti-mouse CD1d	clone 1B1, BD Biosciences 123511	1:100
488 anti-mouse CD5	clone 53-7.3, BD Biosciences 100612	1:100
488 anti-mouse IgM	clone RMM-1, BD Biosciences 406521	1:100
488 anti-mouse CD4	clone Gk1.5, BD Biosciences 100425	1:100
488 anti-mouse CD8a	clone 53-6.7, BD Biosciences 100726	1:100
488 anti-mouse CD19	clone 6D5, BD Biosciences 115524	1:100
PE anti-mouse CD279 (PD-1)	clone J43, eBioscience Monoclonal 12-9985-82	1:100

PE anti-mouse CD274 (PD-L1)	clone MIH5, eBioscience Monoclonal 12-5982-82	1:100

2.3 Tissue processing

For fixed tissue, pups younger than 14 days old were decapitated and brains were removed and placed directly into 4% paraformaldehyde (PFA). Animals 14 days and older were anesthetized and cardiac perfusion was performed using 10 ml of PBS, then 10 ml of 4% PFA, followed by dissection of the brain. Brains used for histological stains, Evans Blue visualization, in situ hybridization or immunostaining were then fixed in 4% PFA overnight at 4°C, whereas brains used for X-gal staining were fixed in 2% PFA with 2 mM MgCl2 and 1.25 mM EGTA (ethylene glycol tetraacetic acid) for 45 min at 4°C. All tissues were then washed in PBS, cryoprotected in 30% sucrose/PBS overnight at 4°C, and embedded in a 50:50 mixture of Optimal cutting temperature compound (OCT compound):30% sucrose by freezing in chilled 2-methylbutane. For fresh frozen tissue, unfixed brains were dissected and embedded as described above. If used for immunostaining, cardiac perfusion was performed using 10 ml of cold PBS before dissection. For lasercapture microdissection, tissue was immediately dissected and embedded without perfusion, for maximum RNA integrity.

2.4 Granule neuron progenitor (GNP) isolation

GNPs from the EGL or lesion-associated GNPs from P14 and P30 $Ptch^{+/-}$ mice were purified from cerebella by percoll gradient separation and pre-plating, as described previously [25]. Cells were then transferred to PDL-coated glass coverslips to proceed with immunostaining, pelleted and immediately resuspended in PBS for flow analysis, or resuspended in lysis buffer for RNA extraction.

2.5 Immunostaining

2.5.1 PFA-fixed brain tissue

Brains were sectioned sagittally in a Leica CM1850 cyrostat at 12 µm onto Superfrost Plus positively charged slides (Fisher Scientific), air dried for 1–2 hr, and stored with desiccant at −20°C. Prior to immunostaining, antigen retrieval was performed in 10 mM sodium citrate buffer (pH 6) in a rice steamer. Slides were blocked with 10% normal serum in TBLS (Tris-buffered saline containing 1% bovine serum albumin and 10 mM lysine) for 30 min at room temperature (RT). Antibodies were diluted in TBLS and incubated overnight at 4°C. Sections were incubated with Alexa fluor secondary antibodies (Molecular Probes) of the desired fluorescence (excitation: 488, 555 and 647) at 1:1000 for 1 hr at RT, and nuclei were stained with Hoechst before coverslipping with fluorescence mounting medium (Dako S3023). For co-immunostaining, both primary and both secondary antibodies were incubated simultaneously.

The following modifications were performed for peroxidase-based immunohistochemistry (IHC): Before blocking, endogenous peroxidases were quenched by incubating slides in 0.3% hydrogen peroxide in PBS for 15 min at RT. Biotinylated secondary antibodies were used at 1:200 (Dako), followed by incubation with avidin-biotin peroxidase (Vector Laboratories, PK-4000) for 40 min at RT, color development with 2.5% diaminobenzidine, and a brief counterstain with hematoxylin before mounting in 50:50 glycerol:PBS.

2.52 Acetone-fixed brain sections

Fresh frozen brains were cryosectioned at 12 µm on to Superfrost Plus positively charged slides (Fisher Scientific), air dried for 1–2 hrs, and slides were dipped in acetone for 20 seconds prior to storage at −80 ^{o}C until staining. Before staining, slides were fixed in ice cold (-20^{o}C) acetone for 10 min, washed in ice cold (-20^{o}C) 70% ethanol for 5 min followed by several washes in RT PBS,

and blocked with 10% normal serum in PBS. Primary antibodies were diluted in 3% normal serum and incubated overnight at 4°C, followed by secondary antibody detection and mounting, as described above. For the Pax6/CD31/EdU triple stain, the EdU was detected immediately following Pax6/CD31 immunostaining, using the Molecular Probes Click-iT EdU Alexa Fluor 647 Imaging Kit according to manufacturer's instructions.

2.5.3 GNP immunostaining

Purified GNPs, directly ex vivo or cultured were washed in sterile PBS before a 10 min fixation step in 4%PFA. Subsequently the cells were washed in sterile PBS and stained, as outlined in section 2.4.1. For the endogenous Fzd4 receptor stain, 10mM of α-Fzd4 or control α-KLH antibody were added into the culture media 10 min prior to wash and fixation. EDU pulses where performed 4 hrs prior to fixation, unless specified otherwise, with 10μM of EDU added directly into the culture media. For each stain or co-stain, at least 1 coverslip from 3 or more different biological samples was stained and examined.

2.5.4 Image stream/flow cytometry

Animals at the desired age were pulsed with 10mg/ kg of EDU IP prior to harvest. Cells were dissociated, as specified in section 2.4.3 and quantified by hemocytometer. 10^6 cells were placed into a 15ml falcon tube, spun down for 5 min at 400gs, washed (1XPBS +2%FBS and 0.1% Sodium aside), spun down again and fixed for 10minutes in 4%PFA (with constant agitation). Subsequently the cells were washed in sterile PBS and permeabilized by re-suspending in PBS + 0.025% Tween20 on the rocker for 5 min at RT. Cells were subsequently spun down, washed in fresh PBS twice and blocked by re-suspension in 1ml 10%GS/PBS on the rocker for 30 min at RT. Primary antibody incubation was performed overnight at 4 ^{o}C with rocking, followed by several

washes in PBS and the secondary antibody incubation was performed at RT for 1hr. Cells were subsequently stained with Hoechst or EdU staining was performed prior to Hoechst staining (Image stream: Hoechst = 2 µl in 2ml of PBS). Cells were then spun down and re-suspended in 500 µl of sterile PBS for imagestream/Flow analysis.

2.6 Retinal whole-mounts

For retinal whole mount analysis, mice were perfused with 10 ml of PBS followed by 10 ml of 4% PFA, eyes were removed and the nasal caruncle was preserved during dissection. The retinas were placed in cold HBSS and a suture was inserted into the dorsal pole. Retinas were dissected into flat mounts with 4 radial incisions, with the longest incision located at the dorsal pole. Following the removal of the pigmented epithelial layer the retinal flat mounts were post dissection fixed in 4%PFA for 10 min. The retinas were washed in PBS + 0.5% TritonX-100 and permeabilized in 500 µl of PBS + 0.5% TritonX-100 for 15 min at -80^{o}C. Afterwards the retinas were removed and thawed at RT, washed several times in PBS + 0.5% Triton X-100 and blocked in 2% normal Goat serum in PBS + 2% Triton X-100 for 1 hr at RT. Isolectin GS-IB4 Alexa Fluor 594 Conjugate (1:100, Life Technologies I21413) was diluted in blocking buffer and incubated over night at 4^{o}C. The following day the retinas were washed several times in PBS + 0.5% Triton X-100, followed by PBS, transferred to a slide with the photoreceptors facing the glass slide, cover slipped with Dako fluorescent mounting medium and sealed with clear nail polish [145].

2.7 X-gal staining

Slides with 12 µm cryosections of 2% PFA-fixed brains were air-dried for 1 hr, placed in X-gal reaction buffer (1 mg/ml X-gal with 5 mM potassium ferrocyanide, 5 mM potassium ferricyanide, 2 mM MgCl2, 0.02% IGEPAL, 0.01% sodium deoxycholate in 0.1 M phosphate buffer), incubated

overnight at 37°C, then washed and mounted with 50:50 glycerol:PBS. For co-X-gal/IHC stains, IHC was performed as described above, immediately after incubation in X-gal reaction buffer. For each X-gal stain or X-gal/IHC co-stain, at least 4 separate sections from n = 3 cerebella were examined.

2.8 In situ hybridization

Digoxigenin (DIG)-labeled antisense RNA riboprobes were prepared by *in vitro* transcription from linearized plasmids containing complete or partial cDNA sequences of the following mouse genes: Atoh1 (a gift from Dr. Carol Schuurmans), Mycn, and Ccnd1. ISH was performed as previously described [221], with the following modifications: Slides were incubated 1 to 5 hrs in staining buffer containing NBT and BCIP, and slides were mounted in 50:50 glycerol:PBS. For each probe, at least 3 separate sections from n = 3 tumors were examined.

2.9 Hematoxylin and eosin staining (H&E)

4%PFA fixed sections were used. Before the staining, fresh ethanol (50%, 70%, 80%, 95% and 100%) was prepared, Eosin Y stain (Ricca 2850-32) was reconstituted as specified by the manufacturer and Mayer's hematoxylin solution (Sigma MHS32) was filtered through a filter paper (Whatman paper). Slides were rinsed in PBS for 2 min and placed into Hematoxylin solution for 3 min. Excess hematoxylin was rinsed off in tap water (until purple coloration stopped coming off of the slides), and briefly dehydrated by incubating the slides for 1 min in increasing concentrations of ethanol (50%, 70%, 80%, 95% and 100%). The slides were then very briefly (3-4 seconds) placed in Eosin. The excess Eosin was rinsed off in tap water (until pink coloration stopped coming off of the slides) and subsequently incubated for 1 min in increasing concentrations of ethanol (50%, 70% and 95%), followed by 1.5 min in 100% EtOH. Afterwards

the slides were incubated in xylene for 5 min prior to mounting with permount (Fisher SP15-100) and glass coverslip. H& E were used for lesion number and lesion volume quantifications.

2.10 Fzd4 blocking antibody, pertussis toxin (Ptx), α-CD20, α-Angpt2 and EdU administration

Anti-Fzd4 and anti-KLH control antibodies were generated as described [222], and functionally tested *in vivo* before use. Antibodies were diluted in PBS to 3 mg/ml immediately prior to administration, and injected intraperitoneally at a dose of 30 mg/kg. $Ptch^{+/-}$ animals in lesion studies were injected once at P7, whereas $Ptch^{+/-}$ animals in the Kaplan-Meier survival study were injected at P7 followed by a booster dose at P16, an age when the phenotypic effects of a P7 injection are still present (Paes et al., 2011).

Ptx was functionally tested *in vivo* before use. Ptx was diluted in PBS to 5 mg/ml and pups received intraperitoneal injections of 120 ng Ptx or PBS vehicle control at P7, P9, P11 and P13.

CD20 and isotype matched control KLH were functionally tested *in vivo* before use. Anti-CD20 monoclonal (clone MB20-11) antibodies were obtained from Genentech, Inc. $Ndp^{-/Y}$;$Ptch^{+/-}$ animals were treated IP at P2, P7 and P11 with 20ug/animal of α-CD20 or isotype matched α-mIgG2A antibody.

Angpt2 and isotype matched control mIgG2A were functionally tested *in vivo* before use. Anti-Angpt2 monoclonal (clone LC06) and isotype match control were obtained from Genentech, Inc. Functional stocks of 1-0.5 μg/μl were generated prior to use, $Ndp^{-/Y}$;$Ptch^{+/-}$ animals were treated IP at P7 and P11 with 10mg/kg of an α-Angpt2 or isotype matched control antibody.

EDU labelling. Animals were injected intraperitoneally with a dose of 10 mg/kg EdU 4 hr prior to sacrifice.

2.11 EGL/lesion measurements and analysis of immunostainings

For EGL/lesion measurements, sagittal 12 µm serial sections of cerebella were collected and examined along the mediolateral axis at intervals 144 µm apart, by hematoxylin and eosin (H and E) or cresyl violet staining, and blinded images at 5x magnification were captured. To quantify EGL thickness, three images (at identical locations at the cerebellar vermis between lobules VII and VIII) from n = 3 animals per genotype were analysed.

To quantify whole cerebella, EGL/ML and IGL area, a composite image of the entire cerebellum was imported into ImageJ, the scale was set based in the scale bar of the image. The desired layers were traced out and ImageJ quantified the area (mm^2) it occupied. 3 neighboring images from 3 different animals were quantified per genotype.

The quantification of the number of PH3+ cells in the EGL, was performed by manually counting the number of PH3+ cells within a composite image of the entire cerebellum. At least 3 neighboring images from 3 different animals were quantified per genotype.

To quantify lesion number or volume, lesions were carefully followed continuously along the entire mediolateral axis, and scored as an individual lesion only if they remained spatially separate from all other lesions in every section. Lesion volume (mm^3) was calculated by measuring the 2-D area (mm^2) of each lesion section using ImageJ, multiplying it by the thickness separating each section from its neighbor (0.144 mm) to obtain the volume of each slice, and adding the individual slice volumes to obtain a total volume.

To assess the vascularized, leaky vessel or CD45 accumulation status of the lesions, sagittal sections between 100 and 250 µm apart were examined along the entire mediolateral axis for Evans blue accumulation or stainings (anti-ColIV, Laminin, CD31, PLVAP or CD45) to sample the entire lesion.

To quantify stains in lesions (PH3, cleaved caspase-3, NeuN, CD31, Laminin, PLVAP or PDGFRβ) immunostaining, 3 to 4 blinded sections from each lesion at 10x or 20x magnification were analyzed. Using ImageJ, the number of PH3+ cells per unit area or percent area stained for caspase-3, NeuN, CD31, Laminin or PLVAP were determined. Quantification involving lesion vasculature included all lesion-associated vessels, whether they were 1) on the outer surface of the cerebellum, 2) deep in the cerebellar folds but still meningeal, or 3) growing into the 'lesion proper'. To quantify the number of PH3+ or Lef1+ cells per endothelial area, 3 sections per lesion were first imaged at 20x magnification by epifluorescence to measure endothelial cell area via tracing of CD31+ vessels and to identify potential double labelled candidates. Sections were then examined by confocal microscopy to confirm double-labelled cells.

2.12 Evans Blue injections and visualization

A 2% weight/per volume Evans Blue (Sigma) solution in 0.9% saline was administered by intraperitoneal injection at 4 µl/ g of body weight and allowed to circulate overnight. Following perfusion and fixation in 4% PFA as described above, whole brains were photographed and 12 µm cryosections were then visualized under the far red fluorescence filter. The same or immediately adjacent section was H& E- or anti-ColIV-stained to provide a matched image.

2.13 Assessment of the lymphatic density

The quantification of lymphatic density was performed by analyzing 3-4 neighboring sections (of the indicated area, e.g. normal EGL) from 3-4 animals of the indicated genotype, imaged at 20x magnification. Using ImageJ, the pixels were quantified and normalized to the blood vasculature. The different vascular density measurement for a specified area from a single animal was averaged and used to generate the figure.

2.14 Quantification of proliferation and DNA damage in GNPs

The quantification of the proliferative index in dissociated GNPs was performed by analyzing 5 images (20x magnification) per coverslip and 3-4 coverslips per condition. The fluorescent pixels of a given channel (e.g. EdU) were quantified and normalized to Hoechst. The images from a coverslip were averaged and used to generate the bar graph.

The quantification of DNA damage in acutely dissociated GNPs of the indicated genotypes was performed by analyzing 3-4 images (40x magnification) per coverslip and 3 coverslips per genotype. In imageJ the individual channels were separated and the Hoechst channel was used to outline the nucleus in an automated fashion, which was superimposed onto the γ-H2AX channel. The γ-H2AX was subsequently converted into a binary image and manually quantified.

2.15 Flow cytometry analysis

Unstained and single stain controls were used to establish the compensation grid and the voltages of the forward and side scatter prior to every experiment. Cells were run on a flow cytometer (CANTOII (BD biosciences)) and the gates were placed post acquisition on the gather data to define and quantify the abundance of the different lymphocyte populations.

2.16 Neurosphere primary and secondary using the limited dilution assay LDA

GNPs were dissociated, as described in section 2.4.3, and cultured in a 96 well plate for 10 days [223], with serum supplementation on day 7. The inner 60 wells (B2-G11) were used for quantification, which was carried out by scoring each well as positive or negative for the presence of neurospheres and the data were analyzed using ELDA online analysis software (http://bioinf.wehi.edu.au/software/elda/). The ELDA analysis tool performs the calculation of the sphere forming cell frequency and the significance of the result by chi squared test. Secondary cultures were performed by dissociating the neurospheres in the first 3 rows with Accutase (sigma A6964-100ML) and subsequent re-plating as described in above for a 10 day incubation and neurosphere quantification.

2.17 Laser capture microdissection

Fresh frozen cerebella were sectioned at 10 µm onto Superfrost microscope slides (Fisher Scientific) and placed immediately on dry ice before storage at −80°C for no more than 5 days before microdissection. Sections were stained and dehydrated by passing through RNase-free coplin jars with solutions made in DEPC-treated distilled water, as follows: 30 s in 75% ethanol, 30 s in distilled water, 2 min in 1% toluidine blue in distilled water, 30 s in distilled water, 30 s in 75% ethanol, 30 s in 95% ethanol, 1 min in 100% ethanol (2 times), and 5 min in xylene. All staining solutions except xylene contained RNase inhibitor (Sigma R7397). Slides were immediately microdissected using the ArcturusXT laser capture microdissection system (Life Technologies) in infrared mode, according to the manufacturer's instructions. 6 to 10 sections from each lesion were captured onto CapSure macro LCM caps (Life Technologies), transferred immediately to RLT plus lysis buffer (Qiagen) with β-mercaptoethanol, briefly vortexed, and stored on dry ice until RNA extraction.

2.18 RNA purification and quantitative RT-PCR

For microdissected lesion tissue, total RNA was extracted using the RNeasy Plus Micro kit (Qiagen) with genomic DNA eliminator columns, and amplified complementary DNA (cDNA) was prepared with the Ovation Pico WTA System V2 (NuGEN) according to the manufacturer's instructions. RNA integrity was assessed by an Agilent 2100 Bioanalyzer (Agilent Technologies) from slide scrapes. For all other samples, total RNA was extracted from freshly isolated/dissected GNPs, cerebellar tumor (with careful preservation of clean margins) or retina tissue using the RNeasy Mini Kit (Qiagen). First-strand cDNA was synthesized using the QuantiTect Reverse Transcription Kit (Qiagen), with and without reverse transcriptase to assess genomic contamination during downstream RT-PCR. For all samples, target gene mRNA levels were determined by quantitative RT-PCR (qRT-PCR) using iQ SYBR Green Supermix (Bio-Rad) and a MyiQ iCycler (Bio-Rad). Primer pairs were designed using PRIMER-blast (http://www.ncbi.nlm.nih.gov/).

Table 2. qRT-PCR primer list

Gene	Primer sequence (5' to 3')
Gapdh Forward	GGCCGGTGCTGAGTATGTCG
Gapdh Reverse	TTCAAGTGGGCCCCGGCCTT
Ndp Forward	CCCACTGTACAAATGTAGCTCAA
Ndp Reverse	AGGACACCAAGGGCTCAGA
Fzd4 Forward	GACAACTTTCACGCCGCTCATC
Fzd4 Reverse	CCAGGCAAACCCAAATTCTCTCAG
Lrp5 Forward	GAGGAGTTCTCAGCCCATCC
Lrp5 Reverse	GATCAGGGGAGCAGGTAGGA
Tspan12 Forward	GATTGCTGTCTGCTGCTTCC
Tspan12 Reverse	ACTGTACTGGCACCATAACCTC
Ptch1 exons2-3 Forward	CTCCTCATATTTGGGGCCTT
Ptch1 exons2-3 Reverse	AATTCTCGACTCACTCGTCCA
Gli1 Forward	ACATGCTGGTGGTGCACAT
Gli1 Reverse	AGGCGTGAATAGGACTTCCG
Mycn Forward	GCGGTAACCACTTTCACGAT
Mycn Reverse	AGTTGTGCTGCTGATGGATG

Esm1 Forward	ACAGGGTGACCGGAAGATGT
Esm1 Reverse	AGTCACGCTCTGTGTGGGAG
Plvap Forward	TGACTACGCGACGTGAGATG
Plvap Reverse	CTCGCTCAGGATGATAGCGG
Emcn Forward	CTCCCGAAGGAACGACCAAAA
Emcn Reverse	GGACCTTCAGTTGTTGTTCCC
Lyve-1 Forward	ACTTGCAGCTATGGATGGGT
Lyve-1 Reverse	GGAGTTAACCCAGGTGTCGG
VEGFR3 Forward	CCGCAAGTGCATTCACAGAG
VEGFR3 Reverse	TCGGACATAGTCGGGGTCTT
Pecam1 Forward	GGAATACCAGTGCAGAGCGG
Pecam1 Reverse	CCTCGTTACTCGACAGGATGG
Angpt2 Forward	AGAGGAGATCAAGGCCTACTGT
Angpt2 Reverse	GCCATCTTCTCGGTGTTGGA
Wnt1 Forward	ATAGCCTCCTCCACGAACCT
Wnt1 Reverse	GATGAACGCTGTTTCTCGGC
Wnt2 Forward	ACCTGATGTAGACGCAAGGG
Wnt2 Reverse	GGCCAAAGAGGCTGTGATCT
Wnt2b Forward	GTGTAGACACGTCCTGGTGG
Wnt2b Reverse	TGTCTGGGTAGCGTTGACAC
Wnt3 Forward	CACAACACGAGGACGGAGA
Wnt3 Reverse	AATCTACCCCTTCCCAGTGC
Wnt3a Forward	AGTGCCAGCACCAGTTCC
Wnt3a Reverse	CATGGACAAAGGCTGACTCC
Wnt4 Forward	CCGGGCACTCATGAATCT
Wnt4 Reverse	CACGCCAGCACGTCTTTAC
Wnt5a Forward	TGAAGCAGGCCGTAGGAC
Wnt5a Reverse	AGCCAGCACGTCTTGAGG
Wnt5b Forward	GAGAGCGTGAGAAGAACTTTGC
Wnt5b Reverse	GGCGACATCAGCCATCTTAT
Wnt6 Forward	CTGCAGCAGGACATCCGAGA
Wnt6 Reverse	TGTGCTGCGCATCCATAAAG
Wnt7a Forward	GGACTATGACCCGGAAAGC
Wnt7a Reverse	CAGAGCTACCACCGAAGAGAA
Wnt7b Forward	CGTTAGTCACTCTTGGCGGG
Wnt7b Reverse	CAATGCTCTGTAAGATGGCGG
Wnt8a Forward	CAGTGAACAACTTCCTGATAACCG
Wnt8a Reverse	GCGGATGGCATGAATGAAGG
Wnt8b Forward	CCAGCCATGGTGGACTTC
Wnt8b Reverse	CGAGGCTGCAGTTTCTAGTCA
Wnt9a Forward	AGACTGCTTTCCTCTACGCC
Wnt9a Reverse	GTTGTGGAAGTCCACTCGGG
Wnt9b Forward	GTGCTCACCTGAAGCAGTGT
Wnt9b Reverse	CTCCTTAAAGCCTCTCTGGAGC
Wnt10a Forward	TTCAGCCGAGGTTTTCGAGAG

Wnt10a Reverse	CTGGGCTGGCAGGAAGTATG
Wnt10b Forward	TTCACGAGTGTCAGCACCA
Wnt10b Reverse	AAAGCACTCTCACGGAAACC
Wnt11 Forward	AGAGCCGAGCACAACTGAC
Wnt11 Reverse	GGATAGGGAGAGTGCGGAAC
Wnt16 Forward	ATGTCCAGTACGGCATGTGG
Wnt16 Reverse	CCAGCAGGTTTTCACAGCAC

All RT-qPCR samples were run in duplicate or triplicate, with a minimum of 3 biological replicates, normalized to Gapdh. The results were expressed relative to a reference tissue or sample as indicated in the figure.

Primers were optimized using a 5-point standard curve of 2-fold diluted composite cDNA from relevant tissue and deemed acceptable with an $R2 > 0.95$, a percent efficiency between 90-110%, a sharp single point melt curve, positive controls with Ct values > 10 cycle difference compared to no RT control samples, and expected amplicon size by agarose gel electrophoresis. All samples were run in triplicate, normalized to Gapdh, and quantified relative to the reference tissue indicated. For qRT-PCR for microdissected lesions, the expression of genes known to be highly expressed in lesions (Gli1, Mycn) were assessed in parallel to Ptch, along with microdissected tumor samples known to have Ptch1 loss of heterozygosity (LOH), or microdissected EGL known to have high levels of Ptch expression. Ptch LOH status was assigned by quantification relative to microdissected tumors with known LOH.

2.19 Microarray analysis of mouse tissue

Total RNA extracted from MB or GNPs was analyzed with the MouseWG-6 v2.0 Expression BeadChip array platform. Illumina BeadStudio outputs were analyzed and annotated with R packages limma [224] and illuminaMousev2.db version 1.26.0. Data were processed with neqc function [225]. The hierarchical clustering and the principal component analysis plots were

prepared from the 1500 most variable probes across all samples in terms of interquartile range, after data processing (background correction, normalization, and log-transformation), and filtering out probes annotated as Bad and No Match. Significantly altered probes were detected with the linear modeling approach and empirical Bayes statistics of limma [226]. Gene Ontology (GO) cellular components enrichment was investigated using DAVID [227] for probes with adjusted P value below 0.05 and higher fold changes (>1.0) between NdpKO;Ptch$^{+/-}$ and Ptch$^{+/-}$ tumors. The tables in Figure 3 display the GO terms with P values<0.05. In an analogous manner we analyzed samples from purified P6 GNPs. The principal component analysis plot was prepared from the 1,500 most variable probes as above.

2.20 Human tumor samples and expression analysis

NDP expression profiles were determined across three independent cohorts with the R2 database analysis tool (http://r2.amc.nl), using publically available datasets from Heidelberg [228], Toronto [57] and Boston [229]. The following probes were used for analysis: Toronto (Affymetrix Exon 1.0 T Probe Accession: 4006280), Heidelberg (Agilent 4 x 44 k Probe Accession: A_23_P73609) and Boston (Affymetrix u133a Probe Accession: 206022_at). P values represent ANOVA across the four subgroups. Survival analysis in Figure 1 was performed on the MAGIC dataset of clinically annotated SHH tumors (Affymetrix Human Gene 1.1 ST, Probe Accession: 8172220) [230, 231]. Log2 transformed expression values of NDP were then ranked as the bottom 10th percentile of expression versus the top 10th percentile. Survival was calculated using the log-rank method in the R-Statistical Environment (v3.1.3) using packages survival (v2.37–7) and ggplot2 (v1.0.0).

2.21 Statistics

Sample sizes and statistical significance are reported in figures and figure legends. Animals that entered survival experiments (Ptx, α-CD20 and α-angpt2 treatment) were randomly assigned to the treatment or control groups. The significance of all presented survival curves were determined with the use of logrank test (GraphPad). Lesion number, vessel or Laminin density, number of endothelial PH3+ cells, Stem cells abundance, proliferation index, qRT-PCR, weight and cerebellar area were analyzed by one-way ANOVA with Tukey post-hoc comparisons. Comparison of lesion volumes, tumor latency and immune cell flow cytometry results were analyzed by two tailed student t-test. The proportion of vascularized and tumor incidence were analyzed by the hypergeometric test. The number of endothelial Lef1+ nuclei was assessed by a one-way ANOVA and Fischer's LSD post hoc comparison. The significance of the neurosphere assay was calculated by the online ELDA website using the chi squared test. The significance of the DNA damage analysis was performed by using the Mann-Whitney U test. A Levene's test for homogeneity of variance and normality tests were used to verify parameters for parametric analysis.

Results

Chapter 3: Characterization of the role of Ndp signaling in cerebellar development and Ndp/Fzd4 signaling in MB initiation and progression.

Statement of Contributions

- Post-doctoral fellow Dr. Erin Bassett
The design and formatting of the manuscript
Assisted with the execution and design of Figure 6 A-E and G-H, 8 10, 11A-E, 12 and 14A and E and Appendix A Figure 1 and 2

- Dr. Carol Perez-Iratxeta analysis of mouse microarray data, assisted with Figure11C-E and Appendix A Figure 1A-C and Figure 2A. In addition to the methods preparation

- Dr. Allan Mears assisted with the mouse microarray data analysis and with Supplemental Figure 1B-C.

- Dr. Michael Taloy analyzed the human microarray data and assisted with Figure 6G-H

- Neno Pokrajac assisted in quantifying the volume of SmoA1 hyperplastic EGL Figure 15B

3.1 Ndp is expressed in GNPs, in addition to mouse and human medulloblastoma (MB)

To assess the potential contributions of an active angiogenic program to PNL formation and progression in $Ptch^{+/-}$ cerebellum, we serial sectioned and sampled entire lesions at postnatal (P) day 14. The samples were immunostained with the vascular basement membrane marker $CollagenIV^{+}$ and counterstained with Haematoxylin to identify lesions. The age P14 was selected as it corresponds to a stage when the external granule layer (EGL) is 2-3 cell layers thick and when PNLs are reliably detectable. In $Ptch^{+/-}$ mice at P14 we observed a minority (24%; Figure 6A) of the identified lesion were vascularized (Figure 6A). Interestingly, the lesions that activated the angiogenic program and recruited novel vasculature were significantly larger in volume ($0.18mm^3$) (a measurement which is often used as an indicator of neoplasia progression in $Ptch^{+/-}$ mice) as compared to their non-angiogenic counterparts ($0.029mm^3$, Figure 6B). The observation of an increased volume size upon vascular recruitment promoted us to explore the lesion-vascular interaction further. We took advantage of the well-characterized Norrin/Fzd4 signaling pathway, which has been shown to activate the canonical Wnt signaling pathway and mediate neuronal-endothelial communication in the cerebellum to maintain BBB integrity [84, 85, 96, 232]. We used male $Ndp^{-/y}$ mice, a mouse line which has a lacZ gene inserted into the Ndp locus to explore the expression pattern of Ndp [85]. We visualized the temporal (P0, P7 and P14) expression pattern of Ndp in the developing cerebellum by examining β-galactosidase (β-gal) activity by X-gal staining (Figure 6D-E). In the developing cerebellum, β-gal activity was detected in the Purkinje cell (PC) layer (Figure 6 D-E), white matter layer (Figure 6D-E) and the external granule layer (EGL) (Figure 6D-E), which is consistent with previously reported expression data using an Alkaline phosphatase (AP)-knockin to the Ndp locus (Ndp-AP) [97]. In the Purkinje cell layer, the β-gal staining pattern is interpreted to indicate the expression in Bergmann glia cells, given the small punctate cellular morphology, in addition to the previously reported radial fibers spanning

the molecular layer observed in the Ndp-AP reporter mouse line [97]. However, in the white matter, β-gal expression overlapped with myelin basic protein (MBP) expression (Figure 6E), potentially implicating oligodendrocytes as a source of Norrin expression.

The expression of Ndp was also detected in the EGL (Figure 6D-E), the cellular layer that is composed predominantly of GNPs and the cells of origin of Shh-MB [55, 233]. GNPs have a period of peak proliferation between postnatal days P5-P8 [234, 235]. Combined X-gal staining and immunohistochemistry (IHC) at P7 revealed that Ndp expression is concentrated in the outer layer of the $Pax6^{+}$ (a marker of granule neurons and their progenitors) EGL (Figure 6E), which is the highly proliferative, phosphohistone H3 $(PH3)^{+}$ portion of the EGL (Figure 6E).

To further examine the role of Norrin expression in tumorigenesis in $Ptch^{+/-}$ mice, we focused our attention on GNPs, the relevant cell type in Shh-MB. We compared Ndp expression in $Ptch^{+/-}$ GNPs isolated from the surface of the cerebellum at different temporal stages in MB progression. While Ndp expression levels were slightly, but not significantly, reduced in $Ptch^{+/-}$ GNPs at pre-lesion (P7) and early lesion (P14) stages (Figure 6F), Ndp expression exhibited a downwards trend in GNPs isolated at the lesion progression stage (P30) and reached significance in the established MB (Figure 6F). Subsequently, we continued our investigation by comparing the expression of Ndp in the different MB subgroups from human samples by micro-array analysis (Figure 6G). MB can be subdivided into Shh and Wnt, MBs which develop from the deregulation of the respective developmental pathways, in addition to group 3 and group 4 MB, which are not as well biologically characterized [59]. We examined Ndp expression in two different sample cohorts, Toronto and Boston, and in both cohorts the expression of Ndp was significantly enriched in the Shh subgroups as compared to the other MB subgroups (Figure 6G). Interestingly, with a limited sample size, we observed a trend towards a reduction in survival in Shh-MB patients with

tumors exhibiting the lowest level of Ndp expression (lowest 10^{th} percentile) as compared to the patients with the highest expression level (highest 10^{th} percentile) (Figure 6H).

These results illustrate that Ndp is expressed by mouse GNPs, the precursor cells to Shh-MB, during a period of peak proliferation and in established human and mouse MB samples. The reduction in Ndp expression correlates with tumor progression in mice, a trend that is reminiscent of the reduced survival outcome in human patients with a reduced expression in Ndp. These results drove us to further our investigation into the role of Norrin in normal cerebellar development and tumorigenesis.

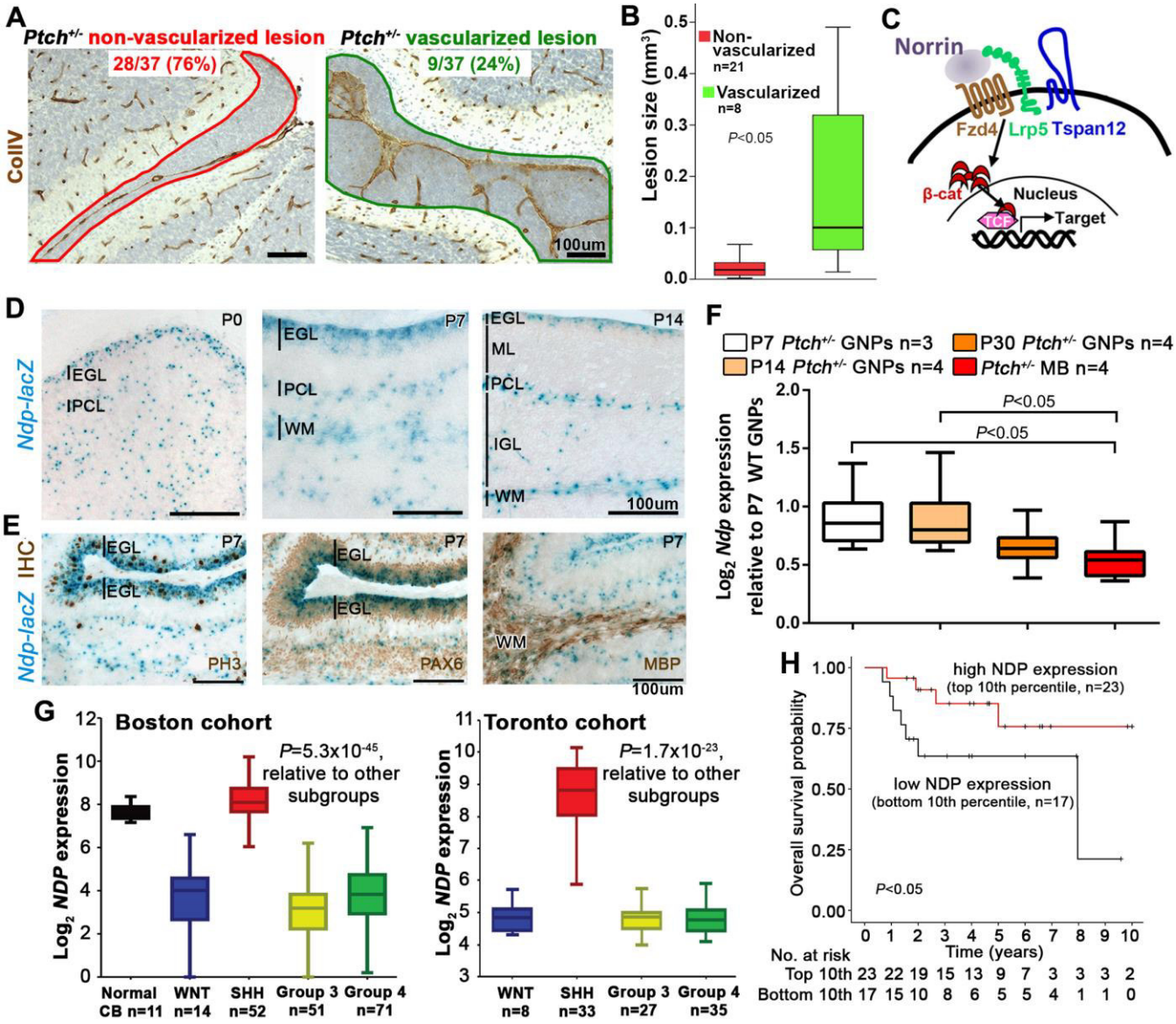
A
Ptch+/- non-vascularized lesion
Ptch+/- vascularized lesion
28/37 (76%)
9/37 (24%)
ColIV
100um
B
Lesion size (mm3)
Non-vascularized n=21
Vascularized n=8
P<0.05
C
Norrin
Fzd4
Lrp5
Tspan12
β-cat
Nucleus
TCF
Target
D
Ndp-lacZ
P0
P7
P14
EGL
IPCL
PCL
WM
ML
IGL
100um
E
Ndp-lacZ IHC
PH3
PAX6
MBP
F
P7 Ptch+/- GNPs n=3
P30 Ptch+/- GNPs n=4
P14 Ptch+/- GNPs n=4
Ptch+/- MB n=4
Log2 Ndp expression relative to P7 WT GNPs
P<0.05
P<0.05
G
Boston cohort
P=5.3x10-45, relative to other subgroups
Log2 NDP expression
Normal CB n=11
WNT n=14
SHH n=52
Group 3 n=51
Group 4 n=71
Toronto cohort
P=1.7x10-23, relative to other subgroups
WNT n=8
SHH n=33
Group 3 n=27
Group 4 n=35
H
high NDP expression (top 10th percentile, n=23)
low NDP expression (bottom 10th percentile, n=17)
P<0.05
Overall survival probability
Time (years)
No. at risk
Top 10th 23 22 19 15 13 9 7 3 3 3 2
Bottom 10th 17 15 10 8 6 5 5 4 1 1 0

Figure 6. Ndp expression in Shh-MB, Shh-MB precursors and in human Shh-MB.
(**A**) Representative Immunohistochemistry staining for Collagen IV (ColIV), counterstained with hematoxylin in $Ptch^{+/-}$ sagittal cerebellum sections, illustrating non-vascularized (red outline) and vascularized (green outline) lesions. (**B**) Quantified volume of identified lesions in (**A**), represented as boxplots, illustrating the statistically larger volume in the vascularized as compared to non-vascularized lesions. (**C**) Simplified schematic diagram of Norrin and associated receptors required to activate canonical, β-catenin (β-cat) dependent, Wnt signaling. (**D**) X-gal stainings (blue) examining Ndp expression in sagittal sections from $Ndp^{-/Y}$ mice, which have an Ndp-lacZ knock in allele, at the indicated ages. (**E**) Combined X-gal (blue) and immunohistochemistry staining (IHC, brown) for phospho-histone H3 (PH3), Pax6, and myelin basic protein (MBP) in P7 $Ndp^{-/Y}$ mice, highlighting the elevated expression of Ndp in the highly proliferative ($PH3^{+}$) external layer of the EGL. (**F**) Box plot representation of the temporal expression profile of Ndp in purified GNPs from $Ptch^{+/-}$ at the indicated ages and $Ptch^{+/-}$ MB lysate (ages ranging from 3 to 10 months of age), normalized to Ndp expression in WT P7 GNP. (**G**) Box plot illustration of the expression of NDP in two different cohorts (Boston, left; Toronto, right) of human MB samples obtained by array profiling and clustered by molecular subgroup (**H**) Kaplan-Meier survival curve illustrating the overall survival of Shh-MB patients with high (top 10^{th} percentile) and low (bottom 10^{th} percentile) of NDP expression in human MB samples. External granule layer (EGL); granule neuron progenitor (GNP); Purkinje cell layer (PCL); molecular layer (ML); white matter (WM); internal granule layer (IGL); cerebellum (CB); medulloblastoma (MB). Scales and number of biological samples examined (n) are indicated in the figure. The error bars of figures (B and F) represent the standard error of the means. Figure adapted from [236]

3.2 Loss of Ndp does not alter normal cerebellar development

To explore the role of Norrin signaling during normal cerebellar development, $Ndp^{+/Y}$ and $Ndp^{-/Y}$ mice were used to assess various gross morphological features such as: the weight (of the animals, the whole brain and the isolated cerebellum), the area (or different cellular layers) and the proliferative index ($PH3^{+}$ - in the EGL) in the cerebellum. We observed no significant difference between the weights of the animals from the two genotypes (Figure 7B). In addition, we observed no significant difference in the weight of the brain and cerebellum between P7 $Ndp^{+/Y}$ and $Ndp^{-/Y}$ littermates, after normalizing to the whole body weight, (Figure 7C-D), indicating that loss of Ndp does not alter gross morphological features such as; whole body, whole brain or cerebellum weight.

To further explore the possible effects of loss of Ndp on normal cerebellum development, we quantified the area of the entire cerebellum, the EGL + molecular layer and the IGL of sagittally sectioned P14 $Ndp^{+/Y}$ and $Ndp^{-/Y}$ samples. The analysis was performed by measuring 3 adjacent sections from the midline of 3 different animals per genotype. We chose to examine the area of the specified layers, as we predicted that gross change in cell number would alter the area measurement. The aforementioned layers of the cerebellum were selected to explore global changes in total cerebellar number (whole cerebellum area), or GNP specific alterations in proliferation (EGL + Molecular layer) or differentiation (the IGL). We observed no significant difference in the area of the entire cerebellum (Figure 7E), EGL+ molecular layer (Figure 7F) or the IGL (Figure 7G) of $Ndp^{-/Y}$ and $Ndp^{+/Y}$ mice. We subsequently performed a cursory exploration of the proliferative index in the cerebellum of these animals by quantifying the number of GNPs in M-phase (PH3+) found in the EGL. We observed no significant difference between the numbers of $PH3^{+}$ GNPs in the EGL of $Ndp^{-/Y}$ or $Ndp^{+/Y}$ mice (Figure 7H). These results are consistent with the literature, where the number of granule neurons within the IGL of Ndp knockout ($Ndp^{-/Y}$) and

NdpWT ($Ndp^{+/Y}$) animals was compared and revealed no significant difference between the two genotypes [237]. This lack of difference in the absence of Norrin could be the result of compensation from other Wnt ligands. We explored this possibility by isolating GNPs from WT P6 cerebella and, using qRT-PCR, examined the mRNA expression, of all the known Wnt molecules normalized to their respective expression in whole P6 WT cerebella. We could readily observe several other Wnt ligands for which expression was enriched in GNPs as compared to whole cerebellum lysate (Figure 7I). Particularly interesting Wnt ligands include Wnt3a and Wnt5a, which have been shown to be able to bind Fzd4 and activate canonical Wnt signaling [238, 239], potentially being able to compensate for the loss of Ndp. The loss of Ndp in WT animals does not adversely affect normal cerebellar development, since we did not observe any signs of gross morphological or proliferative alterations upon its loss.

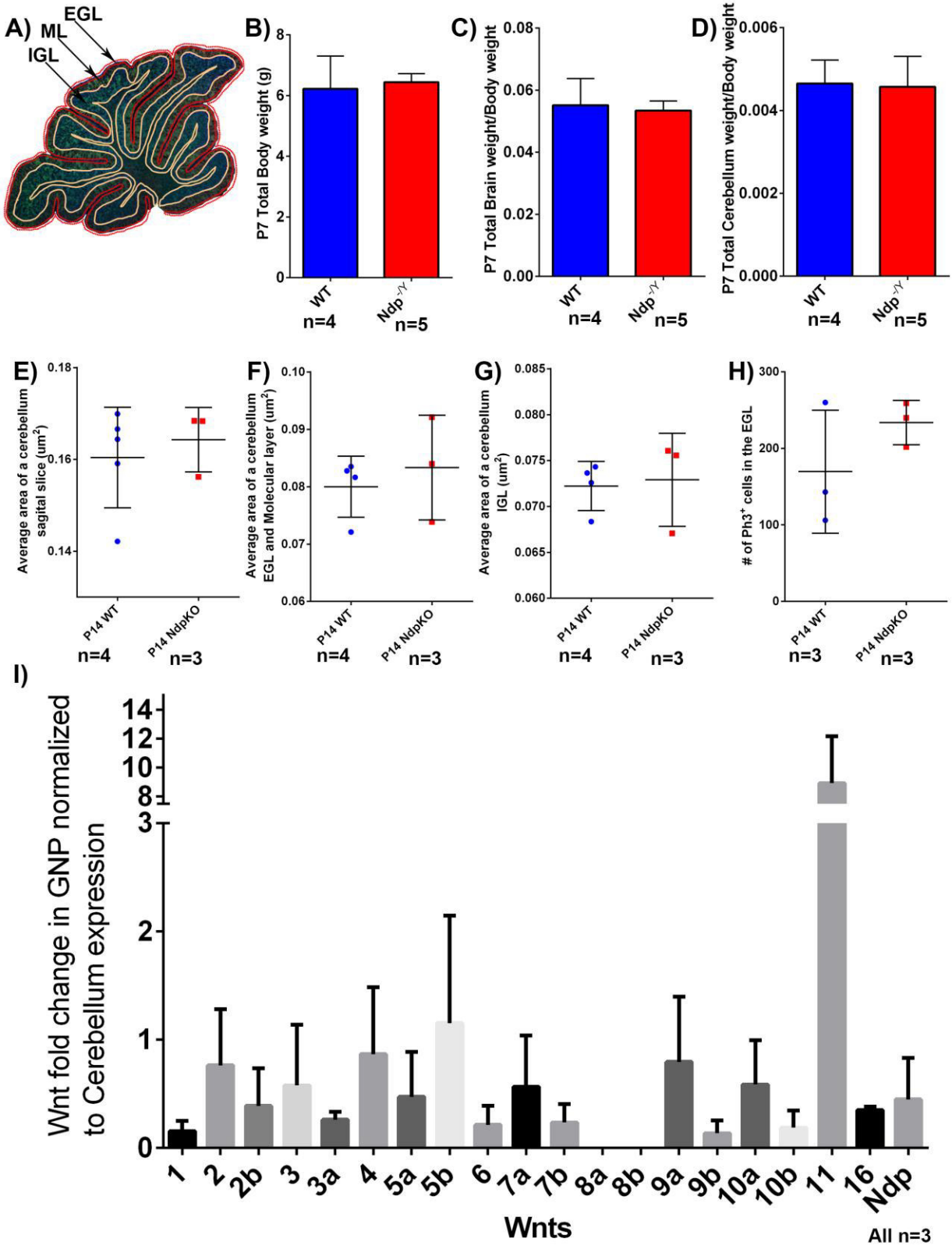
A)
EGL
ML
IGL
B)
P7 Total Body weight (g)
WT
Ndp-/Y
n=4
n=5
C)
P7 Total Brain weight/Body weight
WT
Ndp-/Y
n=4
n=5
D)
P7 Total Cerebellum weight/Body weight
WT
Ndp-/Y
n=4
n=5
E)
Average area of a cerebellum sagital slice (um2)
P14 WT
P14 NdpKO
n=4
n=3
F)
Average area of a cerebellum EGL and Molecular layer (um2)
P14 WT
P14 NdpKO
n=4
n=3
G)
Average area of a cerebellum IGL (um2)
P14 WT
P14 NdpKO
n=4
n=3
H)
# of Ph3+ cells in the EGL
P14 WT
P14 NdpKO
n=3
n=3
I)
Wnt fold change in GNP normalized to Cerebellum expression
1
2
2b
3
3a
4
5a
5b
6
7a
7b
8a
8b
9a
9b
10a
10b
11
16
Ndp
Wnts
All n=3

Figure 7. Gross morphological analysis of NdpKO and NdpWT cerebella and Wnt expression in purified P6 WT GNP.

(**A**) Illustration of a P14 WT cerebellum denoting the EGL (outlined in a dotted red line), ML (apically delimited by dotted red line and basally by the solid beige line) and IGL (outlined in the solid beige line) analyzed in (**F**) and (**G**), respectively. (**B-D**) Analysis of various gross morphological features, such as the weight of: (**B**) the animal, (**C**) the brain normalized to bodyweight and (**D**) the isolated cerebellum normalized to body weight in P7 WT and NdpKO animals. (**E-G**) Analysis of the area of different cellular layers: (**E**) the entire sagittal cerebellar section, (**F**) the EGL + ML and (**G**) the IGL from sagittally sectioned P14 WT and NdpKO animals. (**H**) Quantification of the average number of $PH3^+$ cells identified in the sagittal sections of the EGL from P14 WT and NdpKO littermates. (**I**) qRT-PCR of the expression of all the different known Wnt ligands in purified P6 WT GNPs normalized to Gapdh and expressed relative to the respective Wnt expression in P7 whole cerebella. Results are representatives of three biological replicates. External granule layer (EGL); molecular layer (ML); internal granule layer (IGL); granule neuron progenitor (GNP); N.s. = non-significant; * = No information available. The error bars of all figures represent the standard error of the means. Number of biological samples examined (n) is indicated in the figure.

3.3 Disruption of Norrin/Fzd4 signaling significantly enhances Ptch$^{+/-}$ MB formation

Ndp has an elevated expression in GNPs located in the apical layer of the EGL at P7 (Figure 6D-E), an area that is closely associated to the meningeal layer, which contains the EGL nourishing blood vessels. Interestingly, neuronal Ndp to endothelial Fzd4 signaling has a well-characterized role in neural-endothelial communication, which is important for BBB maintenance [84, 240]. Remarkably, the expression of Ndp in Ptch$^{+/-}$ mice exhibits a downward trend as a function of lesion progression (Figure 6F). In addition, we also showed that lesions that underwent an angiogenic recruitment are significantly larger (Figure 6B), suggesting that the activation of the angiogenic program is associated with tumor progression, an observation that has been observed in other non-CNS multistep tumor models [241-244]. To explore the role of Ndp in tumorigenesis further, we compared tumor development and overall survival of Ptch$^{+/-}$ mice on the WT as compared to the Ndp knockout background. Germ-line deletion of Ndp on the WT background did not generate tumors (Figure 8A), however, the disruption of Ndp on the Ptch$^{+/-}$ background drastically accelerated MB formation and significantly reduced overall survival (Figure 8A). Loss of Ndp also increased MB incidence and reduced latency (≈2 fold – Figure 8B). This observation shows that even though other Wnts are expressed in GNPs (Figure 7I) and may be able to partially compensate for the loss of Ndp, they are not sufficient.

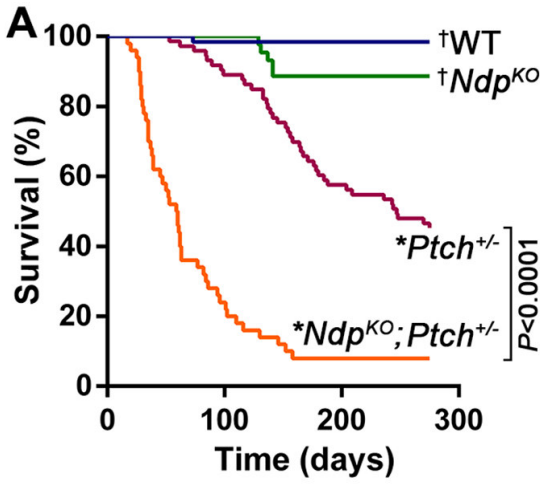

B

Genotype	MB Incidence		Average Latency	
WT	0/60 (0%)		--	
Ndp^KO	0/44 (0%)		--	
Ptch^+/-	35/73 (48%)	P<0.0001	150 days	P<0.001
Ndp^KO;Ptch^+/-	45/49 (92%)		63 days	

<u>Figure 8.</u> Kaplan-Meier survival curve of $Ndp^{-/Y}$;$Ptch^{+/-}$ animals.

(**A**) Kaplan-Meier survival curve of WT, $Ndp^{-/Y}$, $Ptch^{+/-}$ and $Ndp^{-/Y}$;$Ptch^{+/-}$ animals, exploring the impact of systemic deletion of Ndp on the $Ptch^{+/-}$ background. $Ndp^{-/Y}$ mice do not develop tumors, however 5 of 44 animals were euthanized due to advanced skin conditions. (**B**) Survival curve related information, including sample sizes, incidence and latency of the MB cases. *Died with confirmed MB; †Did not develop MB. WT = wild-type; N.s = not significant. Number of biological replicates (incidence) used are indicated in the figure. Figure adapted from [236]

3.4 Ndp signaling in GNP proliferation

Norrin, a non-typical Wnt, has been shown to specifically signal through the Fzd4 receptor and associated co-receptors Lrp5/6 and Tspan12 [83-85] (Figure 6C), which are expressed by ECs [82-85]. Interestingly, we also observed the expression of these essential receptors (Fzd4, Lrp5 and Tspan12) by qRT-PCR in purified GNP samples (Figure 9B). Furthermore, we also detected Fzd4 protein expression on the cell surface of dissociated GNPs (Figure 9A). To further understand the cellular mechanism driving tumorigenesis in the absence of Ndp expression, we focused our attention on determining the respective contributions of GNPs and/or ECs towards the tumorigenic phenotype.

Wnt signaling has been previously shown to antagonize Shh-mediated proliferation in GNPs and Shh-MB [245, 246] and since Norrin is a non-typical Wnt, we began by examining potential contributions that Ndp/Fzd4 signaling may have on GNP proliferation (Figure 9D-E). For this analysis we used purified GNPs from P7 animals (Figure 9C). This time point was selected as it is prior to the establishment of lesions and it corresponds to the stage of maximal GNP proliferation *in vivo* [234, 235]. We modulated Ndp/Fzd4 signaling genetically (Ndp knockout) (Figure 9E) or pharmacologically (Dickkopf-related protein 1 (DKK-1) treatment) (Figure 9D) and assessed proliferation after 3 days in culture by examining EdU incorporation. Inhibition of Ndp/Wnt signaling in Hh-treated GNP cultures resulted in a modest, but significant increase in the proportion of EdU^{+} in $Ptch^{+/-}$ GNPs (Figure 9D-E). Taken together, loss of Ndp/Fzd4 signaling marginally increased proliferation in the context of Ptch heterozygosity.

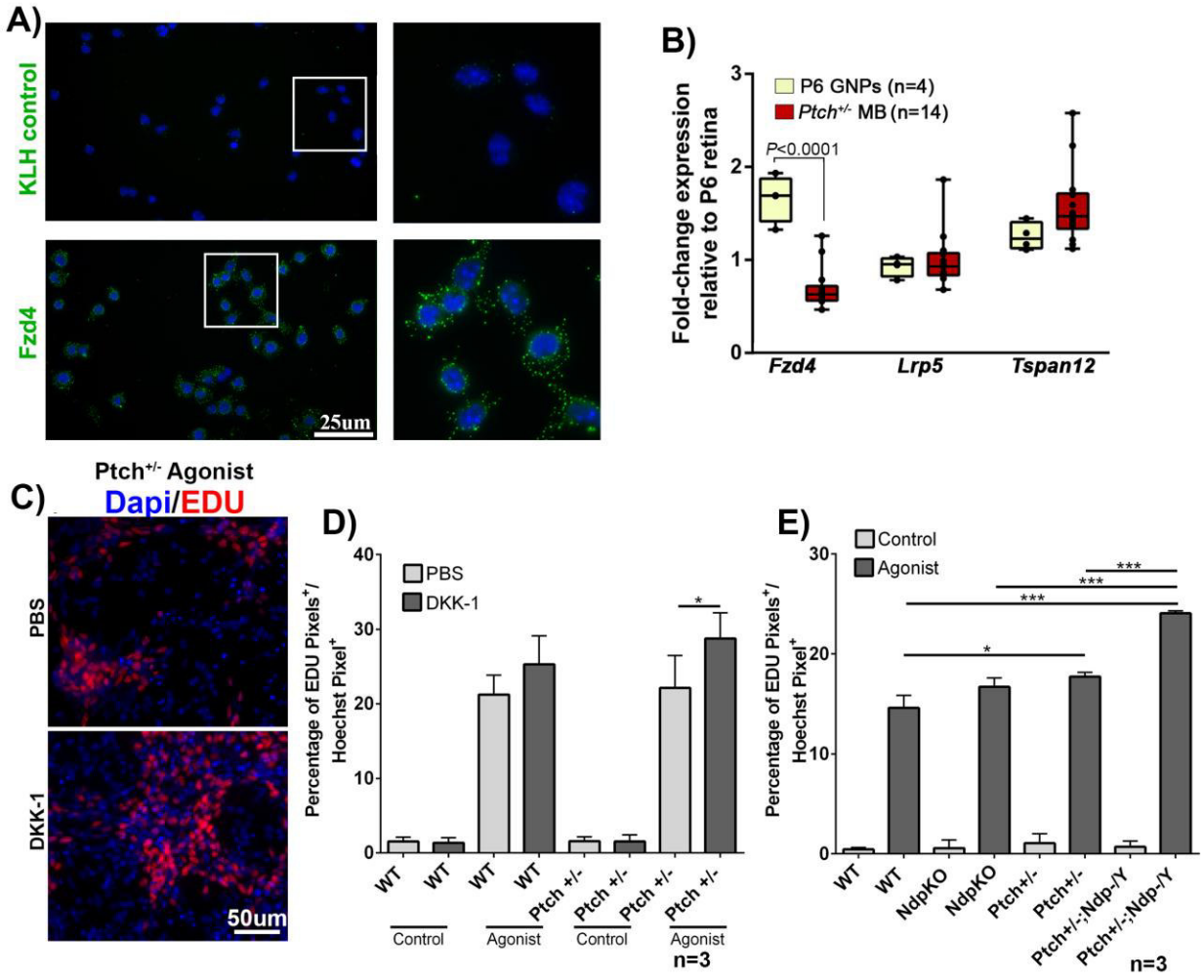

<u>Figure 9.</u> Ndp Receptor expression and *in vitro* GNP proliferation assay.

(**A**)Purified P10 GNPs immunostained for anti-FZD4 or anti-keyhole limpet hemocyanin (KLH), an isotype matched control antibody, (green) and counterstained for Hoechst (blue), white boxes are magnified to the right. (**B**) Box plot representation of qRT-PCR of essential Norrin receptor components (Fzd4, Lrp5 and Tspan12) from isolated mouse P6 GNPs and Ptch$^{+/-}$ MB samples. (**C**) Representative images of cultured GNPs, where we disrupted Ndp/Fzd4 signaling by (**D**) embryonic deletion (**E**) or pharmaceutically with DKK-1 treatment (**C**-**D**) in P7 dissociated GNPs from the indicated genotype. The dissociated GNPs were cultured for 3 days *in vitro* in the indicated conditions and on day 3 the cells were pulsed with EDU for 4 hrs. Subsequently, the cells were fixed, stained and the abundance of EDU was quantified by measuring the pixel fluorescence and normalized to Hoechst pixel fluorescence. The error bars represent the standard error of the means. Number of biological replicates (n) used and scales are indicated in the figure. Figure (**A**-**B**) adapted from [236].

3.5 Disruption of Norrin/Fzd4 signaling in ECs significantly enhances Ptch$^{+/-}$ MB formation

The *in vitro* approach used to assess the role of Norrin/Fzd4 autocrine/paracrine signaling in GNPs may not recapitulate the *in vivo* situation. It is artificial and could be masking the requirement for additional cell types found *in vivo*. To determine the specific contributions of the two cellular compartments to the observed MB phenotype *in vivo*, we selectively deleted the Fzd4 receptor (Fzd4$^{flox/flox}$) by crossing it with a Cre-recombinase (Cre), which was either expressed in endothelial cells (ECs) (Tie2-Cre), or in GNPs (Atoh1-Cre) on the Ptch$^{+/-}$ background (Figure 10A and C). Conditionally deleting the Fzd4 receptor alone in either cellular compartment was not tumorigenic (Figure 10A and C). However, the deletion of Fzd4 from ECs (Tie2Cre$^{+/-}$;Fzd4$^{Flox/Flox}$) was associated with a reduction in survival, which could be the result of esophageal-related feeding defects and progressive auditory and cerebellar degeneration, which has been previously reported in Fzd4 knockout mice [247]. The deletion of Fzd4 from the ECs compartment on the Ptch$^{+/-}$ background significantly reduced latency (≈4 fold) and significantly increased the incidence (≈2 fold) of MB (Figure 10B). However, deletion of the Fzd4 receptor from the GNP cellular compartment did not significantly alter survival, latency or incidence of MB (Figure 10D). Taken together, these results reveal a novel inhibitory role for Norrin/Fzd4 signaling in Ptch$^{+/-}$ MB, which is mediated by a neural-endothelial cell crosstalk within the stroma.

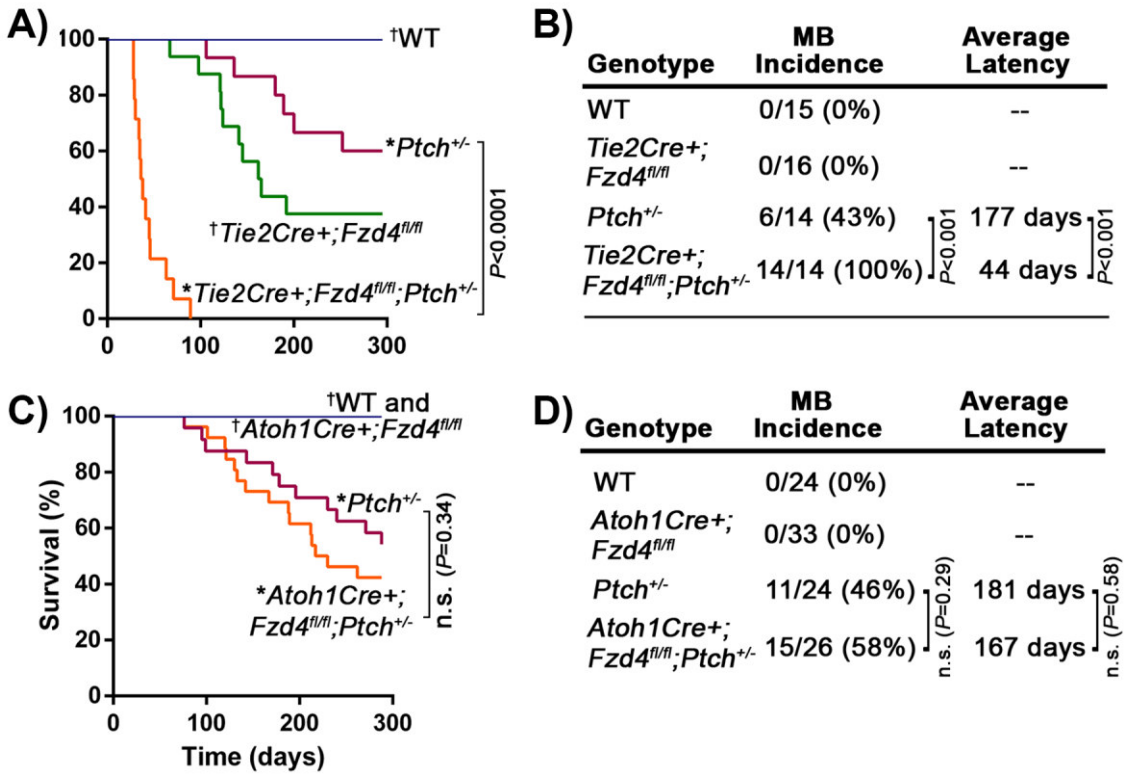

Figure 10. Disruption of Norrin/Fzd4 signaling in ECs promotes Ptch$^{+/-}$ MB.
(**A**) Kaplan-Meier survival curve of WT, Tie2-cre$^{+/-}$;Fzd4$^{Flox/Flox}$; Fzd4$^{Flox/Flox}$;Ptch$^{+/-}$ and Tie2-cre$^{+/-}$;Fzd4$^{Flox/Flox}$;Ptch$^{+/-}$ animals, exploring the impact of endothelial cell targeted deletion of the Fzd4 receptor on the Patch$^{+/-}$ background. Tie2Cre$^{+/-}$;Fzd4$^{Flox/Flox}$ animals do not develop tumors, however they do develop esophageal-related feeding defects and progressive auditory and cerebellar degeneration [247]. (**B**) Survival curve (**A**) related information, including sample sizes, the incidence and latency of the MB cases. (**C**) Kaplan-Meier survival curve of WT, Atoh1-cre$^{+/-}$;Fzd4$^{Flox/Flox}$, Fzd4$^{Flox/Flox}$;Ptch$^{+/-}$ and Atoh1-cre$^{+/-}$;Fzd4$^{Flox/Flox}$;Ptch$^{+/-}$ animals, exploring the impact of GNP targeted Fzd4 deletion on overall survival. (**D**) Survival curve (**C**) related information, including sample sizes, the incidence and latency of the MB cases. *Died with confirmed MB; †Animals that did not develop MB. WT = wild-type; n.s. = not significant. Number of biological replicates (incidence) is are indicated in the figure. Figure adapted from [236]

3.6 Loss of Ndp alters stromal gene expression in Ptch+/- GNP and MB samples

To gain further insight into potential roles for Norrin signaling in driving tumorigenesis, we began by examining histological sections from established $Ndp^{-/Y}$;$Ptch^{+/-}$ and $Ptch^{+/-}$ MB samples. Both $Ndp^{-/Y}$;$Ptch^{+/-}$ and $Ptch^{+/-}$ MB samples displayed a classic MB histology as seen by Haematoxylin and Eosin stains (H&E) (Figure 11A). We further examined the expression of known Shh-MB neural markers (Athoh1, TUBB3 and GFAP) and Hh target genes (Gli1, Mycn and Ccnd1), which appeared comparable between the two genotypes (Figure 11A). Immunohistochemistry of MB samples from both genotypes for CD31 (PECAM1; platelet/endothelial cell adhesion molecule 1), co-stained with extracellular matrix (ECM) protein Laminin, highlighted the abundance of vasculature within the stroma (Figure 11B). With the rare exception, the vast majority of established cancers are very heterogeneous, which can confound and complicate classic histological-based analysis and classification of tumor samples [248]. We therefore isolated whole tumor samples from both genotypes and with the addition of P6 WT GNPs we performed whole genome expression profiling in order to get a better understanding of potential transcriptional alteration between genotypes. Using principal component clustering analysis, we observed that established $Ndp^{-/Y}$;$Ptch^{+/-}$ MB, $Ptch^{+/-}$ MB and P6 WT GNPs samples all had very different gene expression signatures (Figure 11C). We further examined these transcriptional differences by performing hierarchical clustering and cellular component gene ontology analysis, which revealed that several alterations in the $Ndp^{-/Y}$;$Ptch^{+/-}$ MB as compared to $Ptch^{+/-}$ MB samples were composed of stromal genes, particularly ECM components (Figure 11E). Several up-regulated genes in the $Ndp^{-/Y}$;$Ptch^{+/-}$ as compared to $Ptch^{+/-}$ MB samples were endothelial-specific components, such as Endothelial cell-specific molecule 1 (Esm1), Plasmalemmal vesicle associated protein (Plvap), Ephrin type-B receptor 4 (EphB4) and Endomucin (Emcn) (Appendix A Figure 1C-D). The up-regulation of Esm1, Plvap and Emcn was further validated by qRT-PCR

analysis of $Ndp^{-/Y}$;$Ptch^{+/-}$ and $Ptch^{+/-}$ MB samples (Figure 11F). Interestingly, within the up-regulated endothelial genes, EphB4 and Emcn are well-characterized vein specific endothelial cell markers [99, 249, 250], potentially indicating a bias towards vein specific endothelial cell fate. In addition we observed an up-regulation of Plvap, a marker of endothelial transcytosis and fenestration, which could provide an explanation for the observed increase in vascular permeability in $Ndp^{-/Y}$;$Ptch^{+/-}$ as compared to $Ptch^{+/-}$ MB samples, as seen by the increased extravasation of serum protein binding dye Evans blue (Figure 11G). Some additional genes that were up-regulated in the qRT-PCR analysis of $Ndp^{-/Y}$;$Ptch^{+/-}$ as compared to $Ptch^{+/-}$ MB samples were Pecam1 and Angiopoietin-2 (Angpt2), potentially suggestive of increased vascularity and an activated angiogenic program, respectively (Figure 11F). Taken together these results suggest that instead of affecting Shh signaling to drive tumorigenesis in $Ptch^{+/-}$ mice, loss of Ndp could be altering the stromal landscape to create a pro-tumor environment to drive tumorigenesis.

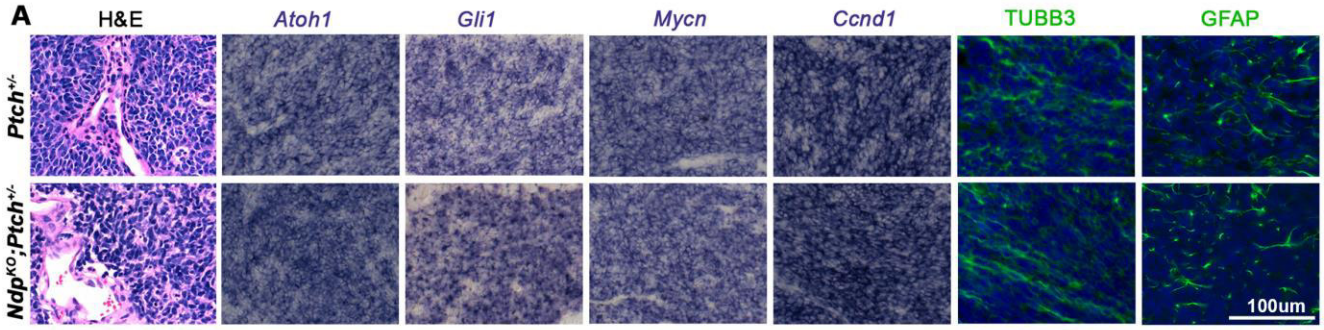

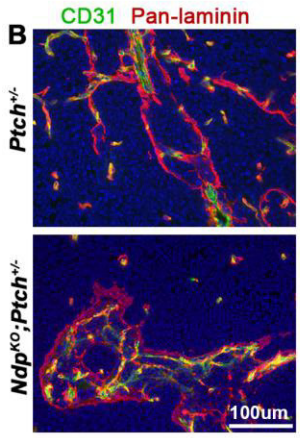

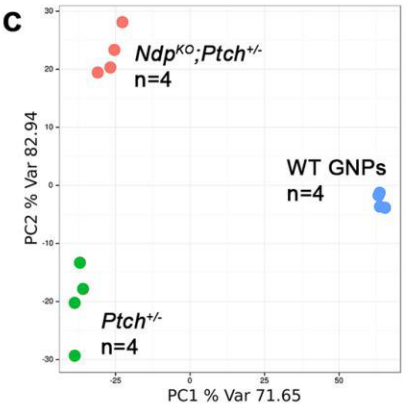

D Down-regulated in *Ndp^{KO};Ptch$^{+/-}$* vs *Ptch$^{+/-}$*

Cellular Component	*P* value
cell surface	3.47×10^{-5}
plasma membrane	4.74×10^{-5}
external side of plasma membrane	7.55×10^{-5}
extracellular region part	5.79×10^{-4}
plasma membrane part	0.0016
proteinaceous extracellular matrix	0.0028
extracellular matrix	0.0037
MHC class II protein complex	0.0049
anchored to membrane	0.0103
anchored to plasma membrane	0.0135
extracellular region	0.0290
extracellular space	0.0325

E Up-regulated in *Ndp^{KO};Ptch$^{+/-}$* vs *Ptch$^{+/-}$*

Cellular Component	*P* value
extracellular region part	0.0034
proteinaceous extracellular matrix	0.0111
extracellular matrix	0.0136
centrosome	0.0427
extracellular space	0.0502

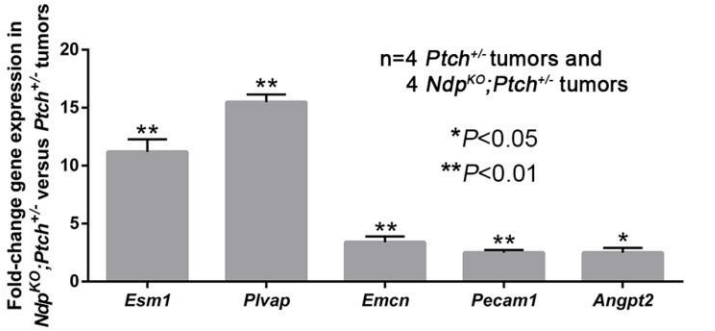

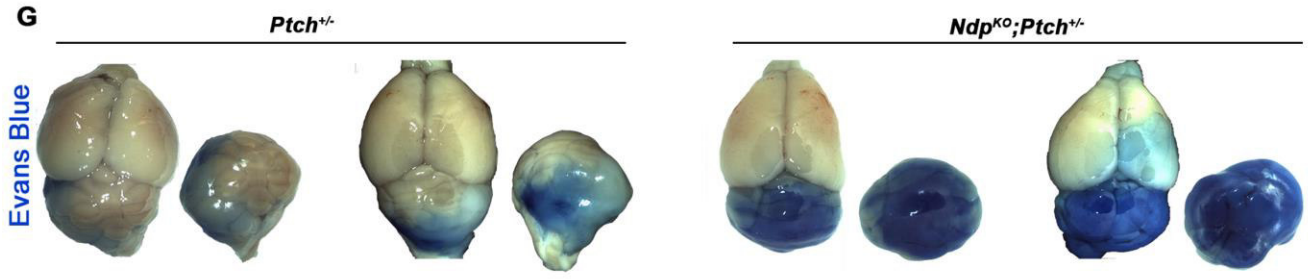

<u>Figure 11.</u> Ptch$^{+/-}$ and Ndp$^{-/Y}$;Ptch$^{+/-}$ MBs samples have different expression profiles.
(**A**) Sections of Ptch$^{+/-}$ and Ndp$^{-/Y}$;Ptch$^{+/-}$ established MB samples were stained by Haematoxylin and Eosin (H&E), by *In Situ Hybridization* for various genes including: Atoh1, Gli1, Mycn and Ccnd1 (purple), or stained by immunohistochemistry for class III β-tubulin (TUBB3) and glial fibrillary acidic protein (GFAP; green) counterstained with Hoechst (blue). For each stain 3 different tumor samples (n = 3) from each genotype were examined. (**B**) Sections of Ptch$^{+/-}$ and Ndp$^{-/Y}$;Ptch$^{+/-}$ established MBs co-immunostained for CD31 (green) and pan-Laminin (red), counterstained with Hoechst (blue). 3 different tumor samples (n = 3) from each genotype were examined. (**C**) Whole genome expression profiles of Ptch$^{+/-}$ MBs, Ndp$^{-/Y}$;Ptch$^{+/-}$ MBs and P6 WT GNPs were used for principal component analysis. The analysis was performed by using the 1500 most variable probes across all samples. (**D-E**) Cellular component gene ontology (GO) analysis of differentially expressed genes between the Ptch$^{+/-}$ and Ndp$^{-/Y}$;Ptch$^{+/-}$ MB samples. (**F**) qRT-PCR analysis of vascular related genes expressed in Ndp$^{-/Y}$;Ptch$^{+/-}$ MB samples, normalized to Gapdh expression and expressed relative to Ptch$^{+/-}$ MB samples. (**G**) Wholemount images of Ptch$^{+/-}$ and Ndp$^{-/Y}$;Ptch$^{+/-}$ MBs from animals injected with Evans Blue dye prior to sacrifice. Scale and number of number of biological replicates (n) used are indicated in the figure. Figure adapted from [236]

3.7 Disruption of stromal Norrin/Fzd4 signaling drives lesion formation

In the $Ptch^{+/-}$ mouse model MB progression is a function of the lesion number and the rate at which lesions transform [251-254]. To explore the potential contributions of loss of Ndp to lesion initiation we serial sectioned cerebella from $Ndp^{-/y}$;$Ptch^{+/-}$, $Tie2Cre^{-/+}$;$Fzd4^{Flox/Flox}$;$Ptch^{+/-}$ and their respective control $Ptch^{+/-}$ littermates at P14, the earliest stage at which lesions are reliably and consistently detected in $Ptch^{+/-}$ mice [255]. In $Ndp^{-/y}$;$Ptch^{+/-}$ and $Tie2Cre^{-/+}$;$Fzd4^{Flox/Flox}$;$Ptch^{+/-}$ we observed a 3.9 fold and 2.4 fold increase in the number of lesions (Figure 12A and C), respectively, as compared to their $Ptch^{+/-}$ littermate control samples. Interestingly, there was no difference in the volume of the established lesions (Figure 12B and D), a measure which is often used as an indicator of lesion progression in $Ptch^{+/-}$ mice [236]. This increase in lesion number was not associated with any other changes at an earlier age, as seen by the similar EGL thickness of $Ndp^{-/Y}$;$Ptch^{+/-}$ and $Ptch^{+/-}$ at P6 (Appendix A Figure 2) and the fact that we could not detect separable GNP expression profiles. These results emphasize an essential role for Ndp/Fzd4 stromal signaling in promoting a tumor suppressive environment and its disruption enhances lesion formation.

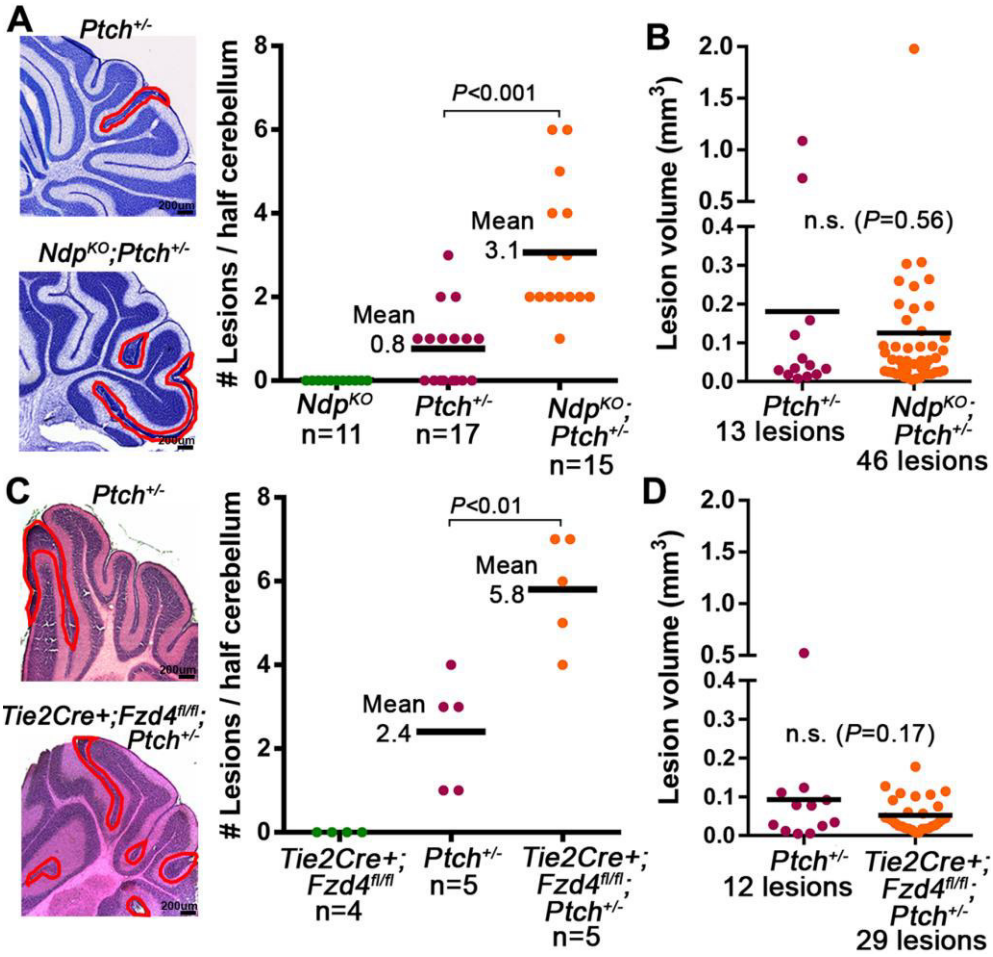

<u>Figure 12.</u> Disruption of Norrin/Fzd4 signaling increases lesion formation in P14 Ptch$^{+/-}$ cerebella.

(**A**) Quantification of the number of lesions from serial sections cresyl violet stained P14 cerebella from 3 genotypes: Ndp$^{-/Y}$ (NdpKO), Ptch$^{+/-}$ and Ndp$^{-/Y}$;Ptch$^{+/-}$ mice. Left: representative cresyl violet stained section of the specified genotype illustrating identified lesions (outlined in red). (**B**) Volume quantification of the identified lesion in (**A**). Quantification of the number of lesions from serial sections Haematoxylin and Eosin (H&E) stained P14 cerebella from 3 genotypes Fzd4$^{Flox/Flox}$; Ptch$^{+/-}$ (Ptch$^{+/-}$), Tie2Cre$^{-/+}$;Fzd4$^{Flox/Flox}$ and Tie2Cre$^{-/+}$;Fzd4$^{Flox/Flox}$; Ptch$^{+/-}$. Left: Representative H&E stained section of the specified genotype illustrating identified lesions (outlined in red). (**D**) Volume quantification of the identified lesion in (**C**). Means are denoted by black horizontal lines on graphs. Scale bars for cresyl violet and H&E stains are indicated (200μm). Number of individual biological replicates (n) is indicated in the figure. Figure adapted from [236]

3.8 Disruption of Norrin/Fzd4 signaling effect on the resident stem cell population

The loss of Ndp could alter or affect closely associated and sensitive cell populations [256], such as tissue-resident stem cells (SC). An important feature of many stem cell niches, including neural stem cell (NSC), mesenchymal stem cells, and many tumor stem cells, is their relative proximity to the vasculature [257]. Interestingly, the vasculature and associated ECM has been shown to play an active role in various stem cell processes, such as quiescence, activation and fate determination [257-261]. We decided to explore the effects of loss of Ndp on the stem cell population, which is a highly relevant component of MB [230]. SRY (sex determining region Y)-box 2 ($Sox2^{+}$) is a reliable NSC marker, and SC in the cerebellum. SC are rare within the EGL, however, they can be readily detected within the GNP population (Figure 13E) as well as in $Ptch^{+/-}$ MB [230]. To investigate the potential effects of Ndp loss of signaling on the cerebellar SC population, we purified GNPs from P14 $Ptch^{+/-}$ and $Ndp^{-/Y}$;$Ptch^{+/-}$ animals, and performd primary and secondary neurosphere culture assays. This enabled the assessment of the proliferative capability and self-renewal [262] of the stem cell pool within this GNP population (Figure 13A). In primary and secondary neurosphere assays, we observed a non-significant trend towards a reduction in stem cell frequency in $Ndp^{-/Y}$;$Ptch^{+/-}$ as compared to $Ptch^{+/-}$ littermate samples (Figure 13B-C). We further corroborated these findings by quantifying the number of $Sox2^{+}$ cells [230] in acutely dissociated GNPs from $Ndp^{-/Y}$;$Ptch^{+/-}$ and $Ptch^{+/-}$ littermates (Figure 13E). $Ndp^{-/Y}$;$Ptch^{+/-}$ animals exhibited a slight, but non-significant decrease in the number of $Sox2^{+}$ stem cells as compared to their $Ptch^{+/-}$ littermates (Figure 13D-E). Taken all together, these results suggest that altered stem cell activity upon disruption of Ndp signaling does not actively contribute to the observed MB phenotypes in our $Ndp^{-/Y}$;$Ptch^{+/-}$ mouse model.

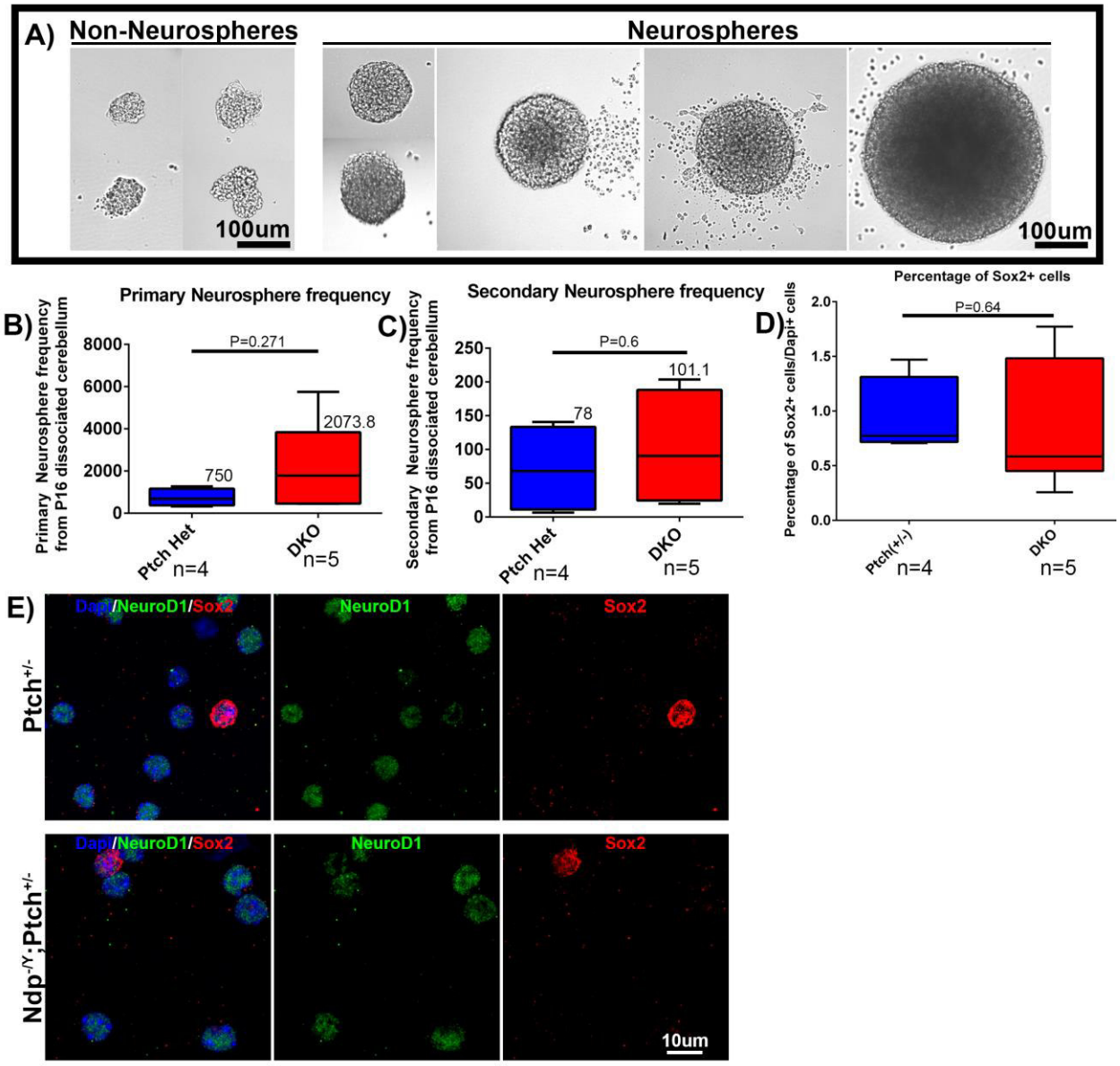

<u>Figure 13.</u> Disruption of Ndp/Fzd4 signaling does not significantly alter the GNP resident stem cell population.

(**A**) Phase microscope images illustrating the strict criteria used for neurosphere quantifications (e.g. size and sphericity). (**B**-**C**) GNP from P16 $Ptch^{+/-}$ and $Ndp^{-/Y}$;$Ptch^{+/-}$ animals were dissociated and used for (**B**) primary and (**C**) secondary neurosphere assays, revealing no significant difference between the genotypes. (**D**-**E**) GNP from P16 $Ptch^{+/-}$ and $Ndp^{-/Y}$;$Ptch^{+/-}$ littermates were acutely dissociated and stained (**E**) for Sox2 expression (red) and (**D**) quantified, revealing no significant difference. Number of biological replicates (n) used and the scales are indicated in the figure. Boxplot figure (**B**-**D**) whiskers are representative of minimal and maximum values.

3.9 Loss of Norrin signaling increases DNA damage and accelerates Ptch LOH

Tumor incidence is a function of lesion formation, which is dependent on both genomic instability [31, 263] and proliferation [254, 264, 265] . An important driver of DNA damage in the context of carcinogenesis is excessive replication, which can increase genomic DNA fragility and DNA damage. This damage manifests in the form of double strand DNA breaks through various mechanisms, such as fork stalling or excessive origin firing [214, 215, 266]. Our initial *in vitro* investigation revealed a modest increase in proliferation (Figure 9C-E), however, our results showed that Ndp is predominantly signaling through the vasculature to prevent tumorigenesis (Figure 10A and C). These results illustrated the need to perform this investigation in an *in vivo* context. As such, we decided to investigate whether loss of Ndp enhances GNP proliferation in the early P14 lesion. In $Ndp^{-/Y}$;$Ptch^{+/-}$ as compared to $Ptch^{+/-}$ samples, there was a moderate but significant increase in the number of GNPs/surface (mm^2) that were positive for the M-phase marker Phospho-Histone H3 ($PH3^+$)(Figure 14A). This result was reminiscent of the *in vitro* P7 dissociated GNP result (Figure 9 C-E). In addition, we observed a modest but significant decrease in the percentage of lesion area that was positive for cleaved caspase 3^+ ($Casp3^+$), an apoptosis marker, in the $Ndp^{-/Y}$;$Ptch^{+/-}$, as compared to $Ptch^{+/-}$ lesions (Figure 15A). This increase in proliferation and decrease in cell death was not counterbalanced by an increase in the area that was positive for the neuronal differentiation marker NeuN, as we observed comparable expression between the two genotypes (Figure 14A). The increase in the replicative index could be promoting genomic instability by driving double strand DNA breaks. To further investigate this, we acutely dissociated P14 $Ptch^{+/-}$ and $Ndp^{-/Y}$;$Ptch^{+/-}$ GNPs and stained for phospho-gammaH2AX (p-γH2AX), an early marker of double strand break repair pathway activation [267, 268] (Figure 15B). We focused our attention on double strand breaks as their repair can promote loss of heterozygosity (LOH) [269, 270], resulting in ligand-independent pathway activation and

malignancy by affecting essential genes such as Ptch1 in $Ptch^{+/-}$ animals [252, 253, 271]. We observed a non-significant increase in the percentage of GNPs containing p-γH2AX foci (Figure 14C) between $Ndp^{-/Y}$;$Ptch^{+/-}$ as compared to $Ptch^{+/-}$ littermates. However, when we examined the number of p-γH2AX foci per cell in GNPs with ≥ 1 p-γH2AX foci, we observed a highly significant increase in the number of p-γH2AX foci/cell in the $Ndp^{-/Y}$;$Ptch^{+/-}$ samples as compared to their $Ptch^{+/-}$ littermates (Figure 14D). These results indicate that while the number of cells affected by DNA damage is not significantly different between genotypes, $Ndp^{-/Y}$;$Ptch^{+/-}$ GNPs, on average, exhibit more evidence of DNA damage as compared to their $Ptch^{+/-}$ littermates. This may indicate enhanced intrinsic or extrinsic sensitivity in $Ndp^{-/Y}$;$Ptch^{+/-}$ GNPs to DNA damage as compared to their $Ptch^{+/-}$ littermates, or conversely, could be related to the increase in replication and could be a consequence of an enhanced replication stress in $Ndp^{-/Y}$;$Ptch^{+/-}$ lesions. To determine whether the observed increase in DNA damage was associated with genetic changes required for malignant transformation [252, 253, 271], we performed qRT-qPCR of laser captured lesions to assess the rate at which lesions from P14 $Ndp^{-/Y}$;$Ptch^{+/-}$ and $Ptch^{+/-}$ littermates, that were converted to LOH for *Ptch1*. We observed an increase in the frequency of lesions that were LOH in $Ndp^{-/Y}$;$Ptch^{+/-}$ (9/17) as compared to $Ptch^{+/-}$ (3/14) samples (Figure 15E). Taken together, these results suggest that the disruption of Ndp/Fzd4 signaling in ECs alters the stroma to increase the sensitivity of GNPs to DNA damage, which accelerates the rate of Ptch1 LOH and drives tumor progression in $Ndp^{-/Y}$;$Ptch^{+/-}$ animals.

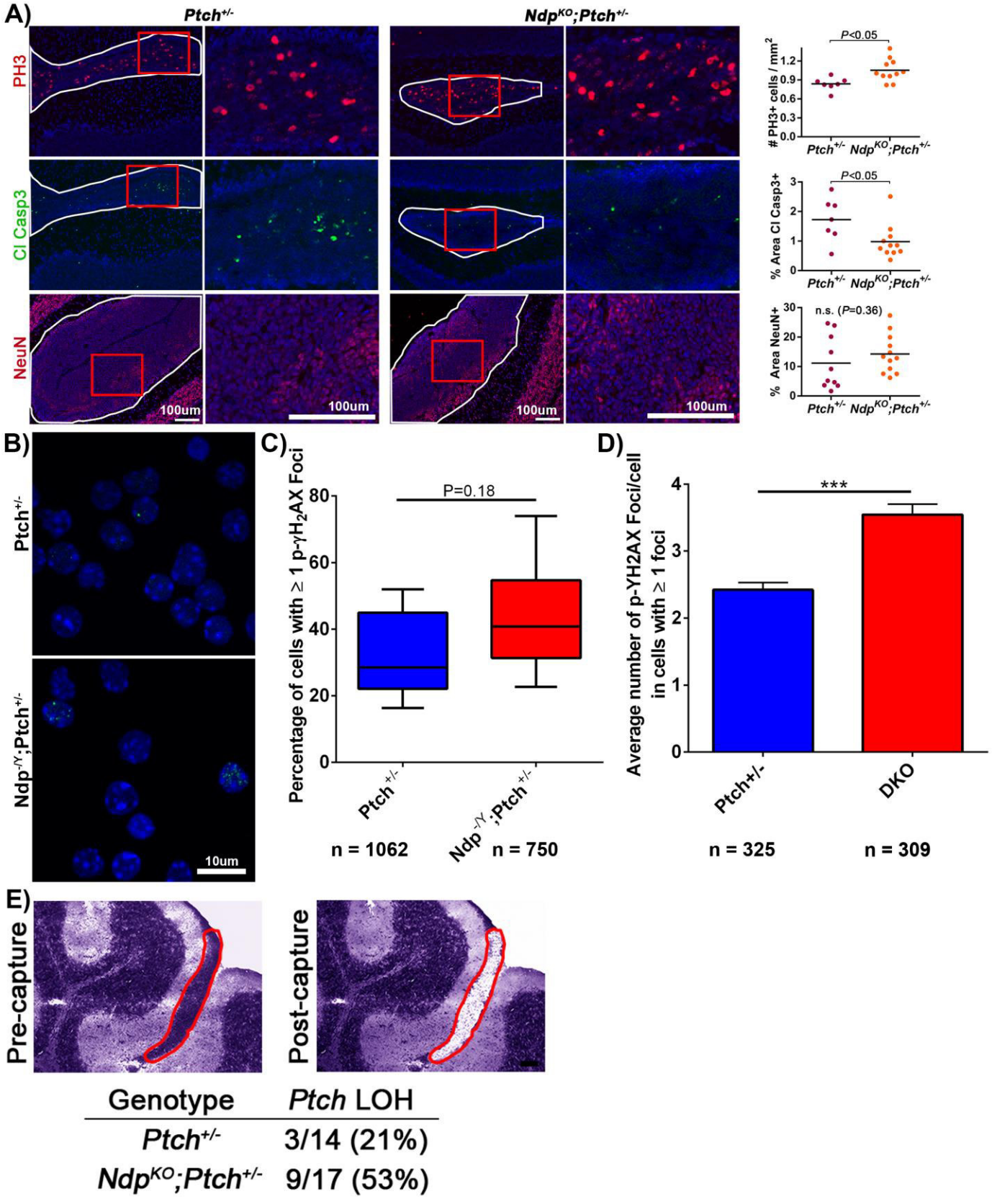

Genotype	*Ptch* LOH
Ptch$^{+/-}$	3/14 (21%)
Ndp^{KO};*Ptch*$^{+/-}$	9/17 (53%)

<u>Figure 14.</u> Loss of Norrin signaling increases DNA damage and accelerates transition to LOH in Ptch$^{+/-}$ lesions.

(**A**) Representative immunostaining and quantification of the proliferative index (PH3), apoptosis (cleaved caspase 3) and differentiation (neuronal nuclear protein - NeuN) in P14 Ptch$^{+/-}$ and Ndp$^{-/Y}$;Ptch$^{+/-}$ cerebellar lesions (outlined in white) and counterstained with Hoechst (blue). Areas in red boxes are magnified on the right. Black horizontal lines in the graphs denote the mean. (**B**) Acutely dissociated Ptch$^{+/-}$ and Ndp$^{-/Y}$;Ptch$^{+/-}$ GNPs were plated for 2 hrs and stained for DNA damage repair pathway marker pγ-H2AX (green) and counterstained with nuclear marker Hoechst (blue). Images were used to quantify (**C**) the average number of cells with ≥ 1 γ-H2AX foci and (**D**) the average number of γ-H2AX foci in cells with ≥ 1 γ-H2AX foci. (**E**) Frequency of Ptch loss of heterozygosity (LOH) in lesions from P14 Ptch$^{+/-}$ and Ndp$^{-/Y}$;Ptch$^{+/-}$ mice. Lesions were laser capture microdissected and used to determine the rate of LOH by qRT-PCR for wild-type allele-specific detection of Ptch1 transcripts. Representative images depict a toluidine blue-stained cerebellar lesion pre- and post-laser capture (lesion outlined in red). Number of biological replicates (n) used and the scales are indicated in the figure, which is adapted from [236] and modified. Box plot in (**C**) whiskers represent the min and Max value, while the bar graph figure in (**D**) illustrated the standard error of the mean.

3.10 Disruption of Ndp signaling in the context of constitutive Hh pathway activation drives lesion progression.

In $Ptch^{+/-}$ animals, we can model both the incidence and latency of lesion development, metrics of lesion number and progression, respectively. Progression is affected by the rate of loss of heterozygosity (LOH) and senescence evasion [217, 272, 273]. To acquire a better understanding of the role that Ndp plays in lesion progression following LOH acquisition, we took advantage of the Neurod2-SmoA1 mouse model, which is a mouse model wherein Patched1 LOH is not required for constitutive Hh pathway activation. Neurod2-SmoA1 (SmoA1) mice express an oncogenic form of human Smo (point mutation at W535L) in GNPs [274], which renders Smo unresponsive to Ptch inhibition [220], effectively driving constitutive Hh pathway activation. We crossed the $SmoA1^{+/+}$ mice with $Ndp^{+/-}$ females to generate $SmoA1^{+/-}$;$Ndp^{+/Y}$ and $SmoA1^{+/-}$;$Ndp^{-/Y}$ littermates. These animals were aged out and continuously monitored for signs of tumor development (Figure 15C). $SmoA1^{+/-}$;$Ndp^{-/Y}$ as compared to $SmoA1^{+/-}$;$Ndp^{+/Y}$ mice exhibited a highly significant (≈ 5 fold) reduction in latency (Figure 15D). Interestingly, there was no difference in lesion incidence (Figure 15D), as all animals (30 animals), except for one $SmoA1^{+/-}$;$Ndp^{+/Y}$ mouse, developed MBs (Figure 15D). To better detail the events surrounding lesion initiation and progression in this model, we turned our attention to the early lesion stage (P14). We observed that all $SmoA1^{+/-}$ mice with or without Ndp expression have a hyperplastic EGL (Figure 15D), rendering lesion quantification impossible [236] and providing an explanation for the similar tumor incidence between genotypes (Figure 15D). Interestingly, however, there was a significant increase in the volume of the hyperplastic EGL of $SmoA1^{+/-}$;$Ndp^{-/Y}$ mice compared to control littermates (Figure 15B), a measurement which is often used as an indicator of lesion progression in $Ptch^{+/-}$ mice [236]. Taken together, these results indicate that the loss of Ndp on the $SmoA1^{+/-}$

background promotes hyperplastic EGL progression towards established MB in the context of a constitutively active Hh pathway.

In summary, neuronal Ndp to endothelial Fzd4 signaling in the presence of aberrant Hh signaling ($Ptch^{+/-}$ mice) promotes the creation of a tumor suppressive environment. The disruption of this signaling pathway induces the creation of a pro-tumor microenvironment, which drives tumorigenesis by promoting lesion formation and lesion progression to established MB. The loss of Ndp signaling enhances the intrinsic or extrinsic susceptibility of GNPs to genomic instability, increasing the rate of Ptch1 LOH, thus driving Hh ligand-independent pathway activation. To better understand the mechanism of action of loss of Ndp on MB initiation and progression we decided to take a closer look at the lesion microenvironment. Knowing that Ndp is acting through the vasculature located in the surrounding microenvironment, and that several vascular associated genes were altered in $Ndp^{-/Y}$;$Ptch^{+/-}$ MB microarrays as compared to $Ptch^{+/-}$ MB samples.

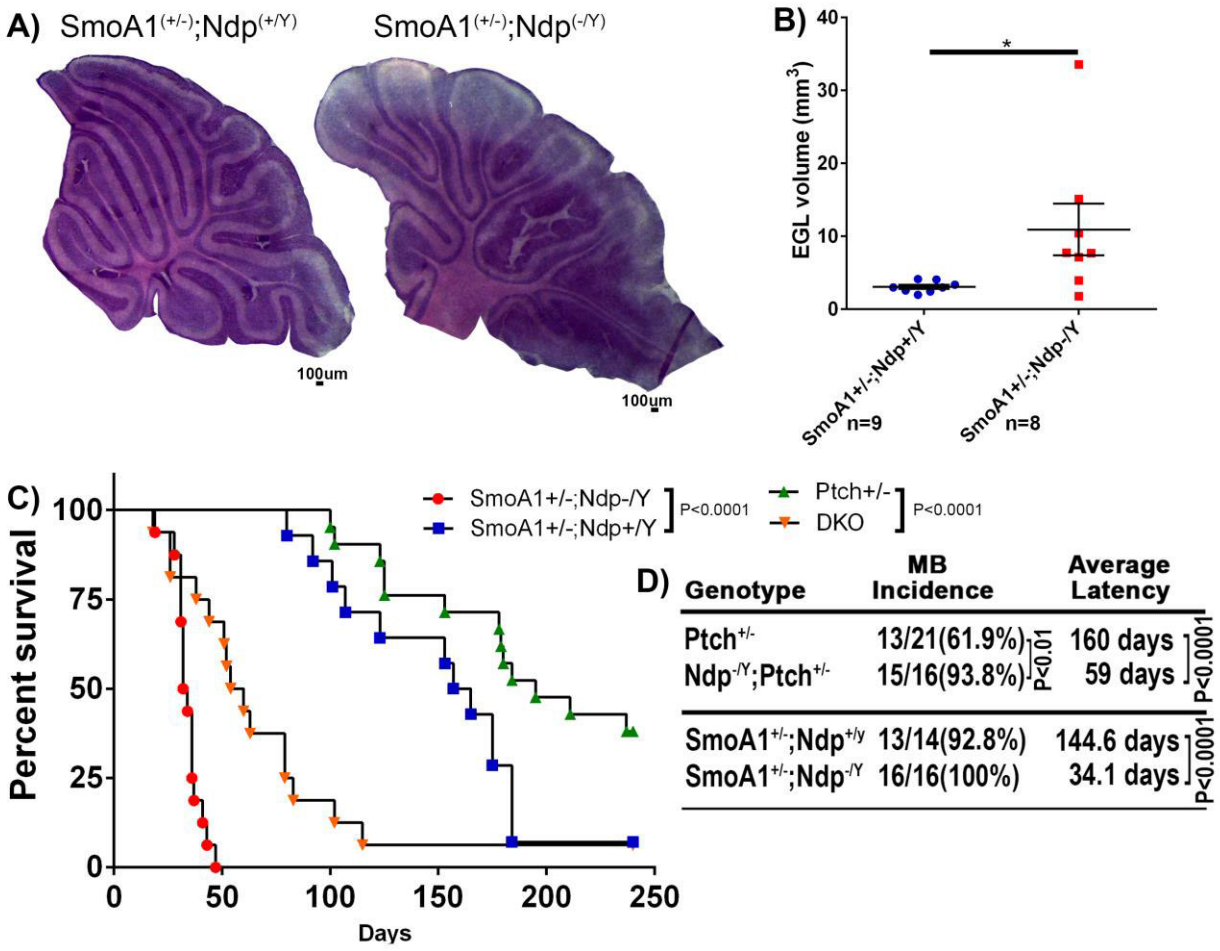

Figure 15. Disruption of Norrin signaling drives MB progression in NeuroD2SmoA1$^{+/-}$ mice. (**A**) Haematoxylin and eosin (H&E) stained section from Ndp$^{+/Y}$;SmoA1$^{+/-}$ and Ndp$^{-/Y}$;SmoA1$^{+/-}$ animals illustrating the hyperplastic EGL. (**B**) Volume quantification of the hyperplastic EGL (A) of the indicated genotype. (**C**) Kaplan-Meier survival curve of Ndp$^{+/Y}$;SmoA1$^{+/-}$, Ndp$^{-/Y}$;SmoA1$^{+/-}$, Ptch$^{+/-}$ and Ndp$^{-/Y}$;Ptch$^{+/-}$ animals, illustrating the impact of systemic Ndp deletion on the SmoA1$^{+/-}$ background. All SmoA1$^{+/-}$ animals in the study developed MB except for 1 Ndp$^{+/Y}$;SmoA1$^{+/-}$ mouse. (**D**) Survival curve (**C**) related information, including sample sizes, incidence and latency of the observed MB cases. Number of individual biological replicates (n) and scales are indicated in the figure. Figure adapted and modified from [236].

Chapter 4. Characterization of stromal alterations as a function of inactivation of endothelial Ndp/Fzd4 signaling

Statement of Contributions

- Post-doctoral student Dr. Erin Bassett

Assisted with the execution and design of Figure 16 A and C-D and 17 and Appendix A supplemental Figure 3 and 4

- Ema A. Allemano assisted with the execution and design of Appendix Figure 3

Ndp signals through the vascular Fzd4 receptor to establish a tumor suppressive micro-environment, which when disrupted, increases incidence and reduces latency of MB by increasing lesion formation, and promoting their progression, respectively. The idea of an early stromal contribution to the formation and progression of lesion is consistent with the observation that stromal genes were among the most altered in $Ndp^{-/Y}$;$Ptch^{+/-}$ MB samples as compared to control. This suggests that loss of Ndp/Fzd4 signaling may induce early stromal alterations, promoting lesion formation that drives progression towards an established MB. To better understand these early stromal alterations, we compared the stromal perturbations upon the loss of Ndp/Fzd4 signaling in the lesion of $Ndp^{-/Y}$;$Ptch^{+/-}$, Tie2-$Cre^{+/-}$;$Fzd4^{flox/flox}$;$Ptch^{+/-}$ and their respective $Ptch^{+/-}$ control littermates.

4.1 Early activation of the angiogenic switch and aberrant ECM deposition

Several of the up-regulated genes detected in micro-array (Esm1, Plvap, EphB4 and Emcn) and qRT-PCR (Pecam and Angpt2) in the $Ndp^{-/Y}$;$Ptch^{+/-}$ as compared to $Ptch^{+/-}$ MB samples were vascular-associated genes. This observation of an increase in vascular gene expression in the established tumor may suggest that vascular alterations are taking place in the early lesion. To investigate this, we examined the vasculature of lesions from serial sections of P14 $Ndp^{-/Y}$;$Ptch^{+/-}$ and Tie2-$Cre^{+/-}$;$Fzd4^{flox/flox}$;$Ptch^{+/-}$ and Ptch+/- littermates. Lesions from $Ndp^{-/Y}$;$Ptch^{+/-}$ (78%) and Tie2-$Cre^{+/-}$;$Fzd4^{flox/flox}$;$Ptch^{+/-}$ (95%) mice were highly vascularized, which was in contrast to the $Ptch^{+/-}$ (24%) samples, where the majority of the lesions were poorly vascularized and only the meningeal-associated vessels could be observed (Figure 16A and D). Upon further investigation, we observed aberrant deposition of ECM components (Laminin) in the lesions of $Ndp^{-/Y}$;$Ptch^{+/-}$ and Tie2-$Cre^{+/-}$;$Fzd4^{flox/flox}$;$Ptch^{+/-}$ animals, as compared to their respective $Ptch^{+/-}$ control littermates (Figure 16A). Furthermore, we observed a significant increase in the vascular density (CD31+) and ECM (Laminin) density (Figure 16 C) in lesions from $Ndp^{-/Y}$;$Ptch^{+/-}$ and Tie2-$Cre^{+/-}$;$Fzd4^{flox/flox}$;$Ptch^{+/-}$ animals as compared to their respective $Ptch^{+/-}$ control littermates. Collectively, these observations are evidence of an early active angiogenic program in the $Ndp^{-/Y}$;$Ptch^{+/-}$ and Tie2-$Cre^{+/-}$;$Fzd4^{flox/flox}$;$Ptch^{+/-}$ animals, as compared to their respective $Ptch^{+/-}$ control littermates. We further corroborated these results by directly assessing the angiogenic program in $Ndp^{-/Y}$;$Ptch^{+/-}$ as compared to $Ptch^{+/-}$ control littermates, by quantifying the number of proliferating ($PH3^{+}$) ECs ($CD31^{+}$) within lesions (normalized to lesion area). We observed a significant increase in the mitotic index of ECs ($PH3^{+}$;$CD31^{+}$) in $Ndp^{-/Y}$;$Ptch^{+/-}$ lesions as compared to $Ptch^{+/-}$ littermates control lesions (Figure 16B), further supporting the observation of an early activation of the angiogenic program following the loss of Ndp/Fzd4 signaling. A particularly interesting observation was the fact that the angiogenic remodeling was restricted to the lesion, with only rare

examples of angiogenic activation, and invasion identified in the normal EGL (Appendix A Figure 3). The observed increase in lesion vascular invasion could be seen in even very small lesions (<0.02mm^3) (Appendix A Figure 3) and was not associated with an increase in lesion volume (Figure 12B and D), as we could not previously detect an increase in lesion volume between Ndp$^{-/Y}$;Ptch$^{+/-}$or Tie2-Cre$^{+/-}$;Fzd4$^{flox/flox}$;Ptch$^{+/-}$ animals and their respective Ptch$^{+/-}$ control littermates (Figure 12B and D). These results illustrate that early vascular recruitment within the lesions of Ndp$^{-/Y}$;Ptch$^{+/-}$and Tie2-Cre$^{+/-}$;Fzd4$^{flox/flox}$;Ptch$^{+/-}$ is independent of lesion size, and may even precede the transformation of the pre-cancerous lesion to established MB.

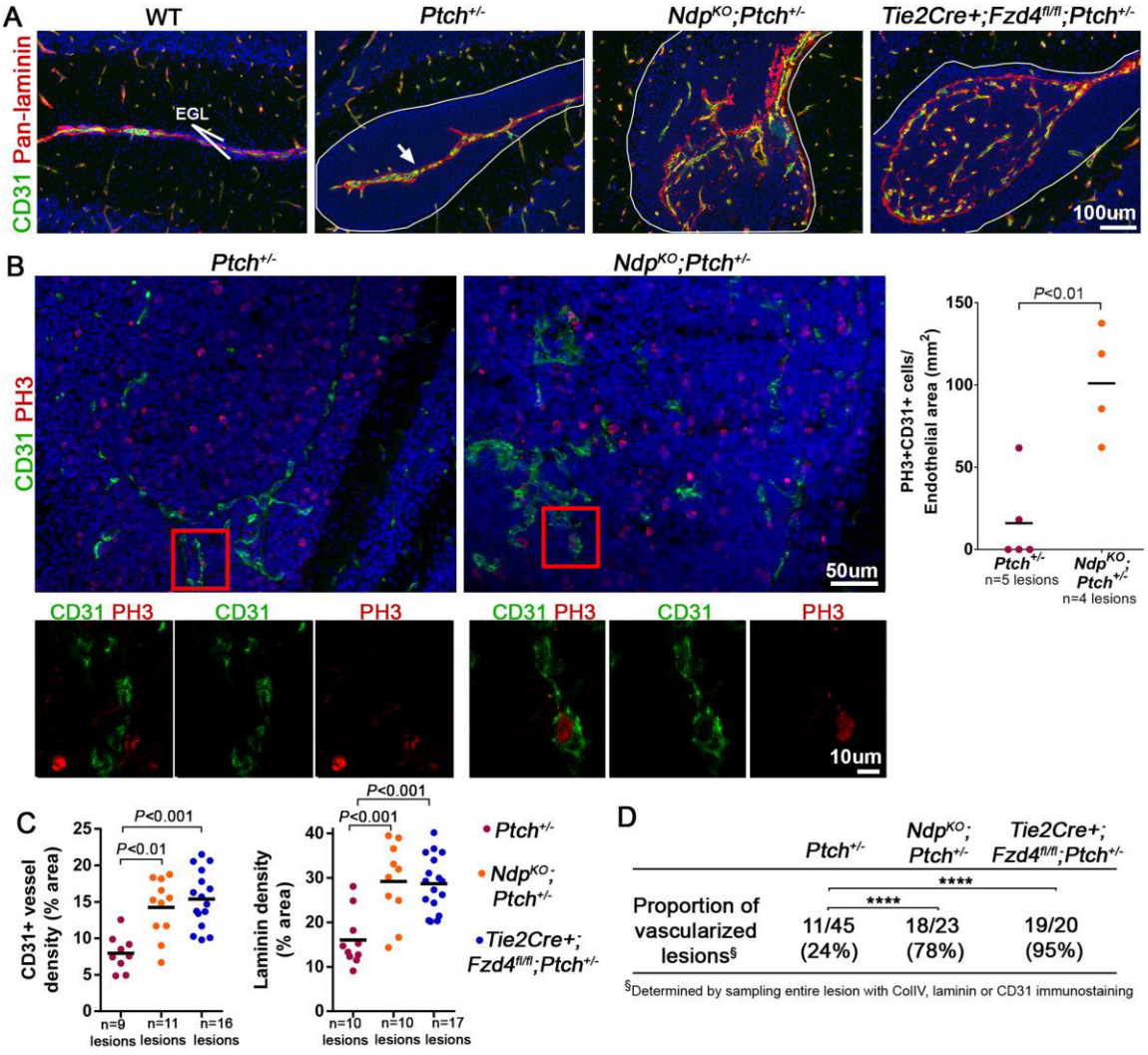

Figure 16. Disruption of Norrin/Fzd4 signaling in ECs drives angiogenic remodeling.
(**A**) Co-immunostaining in the cerebellum from P14 animals of the indicated genotypes for CD31 (green) and pan-Laminin (red), counterstained with Hoechst (blue). Lesions are outlined in white and the white arrow in the Ptch$^{+/-}$ lesion indicates the meningeal blood vessels. (**B**) Quantification of mitotic index in ECs from Ptch$^{+/-}$ and Ndp$^{-/Y}$;Ptch$^{+/-}$ lesions. Top images show a co-immunostaining for CD31 (green) and PH3 (red), counterstained with Hoechst (blue), in vascularized P14 lesions of the indicated genotype. Red squares denote areas shown by confocal scans below, the left image depicts the composite maximum intensity projection, the middle and right images are individual z-stack optical sections of the indicated staining. Blue arrows denote a PH3^{+} cell scored as negative for co-localization, whereas the red arrows denote a positive co-localization. On the far right: a graph summarizing the quantification of double labelled PH3^{+}/CD31^{+} cells normalized to endothelial area within the lesion of the indicated genotype. (**C**) Quantification of (left) CD31+ vessel and (right) Laminin density (percentage of area) in the lesions of the indicated genotypes. (**D**) Summary information on the proportion of vascularized lesions from each genotype. Number of lesions (n) examined is indicated in each graph, means are represented by the black horizontal lines and the scale is indicated in the different figures. ****p<0.0001. Figure adapted from [236]

4.2 Loss of Ndp signaling compromises the BBB

Plvap, a marker of fenestration, trans-endothelial pores and caveolae, and all endothelial structures which increase microvascular permeability [275], was upregulated in the micro-array analysis in the $Ndp^{-/Y}$;$Ptch^{+/-}$, as compared to $Ptch^{+/-}$ MB samples (Appendix A Figure 1C-D). Plvap is repressed in brain ECs by canonical Wnt signaling [94], the pathway that Norrin signaling activates in the cerebellum [84]. Loss of Ndp/Fzd4 signaling increases BBB permeability, as seen by the extravasation of the serum albumin binding dye, Evans blue, into the cerebellum following intraperitoneal injection (IP) in P14 cerebellum and MB samples (Figure 17C and 11G). A closer examination of lesions from $Ndp^{-/Y}$;$Ptch^{+/-}$ and Tie2-$Cre^{+/-}$;$Fzd4^{flox/flox}$;$Ptch^{+/-}$ animals, as compared to their respective $Ptch^{+/-}$ control littermates, revealed a drastic loss of vascular integrity, as indicated by the increased expression of PLVAP (Figure 17A-B) and the variable loss of the endothelial tight junction protein Claudin-5 (Figure 17A). This loss of vascular integrity is associated with an enhanced Evans blue extravasation in the lesions of $Ndp^{-/Y}$;$Ptch^{+/-}$ and Tie2-$Cre^{+/-}$;$Fzd4^{flox/flox}$;$Ptch^{+/-}$ animals, as compared to their respective $Ptch^{+/-}$ control littermates (Figure 17C). The compromised BBB phenotype of $Ndp^{-/Y}$;$Ptch^{+/-}$ and Tie2-$Cre^{+/-}$;$Fzd4^{flox/flox}$;$Ptch^{+/-}$ lesions is in contrast to what was observed in the lesions from $Ptch^{+/-}$ animals, which failed to exhibit leaky vessels, as indicated by the absence of Evans Blue extravasation (Figure 17C). To determine whether the increased vascular permeability in $Ndp^{-/Y}$;$Ptch^{+/-}$ and Tie2-$Cre^{+/-}$;$Fzd4^{flox/flox}$;$Ptch^{+/-}$ was due to vascular development or differentiation defects, we assessed pericyte coverage by immunohistochemistry staining for Platelet-derived growth factor receptor β (PDGFRβ). We observed no noticeable differences in pericyte coverage from any of the genotypes in the lesions or normal EGL area, indicating that vascular development or maturation was not affected upon loss of Ndp/Fzd4 signaling (Figure 17D-E).

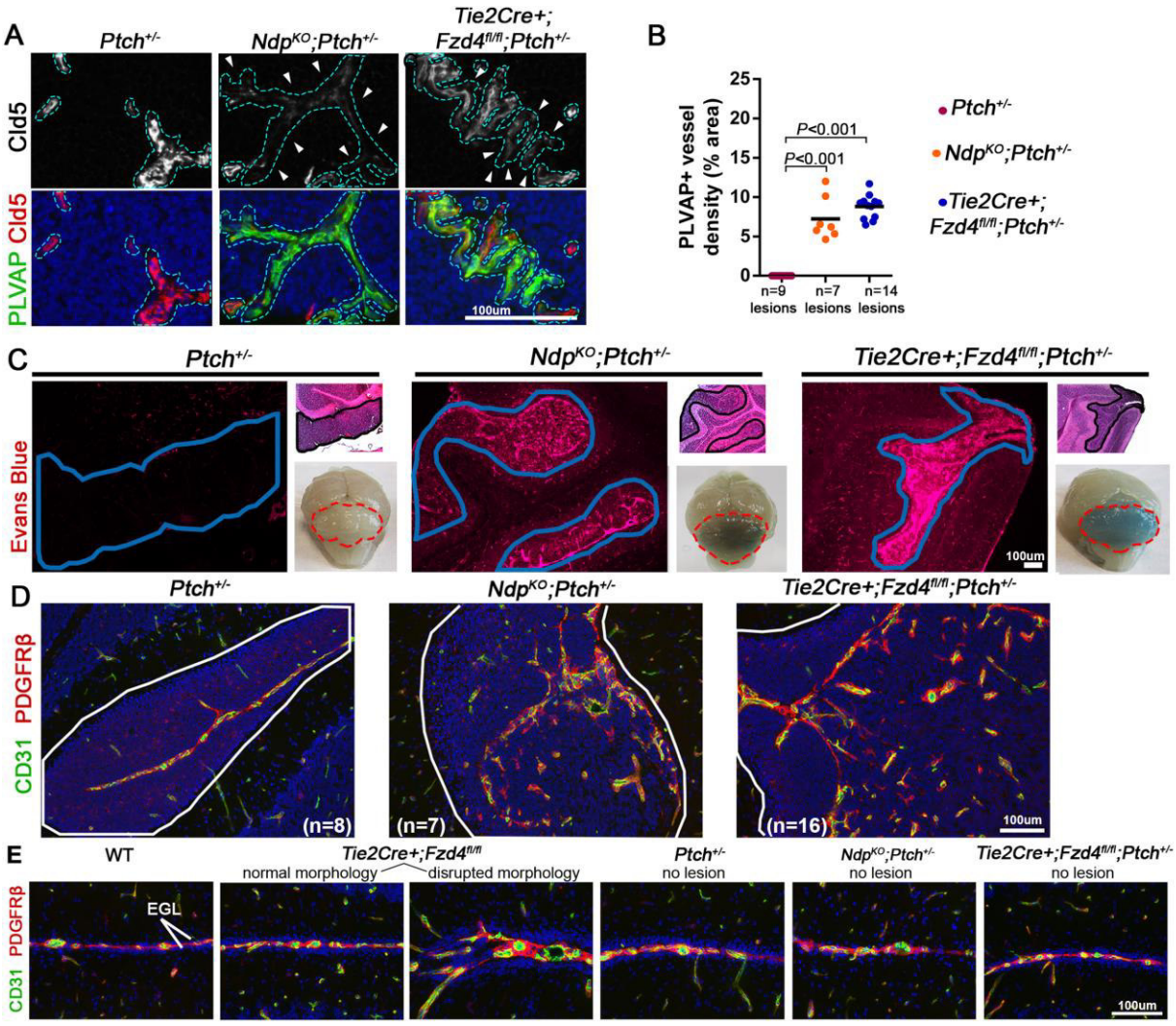

Figure 17. Loss of Norrin/Fzd4 signaling in ECs compromises the BBB in Ptch$^{+/-}$ lesions. (**A**) Co-immunostaining for PLVAP and Claudin-5 (Cld5) counterstained with Hoechst (blue), in lesions of P14 cerebella from the indicated genotypes with the vessels outlined in cyan. Top images show Cld5 channel only to illustrate variable reduction in Cld5 expression (arrowheads). (**B**) Quantification of PLVAP^{+} vessel density in lesions of Ptch$^{+/-}$, Ndp$^{-/Y}$;Ptch$^{+/-}$ and Tie2Cre$^{+/-}$;Fzd4$^{Flox/Flox}$;Ptch$^{+/-}$. (**C**) P14 Ptch$^{+/-}$, Ndp$^{-/Y}$;Ptch$^{+/-}$ and Tie2Cre$^{+/-}$;Fzd4$^{Flox/Flox}$;Ptch$^{+/-}$ mice injected with Evans Blue dye prior to sacrifice. Right bottom, whole brain Evans Blue extravasation in the cerebellum (outlined in red), right, in the lesion (outlined in blue – Evans Blue fluorescence) and left top, the H&E illustrates that the extravasation is enhanced in the lesion as compared to neighboring normal tissue. (**D**) Co-immunostaining for CD31 and the pericyte marker PDGFRβ on P14 cerebellar lesion sections (lesions outlined in white) from Ptch$^{+/-}$, Ndp$^{-/Y}$;Ptch$^{+/-}$ and Tie2Cre$^{+/-}$;Fzd4$^{Flox/Flox}$;Ptch$^{+/-}$.(**E**) Co-immunostaining for CD31 and PDGFRβ in P14 sections from the indicated genotypes. We examined 3 normal EGL areas from at least 3 different cerebella per genotype. External granule layer (EGL); Number of lesions (n) examined is indicated in each figure. Means are represented by the black horizontal lines and the scale is indicated in the different figures. Figure adapted and modified from [236].

4.3 Aberrant immune cell recruitment

Upon a closer examination of the micro-array data we noticed another interesting differentially expressed gene, the chemokine (C-X-C motif) ligand 1 (Cxcl) (Supplemental Figure 1B). Chemokines are cytokines that are important in immune cell trafficking and activation [44]. To explore the potential contributions of the immune cells to the lesion microenvironment, we examined lesions from $Ndp^{-/Y}$;$Ptch^{+/-}$ and $Ptch^{+/-}$ mice by immunohistochemistry for CD45, a pan leukocyte marker (Figure 18A-B). We observed a dramatic enrichment in $CD45^{+}$ cells in lesions from $Ndp^{-/Y}$;$Ptch^{+/-}$. Leukocytes are a broad class of immune cells, which encompass lymphocytes, a particularly interesting sub-class of immune cells which can actively modulate tumor progression in various tissues [32, 276] through their inflammatory function [34, 41] and their ability to stimulate angiogenesis [277]. The initial characterization of the infiltrating immune cells by immunohistochemistry revealed that the recruited leukocytes ($CD45^{+}$) within the lesions of $Ndp^{-/Y}$;$Ptch^{+/-}$ were predominantly localized within the perivascular space (Robin Virchow space), delimited by the vascular basal lamina (Figure 18B), with the rare exception of a few immune cells that extravasated out into the surrounding parenchyma (Figure 18B – red arrow). Interestingly, the recruited leukocytes appeared to be recruited preferentially into the lesions found within the folds of the cerebellum as opposed to the lesions found on the surface. This may be due to the fact that $Ndp^{-/Y}$;$Ptch^{+/-}$ have more lesions located within the fold of the cerebellum (Appendix A Figure 3). Further characterization of the recruited immune cell population by IHC and flow cytometry revealed that the population was very heterogeneous. We could readily identify T-cells ($CD3\varepsilon^{+}$), helper T-cells ($CD4^{+}$), cytotoxic T-cells ($CD8^{+}$), macrophages/dendritic cells ($CD11c^{+}$) and B-cells (IGM^{+}/$CD45R^{+}$). Interestingly, only the B-cell ($CD45R^{+}$/$B220^{+}$) subpopulation was significantly enriched in $Ndp^{-/Y}$;$Ptch^{+/-}$, as seen in flow cytometry analysis of whole cerebella dissociates (Figure 18D), and by immunohistochemistry (Figure 18B). This aberrantly recruited

B-cell population is interesting, as B-cells have been shown to be important in immune suppression and tumor progression [276, 278], with a particular focus in recent years on the B10 cells ($CD1d^+/CD5^+$), a B-cell subtype that has been shown to be a key regulator of this process [276, 278]. Further characterization of the lesion associated B-cell subpopulation revealed that it was comprised nearly exclusively of immature B-cells (IGM^+) (Figure 18C).

The aberrantly recruited B-cell population at the P14 lesion stage could cause alterations in the kinetics of the normal immune response taking place during tumorigenesis in $Ndp^{-/Y};Ptch^{+/-}$ mice. To further explore this possibility, we characterized the recruited lymphocyte population within established MB of $Ndp^{-/Y};Ptch^{+/-}$ and $Ptch^{+/-}$ littermates by IHC and flow cytometry. In $Ndp^{-/Y};Ptch^{+/-}$ tumors, we observed a significant reduction in the total number of lymphocytes ($CD45^+$, $\approx$ 1.5 fold) (Figure 19E-G), T-cells ($CD3^+$, $\approx$ 1.5 fold) (Figure 19F and H) and macrophages/dendritic cells ($CD45+/CD11c^+$, $\approx$ 1.5 fold) (Figure 18E and I) compared with $Ptch^{+/-}$ littermates. Interestingly, the recruited T-cell population in the $Ndp^{-/Y};Ptch^{+/-}$ samples also had a significant reduction in the expression of Programmed cell death protein-1 ($CD3^+/PD\text{-}1^+$, $\approx$ 2 fold), a known marker of lymphocyte activation/exhaustion [279] (Figure 18J). The observed reduction in infiltrating lymphocytes, in addition to the observed down-regulation of the Major histocompatibility complex (MHC) class2 molecules in $Ndp^{-/Y};Ptch^{+/-}$ (Figure 11D), are suggestive of an immune-suppressive environment. The observed down-regulation of PD-1 in $Ndp^{-/Y};Ptch^{+/-}$ is somewhat counterintuitive, as this signaling pathway has been shown to be often up-regulated and exploited by many malignancies to suppress the anti-tumor immune response [280]. This tumor immune-suppressive environment could be initiated or promoted by the early recruited B-cell population [276, 278, 281], rendering them an attractive target for further investigation.

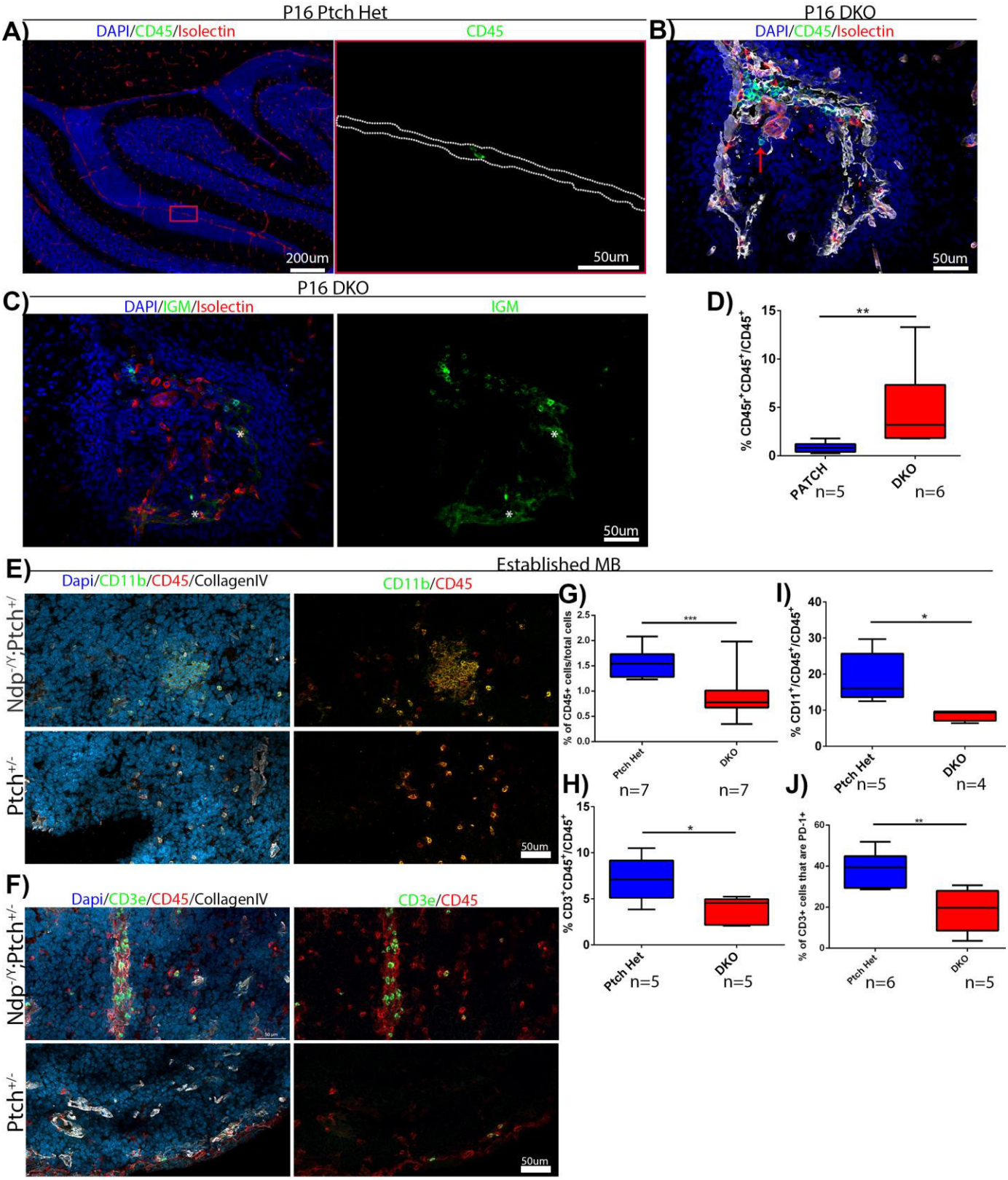
P16 Ptch Het
A)
DAPI/CD45/Isolectin
CD45
200um
50um
P16 DKO
B)
DAPI/CD45/Isolectin
50um
P16 DKO
C)
DAPI/IGM/Isolectin
IGM
50um
D)
% CD45r+CD45+/CD45+
**
PATCH
n=5
DKO
n=6
E)
Established MB
Dapi/CD11b/CD45/CollagenIV
CD11b/CD45
Ndp-/Y;Ptch+/
Ptch+/-
50um
F)
Dapi/CD3e/CD45/CollagenIV
CD3e/CD45
Ndp-/Y;Ptch+/-
Ptch+/-
50um
G)
% of CD45+ cells/total cells
***
Ptch Het
n=7
DKO
n=7
H)
% CD3+CD45+/CD45+
*
Ptch Het
n=5
DKO
n=5
I)
% CD11+/CD45+/CD45+
*
Ptch Het
n=5
DKO
n=4
J)
% of CD3+ cells that are PD-1+
**
Ptch Het
n=6
DKO
n=5

<u>Figure 18.</u> Characterization of the immune cell landscape in $Ndp^{-/Y};Ptch^{+/-}$ early lesion and established MB.

(**A**) Immunohistochemistry of a P16 $Ptch^{+/-}$ lesion. Left: a composite low-resolution image stained for vasculature ($isolectin^{+}$) and lymphocytes ($CD45^{+}$) and counterstained with Hoechst, the lesion outlined (white) with the red box denoting the area zoomed in on the right. Right: lymphocytes (CD45+ - green) which are confined within the meningeal vasculature (isolectin+ - white outline). (**B**) Immunohistochemistry of P16 $Ndp^{-/Y};Ptch^{+/-}$ lesion illustrating lymphocyte ($CD45^{+}$ – green) accumulation within the vasculature ($Isolectin^{+}$ - red) and the perivascular space ($CollagenIV^{+}$ - white) and counterstained with Hoechst (blue). Most of the recruited immune cells are confined within the perivascular space except for the occasional lymphocyte which extravasates out into the surrounding parenchyma (red arrow). (**C**) Immunohistochemistry of P16 $Ndp^{-/Y};Ptch^{+/-}$ lesion illustrating the elevated abundance of the immature B-cells (IGM^{+} - green) within the lesions. Left: composite image of the staining on the right including the vasculature ($Isolectin^{+}$ - red) and counterstained with Hoechst (blue). (**D**) Box-plot representation of flow cytometry quantification of B-cells ($CD45R^{+}/CD45^{+}$) normalized to the number of lymphocytes ($CD45^{+}$) from whole cerebella dissociation preparations from the indicated genotype. (**E-F**) Immunohistochemistry of established tumor samples illustrating the recruitment of lymphocytes ($CD45^{+}$ – red) and (**E**) macrophages/dendritic cells ($CD11b^{+}$ – green) or (**F**) T-cells (CD3ε – Green) within the tumors of the indicated genotypes. The images on the left are composite images of the staining on the right including CollagenIV (white) and counterstained with Hoechst (blue). (**G-I**) Box-plot of flow cytometry quantifications of the abundance of (**G**) lymphocytes ($CD45^{+}$) normalized to all cells of the indicated genotype. Box-plot of flow cytometry quantifications of the percentage of (**I**) macrophages/dendritic cells ($CD11c^{+}$) and (**H**) T-cells (CD3ε+) normalized to the number of lymphocytes ($CD45^{+}$) from whole cerebella dissociation preparations from the indicated genotype. (**J**) Box-plot of the flow cytometry quantification of the percentage of T-cells that are $PD\text{-}1^{+}$ ($PD\text{-}1^{+}/CD3\varepsilon^{+}$) normalized to the total number of T-cells ($CD3\varepsilon^{+}$) from whole cerebella dissociation preparations from the indicated genotypes. Asterisk denotes some background in the stain. Scale and number of biological replicates used (n) are indicated in the figure.

4.4 Reduction in Wnt signaling is associated with lesion progression

Ndp/Fzd4 signaling in the endothelium mediates its actions through the activation of the canonical Wnt-signaling pathway [84, 232]. Upon the loss of Ndp/Fzd4 signaling, we observed an increase in the lesions that activated the angiogenic program (Figure 16A-D). We therefore questioned whether the vascularized lesions in $Ptch^{+/-}$ mice are associated with altered Wnt signaling. To address this question, we examined the expression of Lef1, a canonical Wnt target gene [282], in the vasculature of $Ndp^{-/Y}$;$Ptch^{+/-}$ and $Ptch^{+/-}$ littermates. Lef1 expression in P14 $Ndp^{-/Y}$;$Ptch^{+/-}$ was significantly reduced as compared to P14 $Ptch^{+/-}$ lesions and EGL, validating the requirement for Ndp signaling in the endothelium for this marker. While Lef1 expression in $Ptch^{+/-}$ normal EGL and non-vascularized lesions was similar, we observed a stepwise reduction in Lef1 expression as a function of $Ptch^{+/-}$ lesion vascularization (Figure 19A-B). This reduction in Lef1 expression positively correlated with the decrease in Ndp expression in $Ptch^{+/-}$ GNPs during tumor progression (Figure 6F) and the decrease in Fzd4 expression in $Ptch^{+/-}$ MB samples compared to purified P7 GNPs (Figure 9B). These results suggest that angiogenic activation in $Ptch^{+/-}$ lesions may be associated with a local reduction in Ndp/Fzd4 activation in ECs.

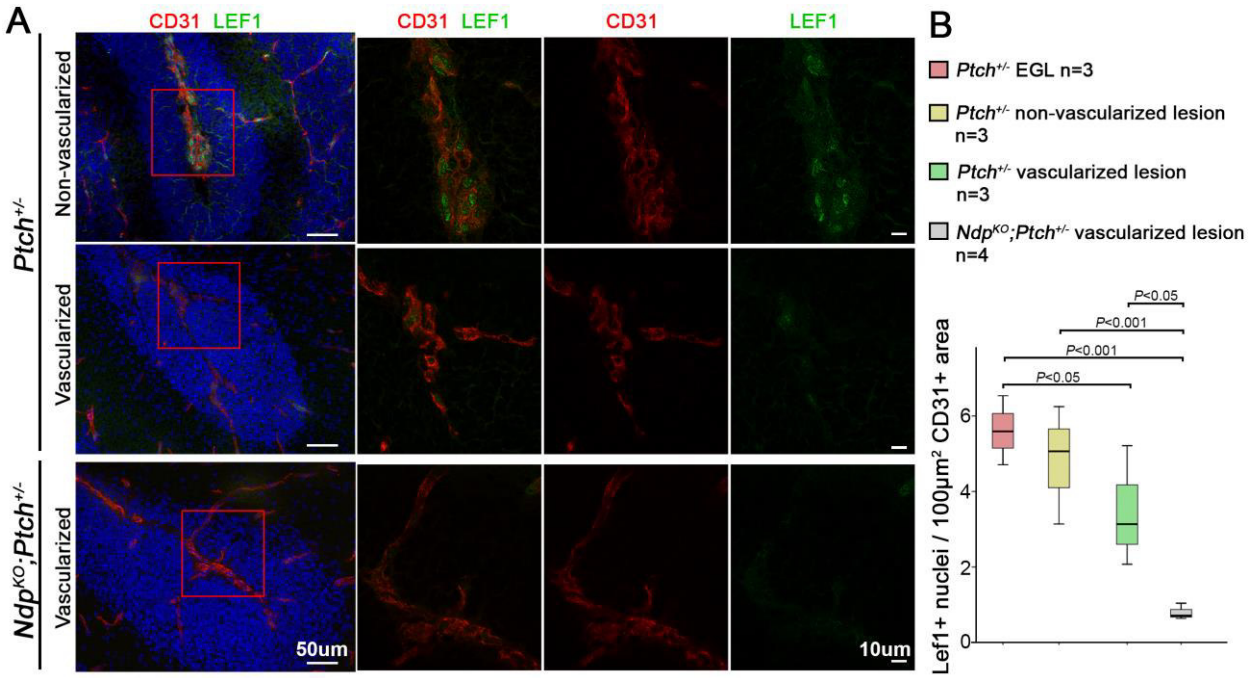

Figure 19. Reduction in Wnt signaling is associated with angiogenic invasion in Ptch+/- lesions.

(**A**) Co-immunostaining for CD31 (Pecam – red) and Lef1 (green), counterstained with Hoechst (blue), in sections from P14 $Ptch^{+/-}$ and $Ndp^{-/Y}$;$Ptch^{+/-}$ lesion. Red squares denote the area magnified on the right, which is a confocal single plane optical slice of the indicated staining. (**B**) Quantification of the number of double labelled $Lef1^{+}/CD31^{+}$ cells per endothelial area in $Ptch^{+/-}$ normal EGL lesions (vascularized and non-vascularized) and vascularized $Ndp^{-/Y}$;$Ptch^{+/-}$ lesions. Number of lesions (n) examined is indicated in the figure, means are represented by the black horizontal lines and the scale is indicated in the different figures. Figure adapted from [236]

4.5 Stromal alterations upon loss of Ndp are independent of Ptch1 status

Ptch1 is a well characterized dependence receptor which has the ability to activate several downstream pathways such as the apoptotic pathway [283], independent of Smoothened activity. To assess any potential contribution of the haploinsufficiency of the Ptch1 receptor in the vasculature to the observed stromal alterations, we took advantage of the SmoA1 mice and examined all the aforementioned phenotypes. We observed all the same phenotypes in the SmoA1 mice as seen in the Ptch+/- mice upon loss of Ndp. The cerebellum of $SmoA1^{+/-};Ndp^{-/Y}$ mice had a compromised BBB compared to $SmoA1^{+/-};Ndp^{+/Y}$ littermates, as visualized by whole brain Evans Blue extravasation (Figure 20A). Interestingly, the SmoA1 mice appeared to have a more severely compromised BBB phenotype as compared to their $Ptch^{+/-}$ counterparts (Figure 20A). The hyperplastic EGL of every animal from both genotypes ($SmoA1^{+/-};Ndp^{+/Y}$ and $SmoA1^{+/-};Ndp^{-/Y}$) exhibited signs of angiogenesis, as seen by vascular ($Isolectin^{+}$) invasion (Figure 20B) and the aberrant deposition of ECM ($CollagenIV^{+}$) (Figure 20B white arrows). In addition, we observed an aberrant recruitment of lymphocytes ($CD45^{+}$) in the hyperplastic EGL of $SmoA1^{+/-};Ndp^{-/Y}$ mice (Figure 20C). Taken together, the loss of Ndp in $SmoA1^{+/-}$ mice recapitulates all the same stromal phenotypes observed in the $Ptch^{-/+}$ mice.

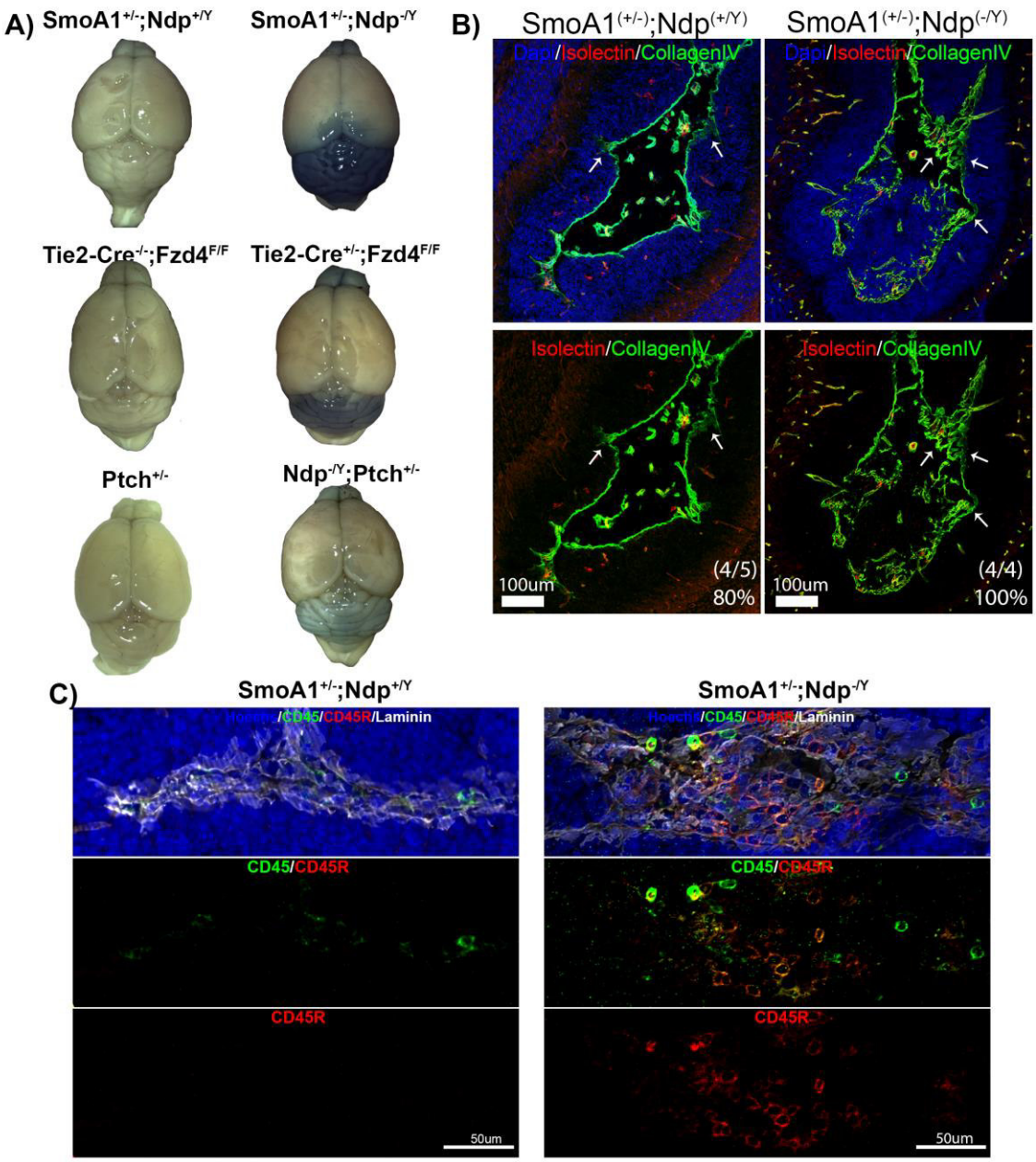

Figure 20. Characterization of the NeuroD2;SmoA1+/- mice upon loss of Ndp signaling. (**A**) Representative whole brain preparation following Evans blue intraperitoneal injection, exemplifying the open BBB phenotype amongst the different genotypes. (**B**) Immunohistochemistry staining of sections from the indicated genotypes stained for Isolectin (red) and collagenIV (green), demonstrating the vascular invasion phenotype in the hyperplastic EGL of both genotypes, and the aberrant deposition of basement membrane protein (CollagenIV - deposition highlighted by white arrows). The ratio and percentage of examined whole cerebella that presented signs of angiogenic invasion are indicated in the bottom right corner of the image in white. (**C**) Immunohistochemistry illustrating the aberrantly recruited lymphocytes ($CD45^+$ – green) and B-cells ($CD45R^+$ - red) from the indicated genotype. For the immune staining we examined 3 normal EGL areas from at least 3 different cerebella per genotype. Scales indicated in the figures.

Collectively, these results highlight the role of Ndp/Fzd4 signaling in creating a tumor suppressive micro-environment. Upon the loss of Ndp/Fzd4 signaling in ECs, a pro-tumor stroma is generated, which is characterized by an open BBB, an active angiogenic program, aberrant ECM deposition, and the enhanced recruitment of B-cells. These stromal alterations are reminiscent of the angiogenic switch, which have been shown to promote lesion progression in some tumors [277].

Chapter 5. Dissecting the requirement for stroma in MB development

Statement of Contributions

-Dr. Arturo Ortín
Assisted with the execution and design of Figure 21B

- Dr. Yuriy Baglaenko
Assisted with the execution and design of Figure 23A

Ndp/Fzd4 signaling in ECs modulates MB development by creating a pro-tumor environment which is characterized by 1) an early activation of the angiogenic program, 2) aberrant ECM deposition, 3) BBB disruption and 4) lymphocyte recruitment. Recently, we uncovered an additional stromal alteration, the reduction in meningeal lymphatic coverage, which may contribute to the MB development. With the exception of the reduction in lymphatic vasculature, all of these stromal modifications have previously been shown to be associated with, or actively participate in, tumor progression inside or outside the CNS [203, 284-288]. To better understand the cellular mechanism driving the observed increase in DNA damage and conversion of the resulting lesions into an established MB, it was necessary to determine the relative contributions of these stromal alterations, and to determine whether there is a predominant stromal alteration that is responsible for driving the MB phenotypes. This assessment was performed by the individual manipulation of the different components of the stroma, and the assessment of their relative contribution to MB initiation and progression.

5.1 Blocking Angpt2 mediated angiogenesis does not affect DKO tumorigenesis

To explore the potential role of active angiogenic remodeling in $Ndp^{-/Y}$;$Ptch^{+/-}$ mice, we pharmacologically targeted angiopoietin-2 (Angpt2) signaling with a functional blocking anti-Angpt2 monoclonal antibody. Angpt2 was selected, as its expression was upregulated in $Ndp^{-/Y}$;$Ptch^{+/-}$ as compared to $Ptch^{+/-}$ MB samples (Figure 11F). Furthermore, Angpt2 is an important angiogenic activato involved in promoting quiescent vascular activation by destabilizing endothelial association with the surrounding mural cells and basement membrane [289]. $Ndp^{-/Y}$;$Ptch^{+/-}$ animals were treated by intraperitoneal (IP) injections at P7 and P11 with 10mg/kg of α-Angpt2 or isotype matched monoclonal control antibody (α-mIgG2A). α-Angpt2 treatment in $Ndp^{-/Y}$;$Ptch^{+/-}$ mice significantly reduced vascular development on the vitreal surface of the retina, as compared to littermates treated with the isotype matched control (α-mIgG2A) antibody, demonstrating the biological effectiveness of α-Angpt2 at blocking *in vivo* angiogenesis (Figure 21A-B). Furthermore, α-Angpt2 treatment resulted in a significant 2-fold reduction in the vascular density of lesions in $Ndp^{-/Y}$;$Ptch^{+/-}$ mice, as compared to control treated animals (Figure 21C-E) and vascular regression (Figure 21D – white arrows). Interestingly, α-Angpt2 treatment significantly reduced overall survival as compared to mIgG2A treated mice and was non-significantly reduced as compared to untreated $Ndp^{-/Y}$;$Ptch^{+/-}$ animals (Figure 21F). This reduction in survival is attributed to a reduction in the latency as both α-Angpt2 and mIgG2A-treated animals had identical incidence (Figure 21F). Furthermore, we observed an apparent reduction in the aberrant deposition of ECM components within established lesions of α-Angpt2 treated animals as compared to control treated samples (Appendix A Figure 4).

In summary, systemic treatment of $Ndp^{-/Y}$;$Ptch^{+/-}$ animals with α-Angpt2 reduced vascular density and overall survival, suggesting that activation of the angiogenic program may not promote tumor progression in the context of Ndp inactivation.

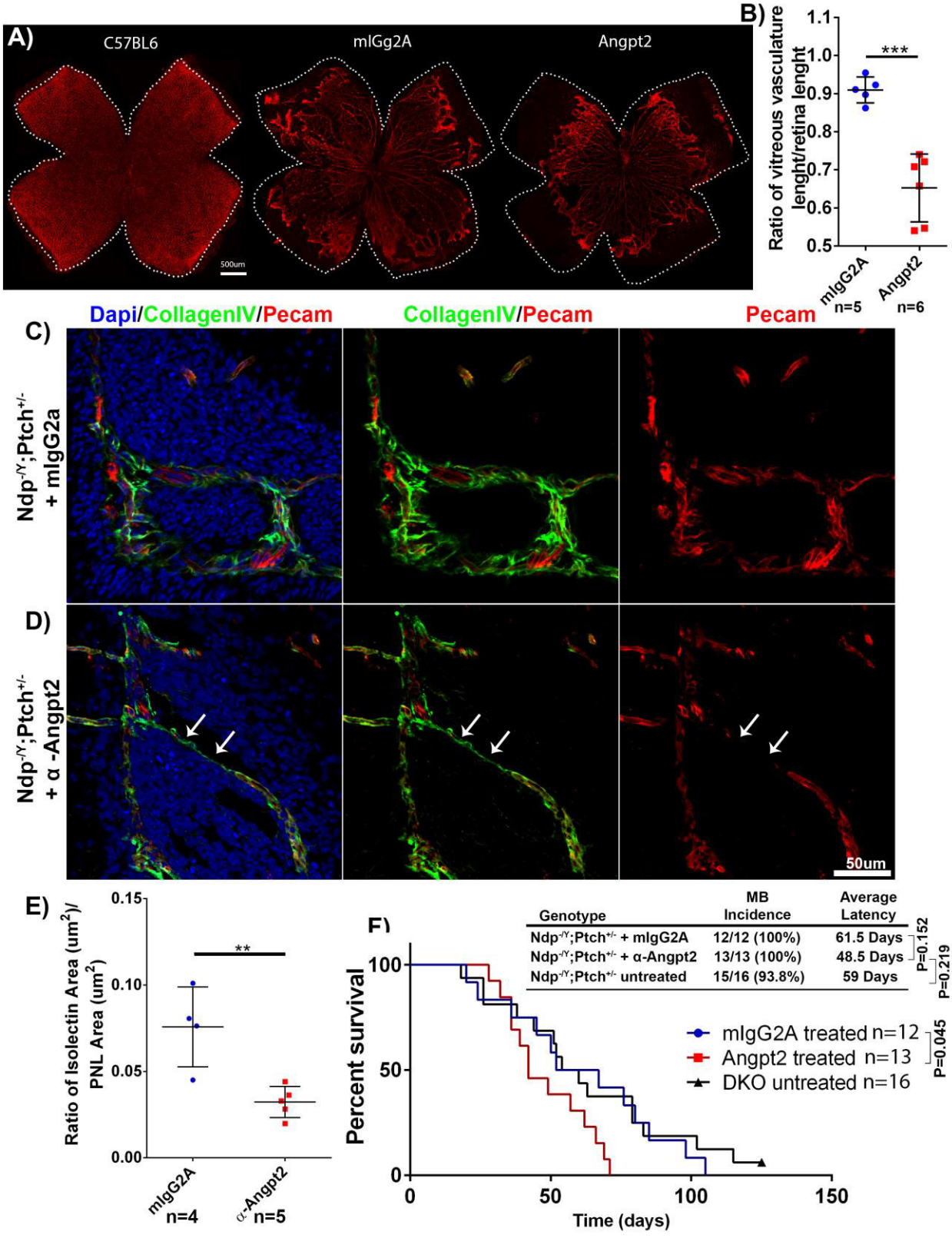
A)
C57BL6
mIgG2A
Angpt2
500um
B)
Ratio of vitreous vasculature lenght/retina lenght
***
mIgG2A n=5
Angpt2 n=6
C)
Dapi/CollagenIV/Pecam
CollagenIV/Pecam
Pecam
Ndp-/Y;Ptch+/- + mIgG2a
D)
Ndp-/Y;Ptch+/- + α -Angpt2
50um
E)
Ratio of Isolectin Area (um2)/ PNL Area (um2)
**
mIgG2A n=4
α-Angpt2 n=5
F)
Genotype | MB Incidence | Average Latency
Ndp-/Y;Ptch+/- + mIgG2A | 12/12 (100%) | 61.5 Days
Ndp-/Y;Ptch+/- + α-Angpt2 | 13/13 (100%) | 48.5 Days
Ndp-/Y;Ptch+/- untreated | 15/16 (93.8%) | 59 Days
P=0.152
P=0.219
P=0.045
Percent survival
mIgG2A treated n=12
Angpt2 treated n=13
DKO untreated n=16
Time (days)

<u>Figure 21.</u> Blocking angiogenesis in $Ndp^{-/Y}$;$Ptch^{+/-}$ with α-Angpt2 treatment does affect survival.

(**A**) $Ndp^{-/Y}$;$Ptch^{+/-}$ were treated at P7 and P11 with α-Angpt2 functional blocking antibodies or the α-mIgG2A isotype control antibody. Whole mounts of P14 the retinas were used to examine the vasculature ($Isolectin^{+}$ - red), far left: an adult WT untreated retina. (**B**) Quantification of the vitreous vasculature, from the optic nerve to the vascular forefront (red line), normalized to the length of the vitreous (outlined in white – white line). (**C-D**) Immunohistochemistry of representative lesion from (**C**) control treated α-mIgG2A and (**D**) α-Angpt2 treated $Ndp^{-/Y}$;$Ptch^{+/-}$ animals stained with CollagenIV (green), CD31 (Pecam – red) and counterstained with Hoechst (blue). Example of vascular regression in the α-Angpt2 treated groups is shown by the white arrow. (**E**) Quantification of the lesion vascular density normalized to the area of the lesion in $Ndp^{-/Y}$;$Ptch^{+/-}$ animals from the indicated treatment group. (**F**) Kaplan-Meier survival curve of $Ndp^{-/Y}$;$Ptch^{+/-}$ animals, treated with α-Angpt2 or α-mIgG2A, exploring the impact of systemically blocking angiogenesis in $Ndp^{-/Y}$;$Ptch^{+/-}$. Right: Survival curve (**F**) related information, including samples sizes, the incidence and latency of the MB cases. Scale and sample size (n) is indicated in the figure. **p<0.01, ***p<0.001

5.2 Ptx-Induced BBB disruption does not affect Ptch$^{+/-}$ tumorigenesis

The disruption of Ndp/Fzd4 signaling destabilized the BBB [84], as visualized by the parenchymal extravasation of Evans Blue in the cerebellum and in lesions (Figure 18C and 21A). We showed that this disruption of the BBB is due to the increased expression of Plasmalemma vesicle-associated protein (Plvap) and the variable loss of the inter-endothelial cell tight junction proteins (claudin-5) (Figure 17A). This opening of the BBB is not believed to be due to vascular maturation defects, as we observed no difference in pericyte coverage upon the disruption of Ndp/Fzd4 signaling (Figure 17D-E).

To assess the contributions that an open BBB may have in promoting lesion formation and progression, we pharmacologically opened the BBB by treating Ptch$^{+/-}$ mice with 120ng/injection of pertussis toxin (Ptx), a mediator of mouse BBB disruption [290], IP at P7, P9, P11 and P13. Ptx treatment in Ptch$^{+/-}$ animals successfully opened the BBB, as seen by whole brain Evans Blue extravasation (Figure 22C). The disruption of the BBB in Ptx-treated mice was mediated by a paracellular mechanism, as seen by the disruption of tight junction complexes (Zo-1 and Claudin-5 – Figure 22 A and B) between ECs. This paracellular opening following Ptx treatment is in contrast to what has been observed upon Ndp/Fzd4 signaling disruption, which opened the BBB in a paracellular (disruption of tight junctions) and transcellular (expression of Plvap) manner [291] (Figure 17A-B and 22D). Interestingly, the disruption of the BBB following Ptx treatment did not significantly alter overall survival or tumor latency as compared to PBS treated control Ptch$^{+/-}$ littermates (Figure 22E). Further investigation at the lesion stage revealed a slight, but not significant ($\approx$ 1.5 fold), increase in the number of established lesions (Figure 22F) and a slight, but not significant reduction in lesion volume in Ptx treated animals as compared to PBS control mice (Figure 22G). Furthermore, we did not observe any alterations in the angiogenic activation, as assessed by the proportion of vascularized lesions (Figure 22H). Taken together these results

indicate that Ptx-mediated BBB disruption does not phenocopy the MB phenotype in $Ndp^{-/Y}$;$Ptch^{+/-}$ mice, which suggests that opening the BBB through the paracellular route is not sufficient to drive tumor progression.

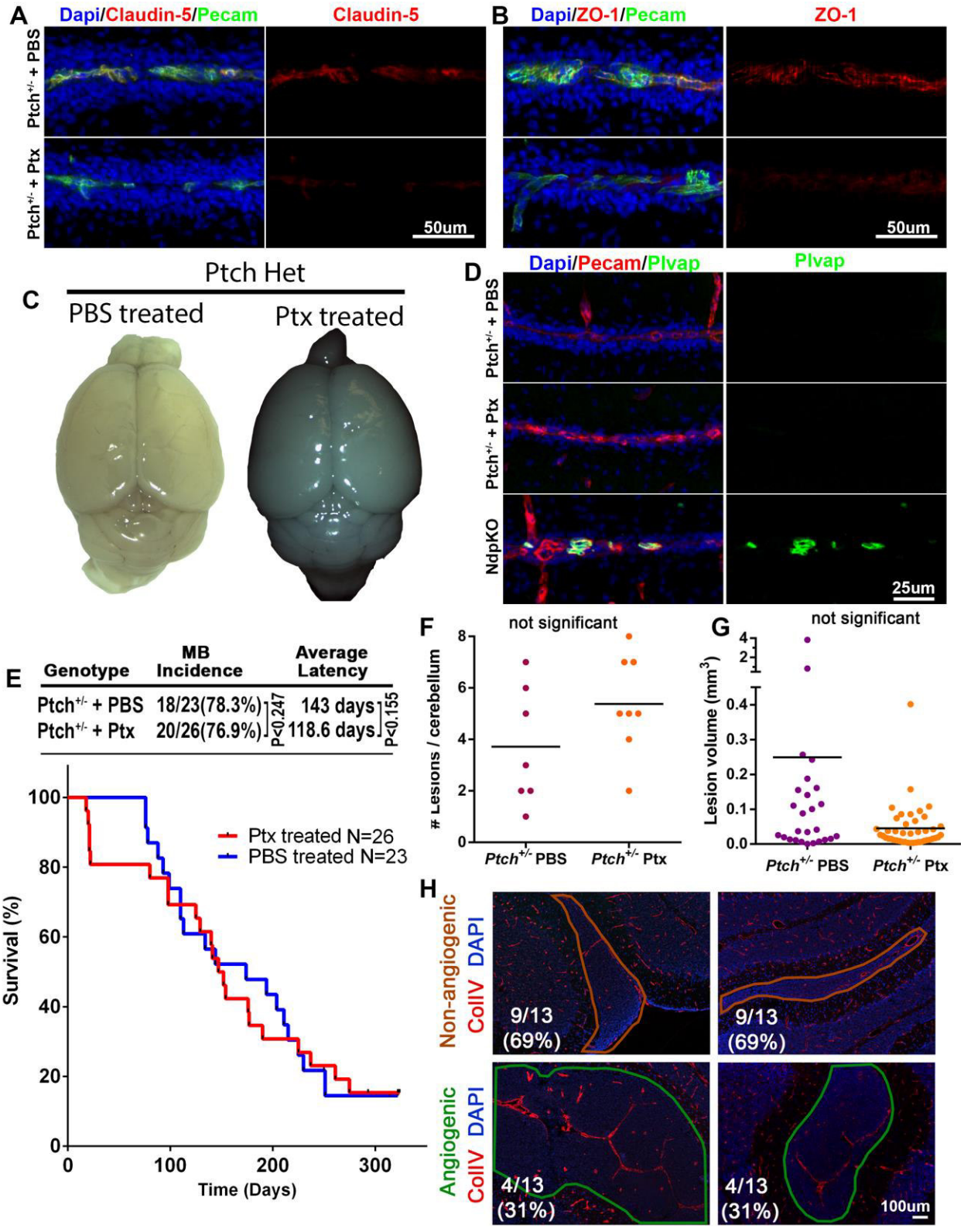
A
Dapi/Claudin-5/Pecam
Claudin-5
Ptch+/- + PBS
Ptch+/- + Ptx
50um
B
Dapi/ZO-1/Pecam
ZO-1
50um
C
Ptch Het
PBS treated
Ptx treated
D
Dapi/Pecam/Plvap
Plvap
Ptch+/- + PBS
Ptch+/- + Ptx
NdpKO
25um
E
Genotype
MB Incidence
Average Latency
Ptch+/- + PBS 18/23(78.3%) 143 days
Ptch+/- + Ptx 20/26(76.9%) 118.6 days
P<0.247
P<0.155
Ptx treated N=26
PBS treated N=23
Survival (%)
Time (Days)
F
not significant
Lesions / cerebellum
Ptch+/- PBS
Ptch+/- Ptx
G
not significant
Lesion volume (mm3)
Ptch+/- PBS
Ptch+/- Ptx
H
Non-angiogenic
CollV DAPI
9/13 (69%)
9/13 (69%)
Angiogenic
CollV DAPI
4/13 (31%)
4/13 (31%)
100um

<u>Figure 22.</u> Opening the BBB with Ptx in Ptch+/- animals does not alter survival or lesion formation.

(**A-B**) Immunohistochemistry of representative EGL from PBS and Ptx treated P14 $Ptch^{+/-}$ animals examining (**A**) Claudin-5 (red) and (**B**) Zo-1 (red) expression. Images on the left are composite images of the staining (right) with the addition of CD31 (Pecam – green) and counterstained with Hoechst (blue). (**C**) Whole brain preparation following Evans blue intraperitoneal injection, illustrating the open BBB phenotype following Ptx treatment in $Ptch^{+/-}$ animals. (**D**) Immunohistochemistry of representative EGL from P14 $Ndp^{-/Y}$, PBS and Ptx treated P14 $Ptch^{+/-}$ animals illustrating Plvap (meca32 – green) expression, images on the left are composite images of the staining on the right, including CD31 (Pecam – green) and counterstained with Hoechst (blue). (**E**) Bottom: Kaplan-Meier survival curve of $Ptch^{+/-}$ treated with PBS or Ptx. The sudden drop in the Ptx-treated survival is due to four animals dying from brain hemorrhages or seizures, in addition three other Ptx-treated animals were euthanized due to malocclusion or unknown causes. All other mice died with confirmed MB. Top: Survival curve (bottom) related information, including samples sizes, the incidence and latency of the fatalities. (**F-G**) Quantification of (**F**) number of lesion and (**G**) their volumes in P14 $Ptch^{+/-}$ mice treated with Ptx (n = 8 mice, 43 lesions total) or PBS (n = 7 mice, 26 lesions total). (**H**) Representative lesion images from PBS or Ptx treated $Ptch^{+/-}$ mice. 13 lesions from each treatment group were stained for CollagenIV (red) and counterstained for Hoechst (blue), to quantify the ratio of non-vascularized (outlined in brown) and vascularized (outlined in green) lesions in the respective treatment groups (ratios and percentages indicated in white). Black bars in (**F-G**) represent the mean value and the scales are indicated in the figures.

5.3 B-cell depletion in $Ndp^{-/Y}$;$Ptch^{+/-}$ mice does not affect tumorigenesis

To explore the potential contribution of the early recruited B-cell population to tumorigenesis in $Ndp^{-/Y}$;$Ptch^{+/-}$ animals, we pharmacologically depleted the B-cell population from $Ndp^{-/Y}$;$Ptch^{+/-}$ animals with α-CD20 depleting antibodies. Based on flow cytometry of dissociated cerebellum (≈4-fold reduction – Figure 23A-B) and IHC analysis of lesion (Figure 23C), α-CD20 treatment significantly reduced the number of B-cells within the whole cerebellum compared to α-mIgG2A treated control animals. Interestingly, the systemic depletion of B-cells induced a reciprocal increase in the number of T-cells ($CD5^+$) in whole cerebellum dissociates (≈ 1.5-fold increase – Figure 23D), an observation which is consistent with the notion that the early recruited B-cells may play a role in establishing an immune suppressive environment in $Ndp^{-/Y}$;$Ptch^{+/-}$ animals. However, the depletion of the B-cell population did not alter overall survival, incidence, or latency, as compared to control α-mIgG2a treated animals or untreated $Ndp^{-/Y}$;$Ptch^{+/-}$ animals (Figure 23E). Taken together these results indicate that the early recruited B-cell population may play a role in establishing an immune suppressive environment, however, they are not driving the observed increase in tumorigenesis in the $Ndp^{-/Y}$;$Ptch^{+/-}$ animals.

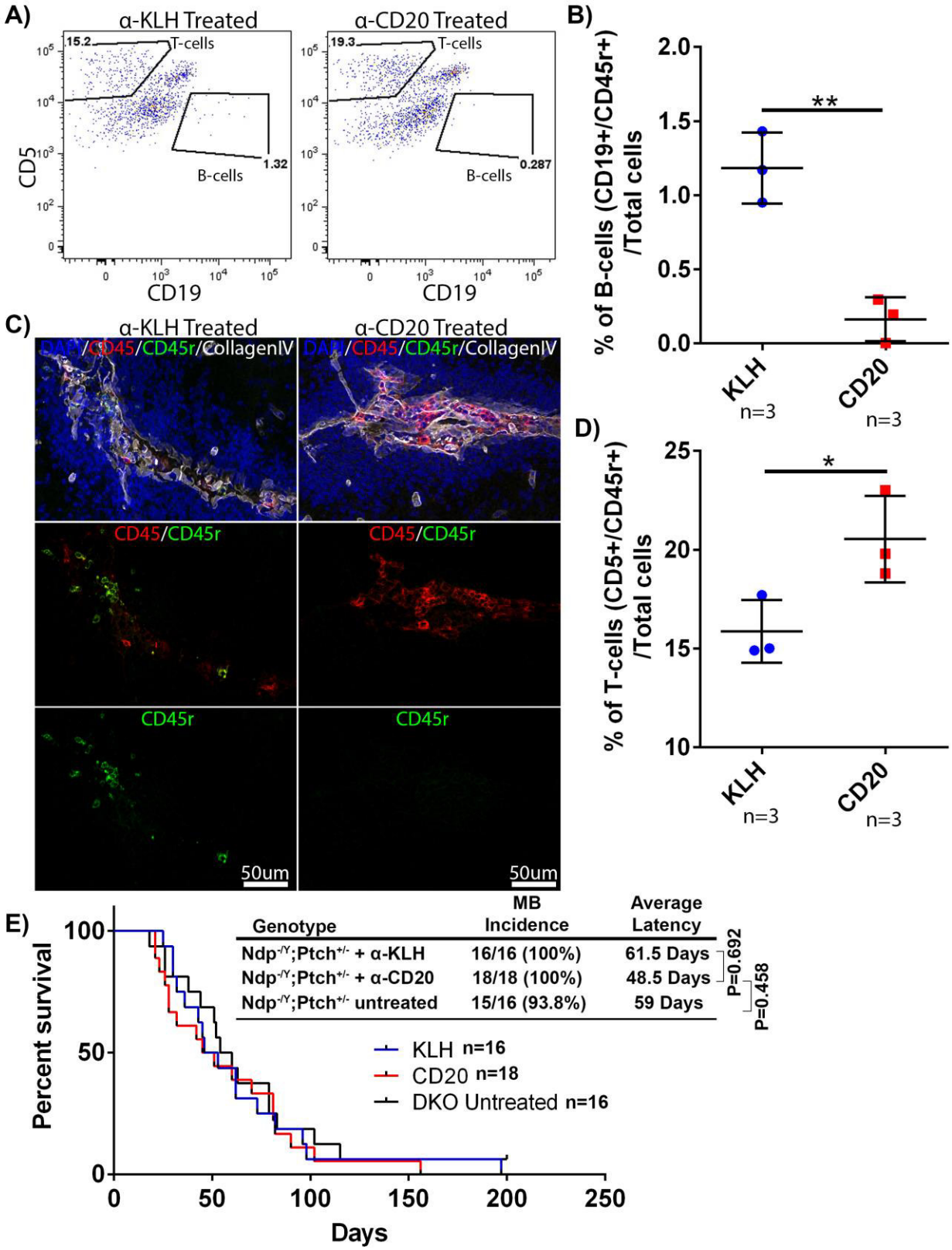
A)
α-KLH Treated
α-CD20 Treated
15.2
T-cells
1.32
B-cells
19.3
0.287
CD5
CD19
B)
% of B-cells (CD19+/CD45r+) /Total cells
**
KLH
CD20
n=3
C)
DAPI/CD45/CD45r/CollagenIV
CD45/CD45r
CD45r
50um
D)
% of T-cells (CD5+/CD45r+) /Total cells
*
E)
Percent survival
Days
Genotype
MB Incidence
Average Latency
Ndp-/Y;Ptch+/- + α-KLH
16/16 (100%)
61.5 Days
Ndp-/Y;Ptch+/- + α-CD20
18/18 (100%)
48.5 Days
Ndp-/Y;Ptch+/- untreated
15/16 (93.8%)
59 Days
P=0.692
P=0.458
KLH n=16
CD20 n=18
DKO Untreated n=16

<u>Figure 23.</u> B-cell depletion in Ndp-/Y;Ptch+/- animals does not alter survival.

(**A**) Flow dot plot illustrating the B-cell and T-cell population in dissociated cerebella from $Ndp^{-/Y}$;$Ptch^{+/-}$ animals treated with either α-CD20 depleting antibody (right) or isotype control α-KLH antibody (left). (**B**) Box plot of flow cytometry quantification of B-cells ($CD19^{+}/CD45^{+}$) normalized to all cells from whole cerebella dissociation preps from $Ndp^{-/Y}$;$Ptch^{+/-}$ that received the indicated treatment. (**C**) Immunohistochemistry of P14 $Ndp^{-/Y}$;$Ptch^{+/-}$ lesion treated with α-KLH (left) or α-CD20 (right), illustrating the recruited B-cells ($CD45R^{+}$ - green) and lymphocytes ($CD45^{+}$ – red). The Top image is a composite image of the staining beneath which includes the perivascular space (CollagenIV+ - white), and is counterstained with Hoechst (blue). (**D**) Box plot of flow cytometry quantification of T-cells ($CD5^{+}$;$CD45^{+}$) normalized to all cells from whole cerebella dissociation preparations from $Ndp^{-/Y}$;$Ptch^{+/-}$ that received the indicated treatment. (**E**) Kaplan-Meier survival curve of $Ndp^{-/Y}$;$Ptch^{+/-}$ treated with α-KLH, α-CD20 or untreated $Ndp^{-/Y}$;$Ptch^{+/-}$ animals. Right: Survival curve (**E**) related information, including sample sizes, the incidence and latency of the MB cases. *$p<0.05$, **$p<0.01$. Scale bars and number of biological replicates used (n) are indicated in the figures.

5.4 Loss of postnatal lymphatic vasculature following disruption of Ndp/Fzd4 signaling

The aberrant recruitment of lymphocytes in early $Ndp^{-/Y}$;$Ptch^{+/-}$ lesions could be due to active recruitment or alternatively, it could be indicative of a defect in lymphocyte trafficking, a function which is mediated by the lymphatic vasculature [292]. Lymphatic vasculature has recently been discovered within the dura meninges along the sinus vein [181, 182]. To characterize the lymphatic vasculature within the cerebellum, we stained serial sections of P14 $Ptch^{+/-}$ cerebella, containing intact pia meninges, with antibodies specific for Lymphatic Vessel Endothelial hyaluronan receptor 1 (Lyve-1^{+} - a known marker of functional lymphatic vessels) [293, 294], Isolectin (a pan vascular marker) and pan-Laminin (a basement membrane protein). We selected Laminin, as it is a component of every vascular basal membrane (endothelial, mural and the parenchymal basement membrane) [132]. We could readily detect lymphatic (Lyve-1^{+}) vasculature confined within the pia layer, on the apical surface (Figure 25B), and deep within the folds of the cerebellum in $Ptch^{+/-}$ animals (Figure 24B-C). We could also detect occasional examples of lymphatic vasculature found within the molecular layer of the cerebellum (Figure 24B – white arrows). We further corroborated this observation of lymphatic vasculature in the pia layer by co-staining Lyve-1 with an additional lymphatic vasculature specific marker Podoplanin (Pdpn) (Figure 24E).Blood vessels within the pia mater were surrounded by a thick basement membrane, which is a composite basement membrane composed of the blood vessel basement membrane and the basement membrane secreted from associated pericytes (Figure 24C white arrows) [143].Lymphatic vasculature was closely associated with blood vessels (Isolectin^{+}), similar to what has been observed in the dura mater [181, 182]. In the meninges, we could readily observe the lymphatic vasculature, which was surrounded by the parenchymal basement membrane. This basement membrane also surrounded blood vessels and delineated the outer layer of the perivascular space (Figure 24C blue arrow and Appendix A Figure 5). The current identity of

lymphatic vessels remains to be determined in our model, however, as we could not readily identify any intraluminal valves [181, 182], we speculate that the lymphatic vessels within the meninges are of the collector subtype [149]. In addition, we could identify meningeal lymphatic vessels expressing low levels of the vascular marker isolectin (Figure 25 C-D red arrows Figure 26C white arrow and white box), an observation which has been previously reported in brain lymphatic vessels with the vascular marker PECAM [182].

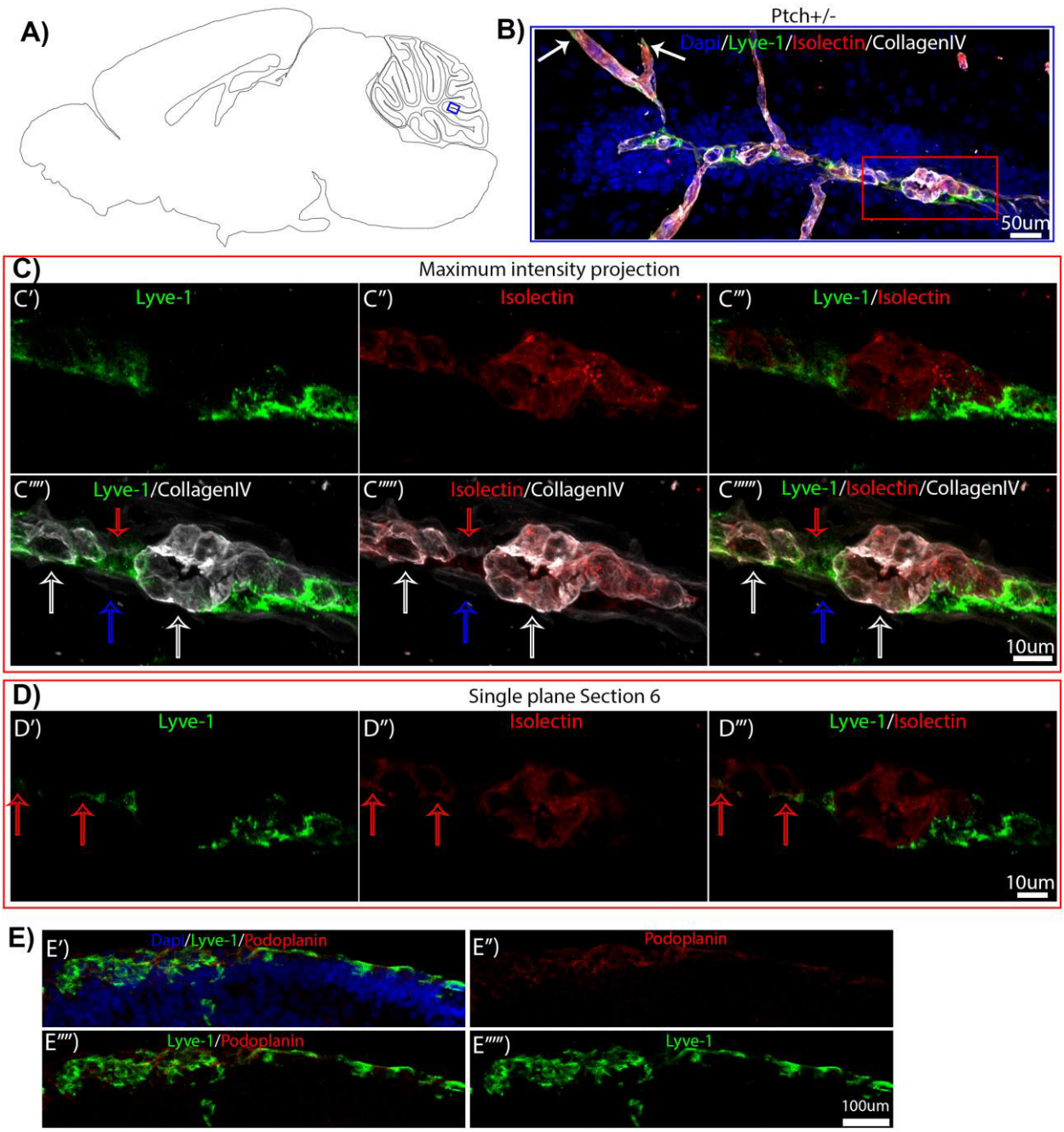
A)
B)
Ptch+/-
Dapi/Lyve-1/Isolectin/CollagenIV
50um
C)
Maximum intensity projection
C′)
Lyve-1
C″)
Isolectin
C‴)
Lyve-1/Isolectin
C⁗)
Lyve-1/CollagenIV
C⁗′)
Isolectin/CollagenIV
C⁗″)
Lyve-1/Isolectin/CollagenIV
10um
D)
Single plane Section 6
D′)
Lyve-1
D″)
Isolectin
D‴)
Lyve-1/Isolectin
10um
E)
E′)
Dapi/Lyve-1/Podoplanin
E″)
Podoplanin
E⁗)
Lyve-1/Podoplanin
E⁗′)
Lyve-1
100um

<u>Figure 24.</u> Lymphatic vasculature in the meningeal layer of the EGL in Ptch+/- cerebellum. (**A**) Schematic diagram of a sagittal sectioned mouse P14 brain, blue box illustrating the zoomed in section in (**B**). (**B**) Immunohistochemistry of P14 Ptch+/- EGL illustrating lymphatic vasculature (Lyve1^{+} - green), blood vasculature (isolectin – red), and basement membrane (CollagenIV – white) and counterstained with Hoechst (blue) White arrow denotes an example of lymphatic vasculature found within the molecular layer. Red box denotes location zoomed in (**C**) and (**D**). (**C**) Maximum intensity projection images of confocal z-stack illustrating lymphatic vasculature in the meningeal layer of the EGL. Red arrow denotes composite basement membrane which surrounds the blood vasculature, Blue arrow denotes the parenchymal basement membrane. Red arrow denotes lymphatic vasculature which also expresses blood vasculature marker isolectin. (**D**) Confocal single optical section images further illustrating the lymphatic which expresses a blood vessel marker isolectin – red arrow. (**E**) Immunohistochemistry of P14 Ptch+/- EGL corroborating lymphatic vasculature stain with two lymphatic markers Lyve-1 (green) and Podoplanin (red), top left is a composite image which also includes the counterstaining Hoechst (blue). We examined several neighboring sections from at least 3 different cerebella per genotype. Scale bars indicated in the figures.

To characterize the presence of the pia lymphatic vasculature within our different models, we performed sagittal serial sectioning of brains from all our mouse models (WT, $Ndp^{-/Y}$, $Ptch^{+/-}$, $Ptch^{+/-}$;$Ndp^{-/Y}$, Tie2-$Cre^{-/-}$;$Fzd4^{Flox/Flox}$, Tie2-$Cre^{+/-}$;$Fzd4^{Flox/Flox}$, $SmoA1^{+/-}$;$Ndp^{+/Y}$ and $SmoA1^{+/-}$;$Ndp^{-/Y}$) and stained them for the lymphatic marker Lyve-1. In the WT and Ptch+/- sections, we observed lymphatic vessels on the surface of the cerebellum and within the folds of the cerebellum (Figure 25B). Upon the loss of Ndp/Fzd4 signaling we could readily observe a loss of pia lymphatic vessels, which appeared exacerbated within the folds of the cerebellum as compared to the apical surface of the cerebellum (Figure 26B). Interestingly, the loss of lymphatic vessels appeared exacerbated when the Fzd4 receptor was removed from the vasculature (Tie2-$cre^{+/-}$;$Fzd4^{Flox/Flox}$) as compared to when the ligand was removed ($Ndp^{-/Y}$ and $Ptch^{+/-}$;$Ndp^{-/Y}$), highlighting partial compensation from other Wnts, which is lost upon the removal of the receptor Fzd4 (Figure 25B). This observation highlights the role for Ndp/Fzd4 signaling in cerebellar lymphatic vessel development. Furthermore, the loss of pia lymphatic vessels appeared to be exacerbated in the mouse model which has an enhanced gain-of-function for the Hh pathway as seen in the $SmoA1^{+/-}$;$Ndp^{-/Y}$ compared to the $Ndp^{-/Y}$;$Ptch^{+/-}$ mice (Figure 25B), implicating Hh signaling in pia lymphatic disruption. Collectively, these observations implicate both the Ndp/Fzd4 and Hh signaling in cerebellar lymphatic maintenance or development.

Given the observation that pia lymphatic vasculature appears to impact both Ndp/Fzd4 and Hh signaling, we focused our attention on characterizing the effect of Ndp signaling on lymphatic development within the context of aberrant Hh signaling (the $Ptch^{+/-}$ animal model). We focused on Ndp as its lymphatic modulatory function has never been described before, although Wnt signaling has previously been shown to be important in lymphatic development outside of the CNS [195]. In P14 $Ptch^{+/-}$ animals, the pia lymphatic vasculature is condensed, streamlined, and closely

associated to the blood vasculature (Figure 25C). This is in striking contrast to what was seen in the P14 $Ndp^{-/Y}$;$Ptch^{+/-}$ animals, where the pia lymphatic vasculature appeared to have a reduced and disorganized expression (Figure 25D). The observed $Ndp^{-/Y}$;$Ptch^{+/-}$ lymphatic vasculature exhibited an inconsistent staining pattern with several irregular protrusions or segments (Figure 25D – Blue arrows). The blood vessels ($Isolectin^{+}$) in $Ptch^{+/-}$ animals exhibited a normal morphology, where the vasculature was completely encapsulated by a thick basement membrane (Figure 24C – white arrows and Figure 25C). Interestingly, $Ndp^{-/Y}$;$Ptch^{+/-}$ animals exhibited several examples of blood vessels ($Isolectin^{+}$) that were not surrounded by a basement membrane (Figure 25D – red arrow), some of which also expressed low levels of the lymphatic marker ($Lyve\text{-}1^{+}$) (Figure 25D - white box). This might be an example of lymphatic vessels that are trans-differentiating or switching fate back into blood vessels [99, 139, 189-191].

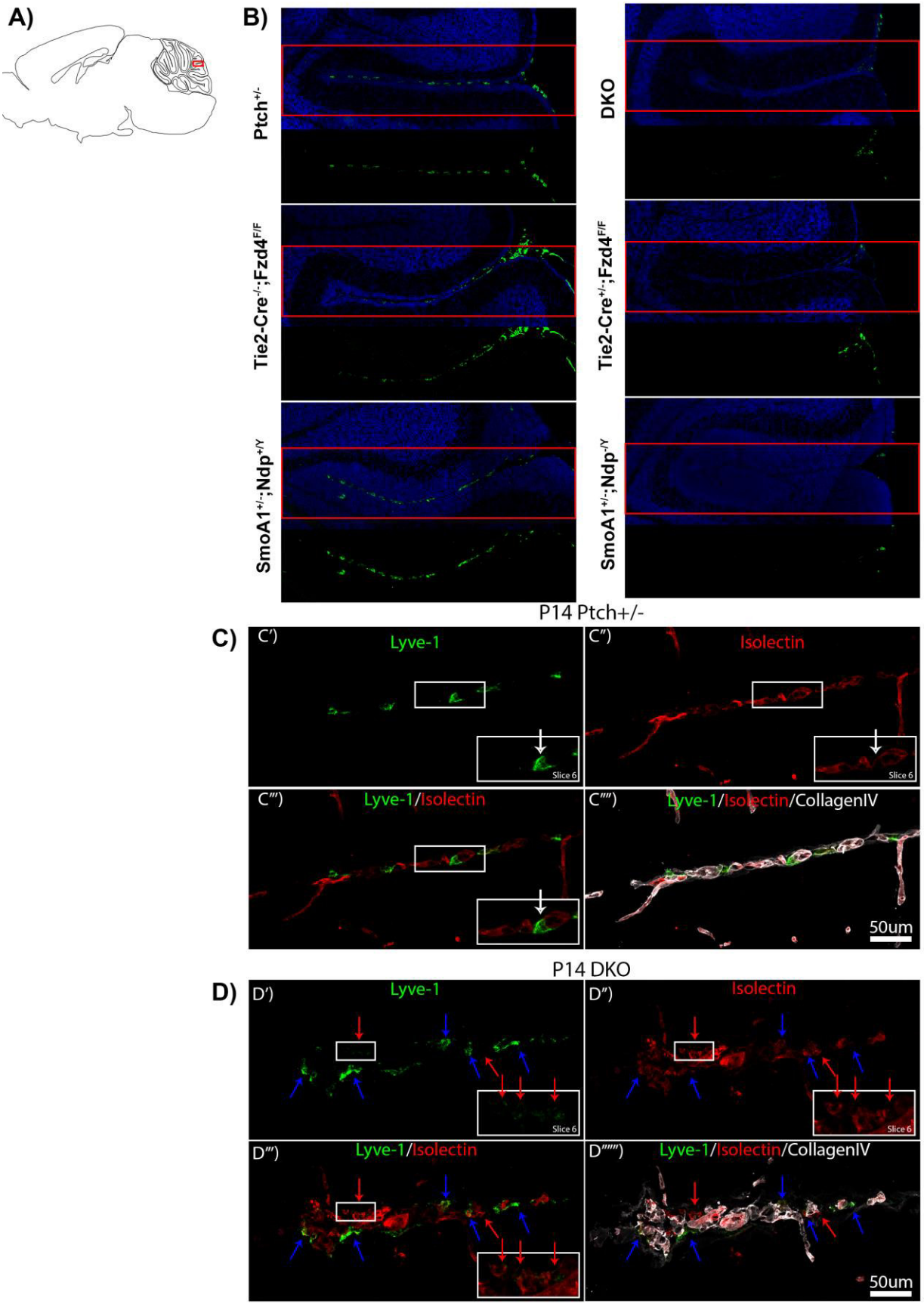
A)
B)
Ptch+/-
DKO
Tie2-Cre-/-;Fzd4F/F
Tie2-Cre+/-;Fzd4F/F
SmoA1+/-;Ndp+/Y
SmoA1+/-;Ndp-/Y
P14 Ptch+/-
C)
C′)
Lyve-1
C″)
Isolectin
Slice 6
C‴)
Lyve-1/Isolectin
C⁗)
Lyve-1/Isolectin/CollagenIV
50um
P14 DKO
D)
D′)
Lyve-1
D″)
Isolectin
Slice 6
D‴)
Lyve-1/Isolectin
D⁗)
Lyve-1/Isolectin/CollagenIV
50um

<u>Figure 25.</u> Lymphatic defect is enhanced by aberrant Hh and the disruption of Ndp signaling. (**A**) Schematic diagram of a sagittal sectioned mouse P14 brain, blue box illustrating the zoomed section in (**B-D**). Immunohistochemistry of lymphatic vasculature (Lyve-1^+ - green) from all mouse lines, illustrating the enhanced lymphatic defect by aberrant Hh, and the disruption of Ndp signaling. The red square denotes the area of the immunohistochemistry staining that is focused in on the below lymphatic only image (Lyve-1^+ - green). The reduction in lymphatic vasculature within the fold of the cerebellum correlates with an increase in Evans Blue extravasation (Figure 21A). (**C**) Representative image of the maximum intensity projection images of P14 $Ptch^{+/-}$ EGL illustrating lymphatic vasculature (Lyve-1^+ - green), which is tightly associated with the blood vasculature ($Isolectin^+$ – red) and confined within the basal membrane ($Laminin^+$ – white). The lymphatic vasculature expresses low levels of Isolectin, highlighted by the white arrow, and further exemplified by the white box, which is a confocal single optical section image. (**D**) Maximum intensity projection images of P14 $Ndp^{-/Y}$;$Ptch^{+/-}$ EGL illustrating lymphatic vasculature (Lyve-1^+ - green), which is highly disorganized (blue arrows). The red arrows denote several examples of blood vessels that are not surrounded by a basement membrane ($Laminin^+$ - white). Some of these blood vessels also express low levels of the lymphatic marker (red arrows), further highlighted by the white box, which is a confocal single optical section image. We examined several neighboring sections from at least 3 different cerebella per genotype. Scale bars indicated in the figures.

The lymphatic defect observed in $Ndp^{-/Y}$;$Ptch^{+/-}$ animals at P14 could result from two sources. First, lymphatic vasculature could fail to develop, or alternatively, they could regress, which could be a function of selective lymphatic death or re-specification to veins. To further explore these two possibilities, we serial sectioned P0, P7 and P14 $Ptch^{+/-}$ and $Ndp^{-/Y}$;Ptch+/- cerebellum and stained selected sections for lymphatic vessels (Lyve-1+) and blood vessels (Isolectin+). Using a confocal microscope, we imaged the entire cerebellum (confocal Z-stack tile scans) and by using the rendered maximum intensity projection images, we performed a temporal quantitative analysis of the lymphatic and blood vasculature within the EGL/meningeal layer (Figure 26B) by quantifying the pixel density of the Lyve-1 and Isolectin stain. Using this data we could subsequently plot the lymphatic vascular density, which was normalized to the blood vascular density ($Lyve\text{-}1^{+}$ pixels/$Isolectin^{+}$ pixels) over time. In addition, we plotted the individual vessel pixel abundances ($Lyve\text{-}1^{+}$ pixels and $Isolectin^{+}$ pixels) separately in order to examine the respective increase in abundance or potential alterations over time. During early postnatal development (P0), the lymphatic vessels were confined to the apical surface of the developing cerebellum in both $Ptch^{+/-}$ and $Ndp^{-/Y}$;$Ptch^{+/-}$ animals (Figure 26A). P0 $Ptch^{+/-}$ and P0 $Ndp^{-/Y}$;$Ptch^{+/-}$ littermates had nearly identical lymphatic ($Lyve\text{-}1^{+}$ pixels – Figure 26D) and blood ($Isolectin^{+}$ pixels – Figure 26D) vessel abundances. Futhermore, lymphatic densities ($Lyve\text{-}1^{+}$ pixels/$Isolectin^{+}$ pixels) were also comparable between genotypes (Figure 26C). In P7 $Ptch^{+/-}$ mice, we detected a slight, but not significant reduction in the lymphatic density ($Lyve\text{-}1^{+}$/$Isolectin^{+}$) as compared to P0 $Ptch^{+/-}$ samples (Figure 26C). This reduction in lymphatic vessel density ($Lyve\text{-}1^{+}$/$Isolectin^{+}$) was attributed to a delay in the increase in blood vessel abundance ($Isolectin^{+}$ Pixels) (Figure 26D) as compared to relative paucity in lymphatic vessel abundance ($Lyve\text{-}1^{+}$ Pixels) (Figure 26D). In P7 $Ndp^{+/-}$;$Ptch^{+/-}$ samples there was also a slight, non-significant, reduction in

lymphatic density (Lyve-1^{+}/Isolectin^{+}) as compared to P0 Ndp$^{-/Y}$;Ptch$^{+/-}$ samples, and a reduction in lymphatic density that was slightly more pronounced, although non-significant, as compared to the P7 Ptch$^{+/-}$ samples (Figure 26C). Again, this observed reduction in lymphatic vessel density was attributed to a delay in increased blood vessel abundance (Isolectin^{+} pixels) (Figure 26D) as compared to lymphatic vessel abundance (Lyve-1^{+} pixels) (Figure 26D). In the P14 Ptch$^{+/-}$ samples, the lymphatic vascular density (Lyve-1^{+}/Isolectin^{+}) was similar to what was seen in the P0 Ptch$^{+/-}$ samples. This was attributed to the proportionate increase in lymphatic vasculature (Lyve-1^{+} pixels) and blood vasculature (Isolectin^{+} pixels) abundance (Figure 26D). This is in contrast to what was seen in the P14 Ndp$^{-/Y}$;Ptch$^{+/-}$ samples, in which the lymphatic vascular density (Lyve-1^{+}/Isolectin^{+}) was lower than in all other ages and genotypes (Figure 26C). This reduction in lymphatic vascular density (Lyve-1^{+}/Isolectin^{+}) was attributed to a reduction in lymphatic vasculature abundance (Lyve-1^{+} pixels) (Figure 26D), which was further exacerbated by a slight, non-significant, increase in blood vessel abundance (Isolectin^{+} pixels) (Figure 26D). The observed reciprocal increase in blood vessel abundance (Isolectin^{+} pixels) and decrease in lymphatic vessel abundance (Lyve-1^{+} pixels) suggests that lymphatic vessels are trans-differentiating back into blood vascular ECs, an observation which is reminiscent of previously described blood vessels that express low levels of the lymphatic marker Lyve-1 (Figure 25D).

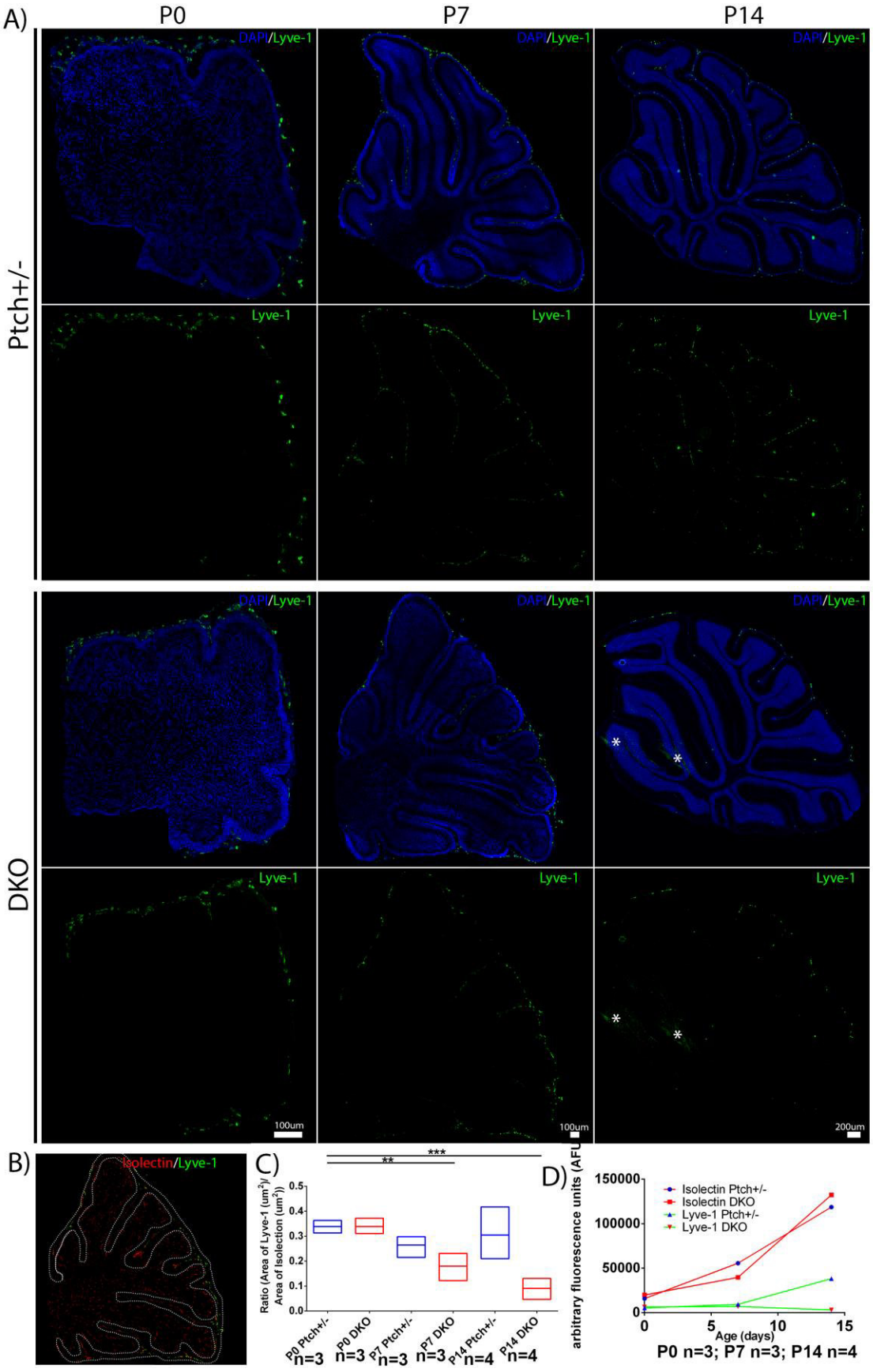
A)
P0
P7
P14
Ptch+/-
DKO
DAPI/Lyve-1
Lyve-1
100um
100um
200um
B)
Isolectin/Lyve-1
C)
***
**
Ratio (Area of Lyve-1 (um²)/ Area of Isolection (um²))
0.5
0.4
0.3
0.2
0.1
0.0
P0 Ptch+/- n=3
P0 DKO n=3
P7 Ptch+/- n=3
P7 DKO n=3
P14 Ptch+/- n=4
P14 DKO n=4
D)
arbitrary fluorescence units (AFU)
150000
100000
50000
0
Isolectin Ptch+/-
Isolectin DKO
Lyve-1 Ptch+/-
Lyve-1 DKO
0
5
10
15
Age (days)
P0 n=3; P7 n=3; P14 n=4

<u>Figure 26.</u> Temporal loss of lymphatic vessels in the cerebellum of Ndp-/Y;Ptch+/- as compared to Ptch+/- animals.

(**A**) Confocal maximum intensity projection images of $Ndp^{-/Y}$;$Ptch^{+/-}$ and $Ptch^{+/-}$ sagittal cerebella sections at P0, P7 and P14 stained for lymphatic vessels (Lyve-1^{+} - green) and counterstained with Hoechst (blue). (**B**) Representative image illustrating the method of quantification that was used, quantifying the lymphatic (Lyve-1^{+} - green) and blood vessel (Isolectin^{+} - red) density strictly in the EGL (white dotted line). (**C**) Quantification of the area ratio of lymphatic (Lyve-1^{+} - green) density normalised to the blood vessel (Isolectin^{+} - red) density in P0, P7 and P14 Ptch+/- and $Ndp^{-/Y}$;$Ptch^{+/-}$ littermates, with 3 to 4 biological replicates, composed of 2-3 images per replicate. (**D**) Plot of the quantified arbitrary fluorescent units for isolectin (red lines) and lyve-1 (green lines) for each genotype at the specified ages, illustrating the progressive loss of lymphatic vasculature between P7 and P14, and the reciprocal slight increase in blood vessel vasculature. White asterisk denotes background in the image, scales are indicated in the figures. * = $P<0.05$, ** = $P<0.01$, *** = $P<0.001$

The observed lymphatic defect in P14 $Ndp^{-/Y}$;$Ptch^{+/-}$ animals as compared to P14 $Ptch^{+/-}$ animals shows a temporal loss of lymphatic vasculature during early postnatal development (Figure 26A-C), an observation which is reminiscent of dermal lymphatic loss during early postnatal development following embryonic deletion of Wnt5a [197]. We further corroborated these results by performing qRT-PCR on P14 whole cerebellar and P14 dissected pia meninges from $Ptch^{+/-}$ and $Ndp^{-/Y}$;$Ptch^{+/-}$ littermates. In whole cerebella qRT-PCR, we observed a significant reduction in the expression of the lymphatic vessel marker Lyve-1 in $Ndp^{-/Y}$;$Ptch^{+/-}$, as compared to $Ptch^{+/-}$ samples (Figure 27G). Furthermore, in pia meninges-specific qRT-PCR, we observed a significant reduction in the expression of the lymphatic vessel marker Lyve-1 and VEGFR3 in $Ndp^{-/Y}$;$Ptch^{+/-}$ as compared to Ptch+/- samples. Interestingly, the qRT-PCR results from the meninges samples showed a slight, but not significant up-regulation in the vein specific marker EMCN in $Ndp^{-/Y}$;$Ptch^{+/-}$ as compared to Ptch+/- samples (Figure 27H). These results further support the observation of a lymphatic vessel defect in P14 $Ndp^{-/Y}$;$Ptch^{+/-}$ as compared to $Ptch^{+/-}$ animals, which is temporally acquired during early postnatal life. Our current data indicates that the loss of lymphatic vasculature may be due to lymphatic vessel fate-switching towards a venous fate.

Previously, we correlated a reduction in both Ndp (Figure 6F) and Fzd4 expression (Figure 9B) with $Ptch^{+/-}$ tumor progression. We also correlated a reduction in vascular canonical Wnt signaling (Figure 19A) with the vascularization of $Ptch^{+/-}$ lesion (Figure 19A-B). Both of these observations highlight a potential role for loss of vascular Wnt signaling in MB progression. As Wnt signaling has been shown to be involved in the expression of the lymphatic master regulator Prox-1 [189], we investigated whether the reduction in lymphatic density also correlates with lesion progression. This investigation was performed by quantifying the lymphatic/vascular

density in P14 $Ndp^{-/Y}$;$Ptch^{+/-}$ as compared to $Ptch^{+/-}$ littermates, within the meningeal layer (Figure 27A-E) of normal untransformed EGL, non-vascularized, and vascularized lesions. In $Ndp^{-/Y}$;$Ptch^{+/-}$ animals, we observed a reduced lymphatic density that was independent of the area examined (normal EGL, non-vascularized and vascularized lesions), as compared to $Ptch^{+/-}$ normal EGL samples (Figure 27B-E). Interestingly, we observed a stepwise decrease in lymphatic density as a function of $Ptch^{+/-}$ lesion vascularization, an expression pattern that appears to positively correlates with previously reported reduction in canonical Wnt signaling (Lef1) (Figure 19A-B). These results highlight a potentially novel role for Norrin signaling in cerebellar lymphatic maintenance, and a novel role for lymphatic vasculature in promoting the establishment of a tumor suppressive micro-environment.

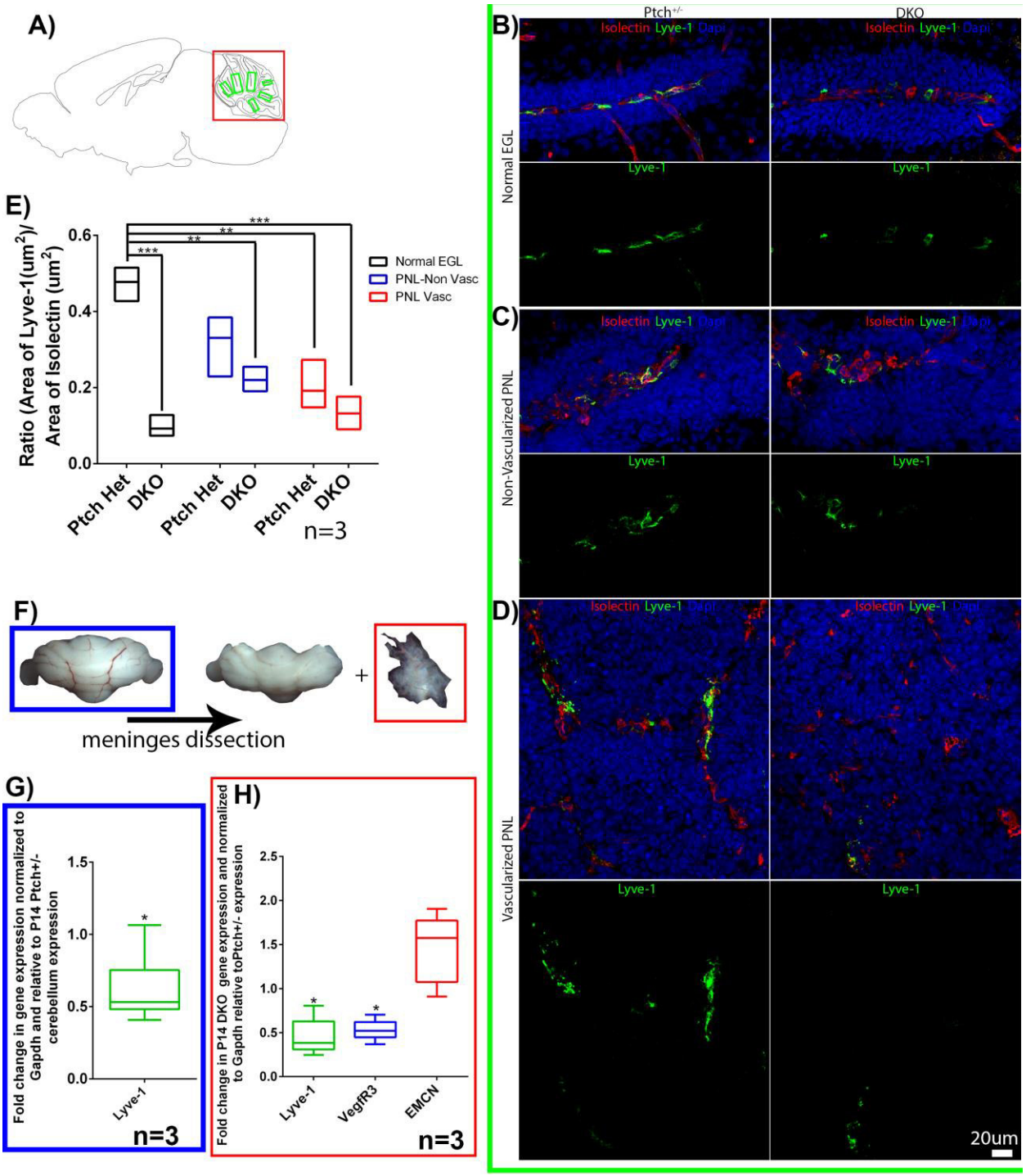
A)
B)
Ptch+/-
DKO
Isolectin Lyve-1 Dapi
Lyve-1
Normal EGL
C)
Non-Vascularized PNL
D)
Vascularized PNL
20um
E)
Ratio (Area of Lyve-1(um2)/ Area of Isolectin (um2)
0.6
0.4
0.2
0.0
***
**
**
***
Normal EGL
PNL-Non Vasc
PNL Vasc
Ptch Het
DKO
Ptch Het
DKO
Ptch Het
DKO
n=3
F)
meninges dissection
G)
Fold change in gene expression normalized to Gapdh and relative to P14 Ptch+/- cerebellum expression
1.5
1.0
0.5
0.0
*
Lyve-1
n=3
H)
Fold change in P14 DKO gene expression and normalized to Gapdh relative toPtch+/- expression
2.5
2.0
1.5
1.0
0.5
0.0
*
*
Lyve-1
VegfR3
EMCN
n=3

<u>Figure 27.</u> Vascularization of Ptch+/- lesions are associated with a reduction in lymphatic vascular density.

(**A**) Schematic diagram of a sagittal sectioned mouse P14 brain, green box illustrating the cerebellar folds which were utilized in subsequent analysis in (**B-E**). (**B-D**) Immunohistochemistry of P14 $Ptch^{+/-}$ and $Ndp^{-/Y}$;$Ptch^{+/-}$ (**B**) normal EGL, (**C**) non-vascularized lesion and (**D**) vascularized lesion illustrating the lymphatic vasculature (Lyve-1^{+} - green), blood vasculature (Isolectin^{+} – red) and counterstained with Hoechst (blue). (**E**) Quantification of the area ratio of lymphatic (Lyve-1^{+} - green) density normalized to the blood vessel (Isolectin^{+} - red) density in the cerebella fold of P14 $Ptch^{+/-}$ and $Ndp^{-/Y}$;$Ptch^{+/-}$ littermates, within the normal EGL, non-vascularized lesion and vascularized lesion. The presented quantification represents 3 biological replicates per sample, composed of 3 analyzed and averaged images per replicate. (**F**) Whole cerebella were removed from P14 $Ptch^{+/-}$ and $Ndp^{-/Y}$;$Ptch^{+/-}$ animals and (**G**) the whole cerebella were used for qRT-PCR or the (**H**) dissected pia meninges were used for qRT-PCR. (**G**) Box plots of qRT-PCR analysis of Lyve-1 expression in whole cerebellar samples isolated from P14 $Ndp^{-/Y}$;$Ptch^{+/-}$ animals and normalized to P14 $Ptch^{+/-}$ littermate expression. (**H**) Box plots of qRT-PCR analysis of Lyve-1, VEGFR3 and EMCN expression in whole cerebellar samples isolated from $Ndp^{-/Y}$;$Ptch^{+/-}$ animals and normalized to P14 $Ptch^{+/-}$ littermate expression. Scales are indicated in the figures. * = $P<0.05$, ** = $P<0.01$, *** = $P<0.001$

Collectively, these results highlight a novel role for Ndp/Fzd4 signaling in cerebellar postnatal lymphatic vessel development and maintenance. The disruption of Ndp/Fzd4 signaling drives the progressive loss in pia meninges, in what is currently believed to be an example of lymphatic ECs fate switching back towards a blood vessel endothelial cell fate.

Chapter 6. Discussion

6.1 Ndp is a novel link between stromal signaling and MB initiation

In tumors with multi-stage progression, such as pancreatic, breast and medulloblastoma (MB), the interactions of the tumor with its surrounding stroma have gained widespread acceptance as an essential process for tumor progression [242, 243, 295]. However, very little is known about the stromal contributions to MB initiation and progression. By taking advantage of the well characterized multistage progression of MB in the $Ptch^{+/-}$ mouse model, we uncovered a novel and previously undescribed angiogenic contribution from the microenvironment to CNS tumorigenesis. Our investigation into the cellular mechanism responsible for this revealed that ECs are the source of potent tumor inhibitory signal(s) which acts during both early preneoplasia formation, and oncogenic progression. We have also shown that the tumor suppressive signal(s) is regulated by the endogenous neuronal to endothelial Norrin/Fzd4 signaling pathway. The importance of Wnt signaling in modulating vasculature in brain malignancies has been previously illustrated in human glioma samples, where conditionally-activated Wnt signaling normalized the vasculature, and reduced tumor growth [157]. An additional example is seen in Wnt-MB samples, which secrete Wnt inhibitors to effectively disrupt the BBB, leading to excessive brain hemorrhaging [296]. The aforementioned studies highlight the importance of tumor-endothelial Wnt signaling in the established carcinoma. In the work presented here, we elaborate the understanding of this concept, and illustrate the importance of stromal Wnt signaling during the earliest events of tumorigenesis in Shh-driven MB.

6.2 Norrin/Fzd4 signaling in human MB and its involvement in progression

The results from human MB micro-array showed a trend towards a reduction in survival in patients with Shh-MB with the lowest (10^{th} percentile) expression of NDP, as compared to the highest (10^{th} percentile). This result would argue for a protective role for Ndp/Fzd4 signaling in

human Shh-MB. Despite this result, we observed Shh-MB as the subgroup with the highest expression of NDP as compared to all other MB subgroups. This apparent contradictory result can be rationalised by several potential explanations. Firstly, the abundance of mRNA is not always a reliable indicator of pathway activation, as NDP might not be heavily regulated at the mRNA level. Rather, this could occur at the translational level or at the level of post-translational stability, as seen for Myc [297] and HIFα [298], respectively. Secondly, NDP, a protein which has been shown to associate with the ECM [83], could be regulated at the level of its bioavailability, such as VEGF and FGF [299]. Thirdly, knowing that human and mouse MB tumors are very heterogeneous, typically arising from multifocal competing clones that evolve over time [300, 301], the expression profile observed in the established MB may not be reflective of early initiating events. Finally, the expression of Ndp in established MB may be slightly protective, since a reduction in Ndp signaling, as seen in our mouse model ($Ndp^{-/Y}$;$Ptch^{+/-}$), may disrupt the BBB, allowing pro-tumor mitogens [302] to exit the circulation and drive tumor progression [157], effectively reducing patient survival. Given the known role for Wnt signaling in CNS vascular development [137] and the role of Ndp/Fzd4 signaling in mediating neuronal-endothelial crosstalk in the cerebellum [97, 240], our presented work exemplifies the need to further investigate the role of Ndp/Fzd4 signaling in mouse and human MB progression.

6.3 The stromal compartment involvement in Ptch+/- MB initiation and progression

In $Ptch^{+/-}$ mice, MB tumorigenesis is governed by two defining features, the incidence, which is the prevalence of the disease within a population, and the latency, which is the rate at which the disease progresses. Several factors which increase DNA damage [253, 254, 303] and proliferation [254, 264, 265] have been shown to alter incidence and latency [26, 304-306]. However, much less is known about factors or events which influence the formation of

preneoplastic lesions and their subsequent transformation. It has been shown that lesion formation in $Ptch^{+/-}$ animals can be modulated by known growth or differentiation regulators (e.g. Igf1, Ccnd1 and Tis21) [254, 264, 265] in addition to events which enhance DNA damage (e.g. radiation) or prevent their subsequent resolution [252, 253, 303]. However, lesion progression to carcinogenesis is enhanced by pro-proliferative factors (e.g. Igf2, Mycn, Boc) and by factors that promote evasion of p53-induced senescence [217, 251, 271, 307, 308]. The present study adds another factor to the aforementioned list, the pro-tumor microenvironment. We showed that disruption of Ndp/Fzd4 signaling in ECs generates a tumor promoting effect(s) which is associated with the acquisition of a pro-tumor stroma. Furthermore, we showed that the disruption of Ndp/Fzd4 signaling promotes increased GNP proliferation and DNA damage, events which have been shown to increase the incidence and reduce the latency of MB in $Ptch^{+/-}$ mice [252, 253, 271, 304, 305]. Interestingly, the conversion to LOH and ligand-independent pathway activation is an important step for tumorigenesis [218, 307], although it is not sufficient for complete transformation and progression, as shown by Ptch1 null GNPs which can properly differentiate and integrate into the IGL [218], illustrating the requirement for additional signals or events. The presented data add to the growing body of literature which highlights the contributions of a pro-tumor microenvironment towards lesion initiation and subsequent transformation [212].

At this point it is worth highlighting some of the observed differences between the survival curves of the different mouse lines. We observed a greater reduction in survival in animals where we deleted the receptor ($Tie2\text{-}Cre^{+/-};Fzd4^{Flox/Flox};Ptch^{+/-}$) as compared to the ligand ($Ndp^{-/Y};Ptch^{+/-}$). We can rationalize that this difference in survival is due to partial compensation in $Ndp^{-/Y};Ptch^{+/-}$ from other Wnt ligands (such as Wnt3a and Wnt5a [238, 239]), which are expressed in GNPs and which have been shown in the literature to bind to Fzd4. However, this compensation is lost upon

the deletion of the receptor (Tie2-Cre$^{+/-}$;Fzd4$^{Flox/Flox}$;Ptch$^{+/-}$), potentially explaining the observed reduction in survival. This compensation from other Wnts upon the loss of Ndp has been previously reported with the exacerbated BBB defect upon the deletion of the Fzd4 receptor from the vasculature as compared to the embryonic deletion of Ndp [84].

6.4 Lesion progression is associated with a reduction in vascular Wnt signaling

In the presented study we examined the stromal influence on the activation of the angiogenic program in early lesions. This was performed by examining the effects of a known neuronal secreted Wnt ligand, Norrin, on canonical Wnt signaling in vascular endothelium and the resulting impact on BBB maintenance and vascular quiescence [84, 137]. Ourresults suggest that the local reduction in Wnt signaling in vascular ECs and vascular invasion are endogenous events, which regulate lesion progression in Ptch$^{+/-}$ animals. This result is consistent with the observation of a step-wise reduction in Norrin expression as a function of tumor progression. By using a mouse line which can expresses a Wnt inhibitors (DKK-1 or SFRPs) specifically in ECs (Tie2-cre^{+}) on the Ptch$^{+/-}$ background, we could further dissect the role of canonical Wnt signaling in the endothelium in Ptch$^{+/-}$ lesion initiation and progression.

6.5 Characterization of the tumor promoting preneoplastic niche

In multi-stage tumors, progression will typically begin with a preneoplastic cell acquiring the ability to maintain its proliferative ability, negating the normal inhibitory cues through the sustained activation of a mitogenic pathway (in Ptch mice it is the Hh pathway), and inactivation of tumor suppressor genes. Nevertheless, for a lesion to progress to a tumor with invasive properties and sustained growth, it requires the recruit and conversion of the normal neighboring stroma cells (e.g. ECs, fibroblast, leukocytes, etc.) to create a tumor promoting microenvironment

[309]. The different cell types that compose the stroma have been shown to possess the ability to modify the tumor microenvironment through various mechanisms, rendering the bidirectional communication between the stroma and preneoplastic cells very important, as it can inhibit and modulate the evolution of the lesion [242, 243, 295, 309]. In the present study we explored the microenvironment of the early preneoplastic lesion at the earliest time during which we could consistently detect lesions in the cerebellum of $Ptch^{+/-}$ animals, which was P14. In the P14 $Ndp^{-/Y}$;$Ptch^{+/-}$ as compared to $Ptch^{+/-}$ littermates, we could readily observe 5 predominant stromal alterations: 1) activated angiogenic program, 2) ECM remodeling and deposition, 3) immune cell infiltration, 4) open BBB and 5) meningeal lymphatic defect. Except for the lymphatic defect, these are all stromal alterations which have been shown to have tumor promoting effects in various tissues [33, 41, 157, 277, 288, 310-312]. To dissect the molecular mechanism promoting tumorigenesis upon Ndp/Fzd4 disruption, we modulated the different stromal phenotypes independently, and assessed their impact on tumorigenesis.

6.6 Activated Angiogenic Switch

In several mouse models of tumors with multistage progression, such as pancreatic and breast cancer, the recruitment of the blood vessels has been shown to happen prior to the progression of the neoplasia, highlighting the importance of the angiogenic switch as a potential rate-limiting step in malignant progression [241, 243, 244, 313]. Disruption of Ndp/Fzd4 signaling activated the angiogenic program in the early lesion, as seen by 1) the increase in the proportion of angiogenic lesions, 2) the increase in the vascular density of lesions, 3) the increase in the number of proliferating ECs and 4) the increase in Ang2 expression. Initially we targeted VEGF-A, a molecule which is normally responsible for initiating the angiogenic cascade [107, 118, 119] and which has a known role in suppressing the anti-tumor immune response [314]. We initially

treated $Ndp^{-/Y}$;$Ptch^{+/-}$ systemically with a monoclonal α-VEGF-A blocking antibody, however, our investigations revealed no difference in the proportion of lesions that underwent an angiogenic switch in $Ndp^{-/Y}$;$Ptch^{+/-}$ animals treated with anti-VEGF-A compared with controls littermates (Bassett and Tokarew, unpublished data). One explanation for the lack of effect of the VEGF-A blockade on lesion vascularity is compensation from other cell types. VEGF-A is secreted by a whole host of cell types, including tumor cells [315], bone derived monocytes [308], fibroblast [316] and other immune cells [317]. It is conceivable that the dose of functional blocking antibodies was not sufficient to neutralize all VEGF-A activity within the lesions. An alternative possibility is that VEGF-A blockade was compensated by the upregulation or activation of VEGF-A-independent angiogenic pathways [41]. To circumvent this issue, we targeted Angiopoietin-2 (Angpt2) with a monoclonal blocking antibody. Angpt2 is an potent angiogenic activator, which is predominantly secreted by ECs and some cancer cell subtypes [318], and the corresponding gene is up-regulated in $Ndp^{-/Y}$;$Ptch^{+/-}$ tumors. Treating $Ndp^{-/Y}$;$Ptch^{+/-}$ mice with α-angpt2 effectively impaired angiogenesis *in vivo*, as seen in whole retina flat mounts. Furthermore, α-angpt2 treatment significantly reduced the vascular density in the lesions, presumably by preventing angiogenic activation and by promoting vascular regression or "pruning" of novel immature blood vessels [319]. In addition, this treatment reduced the ECM deposition in $Ndp^{-/Y}$;$Ptch^{+/-}$ lesions. α-Angpt2 treatment also significantly reduced overall survival of the Angpt2 as compared to mIgG2A treated mice. Meanwhile, the latency was reduced and incidence was comparable in Angpt2 as compared to mIgG2A treated animals. Furthermore, $SmoA1^{+/-}$;$Ndp^{+/Y}$ and $SmoA1^{+/-}$;$Ndp^{-/Y}$ mice had a highly vascularized hyperplastic EGL but their respective survival curves were significantly different, further arguing against the activation of the angiogenic program as the stromal alteration which is responsible for the observed increase in tumorigenesis.

The significant reduction in latency and the non-significant decrease in latency in the α-Angpt2 treated $Ndp^{-/Y}$;$Ptch^{+/-}$ as compared to control animals could represent the selective pressure on lesions to utilize alternative angiogenic programs [277]. In the presence of Angpt2 inhibition, the lesions could be utilizing alternative angiogenic programs to activate the angiogenic switch [243, 320], essentially selecting for pro-angiogenic lesions, and accelerating subsequent tumor progression. This event has been observed with the prolonged use of an anti-angiogenic drug in pre-clinical models [321]. Taken together, these results argue that the activation of the angiogenic program upon Ndp/Fzd4 disruption is not the predominant driving force behind the observed increase in MB. To further determine any potential role of angiogenesis in MB, we will drive angiogenesis by expressing pro-angiogenic factor (VEGF-A) in GNPs (Atoh1-Cre^{+}) on the $Ptch^{+/-}$ background. In addition, we could corroborate this approach by driving the expression of VEG-A in GNPs by intracranial injections of retroviruses encoding the VEGF-A transcript. Finally, we could perform a combinatorial α-VEGF and α-Angpt2 treatment to further reduce angiogenic activation in $Ndp^{-/Y}$;$Ptch^{+/-}$ in order to assess the potential effects of a more substantial angiogenic blockade on lesion initiation and progression.

6.7 Stem cells

A particular cell population which is closely associated to the vasculature and which is particularly sensitive to secreted components from the vasculature and its associated ECM is the stem cell population [257, 322]. Stem cells are particularly interesting as the $Sox2^{+}$ cancer stem cell (CSC) population in $Ptch^{+/-}$ mice has been shown to provide chemotherapy resistance and to drive tumor regrowth following treatment [230]. Furthermore, there is a known population of $Nestin^{+}$ (a neuronal stem cell marker [323]) progenitor cells located within the GNP layer of the cerebellum that is particularly sensitive to genomic instability [256]. Given their proximity to the

vasculature, and their known involvement in $Ptch^{+/-}$ MB, we investigated the stem cell compartment. We analyzed the stem cell pool and their self-renewal capacity by performing neurosphere assays on P16 $Ndp^{-/Y}$;$Ptch^{+/-}$ and $Ptch^{+/-}$ littermates [324]. The primary neurosphere assay revealed a non-significant trend towards a reduction in the frequency of stem cells in the $Ndp^{-/Y}$;$Ptch^{+/-}$ cerebellum. The secondary neurosphere assay revealed a non-significant trend towards a reduction in the self-renewal capacity of the established neurospheres. Although we cannot completely rule out the stem cell population as a potential driver for tumorigenesis in $Ndp^{-/Y}$;$Ptch^{+/-}$ mice, it is important to point out that the role of cancer stem cells is predominantly studied in the context of established tumors [322, 325, 326] and very little is known about its role in lesion initiation and progression [326, 327]. Since DNA damage has been associated with stem cell dysfunction and carcinogenesis [328] and we showed an increase in the amount of DNA in affected GNP cells, a particularly interesting cell population to investigate further would be the $Nestin^{+}$ population, which is a cell population particularly sensitive to DNA damage. To explore any potential contribution from the $Nestin^{+}$ stem cell population towards MB in $Ndp^{-/Y}$;$Ptch^{+/-}$ mice we could generate a new line to selectively eliminate the $Nestin^{+}$ population (Nestin-$CreERT2^{+}$) by the conditional expression of a suicide gene (thymidine kinase or cytosine deaminase) and explore its effects on lesion initiation and progression.

6.8 Lymphocyte recruitment

The establishment of an immune- suppressive environment has been shown to be important for the progression of Shh-MB progression in several mouse models [329, 330]. In the current study, we observed a significant increase in the B-cell population in whole cerebellum dissociates and within the perivascular space of lesions by IHC in $Ndp^{-/Y}$;$Ptch^{+/-}$ samples as compared to controls. This is particularly interesting as B-cells have been shown to be potent antigen presenting cells (APC) for different T-cell subtypes [173, 331, 332], motivating us to investigate whether this

early recruited B-cell population is establishing an immune suppressive environment to promote tumorigenesis.

Initially, we further characterized the B-cell population, predominantly identifying immature (IGM+) B-cells. The observation of immature B-cells could be highlighting the specific recruitment of specific subtypes such as transitional 2-marginal zone precursors (T2-MZP), which have also been shown to be potent immune-suppressors due to their ability to secret interleukin10 (Il-10) [333]. In addition, some studies have shown that during chronic CNS inflammation, B-cells could be readily observed in aggregates in the meningeal space [334]. These reported aggregates in the meninges are similar to what we observed in the cerebellum, potentially indicating that these B-cells are promoting the production of a pro-tumor pro-inflammatory microenvironment. To investigate the role of the early recruited B-cell population in $Ndp^{-/Y}$;$Ptch^{+/-}$, we depleted the B-cell population with an α-CD20 treatment. We confirmed the successful depletion of B-cells by whole cerebellum flow cytometry and IHC of established lesions. Interestingly, the depletion of the B-cell population in $Ndp^{-/Y}$;$Ptch^{+/-}$ animals had no effect on overall survival, incidence or latency. In fact the survival curve of $Ndp^{-/Y}$;$Ptch^{+/-}$ animals was almost identical between B-cell depleted, control treated (α-KLH) and the untreated $Ndp^{-/Y}$;$Ptch^{+/-}$ animals, indicating that the early recruited B-cell population may not be contributing at all to the MB phenotype. In this study, we depleted all B-cells and not just the IgM^+ B-cells, which can have negative effects on innate immune response [335, 336], autoimmunity [337] and T-cell polarization [338]. Furthermore, the observed recruitment of B-cells could be the result of an inflammatory response to the tumor as seen in cases of chronic CNS inflammation [334]. To explore this possibility, we could examine the potential inflammatory response in $Ndp^{-/Y}$;$Ptch^{+/-}$ as compared to $Ptch^{+/-}$ animals by purifying the B-cells from the surface of the cerebellum and analyzing their cytokine production.

Interestingly, upon depletion of the B-cell population we observed (by flow cytometry) a reciprocal increase in the recruitment of $CD3^+$ T-cells in whole cerebellum dissociates. This observation is consistent with the interpretation that the early recruited B-cell population is promoting the establishment of an immune suppressive environment. This immune suppressive environment is also readily observed in the established MB samples, as seen by the reduced representation of lymphocytes and dendritic cells (DCs)/microglia in $Ndp^{-/Y}$;$Ptch^{+/-}$ animals as compared to controls. At this point it is worth mentioning, that this immune-suppressive environment observed in $Ndp^{-/Y}$;$Ptch^{+/-}$ animals could also be the result of the significant difference in ages of the animals. As the average latency of established tumors in $Ndp^{-/Y}$;$Ptch^{+/-}$ is ≈ 63 days as compared to the ≈ 150 days in $Ptch^{+/-}$ animals, it is possible that there was not enough time to mount an effective immune response in $Ndp^{-/Y}$;$Ptch^{+/-}$ animals. This interpretation would be consistent with the observed decrease in $CD3^+PD\text{-}1^+$ cell population in the $Ndp^{-/Y}$;$Ptch^{+/-}$ MB samples. At this point it is worth mentioning that Ndp is expressed in lymphocytes (Tokarew and Baglaenko unpublished data) and the Tie2-Cre recombinase is also active in the hematopoietic lineage [339, 340], as such we cannot negate potential contributions from other immune cell types (T-cells, Mononuclear cells, DC, etc.). To investigate their potential contributions to the MB phenotype in our $Ndp^{-/Y}$;$Ptch^{+/-}$ mouse model, animals could be treated with Fingolimod (FTY720). Fingolimod is an immunomodulating drug which causes sphingosine-1-phosphate receptor (S1PR) internalization, preventing S1P signaling in lymphocytes, effectively preventing lymphocyte entry into the circulatory system, and sequestering them into secondary lymphoid organs. This treatment would effectively deplete the entire adaptive arm of the immune response in an organism by preventing their mobilization [341, 342].

$Ptch^{+/-}$ animals are haploinsufficient for Ptch1, causing a gain of function for the Hh pathway, which could be affecting the recruitment of lymphocytes into the CNS. Shh signaling in ECs can promote CNS immune quiescence by down-regulating the expression of pro-inflammatory cytokine/mediators and by reducing the expression of adhesion molecules on the surface of ECs [12]. However, it is noteworthy that we only observed a significant difference in B-cell recruitment in $Ndp^{-/Y}$;$Ptch^{+/-}$ animals as compared to control animals, and saw no differences in any of the other leukocyte subtypes (such as T-cells or DC). Furthermore, a large proportion of the recruited B-cells were found in the perivascular space, indicating that they have extravagated out of the vasculature, which is a multi-stage, sequential process that requires the coordinated interactions between leukocytes and the vascular ECs [39]. Taken all together, in the context of disrupted Ndp/Fzd4 signaling, B-cells are selectively recruited and potentially contribute to creating an immune suppressive environment. Upon depletion of B-cells, we observed no effect on tumorigenesis, indicating that these early recruited B-cells do not contribute to the observed MB phenotype. Further investigations into the potential contributions from other lymphocytes is required to elucidate their potential contributions to the MB phenotype.

6.9 Endothelial derived factors in MB development

One of the most significantly enriched sets of genes in the gene ontology analysis between $Ndp^{-/Y}$;$Ptch^{+/-}$ animals and $Patch^{+/-}$ littermates was components of the ECM. Although GNP proliferation is predominantly mediated by Shh, other factors have also been shown to influence GNP proliferation, such as Insulin-like Growth Factor Receptor 1 (Igfr1) [343], Notch2 [344] and Transforming Growth Factor- β2 (TGF- β2) [345] signaling, as well as several components of the ECM, such as Vitronectin (VN), Fibronectin (FN) and Laminin. VN is a glycoprotein, which has a known role in promoting cell adhesion/motility, and is highly expressed in the inner layer of the

EGL [346]. In GNPs, VN has been shown to promote the phosphorylation of CREB and drive the differentiation program by down-regulation of Math1 expression [347, 348]. Similarly, FN has been shown to have a role in promoting differentiation of GNP, although its function has predominantly been studied in the context of promoting GNP parallel fiber extension [346]. Laminin on the other hand, is highly expressed in the external layer of the EGL and has been shown to synergize with Shh signaling through a β1 integrin-dependent manner to drive GNP proliferation and to orientate the centrosome and drive the asymmetrical division of proliferating GNPs [49, 349, 350]. In MB, β1 integrin signaling has been shown to have a controversial role in promoting MB cell survival, proliferation and migration [312, 351] to prevent tumor growth by the activation of the ERK pathway following matrix metalloproteinase-9 (MMP-9) blockade [352], and it might even be dispensable in proliferation [353, 354].

In $Ndp^{-/Y}$;$Ptch^{+/-}$ lesion sections we observed a significant increase in the aberrant deposition of Laminin as compared to $Ptch^{+/-}$ samples. This observation lead us to the idea that the increased Laminin deposition could be promoting β1 signaling, which could be responsible for the observed increase in proliferation and reduction in cell death in the lesion of $Ndp^{-/Y}$;$Ptch^{+/-}$ as compared to $Ptch^{+/-}$ littermates. Alternatively, the aberrant deposition of ECM in $Ndp^{-/Y}$;$Ptch^{+/-}$ and Tie-$2Cre^{+/-}$;$Fzd4^{Flox/Flox}$;$Ptch^{+/-}$ mice may not have a role in tumorigenesis and might just be a consequence of the activated angiogenic program. This notion originates from the observation that the increased deposition of Laminin and CollagenIV positively correlates with the angiogenic activation in these animals. Upon α-Angpt2 treatment in $Ndp^{-/Y}$;$Ptch^{+/-}$, we observed a reduction in ECM deposition, which appeared to positively correlate with the observed reduction in angiogenesis and could argue in favor of ECM deposition being a consequence of the activated angiogenic program.

Since we did not quantify Laminin expression in Angpt2-treated animals as compared to control, it is still possible that there is an increase in the ratio of Laminin/vascular endothelial area in the Angpt2 treated mice. Currently, we cannot refute any potential contribution from the aberrantly deposited ECM components (Laminin) to the observed increased MB phenotype in any of our mouse models. The potential contributions of Laminin to tumorigenesis could be studied by analyzing the expression and activity of known downstream components of Laminin-integrin signaling (FAK, JNK, ERK, AKT or MAPK) [312, 355] in $Ndp^{-/Y}$;$Ptch^{+/-}$ as compared to $Ptch^{+/-}$ animals. Subsequently, we could address the potential contributions of integrin signaling in tumorigenesis in $Ndp^{-/Y}$;$Ptch^{+/-}$ mice by treating them with α-β1 function blocking antibodies and examine its impact on overall survival and lesion formation.

Alternatively, the disruption of Ndp/Fzd4 signaling may be altering or deregulating the expression of an endothelial-specific signaling molecule that could affect GNP proliferation. An interesting candidate is Igf-1, which was up-regulated at the mRNA level in Fzd4KO versus Fzd4WT ECs isolated from P16 cerebellum [95]. Igf-1 is predominantly secreted by Purkinje cells and is essential for Shh mediated GNP proliferation. It promotes the stabilization of N-Myc in a PI3K-AKT dependent manner [343], and N-Myc is essential for GNP proliferation and tumorigenesis [356]. Embryonic deletion of Igf-1 is lethal postnatally [357], making systemic depletions or deletion a non-viable option for interrogating tumorigenesis in the Ptch model. However, by using the $Igf\text{-}1^{Flox/Flox}$ mouse [357], we could selectively delete IGF-1 from the vasculature by crossing it onto our Tie2-cre mouse line in order to explore the effect of vascular secreted Igf-1 in $Ndp^{-/Y}$;$Ptch^{+/-}$ tumor progression.

6.10 Disrupted BBB

To assess the role of the open BBB in promoting MB, we pharmacologically opened the BBB in $Ptch^{+/-}$ mice by treating them with Ptx [308]. Ptx opened the BBB, as seen by whole brain and lesion-specific Evans blue extravasation through a peracellular, PLVAP-independent, mechanism by disrupting the inter-endothelial cell expression of Claudin-5 and ZO-1. Opening the BBB in $Ptch^{+/-}$ mice did not alter overall survival, incidence, or latency as compared to the $Ptch^{+/-}$ PBS treated control littermates. This result is consistent with previous reports, which have demonstrated that partially opening the BBB in orthotopic transplants of established mouse MB did not alter survival [296]. Interestingly, we did observe a slight, but non-significant increase in the average number of lesions detected in the Ptx-treated animals as compared to PBS control treated animals, potentially indicating a role for blood serum components in lesion initiation. At this point it is worth noting that the mechanism of action of Ptx is mediated by inhibiting heterotrimeric G coupled proteins, proteins such as Smo [358]. It is possible that Ptx may have dampened Hh signaling, which could explain the observed non-significant reduction in established lesion volumes. However, due to the fact that we could readily detect lesions and that we observed no significant difference in the overall survival of Ptx treated as compared to PBS treated animals, it is possible that Ptx treatment did not significantly alter Shh signaling. Further investigations using Ptx-independent methods are required to better understand the contributions of an open BBB to tumorgenesis in Ndp-/Y;Ptch+/- mice. We could selectively open the BBB by deleting sphingosine 1–phosphate receptor 1 (S1PR1) from ECs as previously described [359]. Deletion of SIPR1 will prevent cadherin-2 surface expression, promoting perycite dissociation and BBB disruption. A caveat with this approach is that many endothelial-specific Cre recombinases (Tie2-Cre) are also active in the immune system [339] and the deletion of S1PR1 in immune cells [360] may have some off-target effects. Alternatively, we could systemically treat (or by means of intra-

cerebellar injections) Ptch$^{+/-}$ animals with VE-cadherin blocking antibodies which would, through a previously described pathway, disrupt endothelial tight junctions by down regulation of Claudin-5 expression [361]. This approach also has its own caveat, as systemic treatment could alter adherent and tight junction expression in various organs and can lead to severe hemorrhages [362]. Furthermore, Ptx opens the BBB by a peracellular mechanism, which is different from the Ndp-mediated, PLVAP-dependent, transcellular mechanism [291]. This difference in BBB opening could also be important for mediating the MB phenotypes. To address the specific effect of the transcellular BBB opening we would need to use an endothelial-specific inducible Cre (Tie2-CreERT2^{+}) to selectively target and control Plvap expression in ECs and cross that on to the Ptch$^{+/-}$ background, enabling us to explore transcellular BBB opening on lesion formation and progression.

A particularly interesting observation which would argue in favor of contributions from the disrupted BBB to the MB phenotypes is the observation of a positive correlation between the degree of BBB disruption, as seen by whole brain Evans Blue extravasation, and a trend towards a reduction in overall survival in our various mouse models.

6.11 Lymphatic vasculature development

Lymphatic vasculature has been predominantly studied in the context of tumorigenesis for its role in promoting established tumor progression and metastasis. In fact, metastasis to regional lymph nodes is a major criteria in cancer staging and prognosis [363, 364]. Interestingly, several lymphatic vessel-specific mitogens, such as VEGF-C and VEGF-D, are actively secreted by cancer cells to drive lymphangiogenesis and metastasis [365, 366]. Furthermore, lymphatic vascular density in various human tumors (including prostate, gastric, thyroid, colorectal, esophageal, and lung carcinoma) [367-369] has been demonstrated to be a powerful prognostic factor which is

associated with poor disease-free and overall patient survival [370]. However, very little is known about the role of lymphatic vasculature in promoting lesion formation and progression. This is especially true in brain malignancies, where the lymphatic vasculature has only recently been discovered, and the local and regional signaling molecules regulating lymphatic development and establishment have not been fully characterized.

With the recent discovery of lymphatic vasculature within the dura mater of the meninges [181, 182] and the observed recruitment of immune cells in the lesions of our $Ndp^{-/Y}$;$Ptch^{+/-}$ animals, we wanted to investigate whether the lymphatic vasculature was affected upon Ndp/Fzd4 disruption. Our investigation revealed the presence of lymphatic vasculature predominantly confined within the pia meninges on the apical surface of the cerebellum and deep within the cerebellar folds in $Ptch^{+/-}$ animals, with the rare example of a lymphatic vessel being found within the molecular layer of the cerebellum. The identity of the lymphatic vessels is believed to be capillary lymphatic vessels, given their small size and geographical positioning. The lymphatic vasculature could be readily identified within the perivascular space and in close association with the blood vessels. Given the role for Ndp in promoting endothelial canonical Wnt signaling and the known role of canonical and non-canonical Wnt signaling in lymphatic vascular development outside the CNS [189-191, 195], we decided to characterize the lymphatic vasculature in our various mouse models. Upon Ndp/Fzd4 disruption, we could readily observe a significant reduction in lymphatic vascular density, demonstrating a role for canonical Wnt signaling in cerebellar CNS lymphatic development. Interestingly, the lymphatic defect appeared exacerbated within the deep folds of the cerebellum, the location where we observed the majority of the established lesions in the $Ndp^{-/Y}$;$Ptch^{+/-}$ animals. The observed lymphatic defect could also be a potential explanation for the observed aberrant accumulation of lymphocytes, as they are

selectively recruited and due to the lack of lymphatic vasculature, have no means of returning to the circulation. A closer examination of the lymphatic defect in $Ndp^{-/Y}$;$Ptch^{+/-}$ cerebella revealed that the lymphatic vessels appear disorganized as compared to the highly organized and stream-lined lymphatic vasculature observed in $Ptch^{+/-}$ animals. Interestingly, in the $Ndp^{-/Y}$;$Ptch^{+/-}$ animals we observed several examples of blood vessels which were devoid of the composite endothelial/Mural cell basement membrane, and only loosely surrounded by a thin parenchymal basement membrane, which is normally seen encapsulating the lymphatic vasculature. Furthermore, several of these blood vessels expressed low levels of the lymphatic marker Lyve-1. These aberrant blood vessels could be examples of previous lymphatic vessels which may have trans-differentiated back into blood vessel ECs, an event which has been shown to take place following the loss of function of Prox-1 in lymphatic ECs [191]. The observed postnatal developmental loss in lymphatic density upon Ndp/Fzd4 disruption is suggestive of a cerebellar-specific role for Ndp signaling in lymphatic vessel identity maintenance.

To better understand the lymphatic defect, we temporally analyzed (P0, P7 and P14) the lymphatic vascular density within the meningeal and EGL layer of $Ptch^{+/-}$ and $Ndp^{-/Y}$;$Ptch^{+/-}$. The lymphatic density in $Ptch^{+/-}$ mice throughout postnatal development remained relatively constant, with the exception of a minor, non-significant reduction in vascular density at P7. This reduction in lymphatic density is associated to a delay in increasing blood vasculature and lymphatic vasculature abundances. The lymphatic density was identical between the $Ndp^{-/Y}$;$Ptch^{+/-}$ littermates as compared to $Ptch^{+/-}$ samples at P0. However, as development ensued, we observed a significant temporal decrease in lymphatic density, with the lowest lymphatic density observed at P14. This significant reduction in lymphatic density was associated with a reduction in lymphatic vascular abundance at P14 as compared to P14 $Patch^{+/-}$ samples, and a moderate non-

significant increase in blood vessel abundance in P14 Ndp^{-Y};$Ptch^{+/-}$ as compared to P14 $Ptch^{+/-}$ samples. This result is consistent with our observed increase in vascular density in the lesions of $Ndp^{-/Y}$;$Ptch^{+/-}$ as compared to $Ptch^{+/-}$ animals.

We subsequently explored whether alteration in lymphatic vasculature density could be associated with lesion progression. In $Ndp^{-/Y}$;$Ptch^{+/-}$ animals, we observed a consistent reduction in lymphatic vascular density in the EGL, non-vascularized and vascularized lesions. In the $Ptch^{+/-}$ animals, however, we observed a stepwise decrease in lymphatic vascular density as a function of lesion vascularity. This trend was reminiscent of the stepwise decrease in Ndp expression as a function of tumor progression and positively correlated with the observed reduction in Wnt signaling ($Lef1^{+}$ expression) as a function of lesion vascularity. We further corroborated these results by whole cerebellum and meningeal-specific qRT-PCR, in which we observed a significant decrease in the expression of Lyve-1 and VEGFR3, respectively, in P14 $Ndp^{-/y}$;$Ptch^{+/-}$ samples as compared to P14 $Ptch^{+/-}$ samples. These results suggest that the observed reduction in lymphatic vascular density positively correlated with a local reduction in Wnt signaling in ECs, which is also associated with increased vascular invasion and lesion progression in $Ptch^{+/-}$ animals.

Interestingly, in the meningeal specific qRT-PCR, we also observed a slight but not significant increase in Endomucin (EMCN - a vein specific marker) in $Ndp^{-/y}$;$Ptch^{+/-}$ as compared to $Ptch^{+/-}$ samples. This result is particularly interesting given the fact that we have previously reported an increase in EMCN and Ephb4 (both vein markers) expression in $Ndp^{-/y}$;$Ptch^{+/-}$ MB as compared to $Ptch^{+/-}$ MB samples by micro-array analysis, and we further corroborated the EMCN results by MB specific qRT-PCR [236]. These results highlight the increased expression of vein-specific markers in the early lesion, which is significant in the established MB. Taken together, these results support a model within which Norrin is an endogenous, cerebellum-specific ligand

that is involved in the post-natal maintenance of lymphatic fate. Upon the loss of Norrin/Fzd4 signaling, LEC are trans-differentiating back into vein ECs, a process that would require the modulation of Prox-1, either at the protein or mRNA level [189, 191, 371].

These results are also very interesting as the majority of the research surrounding lymphatic vasculature in cancer revolve around its role in promoting metastasis and immune suppression [183, 364, 369, 370, 372]. In the presented study we highlight a potential role for lymphatic vessels in preventing lesion formation and progression. To explore the effect of the meningeal lymphatic defect in tumorigenesis, we could attempt to rescue the lymphatic defect in $Ndp^{-/Y}$;$Ptch^{+/-}$ mice by crossing on an endothelial specific Cre-inducible (Tie2-CreERT2^{+}) crossed with a Prox-1-driven constitutively active β-catenin. This complicated mouse line would allow us to control the timing of the induction of the constitutively active β-catenin in Prox-1 expressing lymphatic cells. Alternatively, we could use the VEGF-C/D trap protein expressing mouse line (K14-VEGFR3-Ig) [182, 373], a line which expresses a VEGFR3 binding domain fused to the FC domain of immunoglobulin, effectively producing a soluble form of the VEGFR3 receptor. We could cross this mouse line on to the $Ptch^{+/-}$ mice to investigate the role of lymphatic loss in lesion initiation and progression.

6.12 Summary

The disruption of neuronal-endothelial Norrin/Fzd4 signaling in $Ptch^{+/-}$ mice increases GNP proliferation and DNA damage, culminating in a faster conversion to LOH and tumorigenesis. Loss of Ndp/Fzd4 signaling alters the early microenvironment into a pro-tumor microenvironment, which is characterized by 5 essential stromal alterations. To uncover the molecular underpinning which is responsible for the observed increase in tumorigenesis, we modulated the different stromal phenotypes to determine their relative contributions. Our investigation enabled us to stratify the different cellular compartments (stem cells) and stromal alterations as potential driving factors on a probability spectrum from high to low. Our investigation of the potential contributions from the stem cell compartment placed it on the lower end of the probability spectrum as we observed no difference in the abundance, proliferative ability or potential for renewal in the stem cell pool between $Ndp^{-/Y}$;$Ptch^{+/-}$ and $Ptch^{+/-}$ littermates. Our investigations also placed the aberrantly recruited B-cells on the lower end of the probability spectrum, as their depletion had no effect on overall survival. However, knowing that Ndp is expressed in lymphocytes and the Tie2-Cre recombinase is also active in the hematopoietic lineage [339, 340], we cannot negate potential contributions from other lymphocytes, which still remain to be determined. In addition, we placed the activation of the angiogenic program on the lower end of the probability spectrum as inhibiting angiogenic remodeling and decreasing the vascular density in $Ndp^{-/Y}$;$Ptch^{+/-}$ lesion, presumably by halting *de novo* vessel formation and promoting vascular regression significantly, reduced overall survival. We also acknowledge that the disruption of Ndp/Fzd4 signaling could be promoting the secretion of an endothelium-specific factor (factor X, such as Igf1), which could be altering GNP proliferation. However, following Angpt2 treatment in $Ndp^{-/Y}$;$Ptch^{+/-}$, we observed a significant reduction in vascular density, which would presumably also reduce the secretion of the endothelial paracrine factor. Given the fact that

the overall survival of $Ndp^{-/Y}$;$Ptch^{+/-}$ animals was significantly reduced following Angpt2 treatment, we would argue against the role of a secreted paracrine factor (Factor X) as a strong driving force in tumorigenesis. As such, we would place it as a medium section of the probability spectrum until additional investigations can more precisely determine its contributions. Furthermore, we also observed a reduction in the aberrant deposition of ECM components (collagenIV) in the $Ndp^{-/Y}$;$Ptch^{+/-}$ animals treated with α-Angpt2, which would argue against the ECM as being the predominant driver in our MB mouse model. Currently, these observations were only qualitative and still require quantification, effectively placing the ECM in the medium section of the probability spectrum until additional investigations can more precisely determine its contributions. The remaining stromal alterations are: the open BBB and the reduction in lymphatic vascular density, which we both placed on the medium to high end of the probability spectrum. This assignment was the result of a positive correlation between an exacerbated opening of the BBB and a reduced survival between the different animal models. The assignment for the reduction in meningeal lymphatic vessels was also due to the observed positive correlation between the apparent reduction in lymphatic vasculature in the folds of the cerebellum, and a reduction in survival between the different animal models. Furthermore, the reduction in lymphatic vasculature in $Ptch^{+/-}$ mice also positively correlated with the observed reduction in lesion vascularization and progression. Both of these phenotypes can contribute individually or synergistically to the observed increase in tumorigenesis in $Ndp^{-/Y}$;$Ptch^{+/-}$ animals.

6.13 Working model

(Figure 28) Currently, we conceptualize both the open BBB and loss of meningeal lymphatic vessels are co-operating together. The open BBB enables the extravasation of pro-proliferative (e.g. Insulin) [302, 374] signaling molecules from the blood serum into the

cerebellum parenchyma. This increase in serum components could drive ectopic activation of various pathways associated with proliferation, increase the replicative stress or alternatively activate metabolic pathways which could produce potentially detrimental metabolites and/or reactive oxygen species (ROS) and reactive nitrogen species (RNI), resulting in increased DNA damage [214, 375]. In addition, the lack of lymphatic vasculature could be cooperating with the open BBB by increasing ISF stagnation, which would limit oxygen and nutrient diffusion, increasing hypoxia, and further exacerbating ROS and RNI production and DNA damage [219, 376]. To assess the relative contributions from the open BBB and the loss of meningeal lymphatic vasculature towards tumorigenesis in $Ndp^{-/Y}$;$Ptch^{+/-}$ animals, we would have to individually modulate these two stromal alterations.

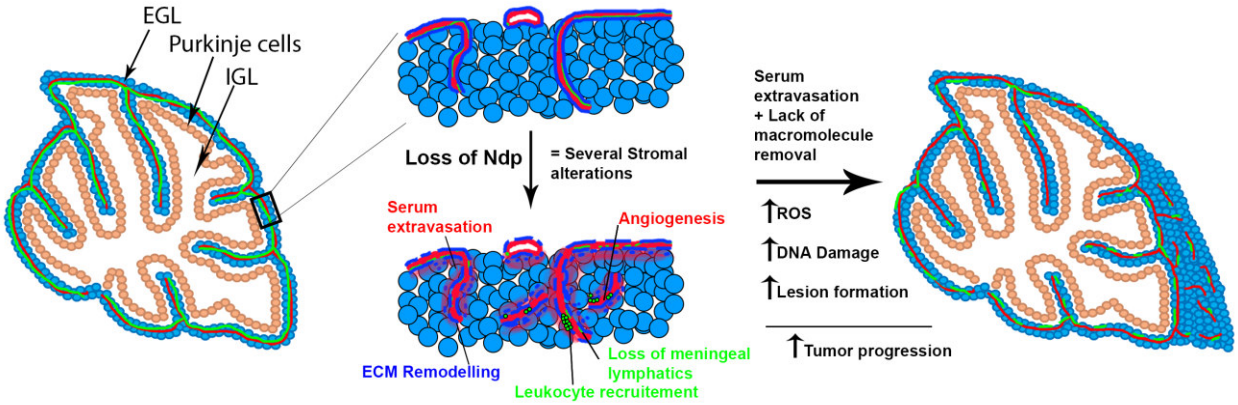

Figure 28. Working model.

Disruption of Ndp/Fzd4 signaling promotes several stromal alterations such as an open BBB, activation of the angiogenic program, ECM deposition, aberrant lymphocyte recruitment and a loss of meningeal lymphatic vessels. We believe that the open BBB and the loss of lymphatic vasculature are cooperating to promote tumorigenesis. The open BBB enables the extravasation of pro-proliferative (e.g. Insulin) [302, 374] signaling molecules from the blood serum. This could ectopically activate various pathways associated with proliferation, or metabolic pathways which could potentially produce detrimental metabolites and/or reactive oxygen species (ROS) and reactive nitrogen species (RNI) [214, 375]. In addition, the lack of lymphatic vasculature could be cooperating with the open BBB by increasing ISF stagnation, which would limit oxygen and nutrient diffusion, increasing hypoxia and further exacerbate ROS and RNI production. Together they would increase replicative stress and DNA damage through ROS and RNI [219, 376], promoting LOH conversion of the lesions, effectively driving tumorigenesis.

6.14 Significance of the study

This work highlights several important notions. First, the Ndp/Fzd4 signaling axis has never before been shown to be involved in brain tumorigenesis. Second, we showed a novel mechanism by which Hh-driven tumors can interact with the surrounding stroma. Third, we are the first group to describe a novel role for Ndp/Fzd4 signaling in lymphatic vasculature development and maintenance in the pia meninges of the cerebellum.

These results are clinically relevant and particularly interesting in the context of future patient management, especially in the context of Shh-MB. Wnt-MB is regarded as a MB with a good prognosis and an excellent responsiveness to classical treatments (such as chemotherapy), a trait that has been attributed to an open BBB [296]. In the presented work we describe an endogenous signaling network (Ndp/Fzd4), which is enriched in Shh-MB, and which can be targeted *in vivo* [236], effectively opening the BBB in Shh-MB and potentially enhancing the responsiveness of human Shh-MB to classical treatment and reducing the need for invasive surgical resection.

Furthermore, given the known role of Ndp signaling in the regulation of cerebellar BBB integrity, and the observed correlation of a reduced survival in human patients with lower levels of Ndp expression; it would be interesting to see if these human patients do in fact have a more compromised BBB due to the reduced expression of Ndp. Furthermore, if the lower levels of Ndp expression translates to an exacerbation of the BBB phenotype in the established MB, it would be interesting to determine whether these patients are better responders to classic treatments, such as chemotherapy.

References

1. Parkin, D.M., et al., *Global Cancer Statistics, 2002.* CA: A Cancer Journal for Clinicians, 2005. **55**(2): p. 74-108.
2. Anderson, D.E., *Familial versus sporadic breast cancer.* Cancer, 1992. **70**(S4): p. 1740-1746.
3. Dhillon, A.S., et al., *MAP kinase signalling pathways in cancer.* Oncogene, 0000. **26**(22): p. 3279-3290.
4. Giancotti, F.G., *Deregulation of cell signaling in cancer.* FEBS Letters, 2014. **588**(16): p. 2558-2570.
5. Michel, M., et al., *Hh signalling is essential for somatic stem cell maintenance in the Drosophila testis niche.* Development, 2012. **139**(15): p. 2663.
6. Zhao, C., et al., *Hedgehog signalling is essential for maintenance of cancer stem cells in myeloid leukaemia.* Nature, 2009. **458**(7239): p. 776-779.
7. Plaisant, M., et al., *Activation of Hedgehog Signaling Inhibits Osteoblast Differentiation of Human Mesenchymal Stem Cells.* STEM CELLS, 2009. **27**(3): p. 703-713.
8. Domínguez, M. and E. Hafen, *Hedgehog directly controls initiation and propagation of retinal differentiation in the Drosophila eye.* Genes & Development, 1997. **11**(23): p. 3254-3264.
9. Jiang, J. and C.-c. Hui, *Hedgehog Signaling in Development and Cancer.* Developmental Cell, 2008. **15**(6): p. 801-812.
10. Jia, Y., Y. Wang, and J. Xie, *The Hedgehog pathway: role in cell differentiation, polarity and proliferation.* Archives of toxicology, 2015. **89**(2): p. 179-191.
11. Le, H., et al., *Hedgehog signaling is essential for normal wound healing.* Wound Repair and Regeneration, 2008. **16**(6): p. 768-773.
12. Alvarez, J.I., et al., *The Hedgehog Pathway Promotes Blood-Brain Barrier Integrity and CNS Immune Quiescence.* Science, 2011. **334**(6063): p. 1727.
13. Briscoe, J. and P.P. Therond, *The mechanisms of Hedgehog signalling and its roles in development and disease.* Nat Rev Mol Cell Biol, 2013. **14**(7): p. 416-429.
14. Goetz, S.C. and K.V. Anderson, *The primary cilium: a signalling centre during vertebrate development.* Nat Rev Genet, 2010. **11**(5): p. 331-344.
15. Tsanev, R., et al., *Identification of the gene transcription repressor domain of Gli3.* Febs Letters, 2009. **583**(1): p. 224-228.
16. Brennan, D., et al., *Noncanonical Hedgehog Signaling.* Vitamins & Hormones, 2012. **88**: p. 55-72.
17. Tukachinsky, H., L.V. Lopez, and A. Salic, *A mechanism for vertebrate Hedgehog signaling: recruitment to cilia and dissociation of SuFu–Gli protein complexes.* The Journal of Cell Biology, 2010. **191**(2): p. 415.
18. Zhang, Z., et al., *Suppressor of Fused Chaperones Gli Proteins To Generate Transcriptional Responses to Sonic Hedgehog Signaling.* Molecular and Cellular Biology, 2017. **37**(3).
19. Pan, Y. and B. Wang, *A Novel Protein-processing Domain in Gli2 and Gli3 Differentially Blocks Complete Protein Degradation by the Proteasome.* Journal of Biological Chemistry, 2007. **282**(15): p. 10846-10852.
20. Pan, Y., C. Wang, and B. Wang, *Phosphorylation of Gli2 by protein kinase A is required for Gli2 processing and degradation and the Sonic Hedgehog-regulated mouse development.* Developmental biology, 2009. **326**(1): p. 177-189.
21. Teglund, S. and R. Toftgård, *Hedgehog beyond medulloblastoma and basal cell carcinoma.* Biochimica et Biophysica Acta (BBA) - Reviews on Cancer, 2010. **1805**(2): p. 181-208.
22. Cheng, S.Y. and J.M. Bishop, *Suppressor of Fused represses Gli-mediated transcription by recruiting the SAP18-mSin3 corepressor complex.* Proceedings of the National Academy of Sciences, 2002. **99**(8): p. 5442-5447.
23. BeachyPhilip, A., S. KarhadkarSunil, and M. BermanDavid, *Tissue repair and stem cell renewal in carcinogenesis.* Nature, 2004. **432**(7015): p. 324-331.

24. Gupta, S., N. Takebe, and P. LoRusso, *Targeting the Hedgehog pathway in cancer.* Therapeutic Advances in Medical Oncology, 2010. **2**(4): p. 237-250.
25. Oliver, T.G., et al., *Loss of patched and disruption of granule cell development in a pre-neoplastic stage of medulloblastoma.* Development, 2005. **132**(10): p. 2425.
26. Wetmore, C., D.E. Eberhart, and T. Curran, *Loss of p53 but not ARF Accelerates Medulloblastoma in Mice Heterozygous for <em>patched</em&gt.* Cancer Research, 2001. **61**(2): p. 513.
27. Lindemann, R.K., *Stroma-Initiated Hedgehog Signaling Takes Center Stage in B-Cell Lymphoma.* Cancer Research, 2008. **68**(4): p. 961.
28. Yauch, R.L., et al., *A paracrine requirement for hedgehog signalling in cancer.* Nature, 2008. **455**(7211): p. 406-410.
29. Calabrese, C., et al., *A Perivascular Niche for Brain Tumor Stem Cells.* Cancer Cell, 2007. **11**(1): p. 69-82.
30. Matsuda, Y., et al., *DNA Damage Sensor γ-H2AX Is Increased in Preneoplastic Lesions of Hepatocellular Carcinoma.* The Scientific World Journal, 2013. **2013**: p. 597095.
31. Gorgoulis, V.G., et al., *Activation of the DNA damage checkpoint and genomic instability in human precancerous lesions.* Nature, 2005. **434**(7035): p. 907-913.
32. Quail, D.F. and J.A. Joyce, *Microenvironmental regulation of tumor progression and metastasis.* Nat Med, 2013. **19**(11): p. 1423-1437.
33. Nishida, N., et al., *Angiogenesis in Cancer.* Vascular Health and Risk Management, 2006. **2**(3): p. 213-219.
34. Lu, H., W. Ouyang, and C. Huang, *Inflammation, a Key Event in Cancer Development.* Molecular Cancer Research, 2006. **4**(4): p. 221.
35. Tlsty, T.D. and L.M. Coussens, *TUMOR STROMA AND REGULATION OF CANCER DEVELOPMENT.* Annual Review of Pathology: Mechanisms of Disease, 2006. **1**(1): p. 119-150.
36. Tommelein, J., et al., *Cancer-Associated Fibroblasts Connect Metastasis-Promoting Communication in Colorectal Cancer.* Frontiers in Oncology, 2015. **5**: p. 63.
37. Yeung, T.-L., C.S. Leung, and S.C. Mok, *CAF reprogramming inhibits ovarian cancer progression.* Cell Cycle, 2014. **13**(24): p. 3783-3784.
38. Raica, M., A.M. Cimpean, and D. Ribatti, *Angiogenesis in pre-malignant conditions.* European Journal of Cancer. **45**(11): p. 1924-1934.
39. Muller, W.A., *Getting Leukocytes to the Site of Inflammation.* Veterinary pathology, 2013. **50**(1): p. 7-22.
40. Schoenfeld, J.D. and G. Dranoff, *Anti-angiogenic immunotherapy.* Human Vaccines, 2011. **7**(9): p. 976-981.
41. Grivennikov, S.I., F.R. Greten, and M. Karin, *Immunity, Inflammation, and Cancer.* Cell, 2010. **140**(6): p. 883-899.
42. Stewart, T., et al., *Incidence of de-novo breast cancer in women chronically immunosuppressed after organ transplantation.* The Lancet. **346**(8978): p. 796-798.
43. Gallagher, B., et al., *Cancer Incidence in New York State Acquired Immunodeficiency Syndrome Patients.* American Journal of Epidemiology, 2001. **154**(6): p. 544-556.
44. Chow, M.T. and A.D. Luster, *Chemokines in Cancer.* Cancer immunology research, 2014. **2**(12): p. 1125-1131.
45. Palumbo, A., et al., *Genetic instability in the tumor microenvironment: a new look at an old neighbor.* Molecular Cancer, 2015. **14**: p. 145.
46. Ramnani, N., *The primate cortico-cerebellar system: anatomy and function.* Nat Rev Neurosci, 2006. **7**(7): p. 511-522.
47. Ito, M., *Cerebellar learning in the vestibulo–ocular reflex.* Trends in Cognitive Sciences. **2**(9): p. 313-321.
48. Wallace, V.A., *Purkinje-cell-derived Sonic hedgehog regulates granule neuron precursor cell proliferation in the developing mouse cerebellum.* Current Biology. **9**(8): p. 445-448.

49. Gupta, S.K., et al., *Coordination between extrinsic extracellular matrix cues and intrinsic responses to orient the centrosome in polarizing cerebellar granule neurons.* The Journal of neuroscience : the official journal of the Society for Neuroscience, 2010. **30**(7): p. 2755-2766.
50. Butts, T., M.J. Green, and R.J.T. Wingate, *Development of the cerebellum: simple steps to make a 'little brain'.* Development, 2014. **141**(21): p. 4031.
51. Roussel, M.F. and M.E. Hatten, *Cerebellum: Development and Medulloblastoma.* Current topics in developmental biology, 2011. **94**: p. 235-282.
52. Ho, K.S. and M.P. Scott, *Sonic hedgehog in the nervous system: functions, modifications and mechanisms.* Current Opinion in Neurobiology, 2002. **12**(1): p. 57-63.
53. Kenney, A.M. and D.H. Rowitch, *Sonic hedgehog Promotes G(1) Cyclin Expression and Sustained Cell Cycle Progression in Mammalian Neuronal Precursors.* Molecular and Cellular Biology, 2000. **20**(23): p. 9055-9067.
54. Vaillant, C. and D. Monard, *SHH Pathway and Cerebellar Development.* The Cerebellum, 2009. **8**(3): p. 291-301.
55. Romer, J. and T. Curran, *Targeting Medulloblastoma: Small-Molecule Inhibitors of the Sonic Hedgehog Pathway as Potential Cancer Therapeutics.* Cancer Research, 2005. **65**(12): p. 4975.
56. Northcott, P.A., et al., *The clinical implications of medulloblastoma subgroups.* Nat Rev Neurol, 2012. **8**(6): p. 340-351.
57. Northcott, P.A., et al., *Medulloblastoma Comprises Four Distinct Molecular Variants.* Journal of Clinical Oncology, 2011. **29**(11): p. 1408-1414.
58. Ramaswamy, V., et al., *Recurrence patterns across medulloblastoma subgroups: an integrated clinical and molecular analysis.* The lancet oncology, 2013. **14**(12): p. 1200-1207.
59. Kool, M., et al., *Molecular subgroups of medulloblastoma: an international meta-analysis of transcriptome, genetic aberrations, and clinical data of WNT, SHH, Group 3, and Group 4 medulloblastomas.* Acta Neuropathologica, 2012. **123**(4): p. 473-484.
60. Manoranjan, B., et al., *Medulloblastoma stem cells: where development and cancer cross pathways.* Pediatr Res, 2012. **71**(4-2): p. 516-522.
61. Yang, Z.-J., et al., *Medulloblastoma can be Initiated by Deletion of patched in Lineage-Restricted Progenitors or Stem Cells.* Cancer cell, 2008. **14**(2): p. 135-145.
62. Cavalli, F.M.G., et al., *Intertumoral Heterogeneity within Medulloblastoma Subgroups.* Cancer Cell. **31**(6): p. 737-754.e6.
63. Grill, J. and C. Dufour, *Neuro-oncology: Stability of medulloblastoma subgroups at tumour recurrence.* Nat Rev Neurol, 2014. **10**(1): p. 5-6.
64. Pei, Y., et al., *WNT signaling increases proliferation and impairs differentiation of stem cells in the developing cerebellum.* Development, 2012. **139**(10): p. 1724.
65. Goessling, W., et al., *Genetic Interaction of PGE2 and Wnt Signaling Regulates Developmental Specification of Stem Cells and Regeneration.* Cell. **136**(6): p. 1136-1147.
66. Polakis, P., *Wnt Signaling in Cancer.* Cold Spring Harbor Perspectives in Biology, 2012. **4**(5): p. a008052.
67. Loh, Kyle M., R. van Amerongen, and R. Nusse, *Generating Cellular Diversity and Spatial Form: Wnt Signaling and the Evolution of Multicellular Animals.* Developmental Cell. **38**(6): p. 643-655.
68. Nusse, R., *Wnt signaling in disease and in development.* Cell Res, 2005. **15**(1): p. 28-32.
69. Yang, Y., *Wnt signaling in development and disease.* Cell & Bioscience, 2012. **2**: p. 14-14.
70. Anastas, J.N. and R.T. Moon, *WNT signalling pathways as therapeutic targets in cancer.* Nat Rev Cancer, 2013. **13**(1): p. 11-26.
71. Nusse, R. and H. Clevers, *Wnt/b-Catenin Signaling, Disease, and Emerging Therapeutic Modalities.* Cell. **169**(6): p. 985-999.
72. Angers, S. and R.T. Moon, *Proximal events in Wnt signal transduction.* Nat Rev Mol Cell Biol, 2009. **10**(7): p. 468-477.
73. Kohn, A.D. and R.T. Moon, *Wnt and calcium signaling: β-Catenin-independent pathways.* Cell Calcium, 2005. **38**(3): p. 439-446.

74. Nusse, R., *Wnt signaling and stem cell control.* Cell Res, 2008. **18**(5): p. 523-527.
75. Reya, T. and H. Clevers, *Wnt signalling in stem cells and cancer.* Nature, 2005. **434**(7035): p. 843-850.
76. Clevers, H. and R. Nusse, *Wnt/β-Catenin Signaling and Disease.* Cell. **149**(6): p. 1192-1205.
77. Fagotto, F., U. Glück, and B.M. Gumbiner, *Nuclear localization signal-independent and importin/karyopherin-independent nuclear import of β-catenin.* Current Biology. **8**(4): p. 181-190.
78. Eastman, Q. and R. Grosschedl, *Regulation of LEF-1/TCF transcription factors by Wnt and other signals.* Current Opinion in Cell Biology, 1999. **11**(2): p. 233-240.
79. Giles, R.H., J.H. van Es, and H. Clevers, *Caught up in a Wnt storm: Wnt signaling in cancer.* Biochimica et Biophysica Acta (BBA) - Reviews on Cancer, 2003. **1653**(1): p. 1-24.
80. Inestrosa, N.C. and L. Varela-Nallar, *Wnt Signaling Roles on the Structure and Function of the Central Synapses: Involvement in Alzheimer's Disease*, in *Trends in Cell Signaling Pathways in Neuronal Fate Decision*, S. Wislet-Gendebien, Editor 2013, InTech: Rijeka. p. Ch. 04.
81. Ke, J., et al., *Structure and function of Norrin in assembly and activation of a Frizzled 4–Lrp5/6 complex.* Genes & Development, 2013. **27**(21): p. 2305-2319.
82. Ye, X., Y. Wang, and J. Nathans, *The Norrin/Frizzled4 signaling pathway in retinal vascular development and disease.* Trends in Molecular Medicine. **16**(9): p. 417-425.
83. Perez-Vilar, J. and R.L. Hill, *Norrie Disease Protein (Norrin) Forms Disulfide-linked Oligomers Associated with the Extracellular Matrix.* Journal of Biological Chemistry, 1997. **272**(52): p. 33410-33415.
84. Wang, Y., et al., *Norrin/Frizzled4 signaling in retinal vascular development and blood brain barrier plasticity.* Cell, 2012. **151**(6): p. 1332-1344.
85. Junge, H.J., et al., *TSPAN12 Regulates Retinal Vascular Development by Promoting Norrin- but Not Wnt-Induced FZD4/β-Catenin Signaling.* Cell. **139**(2): p. 299-311.
86. Musada, G.R., et al., *Mutation spectrum of the Norrie disease pseudoglioma (NDP) gene in Indian patients with FEVR.* Molecular Vision, 2016. **22**: p. 491-502.
87. Yang, H., et al., *Identification of FZD4 and LRP5 mutations in 11 of 49 families with familial exudative vitreoretinopathy.* Molecular Vision, 2012. **18**: p. 2438-2446.
88. University of Utah Scholar, W., *Spectrum and Frequency of FZD4 Mutations in Familial Exudative Vitreoretinopathy*2004: Association for Research in Vision and Ophthalmology.
89. Kondo, H., et al., *Mutations in the TSPAN12 Gene in Japanese Patients with Familial Exudative Vitreoretinopathy.* American Journal of Ophthalmology. **151**(6): p. 1095-1100.e1.
90. Jiao, X., et al., *Autosomal Recessive Familial Exudative Vitreoretinopathy Is Associated with Mutations in LRP5.* American Journal of Human Genetics, 2004. **75**(5): p. 878-884.
91. Poulter, J.A., et al., *Recessive Mutations in TSPAN12 Cause Retinal Dysplasia and Severe Familial Exudative Vitreoretinopathy (FEVR)TSPAN12 Recessive Mutations.* Investigative Ophthalmology & Visual Science, 2012. **53**(6): p. 2873-2879.
92. Chamney, S., E. McLoone, and C.E. Willoughby, *A mutation in the Norrie disease gene (NDP) associated with familial exudative vitreoretinopathy.* Eye, 2011. **25**(12): p. 1658-1658.
93. Pelcastre, E.L., C. Villanueva-Mendoza, and J.C. Zenteno, *Novel and recurrent NDP gene mutations in familial cases of Norrie disease and X-linked exudative vitreoretinopathy.* Clinical & Experimental Ophthalmology, 2010. **38**(4): p. 367-374.
94. Liebner, S. and K.H. Plate, *Differentiation of the brain vasculature: the answer came blowing by the Wnt.* Journal of Angiogenesis Research, 2010. **2**: p. 1-1.
95. Ye, X., et al., *Norrin, Frizzled-4, and Lrp5 Signaling in ECs Controls a Genetic Program for Retinal Vascularization.* Cell. **139**(2): p. 285-298.
96. Smallwood, P.M., et al., *Mutational Analysis of Norrin-Frizzled4 Recognition.* Journal of Biological Chemistry, 2007. **282**(6): p. 4057-4068.

97. Ye, X., P. Smallwood, and J. Nathans, *Expression of the Norrie disease gene (Ndp) in developing and adult mouse eye, ear, and brain.* Gene Expression Patterns, 2011. **11**(1–2): p. 151-155.
98. Swartz, M.A. and M. Skobe, *Lymphatic function, lymphangiogenesis, and cancer metastasis.* Microscopy Research and Technique, 2001. **55**(2): p. 92-99.
99. dela Paz, N.G. and P.A. D'Amore, *Arterial versus venous ECs.* Cell and tissue research, 2009. **335**(1): p. 5-16.
100. Makrilia, N., et al., *The role of angiogenesis in solid tumours: An overview.* European Journal of Internal Medicine. **20**(7): p. 663-671.
101. Vaupel, P., F. Kallinowski, and P. Okunieff, *Blood Flow, Oxygen and Nutrient Supply, and Metabolic Microenvironment of Human Tumors: A Review.* Cancer Research, 1989. **49**(23): p. 6449.
102. Lawson, N.D., et al., *Notch signaling is required for arterial-venous differentiation during embryonic vascular development.* Development, 2001. **128**(19): p. 3675.
103. Corada, M., et al., *The Wnt/β-Catenin Pathway Modulates Vascular Remodeling and Specification by Upregulating Dll4/Notch Signaling.* Developmental Cell. **18**(6): p. 938-949.
104. Risau, W., *Mechanisms of angiogenesis.* Nature, 1997. **386**(6626): p. 671-674.
105. Potente, M., H. Gerhardt, and P. Carmeliet, *Basic and Therapeutic Aspects of Angiogenesis.* Cell. **146**(6): p. 873-887.
106. Adams, R.H. and K. Alitalo, *Molecular regulation of angiogenesis and lymphangiogenesis.* Nat Rev Mol Cell Biol, 2007. **8**(6): p. 464-478.
107. Blanco, R. and H. Gerhardt, *VEGF and Notch in Tip and Stalk Cell Selection.* Cold Spring Harbor Perspectives in Medicine, 2013. **3**(1).
108. Paleolog, E.M., *The vasculature in rheumatoid arthritis: cause or consequence?* International Journal of Experimental Pathology, 2009. **90**(3): p. 249-261.
109. Tsai, M.-J., et al., *Acute Midbrain Infarction in a Child With Intracranial Carotid Artery Hypoplasia and Aberrant Cerebral Vasculature: A Case Report.* Journal of Child Neurology, 2007. **22**(4): p. 465-470.
110. Mulligan-Kehoe, M.J. and M. Simons, *Vascular Disease in Scleroderma: Angiogenesis and Vascular Repair.* Rheumatic Disease Clinics. **34**(1): p. 73-79.
111. Xia, Y.-P., et al., *Transgenic delivery of VEGF to mouse skin leads to an inflammatory condition resembling human psoriasis.* Blood, 2003. **102**(1): p. 161.
112. Gacche, R.N. and R.J. Meshram, *Angiogenic factors as potential drug target: Efficacy and limitations of anti-angiogenic therapy.* Biochimica et Biophysica Acta (BBA) - Reviews on Cancer, 2014. **1846**(1): p. 161-179.
113. Dayan, F., et al., *A Dialogue between the Hypoxia-Inducible Factor and the Tumor Microenvironment.* Cancer Microenvironment, 2008. **1**(1): p. 53-68.
114. Krock, B.L., N. Skuli, and M.C. Simon, *Hypoxia-Induced Angiogenesis: Good and Evil.* Genes & Cancer, 2011. **2**(12): p. 1117-1133.
115. Semenza, G.L., *Hydroxylation of HIF-1: Oxygen Sensing at the Molecular Level.* Physiology, 2004. **19**(4): p. 176.
116. Yang, J., et al., *Functions of the Per/ARNT/Sim Domains of the Hypoxia-inducible Factor.* Journal of Biological Chemistry, 2005. **280**(43): p. 36047-36054.
117. Vallon, M., et al., *Developmental and pathological angiogenesis in the central nervous system.* Cellular and Molecular Life Sciences, 2014. **71**(18): p. 3489-3506.
118. Phng, L.K. and H. Gerhardt, *Angiogenesis: A Team Effort Coordinated by Notch.* Developmental Cell. **16**(2): p. 196-208.
119. Park, J.E., et al., *Placenta growth factor. Potentiation of vascular endothelial growth factor bioactivity, in vitro and in vivo, and high affinity binding to Flt-1 but not to Flk-1/KDR.* Journal of Biological Chemistry, 1994. **269**(41): p. 25646-25654.

120. Wang, S., et al., *Control of endothelial cell proliferation and migration by VEGF signaling to histone deacetylase 7.* Proceedings of the National Academy of Sciences of the United States of America, 2008. **105**(22): p. 7738-7743.
121. Gerhardt, H., et al., *VEGF guides angiogenic sprouting utilizing endothelial tip cell filopodia.* The Journal of Cell Biology, 2003. **161**(6): p. 1163-1177.
122. Hellstrom, M., et al., *Dll4 signalling through Notch1 regulates formation of tip cells during angiogenesis.* Nature, 2007. **445**(7129): p. 776-780.
123. Ucuzian, A.A., et al., *Molecular Mediators of Angiogenesis.* Journal of burn care & research : official publication of the American Burn Association, 2010. **31**(1): p. 158.
124. Fagiani, E. and G. Christofori, *Angiopoietins in angiogenesis.* Cancer Letters. **328**(1): p. 18-26.
125. Gaengel, K., et al., *Endothelial-Mural Cell Signaling in Vascular Development and Angiogenesis.* Arteriosclerosis, Thrombosis, and Vascular Biology, 2009. **29**(5): p. 630.
126. Ostman, A., et al., *Identification of a cell retention signal in the B-chain of platelet-derived growth factor and in the long splice version of the A-chain.* Cell Regulation, 1991. **2**(7): p. 503-512.
127. Lindahl, P., et al., *Pericyte Loss and Microaneurysm Formation in PDGF-B-Deficient Mice.* Science, 1997. **277**(5323): p. 242.
128. Hirschi, K.K., et al., *ECs Modulate the Proliferation of Mural Cell Precursors via Platelet-Derived Growth Factor-BB and Heterotypic Cell Contact.* Circulation Research, 1999. **84**(3): p. 298.
129. Hellstrom, M., et al., *Role of PDGF-B and PDGFR-beta in recruitment of vascular smooth muscle cells and pericytes during embryonic blood vessel formation in the mouse.* Development, 1999. **126**(14): p. 3047.
130. Abramsson, A., P. Lindblom, and C. Betsholtz, *Endothelial and nonendothelial sources of PDGF-B regulate pericyte recruitment and influence vascular pattern formation in tumors.* Journal of Clinical Investigation, 2003. **112**(8): p. 1142-1151.
131. Iruela-Arispe, M.L. and G.E. Davis, *Cellular and Molecular Mechanisms of Vascular Lumen Formation.* Developmental Cell. **16**(2): p. 222-231.
132. Hallmann, R., et al., *Expression and Function of Laminins in the Embryonic and Mature Vasculature.* Physiological Reviews, 2005. **85**(3): p. 979.
133. Norton, K.-A. and A.S. Popel, *Effects of endothelial cell proliferation and migration rates in a computational model of sprouting angiogenesis.* 2016. **6**: p. 36992.
134. Gerhardt, H. and C. Betsholtz, *Endothelial-pericyte interactions in angiogenesis.* Cell and Tissue Research, 2003. **314**(1): p. 15-23.
135. Abbott, N.J., L. Ronnback, and E. Hansson, *Astrocyte-endothelial interactions at the blood-brain barrier.* Nat Rev Neurosci, 2006. **7**(1): p. 41-53.
136. Murakami, M., *Signaling Required for Blood Vessel Maintenance: Molecular Basis and Pathological Manifestations.* International Journal of Vascular Medicine, 2012. **2012**: p. 293641.
137. Daneman, R., et al., *Wnt/β-catenin signaling is required for CNS, but not non-CNS, angiogenesis.* Proceedings of the National Academy of Sciences of the United States of America, 2009. **106**(2): p. 641-646.
138. Clapp, C., et al., *Peptide Hormone Regulation of Angiogenesis.* Physiological Reviews, 2009. **89**(4): p. 1177.
139. Oliver, G. and R.S. Srinivasan, *Endothelial cell plasticity: how to become and remain a lymphatic endothelial cell.* Development (Cambridge, England), 2010. **137**(3): p. 363-372.
140. Nombela-Arrieta, C., et al., *Quantitative imaging of haematopoietic stem and progenitor cell localization and hypoxic status in the bone marrow microenvironment.* Nat Cell Biol, 2013. **15**(5): p. 533-543.
141. Tanaka, M. and Y. Iwakiri, *The Hepatic Lymphatic Vascular System: Structure, Function, Markers, and Lymphangiogenesis.* Cellular and Molecular Gastroenterology and Hepatology, 2016. **2**(6): p. 733-749.

142. Satchell, S.C. and F. Braet, *Glomerular endothelial cell fenestrations: an integral component of the glomerular filtration barrier.* American Journal of Physiology - Renal Physiology, 2009. **296**(5): p. F947-F956.
143. Obermeier, B., R. Daneman, and R.M. Ransohoff, *Development, maintenance and disruption of the blood-brain barrier.* Nature medicine, 2013. **19**(12): p. 1584-1596.
144. Butt, A.M., H.C. Jones, and N.J. Abbott, *Electrical resistance across the blood-brain barrier in anaesthetized rats: a developmental study.* The Journal of Physiology, 1990. **429**: p. 47-62.
145. Bauer, H.-C., et al., *"You Shall Not Pass"—tight junctions of the blood brain barrier.* Frontiers in Neuroscience, 2014. **8**: p. 392.
146. Alvarez, J.I., T. Katayama, and A. Prat, *Glial influence on the Blood Brain Barrier.* Glia, 2013. **61**(12): p. 1939-1958.
147. Lampugnani, M.G. and E. Dejana, *Adherens junctions in ECs regulate vessel maintenance and angiogenesis.* Thrombosis Research, 2007. **120**: p. S1-S6.
148. Sanchez-Covarrubias, L., et al., *Transporters at CNS Barrier Sites: Obstacles or Opportunities for Drug Delivery?* Current pharmaceutical design, 2014. **20**(10): p. 1422-1449.
149. Redzic, Z., *Molecular biology of the blood-brain and the blood-cerebrospinal fluid barriers: similarities and differences.* Fluids and Barriers of the CNS, 2011. **8**: p. 3-3.
150. Banks, W.A., *From blood-brain barrier to blood-brain interface: new opportunities for CNS drug delivery.* Nat Rev Drug Discov, 2016. **15**(4): p. 275-292.
151. Hawkins, B.T. and T.P. Davis, *The Blood-Brain Barrier/Neurovascular Unit in Health and Disease.* Pharmacological Reviews, 2005. **57**(2): p. 173.
152. Stewart, P.A. and M.J. Wiley, *Developing nervous tissue induces formation of blood-brain barrier characteristics in invading ECs: A study using quail-chick transplantation chimeras.* Developmental Biology, 1981. **84**(1): p. 183-192.
153. Daneman, R., et al., *Pericytes are required for blood–brain barrier integrity during embryogenesis.* Nature, 2010. **468**(7323): p. 562-566.
154. Shalaby, F., et al., *Failure of blood-island formation and vasculogenesis in Flk-1-deficient mice.* Nature, 1995. **376**(6535): p. 62-66.
155. Liebner, S., et al., *Wnt/β-catenin signaling controls development of the blood–brain barrier.* The Journal of Cell Biology, 2008. **183**(3): p. 409-417.
156. Stenman, J.M., et al., *Canonical Wnt Signaling Regulates Organ-Specific Assembly and Differentiation of CNS Vasculature.* Science, 2008. **322**(5905): p. 1247.
157. Reis, M., et al., *Endothelial Wnt/β-catenin signaling inhibits glioma angiogenesis and normalizes tumor blood vessels by inducing PDGF-B expression.* The Journal of Experimental Medicine, 2012. **209**(9): p. 1611-1627.
158. Kuhnert, F., et al., *Essential regulation of CNS angiogenesis by the orphan G protein-coupled receptor GPR124.* Science (New York, N.Y.), 2010. **330**(6006): p. 985-989.
159. Anderson, K.D., et al., *Angiogenic sprouting into neural tissue requires Gpr124, an orphan G protein-coupled receptor.* Proceedings of the National Academy of Sciences of the United States of America, 2011. **108**(7): p. 2807-2812.
160. Cullen, M., et al., *GPR124, an orphan G protein-coupled receptor, is required for CNS-specific vascularization and establishment of the blood–brain barrier.* Proceedings of the National Academy of Sciences, 2011. **108**(14): p. 5759-5764.
161. Chang, J., et al., *Gpr124 is essential for blood–brain barrier integrity in central nervous system disease.* Nature medicine, 2017. **23**(4): p. 450-460.
162. Winkler, E.A., R.D. Bell, and B.V. Zlokovic, *Central nervous system pericytes in health and disease.* Nature neuroscience, 2011. **14**(11): p. 1398-1405.
163. Armulik, A., G. Genové, and C. Betsholtz, *Pericytes: Developmental, Physiological, and Pathological Perspectives, Problems, and Promises.* Developmental Cell. **21**(2): p. 193-215.
164. Li, F., et al., *Endothelial Smad4 Maintains Cerebrovascular Integrity by Activating N-Cadherin through Cooperation with Notch.* Developmental Cell. **20**(3): p. 291-302.

165. Iliff, J.J., et al., *A Paravascular Pathway Facilitates CSF Flow Through the Brain Parenchyma and the Clearance of Interstitial Solutes, Including Amyloid β.* Science translational medicine, 2012. **4**(147): p. 147ra111-147ra111.
166. Xie, L., et al., *Sleep Drives Metabolite Clearance from the Adult Brain.* Science (New York, N.Y.), 2013. **342**(6156): p. 10.1126/science.1241224.
167. Neuhaus, J., *Orthogonal arrays of particles in astroglial cells: Quantitative analysis of their density, size, and correlation with intramembranous particles.* Glia, 1990. **3**(4): p. 241-251.
168. Zhang, E.T., C.B. Inman, and R.O. Weller, *Interrelationships of the pia mater and the perivascular (Virchow-Robin) spaces in the human cerebrum.* Journal of Anatomy, 1990. **170**: p. 111-123.
169. Hutchings, M. and R.O. Weller, *Anatomical relationships of the pia mater to cerebral blood vessels in man.* Journal of Neurosurgery, 1986. **65**(3): p. 316-325.
170. Pollock, H., et al., *Perivascular spaces in the basal ganglia of the human brain: their relationship to lacunes.* Journal of Anatomy, 1997. **191**(Pt 3): p. 337-346.
171. Bechmann, I., et al., *Immune surveillance of mouse brain perivascular spaces by blood-borne macrophages.* European Journal of Neuroscience, 2001. **14**(10): p. 1651-1658.
172. Hussain, R.Z., et al., *Immune surveillance of the central nervous system in multiple sclerosis–Relevance for therapy and experimental models.* Journal of neuroimmunology, 2014. **276**(0): p. 9-17.
173. Korn, T. and A. Kallies, *T cell responses in the central nervous system.* Nat Rev Immunol, 2017. **17**(3): p. 179-194.
174. Matsumae, M., et al., *Research into the Physiology of Cerebrospinal Fluid Reaches a New Horizon: Intimate Exchange between Cerebrospinal Fluid and Interstitial Fluid May Contribute to Maintenance of Homeostasis in the Central Nervous System.* Neurologia medico-chirurgica, 2016. **56**(7): p. 416-441.
175. McLaughlin, N. and N.A. Martin, *Meningeal management for optimal revascularization from middle meningeal artery.* Journal of Neurosurgery, 2012. **118**(1): p. 104-108.
176. Hartmann, D., M. Schulze, and J. Sievers, *Meningeal cells stimulate and direct the migration of cerebellar external granule cells in vitro.* Journal of Neurocytology, 1998. **27**(6): p. 395-409.
177. Ichimura, T., P.A. Fraser, and H.F. Cserr, *Distribution of extracellular tracers in perivascular spaces of the rat brain.* Brain Research, 1991. **545**(1–2): p. 103-113.
178. Simon, M.J. and J.J. Iliff, *Regulation of cerebrospinal fluid (CSF) flow in neurodegenerative, neurovascular and neuroinflammatory disease.* Biochimica et Biophysica Acta (BBA) - Molecular Basis of Disease, 2016. **1862**(3): p. 442-451.
179. Hadaczek, P., et al., *The "Perivascular Pump" Driven by Arterial Pulsation is a Powerful Mechanism for the Distribution of Therapeutic Molecules within the Brain.* Molecular therapy : the journal of the American Society of Gene Therapy, 2006. **14**(1): p. 69-78.
180. Krisch, B., H. Leonhardt, and A. Oksche, *Compartments and perivascular arrangement of the meninges covering the cerebral cortex of the rat.* Cell and Tissue Research, 1984. **238**(3): p. 459-474.
181. Louveau, A., et al., *Structural and functional features of central nervous system lymphatic vessels.* Nature, 2015. **523**(7560): p. 337-341.
182. Aspelund, A., et al., *A dural lymphatic vascular system that drains brain interstitial fluid and macromolecules.* The Journal of Experimental Medicine, 2015. **212**(7): p. 991.
183. Alitalo, K., *The lymphatic vasculature in disease.* Nat Med, 2011. **17**(11): p. 1371-1380.
184. Yang, Y., et al., *Lymphatic endothelial progenitors bud from the cardinal vein and intersomitic vessels in mammalian embryos.* Blood, 2012. **120**(11): p. 2340-2348.
185. Oliver, G., *Lymphatic vasculature development.* Nat Rev Immunol, 2004. **4**(1): p. 35-45.
186. Semo, J., J. Nicenboim, and K. Yaniv, *Development of the lymphatic system: new questions and paradigms.* Development, 2016. **143**(6): p. 924.
187. Martinez-Corral, I., et al., *Nonvenous Origin of Dermal Lymphatic Vasculature<span*

hwp:id="article-title-15" class="sub-article-title">Novelty and Significance</span&gt. Circulation Research, 2015. **116**(10): p. 1649.
188. Stanczuk, L., et al., *cKit Lineage Hemogenic Endothelium-Derived Cells Contribute to Mesenteric Lymphatic Vessels.* Cell Reports, 2015. **10**(10): p. 1708-1721.
189. Hong, Y.-K. and M. Detmar, *Prox1, master regulator of the lymphatic vasculature phenotype.* Cell and Tissue Research, 2003. **314**(1): p. 85-92.
190. Karalay, Ö., et al., *Prospero-related homeobox 1 gene (Prox1) is regulated by canonical Wnt signaling and has a stage-specific role in adult hippocampal neurogenesis.* Proceedings of the National Academy of Sciences of the United States of America, 2011. **108**(14): p. 5807-5812.
191. Johnson, N.C., et al., *Lymphatic endothelial cell identity is reversible and its maintenance requires Prox1 activity.* Genes & Development, 2008. **22**(23): p. 3282-3291.
192. Norrmén, C., et al., *FOXC2 controls formation and maturation of lymphatic collecting vessels through cooperation with NFATc1.* The Journal of Cell Biology, 2009. **185**(3): p. 439-457.
193. Srinivasan, R.S., et al., *The Prox1–Vegfr3 feedback loop maintains the identity and the number of lymphatic endothelial cell progenitors.* Genes & Development, 2014. **28**(19): p. 2175-2187.
194. Planas-Paz, L., et al., *Mechanoinduction of lymph vessel expansion.* The EMBO Journal, 2012. **31**(4): p. 788-804.
195. Cha, B., et al., *Mechanotransduction activates canonical Wnt/β-catenin signaling to promote lymphatic vascular patterning and the development of lymphatic and lymphovenous valves.* Genes & Development, 2016. **30**(12): p. 1454-1469.
196. Nicenboim, J., et al., *Lymphatic vessels arise from specialized angioblasts within a venous niche.* Nature, 2015. **522**(7554): p. 56-61.
197. Buttler, K., et al., *Maldevelopment of dermal lymphatics in Wnt5a-knockout-mice.* Developmental Biology, 2013. **381**(2): p. 365-376.
198. Bussard, K.M., et al., *Tumor-associated stromal cells as key contributors to the tumor microenvironment.* Breast Cancer Research : BCR, 2016. **18**: p. 84.
199. Holmgren, L., M.S. O'Reilly, and J. Folkman, *Dormancy of micrometastases: Balanced proliferation and apoptosis in the presence of angiogenesis suppression.* Nat Med, 1995. **1**(2): p. 149-153.
200. Parangi, S., et al., *Antiangiogenic therapy of transgenic mice impairs de novo tumor growth.* Proceedings of the National Academy of Sciences of the United States of America, 1996. **93**(5): p. 2002-2007.
201. Madden, S.L., et al., *Vascular Gene Expression in Nonneoplastic and Malignant Brain.* The American Journal of Pathology, 2004. **165**(2): p. 601-608.
202. Maher, E.A., et al., *Malignant glioma: genetics and biology of a grave matter.* Genes & Development, 2001. **15**(11): p. 1311-1333.
203. Shue, E.H., et al., *Plasmalemmal Vesicle Associated Protein-1 (PV-1) is a marker of blood-brain barrier disruption in rodent models.* BMC Neuroscience, 2008. **9**(1): p. 29.
204. Vasudevan, A. and P.G. Bhide, *Angiogenesis in the embryonic CNS: A new twist on an old tale.* Cell Adhesion & Migration, 2008. **2**(3): p. 167-169.
205. Tam, S.J. and R.J. Watts, *Connecting Vascular and Nervous System Development: Angiogenesis and the Blood-Brain Barrier.* Annual Review of Neuroscience, 2010. **33**(1): p. 379-408.
206. Font, M.A., A. Arboix, and J. Krupinski, *Angiogenesis, Neurogenesis and Neuroplasticity in Ischemic Stroke.* Current Cardiology Reviews, 2010. **6**(3): p. 238-244.
207. Xiong, Y., A. Mahmood, and M. Chopp, *Angiogenesis, neurogenesis and brain recovery of function following injury.* Current opinion in investigational drugs (London, England : 2000), 2010. **11**(3): p. 298-308.
208. Sun, Y., et al., *VEGF-induced neuroprotection, neurogenesis, and angiogenesis after focal cerebral ischemia.* Journal of Clinical Investigation, 2003. **111**(12): p. 1843-1851.
209. Charron, F., et al., *The Morphogen Sonic Hedgehog Is an Axonal Chemoattractant that Collaborates with Netrin-1 in Midline Axon Guidance.* Cell, 2003. **113**(1): p. 11-23.

210. Lyuksyutova, A.I., et al., *Anterior-Posterior Guidance of Commissural Axons by Wnt-Frizzled Signaling*. Science, 2003. **302**(5652): p. 1984.
211. Yoshikawa, S., et al., *Wnt-mediated axon guidance via the Drosophila Derailed receptor.* Nature, 2003. **422**(6932): p. 583-588.
212. Barcellos-Hoff, M.H., D. Lyden, and T.C. Wang, *The evolution of the cancer niche during multistage carcinogenesis*. Nat Rev Cancer, 2013. **13**(7): p. 511-518.
213. Gopalakrishnan, V., et al., *Medulloblastoma development: tumor biology informs treatment decisions*. CNS oncology, 2015. **4**(2): p. 79-89.
214. Zeman, M.K. and K.A. Cimprich, *Causes and Consequences of Replication Stress*. Nature cell biology, 2014. **16**(1): p. 2-9.
215. Mazouzi, A., G. Velimezi, and J.I. Loizou, *DNA replication stress: Causes, resolution and disease.* Experimental Cell Research, 2014. **329**(1): p. 85-93.
216. Tamayo-Orrego, L., S.M. Swikert, and F. Charron, *Evasion of cell senescence in SHH medulloblastoma.* Cell Cycle, 2016. **15**(16): p. 2102-2107.
217. Tamayo-Orrego, L., et al., *Evasion of Cell Senescence Leads to Medulloblastoma Progression.* Cell Reports. **14**(12): p. 2925-2937.
218. Yang, Z.-J., et al., *Medulloblastoma Can Be Initiated by Deletion of Patched in Lineage-Restricted Progenitors or Stem Cells.* Cancer Cell. **14**(2): p. 135-145.
219. Reynolds, T.Y., S. Rockwell, and P.M. Glazer, *Genetic Instability Induced by the Tumor Microenvironment.* Cancer Research, 1996. **56**(24): p. 5754.
220. Hallahan, A.R., et al., *The SmoA1 Mouse Model Reveals That Notch Signaling Is Critical for the Growth and Survival of Sonic Hedgehog-Induced Medulloblastomas.* Cancer Research, 2004. **64**(21): p. 7794.
221. Jensen, A.M. and V.A. Wallace, *Expression of Sonic hedgehog and its putative role as a precursor cell mitogen in the developing mouse retina.* Development, 1997. **124**(2): p. 363-71.
222. Paes, K.T., et al., *Frizzled 4 Is Required for Retinal Angiogenesis and Maintenance of the Blood-Retina Barrier.* Investigative Ophthalmology & Visual Science, 2011. **52**(9): p. 6452-6461.
223. Guerrero-Cázares, H., K.L. Chaichana, and A. Quiñones-Hinojosa, *Neurosphere Culture and Human Organotypic Model to Evaluate Brain Tumor Stem Cells.* Methods in molecular biology (Clifton, N.J.), 2009. **568**: p. 73-83.
224. Ritchie, M.E., et al., *limma powers differential expression analyses for RNA-sequencing and microarray studies*. Nucleic Acids Research, 2015. **43**(7): p. e47-e47.
225. Shi, W., A. Oshlack, and G.K. Smyth, *Optimizing the noise versus bias trade-off for Illumina whole genome expression BeadChips*. Nucleic Acids Research, 2010. **38**(22): p. e204-e204.
226. Smyth Gordon, K., *Linear Models and Empirical Bayes Methods for Assessing Differential Expression in Microarray Experiments*, in *Statistical Applications in Genetics and Molecular Biology*2004. p. 1.
227. Huang, D.W., B.T. Sherman, and R.A. Lempicki, *Systematic and integrative analysis of large gene lists using DAVID bioinformatics resources.* Nat. Protocols, 2008. **4**(1): p. 44-57.
228. Remke, M., et al., *FSTL5 Is a Marker of Poor Prognosis in Non-WNT/Non-SHH Medulloblastoma.* Journal of Clinical Oncology, 2011. **29**(29): p. 3852-3861.
229. Cho, Y.-J., et al., *Integrative Genomic Analysis of Medulloblastoma Identifies a Molecular Subgroup That Drives Poor Clinical Outcome*. Journal of Clinical Oncology, 2011. **29**(11): p. 1424-1430.
230. Vanner, Robert J., et al., *Quiescent Sox2⁺ Cells Drive Hierarchical Growth and Relapse in Sonic Hedgehog Subgroup Medulloblastoma.* Cancer Cell. **26**(1): p. 33-47.
231. Northcott, P.A., et al., *Subgroup specific structural variation across 1,000 medulloblastoma genomes*. Nature, 2012. **488**(7409): p. 49-56.
232. Xu, Q., et al., *Vascular Development in the Retina and Inner Ear.* Cell. **116**(6): p. 883-895.

233. Hooper, C.M., et al., *Gene Expression Analyses of the Spatio-Temporal Relationships of Human Medulloblastoma Subgroups during Early Human Neurogenesis.* PLoS ONE, 2014. **9**(11): p. e112909.
234. Yun, J.-S., et al., *A Novel Role of the Mad Family Member Mad3 in Cerebellar Granule Neuron Precursor Proliferation.* Molecular and Cellular Biology, 2007. **27**(23): p. 8178-8189.
235. Hatten, M.E., et al., *Genes involved in cerebellar cell specification and differentiation.* Current Opinion in Neurobiology, 1997. **7**(1): p. 40-47.
236. Bassett, E.A., et al., *Norrin/Frizzled4 signalling in the preneoplastic niche blocks medulloblastoma initiation.* eLife, 2016. **5**: p. e16764.
237. Luhmann, U.F.O., et al., *Vascular changes in the cerebellum of Norrin?/Ndph knockout mice correlate with high expression of Norrin and Frizzled-4.* European Journal of Neuroscience, 2008. **27**(10): p. 2619-2628.
238. Dijksterhuis, J.P., J. Petersen, and G. Schulte, *International Union of Basic and Clinical Pharmacology Review: WNT/Frizzled signalling: receptor–ligand selectivity with focus on FZD-G protein signalling and its physiological relevance: IUPHAR Review 3.* British Journal of Pharmacology, 2014. **171**(5): p. 1195-1209.
239. Dijksterhuis, J.P., et al., *Systematic Mapping of WNT-FZD Protein Interactions Reveals Functional Selectivity by Distinct WNT-FZD Pairs.* The Journal of Biological Chemistry, 2015. **290**(11): p. 6789-6798.
240. Zhou, Y., et al., *Canonical WNT signaling components in vascular development and barrier formation.* The Journal of Clinical Investigation, 2014. **124**(9): p. 3825-3846.
241. Giraudo, E., M. Inoue, and D. Hanahan, *An amino-bisphosphonate targets MMP-9–expressing macrophages and angiogenesis to impair cervical carcinogenesis.* Journal of Clinical Investigation, 2004. **114**(5): p. 623-633.
242. Coussens, L.M., D. Hanahan, and J.M. Arbeit, *Genetic predisposition and parameters of malignant progression in K14-HPV16 transgenic mice.* The American Journal of Pathology, 1996. **149**(6): p. 1899-1917.
243. Lin, E.Y., et al., *Macrophages Regulate the Angiogenic Switch in a Mouse Model of Breast Cancer.* Cancer Research, 2006. **66**(23): p. 11238.
244. Smith-McCune, K., et al., *Cross-Species Comparison of Angiogenesis during the Premalignant Stages of Squamous Carcinogenesis in the Human Cervix and K14-HPV16 Transgenic Mice.* Cancer Research, 1997. **57**(7): p. 1294.
245. Lorenz, A., et al., *Severe Alterations of Cerebellar Cortical Development after Constitutive Activation of Wnt Signaling in Granule Neuron Precursors.* Molecular and Cellular Biology, 2011. **31**(16): p. 3326-3338.
246. Pöschl, J., et al., *Wnt/β-catenin signaling inhibits the Shh pathway and impairs tumor growth in Shh-dependent medulloblastoma.* Acta Neuropathologica, 2014. **127**(4): p. 605-607.
247. Wang, Y., et al., *Progressive Cerebellar, Auditory, and Esophageal Dysfunction Caused by Targeted Disruption of thefrizzled -4 Gene.* The Journal of Neuroscience, 2001. **21**(13): p. 4761.
248. Marusyk, A. and K. Polyak, *Tumor heterogeneity: causes and consequences.* Biochimica et biophysica acta, 2010. **1805**(1): p. 105.
249. Kusumbe, A.P., S.K. Ramasamy, and R.H. Adams, *Coupling of angiogenesis and osteogenesis by a specific vessel subtype in bone.* Nature, 2014. **507**(7492): p. 323-328.
250. Sacilotto, N., et al., *Analysis of Dll4 regulation reveals a combinatorial role for Sox and Notch in arterial development.* Proceedings of the National Academy of Sciences, 2013. **110**(29): p. 11893-11898.
251. Corcoran, R.B., et al., *Insulin-like Growth Factor 2 Is Required for Progression to Advanced Medulloblastoma in patched1 Heterozygous Mice.* Cancer Research, 2008. **68**(21): p. 8788.

252. Pazzaglia, S., et al., *Two-hit model for progression of medulloblastoma preneoplasia in Patched heterozygous mice.* Oncogene, 2006. **25**(40): p. 5575-5580.
253. Pazzaglia, S., et al., *Linking DNA damage to medulloblastoma tumorigenesis in patched heterozygous knockout mice.* Oncogene, 2006. **25**(8): p. 1165-1173.
254. Tanori, M., et al., *Developmental and oncogenic effects of Insulin-like Growth Factor-I in Ptc1(+/-)mouse cerebellum.* Molecular Cancer, 2010. **9**: p. 53-53.
255. Suero-Abreu, G.A., et al., *In Vivo Mn-Enhanced MRI for Early Tumor Detection and Growth Rate Analysis in a Mouse Medulloblastoma Model()().* Neoplasia (New York, N.Y.), 2014. **16**(12): p. 993-1006.
256. Li, P., et al., *A population of Nestin expressing progenitors in the cerebellum exhibits increased tumorigenicity.* Nature neuroscience, 2013. **16**(12): p. 1737-1744.
257. Putnam, A.J., *The Instructive Role of the Vasculature in Stem Cell Niches.* Biomaterials science, 2014. **2**(11): p. 1562-1573.
258. Jones, D.L. and A.J. Wagers, *No place like home: anatomy and function of the stem cell niche.* Nat Rev Mol Cell Biol, 2008. **9**(1): p. 11-21.
259. Wagers, Amy J., *The Stem Cell Niche in Regenerative Medicine.* Cell Stem Cell. **10**(4): p. 362-369.
260. Lane, S.W., D.A. Williams, and F.M. Watt, *Modulating the stem cell niche for tissue regeneration.* Nat Biotech, 2014. **32**(8): p. 795-803.
261. Shen, Q., et al., *ECs Stimulate Self-Renewal and Expand Neurogenesis of Neural Stem Cells.* Science, 2004. **304**(5675): p. 1338.
262. Reynolds, B.A. and R.L. Rietze, *Neural stem cells and neurospheres[mdash]re-evaluating the relationship.* Nat Meth, 2005. **2**(5): p. 333-336.
263. Marongiu, F., et al., *Cancer as a disease of tissue pattern formation.* Progress in Histochemistry and Cytochemistry, 2012. **47**(3): p. 175-207.
264. Farioli-Vecchioli, S., et al., *Tis21 Knock-Out Enhances the Frequency of Medulloblastoma in Patched1 Heterozygous Mice by Inhibiting the Cxcl3-Dependent Migration of Cerebellar Neurons.* The Journal of Neuroscience, 2012. **32**(44): p. 15547.
265. Pogoriler, J., et al., *Loss of cyclin D1 impairs cerebellar development and suppresses medulloblastoma formation.* Development (Cambridge, England), 2006. **133**(19): p. 3929-3937.
266. Gaillard, H., T. Garcia-Muse, and A. Aguilera, *Replication stress and cancer.* Nat Rev Cancer, 2015. **15**(5): p. 276-289.
267. Kuo, L.J. and L.-X. Yang, *γ-H2AX - A Novel Biomarker for DNA Double-strand Breaks.* In Vivo, 2008. **22**(3): p. 305-309.
268. Podhorecka, M., A. Skladanowski, and P. Bozko, *H2AX Phosphorylation: Its Role in DNA Damage Response and Cancer Therapy.* Journal of Nucleic Acids, 2010. **2010**: p. 920161.
269. Moynahan, M.E. and M. Jasin, *Loss of heterozygosity induced by a chromosomal double-strand break.* Proceedings of the National Academy of Sciences of the United States of America, 1997. **94**(17): p. 8988-8993.
270. Stark, J.M. and M. Jasin, *Extensive Loss of Heterozygosity Is Suppressed during Homologous Repair of Chromosomal Breaks.* Molecular and Cellular Biology, 2003. **23**(2): p. 733-743.
271. Mille, F., et al., *The Shh Receptor Boc Promotes Progression of Early Medulloblastoma to Advanced Tumors.* Developmental Cell. **31**(1): p. 34-47.
272. Hanahan, D. and Robert A. Weinberg, *Hallmarks of Cancer: The Next Generation.* Cell. **144**(5): p. 646-674.
273. Vinay, D.S., et al., *Immune evasion in cancer: Mechanistic basis and therapeutic strategies.* Seminars in Cancer Biology, 2015. **35**: p. S185-S198.
274. Xie, J., et al., *Activating Smoothened mutations in sporadic basal-cell carcinoma.* Nature, 1998. **391**(6662): p. 90-92.
275. Guo, L., et al., *Plasmalemma vesicle-associated protein: A crucial component of vascular homeostasis.* Experimental and Therapeutic Medicine, 2016. **12**(3): p. 1639-1644.

276. Schwartz, M., Y. Zhang, and J.D. Rosenblatt, *B cell regulation of the anti-tumor response and role in carcinogenesis.* Journal for Immunotherapy of Cancer, 2016. **4**: p. 40.
277. Baeriswyl, V. and G. Christofori, *The angiogenic switch in carcinogenesis.* Seminars in Cancer Biology, 2009. **19**(5): p. 329-337.
278. Maseda, D., et al., *Regulatory B10 Cells Differentiate Into Antibody-Secreting Cells After Transient IL-10 Production In Vivo.* Journal of Immunology (Baltimore, Md. : 1950), 2012. **188**(3): p. 1036-1048.
279. Hong, J.J., et al., *Re-Evaluation of PD-1 Expression by T Cells as a Marker for Immune Exhaustion during SIV Infection.* PLOS ONE, 2013. **8**(3): p. e60186.
280. Zitvogel, L. and G. Kroemer, *Targeting PD-1/PD-L1 interactions for cancer immunotherapy.* Oncoimmunology, 2012. **1**(8): p. 1223-1225.
281. Yang, C., et al., *B Cells Promote Tumor Progression via STAT3 Regulated-Angiogenesis.* PLOS ONE, 2013. **8**(5): p. e64159.
282. Logan, C.Y. and R. Nusse, *The Wnt signaling pathway in development and disease.* Annu. Rev. Cell. Dev. Biol, 2004. **20**: p. 781-810.
283. Fombonne, J., et al., *Patched dependence receptor triggers apoptosis through ubiquitination of caspase-9.* Proceedings of the National Academy of Sciences of the United States of America, 2012. **109**(26): p. 10510-10515.
284. Lu, P., V.M. Weaver, and Z. Werb, *The extracellular matrix: A dynamic niche in cancer progression.* The Journal of Cell Biology, 2012. **196**(4): p. 395.
285. Perng, P. and M. Lim, *Immunosuppressive Mechanisms of Malignant Gliomas: Parallels at Non-CNS Sites.* Frontiers in Oncology, 2015. **5**: p. 153.
286. Jain, R.K., et al., *Angiogenesis in brain tumours.* Nat Rev Neurosci, 2007. **8**(8): p. 610-622.
287. Swartz, M.A., *Immunomodulatory Roles of Lymphatic Vessels in Cancer Progression.* Cancer Immunology Research, 2014. **2**(8): p. 701.
288. Stachura, J., et al., *The dual role of tumor lymphatic vessels in dissemination of metastases and immune response development.* Oncoimmunology, 2016. **5**(7): p. e1182278.
289. Gerald, D., et al., *Angiopoietin-2: An Attractive Target for Improved Antiangiogenic Tumor Therapy.* Cancer Research, 2013. **73**(6): p. 1649.
290. Clifford, P.M., et al., *Aβ peptides can enter the brain through a defective blood–brain barrier and bind selectively to neurons.* Brain Research, 2007. **1142**: p. 223-236.
291. Stan, R.V., E. Tkachenko, and I.R. Niesman, *PV1 Is a Key Structural Component for the Formation of the Stomatal and Fenestral Diaphragms.* Molecular Biology of the Cell, 2004. **15**(8): p. 3615-3630.
292. Girard, J.-P., C. Moussion, and R. Forster, *HEVs, lymphatics and homeostatic immune cell trafficking in lymph nodes.* Nat Rev Immunol, 2012. **12**(11): p. 762-773.
293. Koltowska, K., et al., *Getting out and about: the emergence and morphogenesis of the vertebrate lymphatic vasculature.* Development, 2013. **140**(9): p. 1857.
294. Alitalo, K., T. Tammela, and T.V. Petrova, *Lymphangiogenesis in development and human disease.* Nature, 2005. **438**(7070): p. 946-953.
295. Hanahan, D. and J. Folkman, *Patterns and Emerging Mechanisms of the Angiogenic Switch during Tumorigenesis.* Cell. **86**(3): p. 353-364.
296. Phoenix, T.N., et al., *Medulloblastoma genotype dictates blood brain barrier phenotype.* Cancer cell, 2016. **29**(4): p. 508-522.
297. Conacci-Sorrell, M. and R.N. Eisenman, *Post-translational control of Myc function during differentiation.* Cell Cycle, 2011. **10**(4): p. 604-610.
298. Lee, J.-W., et al., *Hypoxia-inducible factor (HIF-1)[alpha]: its protein stability and biological functions.* Exp Mol Med, 0000. **36**: p. 1-12.
299. Hynes, R.O., *Extracellular matrix: not just pretty fibrils.* Science (New York, N.Y.), 2009. **326**(5957): p. 1216-1219.

300. Morrissy, A.S., et al., *Divergent clonal selection dominates medulloblastoma at recurrence.* Nature, 2016. **529**(7586): p. 351-357.
301. Wu, X., et al., *Clonal selection drives genetic divergence of metastatic medulloblastoma.* Nature, 2012. **482**(7386): p. 529-533.
302. Rubin, H., *Promotion and selection by serum growth factors drive field cancerization, which is anticipated in vivo by type 2 diabetes and obesity.* Proceedings of the National Academy of Sciences of the United States of America, 2013. **110**(34): p. 13927-13931.
303. Malek, R., et al., *The p53 Inhibitor MDM2 Facilitates Sonic Hedgehog-Mediated Tumorigenesis and Influences Cerebellar Foliation.* PLOS ONE, 2011. **6**(3): p. e17884.
304. Ayrault, O., et al., *Two tumor suppressors, p27(Kip1) and Patched-1, collaborate to prevent medulloblastoma.* Molecular cancer research : MCR, 2009. **7**(1): p. 33-40.
305. Uziel, T., et al., *The tumor suppressors Ink4c and p53 collaborate independently with Patched to suppress medulloblastoma formation.* Genes & Development, 2005. **19**(22): p. 2656-2667.
306. Briggs, K.J., et al., *Cooperation between the Hic1 and Ptch1 tumor suppressors in medulloblastoma.* Genes & Development, 2008. **22**(6): p. 770-785.
307. Kessler, J.D., et al., *N-myc alters the fate of preneoplastic cells in a mouse model of medulloblastoma.* Genes & Development, 2009. **23**(2): p. 157-170.
308. !!! INVALID CITATION !!! {}.
309. Lorusso, G. and C. Rüegg, *The tumor microenvironment and its contribution to tumor evolution toward metastasis.* Histochemistry and Cell Biology, 2008. **130**(6): p. 1091-1103.
310. Topalian, S.L., C.G. Drake, and D.M. Pardoll, *Immune checkpoint blockade: a common denominator approach to cancer therapy.* Cancer Cell, 2015. **27**.
311. Schaffner, F., A.M. Ray, and M. Dontenwill, *Integrin α5β1, the Fibronectin Receptor, as a Pertinent Therapeutic Target in Solid Tumors.* Cancers, 2013. **5**(1): p. 27-47.
312. Fiorilli, P., et al., *Integrins mediate adhesion of medulloblastoma cells to tenascin and activate pathways associated with survival and proliferation.* Laboratory investigation; a journal of technical methods and pathology, 2008. **88**(11): p. 1143-1156.
313. Hanahan, D., et al., *Transgenic mouse models of tumour angiogenesis: the angiogenic switch, its molecular controls, and prospects for preclinical therapeutic models.* European Journal of Cancer. **32**(14): p. 2386-2393.
314. Zhang, L., et al., *Generation of a Syngeneic Mouse Model to Study the Effects of Vascular Endothelial Growth Factor in Ovarian Carcinoma.* The American Journal of Pathology, 2002. **161**(6): p. 2295-2309.
315. Bergers, G. and D. Hanahan, *Modes of resistance to anti-angiogenic therapy.* Nature reviews. Cancer, 2008. **8**(8): p. 592-603.
316. Raffaghello, L., et al., *Cancer associated fibroblasts in hematological malignancies.* Oncotarget, 2015. **6**(5): p. 2589-2603.
317. Ribatti, D., *Mast cells and macrophages exert beneficial and detrimental effects on tumor progression and angiogenesis.* Immunology Letters, 2013. **152**(2): p. 83-88.
318. Sfiligoi, C., et al., *Angiopoietin-2 expression in breast cancer correlates with lymph node invasion and short survival.* International Journal of Cancer, 2003. **103**(4): p. 466-474.
319. Jain, R.K., *Normalization of Tumor Vasculature: An Emerging Concept in Antiangiogenic Therapy.* Science, 2005. **307**(5706): p. 58.
320. Folkman, J., et al., *Induction of angiogenesis during the transition from hyperplasia to neoplasia.* Nature, 1989. **339**(6219): p. 58-61.
321. Loges, S., T. Schmidt, and P. Carmeliet, *Mechanisms of Resistance to Anti-Angiogenic Therapy and Development of Third-Generation Anti-Angiogenic Drug Candidates.* Genes & Cancer, 2010. **1**(1): p. 12-25.
322. Butler, J.M., H. Kobayashi, and S. Rafii, *Instructive role of the vascular niche in promoting tumour growth and tissue repair by angiocrine factors.* Nature reviews. Cancer, 2010. **10**(2): p. 138-146.

323. Singh, S.K., et al., *Identification of a Cancer Stem Cell in Human Brain Tumors.* Cancer Research, 2003. **63**(18): p. 5821.
324. Pastrana, E., V. Silva-Vargas, and F. Doetsch, *Eyes Wide Open: A Critical Review of Sphere-Formation as an Assay For Stem Cells.* Cell stem cell, 2011. **8**(5): p. 486-498.
325. Read, T.-A., et al., *Identification of CD15 as a Marker for Tumor-Propagating Cells in a Mouse Model of Medulloblastoma.* Cancer cell, 2009. **15**(2): p. 135-147.
326. Boumahdi, S., et al., *SOX2 controls tumour initiation and cancer stem-cell functions in squamous-cell carcinoma.* Nature, 2014. **511**(7508): p. 246-250.
327. Li, C., et al., *CD54-NOTCH1 axis controls tumor initiation and cancer stem cell functions in human prostate cancer.* Theranostics, 2017. **7**(1): p. 67-80.
328. Behrens, A., et al., *Impact of genomic damage and ageing on stem cell function.* Nat Cell Biol, 2014. **16**(3): p. 201-207.
329. Gate, D., et al., *T-cell TGF-β signaling abrogation restricts medulloblastoma progression.* Proceedings of the National Academy of Sciences, 2014. **111**(33): p. E3458-E3466.
330. Pham, C.D., et al., *Differential immune microenvironments and response to immune checkpoint blockade amongst molecular subtypes of murine medulloblastoma.* Clinical cancer research : an official journal of the American Association for Cancer Research, 2016. **22**(3): p. 582-595.
331. Lanzavecchia, A., *Antigen-specific interaction between T and B cells.* Nature, 1985. **314**(6011): p. 537-539.
332. Molnarfi, N., et al., *MHC class II–dependent B cell APC function is required for induction of CNS autoimmunity independent of myelin-specific antibodies.* The Journal of Experimental Medicine, 2013. **210**(13): p. 2921-2937.
333. Mauri, C. and M. Menon, *The expanding family of regulatory B cells.* International Immunology, 2015. **27**(10): p. 479-486.
334. Magliozzi, R., et al., *Meningeal B-cell follicles in secondary progressive multiple sclerosis associate with early onset of disease and severe cortical pathology.* Brain, 2007. **130**(4): p. 1089-1104.
335. Zouali, M. and Y. Richard, *Marginal Zone B-Cells, a Gatekeeper of Innate Immunity.* Frontiers in Immunology, 2011. **2**: p. 63.
336. Belperron, A.A., et al., *Marginal Zone B-Cell Depletion Impairs Murine Host Defense against Borrelia burgdorferi Infection.* Infection and Immunity, 2007. **75**(7): p. 3354-3360.
337. Ray, A. and B.N. Dittel, *Mechanisms of Regulatory B cell Function in Autoimmune and Inflammatory Diseases beyond IL-10.* Journal of Clinical Medicine, 2017. **6**(1): p. 12.
338. Barr, T.A., et al., *TLR-mediated stimulation of APC: Distinct cytokine responses of B cells and dendritic cells.* European Journal of Immunology, 2007. **37**(11): p. 3040-3053.
339. Tang, Y., et al., *The contribution of the Tie2(+) lineage to primitive and definitive hematopoietic cells.* Genesis (New York, N.Y. : 2000), 2010. **48**(9): p. 563-567.
340. De Palma, M., et al., *Tie2 identifies a hematopoietic lineage of proangiogenic monocytes required for tumor vessel formation and a mesenchymal population of pericyte progenitors.* Cancer Cell. **8**(3): p. 211-226.
341. Brinkmann, V., et al., *The Immune Modulator FTY720 Targets Sphingosine 1-Phosphate Receptors.* Journal of Biological Chemistry, 2002. **277**(24): p. 21453-21457.
342. Gandhi, R. and M. Mazzola, *Immune regulatory effects of Fingolimod (FTY720) on T cells (THER7P.959).* The Journal of Immunology, 2015. **194**(1 Supplement): p. 208.19.
343. Fernandez, C., et al., *Differential Modulation of Sonic-Hedgehog-Induced Cerebellar Granule Cell Precursor Proliferation by the IGF Signaling Network.* Developmental Neuroscience, 2010. **32**(1): p. 59-70.
344. Solecki, D.J., et al., *Activated Notch2 Signaling Inhibits Differentiation of Cerebellar Granule Neuron Precursors by Maintaining Proliferation.* Neuron. **31**(4): p. 557-568.

345. Elvers, M., et al., *TGF-β2 neutralization inhibits proliferation and activates apoptosis of cerebellar granule cell precurors in the developing cerebellum.* Mechanisms of Development, 2005. **122**(4): p. 587-602.
346. Murase, S.-I.a.H.Y., *Concomitant expression of genes encoding integrin αvβ5 heterodimer and vitronectin in growing parallel fibers of postnatal rat cerebellum: A possible role as mediators of parallel fiber elongation.* The Journal of Comparative Neurology, 1998. **397**(2): p. 199--212.
347. Wechsler-Reya, R.J., *Caught in the matrix: how vitronectin controls neuronal differentiation.* Trends in Neurosciences, 2001. **24**(12): p. 680-682.
348. Pons, S., et al., *Vitronectin regulates Sonic hedgehog activity during cerebellum development through CREB phosphorylation.* Development, 2001. **128**(9): p. 1481.
349. Blaess, S., et al., *β1-Integrins Are Critical for Cerebellar Granule Cell Precursor Proliferation.* The Journal of neuroscience : the official journal of the Society for Neuroscience, 2004. **24**(13): p. 3402-3412.
350. Wechsler-Reya, R.J., *Caught in the matrix: how vitronectin controls neuronal differentiation.* Trends in Neurosciences. **24**(12): p. 680-682.
351. Nalla, A.K., et al., *Suppression of uPAR Retards Radiation-Induced Invasion and Migration Mediated by Integrin β1/FAK Signaling in Medulloblastoma.* PLOS ONE, 2010. **5**(9): p. e13006.
352. Bhoopathi, P., et al., *Blockade of tumor growth due to MMP-9 inhibition is mediated by sequential activation of β1 integrin, ERK and NFκB.* The Journal of biological chemistry, 2008. **283**(3): p. 1545-1552.
353. Frick, A., et al., *Proper cerebellar development requires expression of β1-integrin in Bergmann glia, but not in granule neurons.* Glia, 2012. **60**(5): p. 820-832.
354. Marchetti, G., et al., *α6 integrin subunit regulates cerebellar development.* Cell Adhesion & Migration, 2013. **7**(3): p. 325-332.
355. Patsenker, E. and F. Stickel, *Role of integrins in fibrosing liver diseases.* American Journal of Physiology - Gastrointestinal and Liver Physiology, 2011. **301**(3): p. G425.
356. Kenney, A.M., M.D. Cole, and D.H. Rowitch, *Nmyc upregulation by sonic hedgehog signaling promotes proliferation in developing cerebellar granule neuron precursors.* Development, 2003. **130**(1): p. 15.
357. Liu, J.-L., S. Yakar, and D. Leroith, *Conditional Knockout of Mouse Insulin-Like Growth Factor-1 Gene Using The Cre/Loxp System (44500).* Proceedings of the Society for Experimental Biology and Medicine, 2000. **223**(4): p. 344-351.
358. Riobo, N.A., et al., *Activation of heterotrimeric G proteins by Smoothened.* Proceedings of the National Academy of Sciences of the United States of America, 2006. **103**(33): p. 12607-12612.
359. Yanagida, K., et al., *Size-selective opening of the blood–brain barrier by targeting endothelial sphingosine 1–phosphate receptor 1.* Proceedings of the National Academy of Sciences, 2017. **114**(17): p. 4531-4536.
360. Pappu, R., et al., *Promotion of Lymphocyte Egress into Blood and Lymph by Distinct Sources of Sphingosine-1-Phosphate.* Science, 2007. **316**(5822): p. 295.
361. Taddei, A., et al., *Endothelial adherens junctions control tight junctions by VE-cadherin-mediated upregulation of claudin-5.* Nat Cell Biol, 2008. **10**(8): p. 923-934.
362. Corada, M., et al., *Vascular endothelial–cadherin is an important determinant of microvascular integrity in vivo.* Proceedings of the National Academy of Sciences, 1999. **96**(17): p. 9815-9820.
363. Rinderknecht, M. and M. Detmar, *Tumor lymphangiogenesis and melanoma metastasis.* Journal of Cellular Physiology, 2008. **216**(2): p. 347-354.
364. McAllaster, J.D. and M.S. Cohen, *Role of the lymphatics in cancer metastasis and chemotherapy applications.* Advanced Drug Delivery Reviews, 2011. **63**(10): p. 867-875.
365. Nakamura, Y., et al., *Lymph vessel density correlates with nodal status, VEGF-C expression, and prognosis in breast cancer.* Breast Cancer Research and Treatment, 2005. **91**(2): p. 125-132.
366. Stacker, S.A., et al., *VEGF-D promotes the metastatic spread of tumor cells via the lymphatics.* Nat Med, 2001. **7**(2): p. 186-191.

367. Stacker, S.A., et al., *Metastasis: Lymphangiogenesis and cancer metastasis.* Nat Rev Cancer, 2002. **2**(8): p. 573-583.
368. Stacker, S.A., M.E. Baldwin, and M.G. Achen, *The role of tumor lymphangiogenesis in metastatic spread.* The FASEB Journal, 2002. **16**(9): p. 922-934.
369. Achen, M.G. and S.A. Stacker, *Molecular Control of Lymphatic Metastasis.* Annals of the New York Academy of Sciences, 2008. **1131**(1): p. 225-234.
370. Dadras, S.S., et al., *Tumor Lymphangiogenesis : A Novel Prognostic Indicator for Cutaneous Melanoma Metastasis and Survival.* The American Journal of Pathology, 2003. **162**(6): p. 1951-1960.
371. Wigle, J.T., et al., *An essential role for Prox1 in the induction of the lymphatic endothelial cell phenotype.* The EMBO Journal, 2002. **21**(7): p. 1505-1513.
372. Weller, R.O., et al., *Pathophysiology of the lymphatic drainage of the central nervous system: Implications for pathogenesis and therapy of multiple sclerosis.* Pathophysiology, 2010. **17**(4): p. 295-306.
373. Makinen, T., et al., *Inhibition of lymphangiogenesis with resulting lymphedema in transgenic mice expressing soluble VEGF receptor-3.* Nat Med, 2001. **7**(2): p. 199-205.
374. Li, Y., et al., *Transforming Growth Factor-Alpha: A Major Human Serum Factor that Promotes Human Keratinocyte Migration.* Journal of Investigative Dermatology. **126**(9): p. 2096-2105.
375. Jossen, R. and R. Bermejo, *The DNA damage checkpoint response to replication stress: A Game of Forks.* Frontiers in Genetics, 2013. **4**: p. 26.
376. Asgari, M., D. de Zélicourt, and V. Kurtcuoglu, *Glymphatic solute transport does not require bulk flow.* Scientific Reports, 2016. **6**: p. 38635.

Appendix A

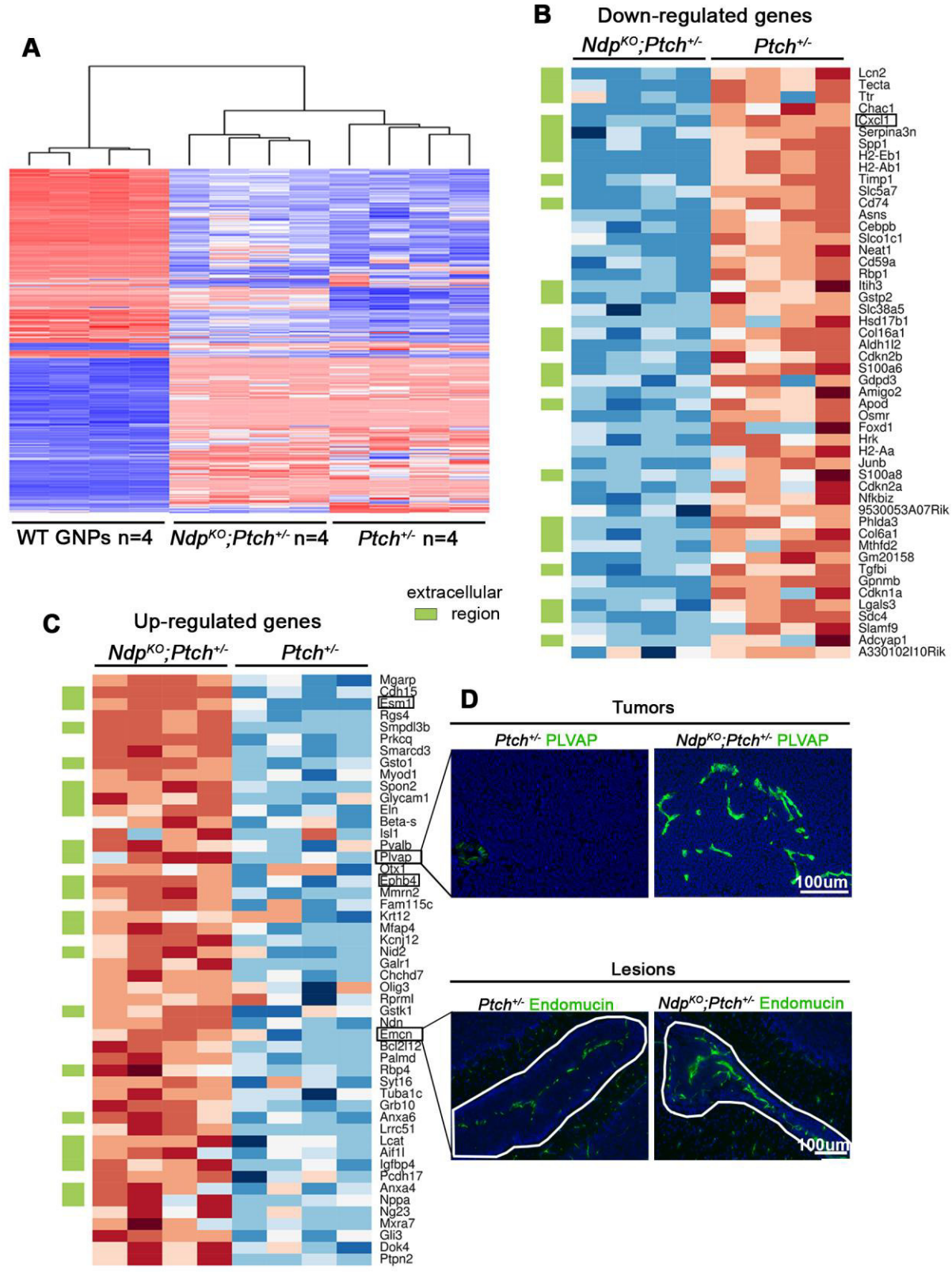
A
WT GNPs n=4
Ndp^KO;Ptch^+/- n=4
Ptch^+/- n=4
B
Down-regulated genes
Ndp^KO;Ptch^+/-
Ptch^+/-
Lcn2
Tecta
Ttr
Chac1
Cxcl1
Serpina3n
Spp1
H2-Eb1
H2-Ab1
Timp1
Slc5a7
Cd74
Asns
Cebpb
Slco1c1
Neat1
Cd59a
Rbp1
Itih3
Gstp2
Slc38a5
Hsd17b1
Col16a1
Aldh1l2
Cdkn2b
S100a6
Gdpd3
Amigo2
Apod
Osmr
Foxd1
Hrk
H2-Aa
Junb
S100a8
Cdkn2a
Nfkbiz
9530053A07Rik
Phlda3
Col6a1
Mthfd2
Gm20158
Tgfbi
Gpnmb
Cdkn1a
Lgals3
Sdc4
Slamf9
Adcyap1
A330102I10Rik
extracellular region
C
Up-regulated genes
Ndp^KO;Ptch^+/-
Ptch^+/-
Mgarp
Cdh15
Esm1
Rgs4
Smpdl3b
Prkcq
Smarcd3
Gsto1
Myod1
Spon2
Glycam1
Eln
Beta-s
Isl1
Pvalb
Plvap
Otx1
Ephb4
Mmrn2
Fam115c
Krt12
Mfap4
Kcnj12
Nid2
Galr1
Chchd7
Olig3
Rprml
Gstk1
Ndn
Emcn
Bcl2l12
Palmd
Rbp4
Syt16
Tuba1c
Grb10
Anxa6
Lrrc51
Lcat
Aif1l
Igfbp4
Pcdh17
Anxa4
Nppa
Ng23
Mxra7
Gli3
Dok4
Ptpn2
D
Tumors
Ptch^+/- PLVAP
Ndp^KO;Ptch^+/- PLVAP
100um
Lesions
Ptch^+/- Endomucin
Ndp^KO;Ptch^+/- Endomucin
100um

<u>Supplemental Figure 1.</u> Loss of Ndp causes alterations in stromal associated gene expression in Ptch$^{+/-}$ MB samples.

(**A**) Hierarchical clustering calculated from the 1500 probes with the largest midspread ranges across all biological replicates from Ptch$^{+/-}$ MB, Ndp$^{-/Y}$;Ptch$^{+/-}$ MB and P6 WT GNP samples following whole genome expression analyses. (**B**-**C**) A total of 1586 mRNA transcripts were detected as differentially expressed in Ptch$^{+/-}$ as compared to Ndp$^{-/Y}$;Ptch$^{+/-}$ MB samples by using limma[226], with a P value threshold of 0.05. The presented heatmap figures display the top 50 most up- and down-regulated genes between Ptch$^{-/+}$ and Ndp$^{-/Y}$;Ptch$^{+/-}$ MB samples. Genes marked by a green rectangle (on the left of the heatmaps) fall into the extracellular region of the Gene Ontology (GO) classification. (**D**) Immunostainings of PLVAP and Endomucin (green) on Ndp$^{-/Y}$;Ptch$^{+/-}$ and Ptch$^{+/-}$ MBs (top) and lesions (bottom) demonstrate validation of up-regulated genes at the protein level. The black box denotes particularly interesting blood vessel specific genes (Plvap and Esm1) and more specifically vein associated genes (Ephb4 and EMCN). Wild Type = WT; Scale bars indicated in the figures. Figure adapted from [236]

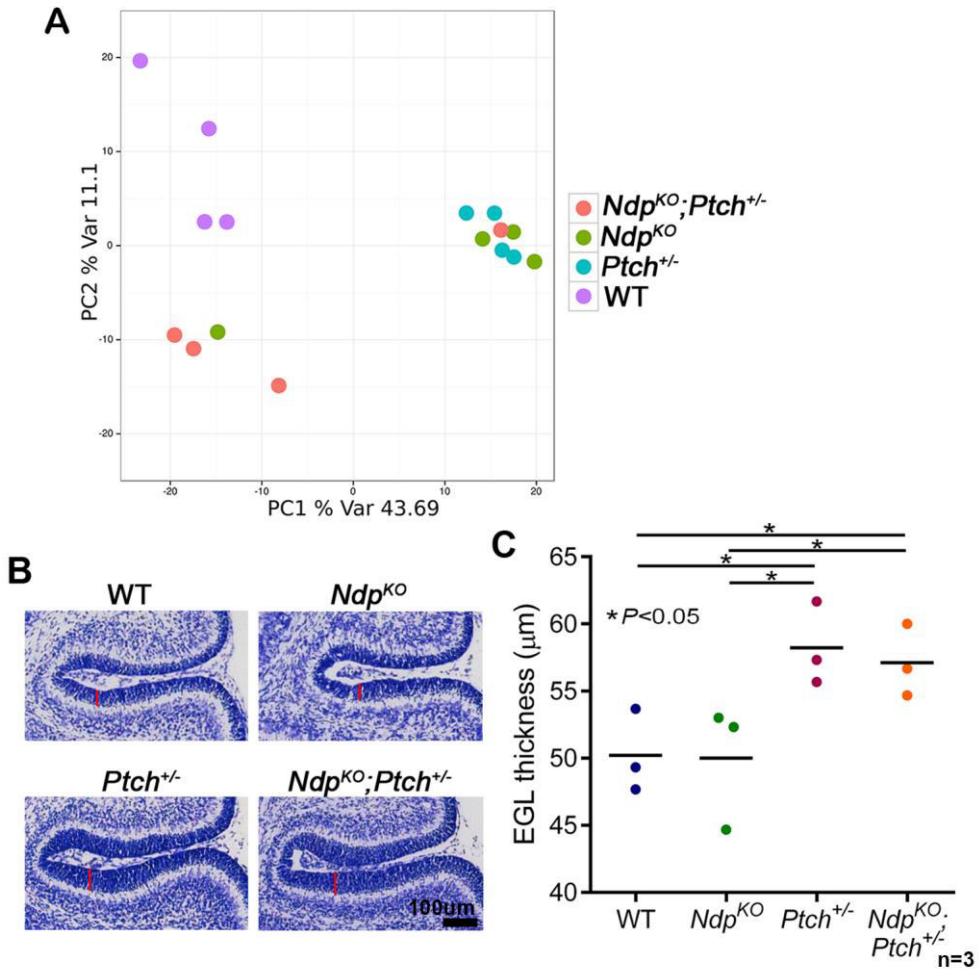

<u>Supplemental Figure 2.</u> Loss of Norrin signaling in Ptch$^{+/-}$ mice does not enhance EGL overgrowth or significantly alter GNP gene expression profile.

(**A**) Principal component analysis following genome-wide expression array profiling of acutely isolated WT (wild-type), Ptch$^{+/-}$, Ndp$^{-/Y}$ and Ndp$^{-/Y}$;Ptch$^{+/-}$ GNPs (n = 4 animals per group) does not reveal clear separation of the different GNP genotypes. (**B**) Representative Haematoxylin stainings of the EGL from equivalent cerebellar regions from the 4 different genotypes (WT, Ptch$^{+/-}$, Ndp$^{-/Y}$ and Ndp$^{-/Y}$;Ptch$^{+/-}$), red bar denotes EGL thickness. (**C**) Scatterplot quantification of the EGL thickness in (**B**), which shows that loss of Ndp does not increase EGL thickness on the WT background or on the Ptch$^{+/-}$ background. Means are denoted by black horizontal lines on the graph. Scale bar indicated in the figure. Figure adapted from [236]

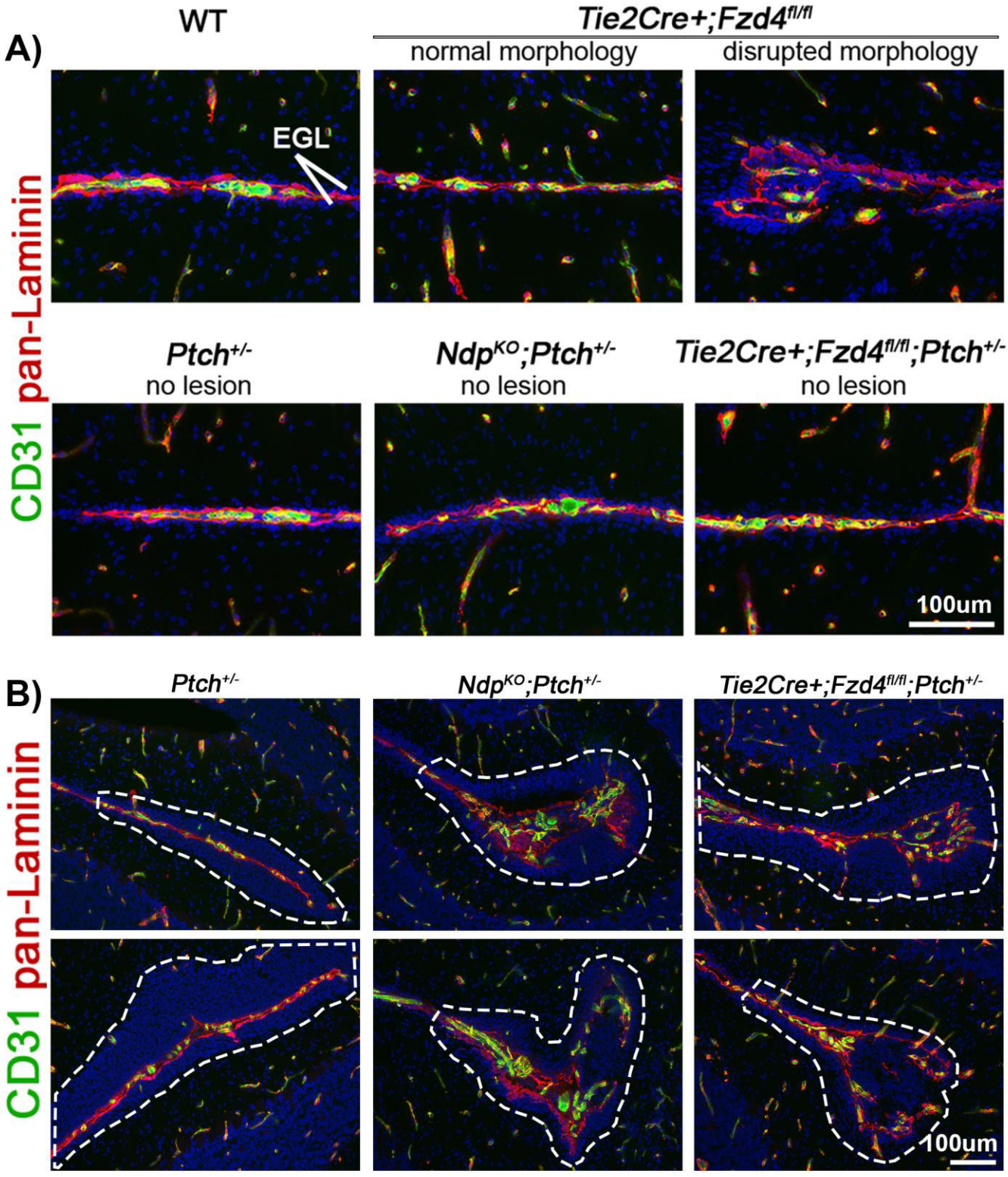
A)
WT
Tie2Cre+;Fzd4fl/fl
normal morphology
disrupted morphology
EGL
CD31 pan-Laminin
Ptch+/-
no lesion
Ndp^KO;Ptch+/-
no lesion
Tie2Cre+;Fzd4fl/fl;Ptch+/-
no lesion
100um
B)
Ptch+/-
Ndp^KO;Ptch+/-
Tie2Cre+;Fzd4fl/fl;Ptch+/-
CD31 pan-Laminin
100um

<u>Supplemental Figure 3.</u> EGL-associated morphology in WT, $Ptch^{+/-}$, $Ndp^{-/Y}$;$Ptch^{+/-}$, $Cre^{+/-}$;$Fzd4^{flox/flox}$ and Tie2-$Cre^{+/-}$;$Fzd4^{flox/flox}$;$Ptch^{+/-}$ cerebella.

(**A**) Cerebellar sections from P14 animals of the indicated genotypes where stained with CD31 (ECs marker), pan-Laminin (vascular basement membrane marker) and counterstained with Hoechst (nuclear marker). Although $Tie2Cre^{+/-}$;$Fzd4^{Flox/Flox}$ cerebella do not develop preneoplastic lesions we can find the rare foci of a disrupted EGL morphology. 3 lesion-free regions from at least 3 cerebella per genotype were examined. (**B**) Co-immunostaining for CD31 and pan-Laminin on cerebellar lesion sections from P14 Cerebellar sections from P14 animals of the indicated genotypes where stained with CD31 (ECs marker), pan-Laminin (vascular basement membrane marker) and counterstained with Hoechst (nuclear marker) with the lesions outlined in white dashed line. Figure is to illustrate the vascular remodeling in small (<0.02 mm3) compound mutant lesions. External granule layer = EGL. Scale bar indicated in the figure.

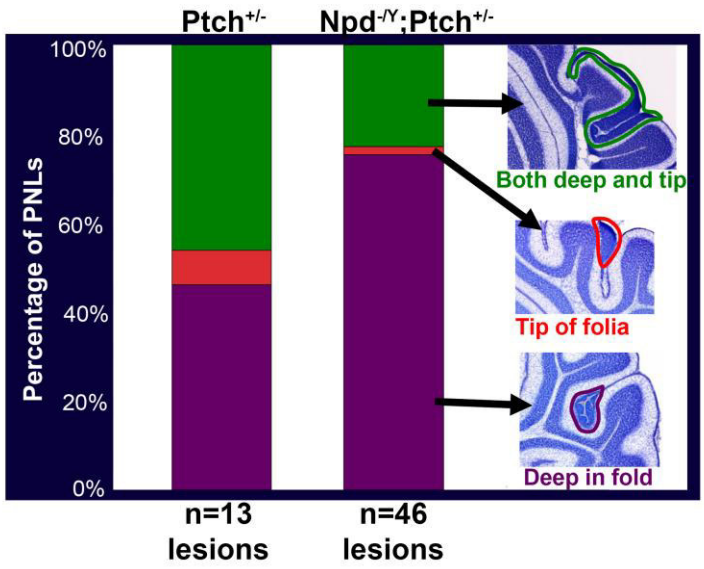

Supplemental Figure 4. Lesion distribution in $Ndp^{-/Y}$;$Ptch^{+/-}$ and $Ptch^{+/-}$ animals.
Whole cerebella were serial sectioned and lesions were followed throughout the cerebellum and scored depending on their location as within the deep cerebellar fold, tip of folia or both the tip and deep in the fold. In $Ndp^{-/Y}$;$Ptch^{+/-}$ animals we see an increase in lesions found within the fold. Although $Ptch^{+/-}$ animals have a large portion of lesions found in both the fold and the tip, this type of lesion does not allow for a proper determination of its origin (the lesion could have originated in the tip and spread inwards or vice versa). Number of lesions investigated per genotype are indicated in the figure (Bassett and Allemano unpublished data).

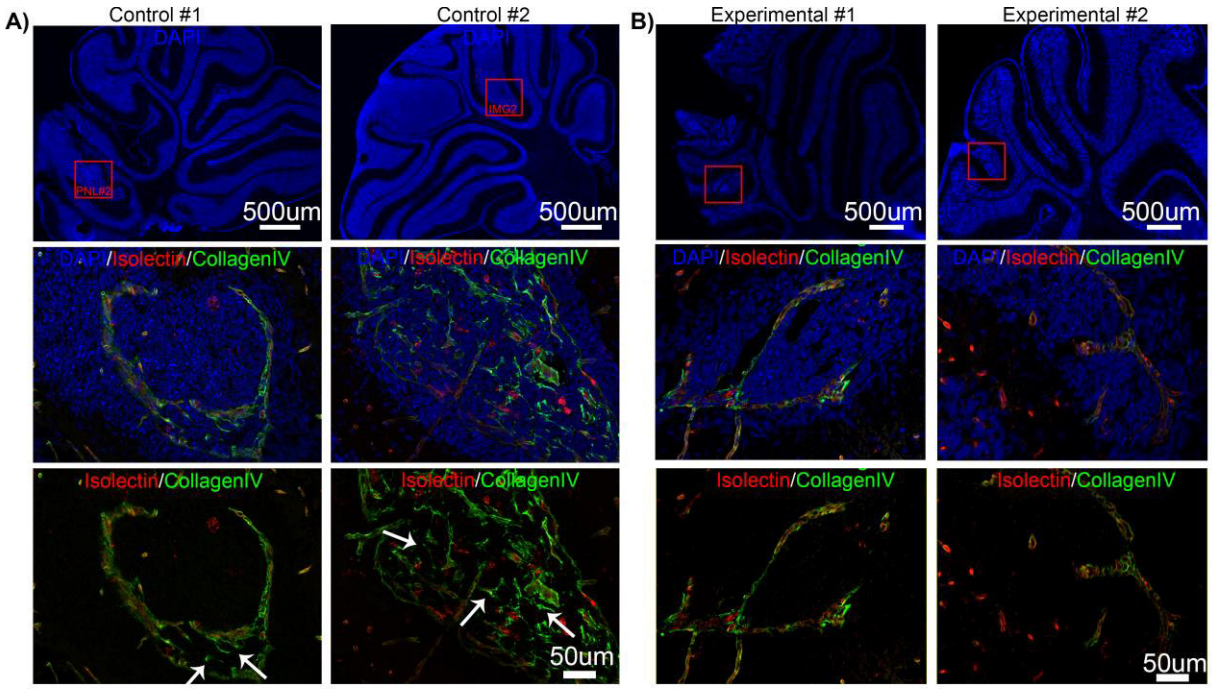

<u>Supplemental Figure 5.</u> Reduction in ECM deposition following α-Angpt2 in Ndp-/Y;Ptch+/- animals.

(**A**) Aberrant deposition of ECM (CollagenIV^{+}) in the Ndp-/Y;Ptch+/- animals treated with α-mIgG2a, highlighted by the white arrows. (**B**) The aberrant deposition of ECM (CollagenIV^{+}) is significantly reduced in the Ndp-/Y;Ptch+/- animals treated with α-Angpt2. For the immunohistochemical stainings we examined 3 neighboring sections from at least 3 different cerebella per genotype. Scale bars indicated in the figures.

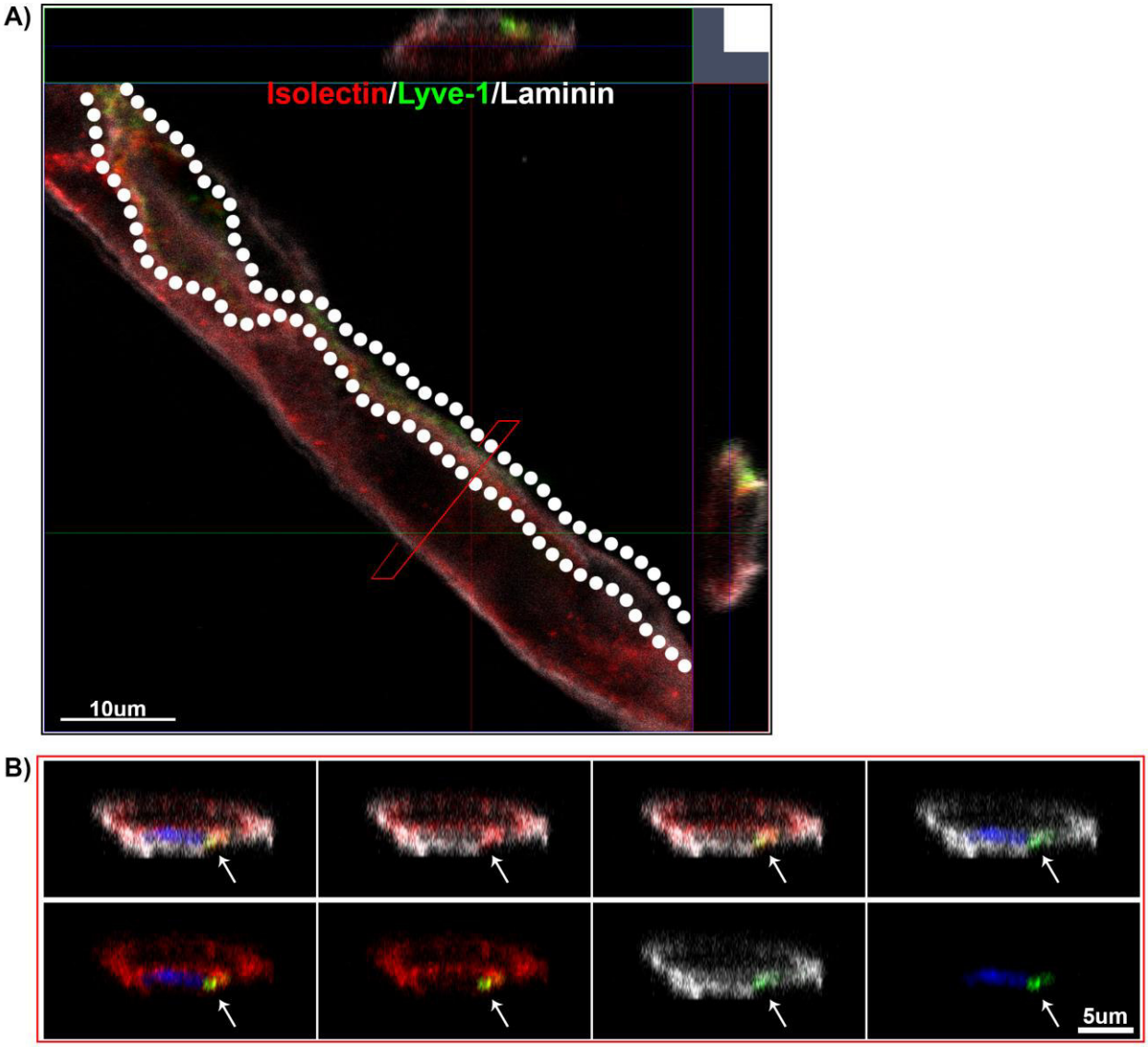

<u>Supplemental Figure 6.</u> Meningeal lymphatic are confined within the perivascular space.
(**A**) Orthogonal confocal cross section image of a meningeal vessel, with the dotted line illustrating the lymphatic vessel. The vasculature (Isolectin – red) and lymphatic (Lyve-1 – green) are found confined within the Laminin (white) basement membrane. The red box is the sliced image found in (**B**). (**B**) Confocal cut section illustrating the lymphatic vasculature (white arrow) is found within the perivascular space and closely associated to the endothelial nucleus. Scale bars indicated in the figures.

Personal Information

Name: Nicholas Tokarew

Nationality: Canadian

Personal summary

I am a highly motivated, hardworking researcher that is objective and result orientated. I excel in various positions including but not limited to: bench work, writing, illustrating, experimental design, project coordination, educating and mentoring. I am an open minded individual that utilises and integrates current information in various fields to help shape and guide research questions, always looking for new avenues and challenges in order to broaden my knowledge and understanding in my research and various other fields.

Education

January 2013 – Present Ottawa University Ottawa Ont.

- Ph.D. candidate in Biochemistry at the University of Ottawa under the supervision of senior scientist Valerie Wallace, PhD. My Ph.D was carried out by working at two different campuses, the Ottawa Hospital Research Institute and at the prestigious Krembil Discovery Tower in Toronto. My project was focused on examining the cellular and molecular underpinnings involved in Ndp-Fzd4 driven medulloblastoma formation and progression and its relationship with the sonic hedgehog pathway.

September 2011 – November 2012 Ottawa University Ottawa Ont.

- Masters in Biochemistry at the University of Ottawa under the supervision of senior scientist Valerie Wallace, PhD. The project was entitled "Functional analysis of Norrie Disease Pseudogliaoma (Ndp) in cerebellar development".

September 2006 – April 2011 Ottawa University Ottawa Ont.

- Bachelor in Biology at the University of Ottawa. Graduated Cum laude B.Sc. in with a specialization in Biomedical Science and a minor in Biochemistry at the University of Ottawa.

Responsibility and achievements

- Teachers assistant during my Bachelor studies
- Developing and optimising research projects and procedures
- Coordinating collaborations with various laboratories
- Supervising and mentoring of bachelor and master candidate students
- Presenting research projects and results at group and scientific meetings
- First co-author publication

Techniques and Skills

- Animal husbandry. Generating compound mutants, breeding, maintaining and genotyping of mice

- Performing experimental tumor studies, assessing drug and biopharmaceutical treatment effects on animal's survival
- Intracranial intraperitoneal injections
- Molecular techniques: PCR, qRT-PCR, cloning, in situ hybridization
- Biochemical techniques: immunocytochemistry, immunohistochemistry, Western Blot, protein expression and purification, Flow Cytometry
- Epifluorescence and Confocal microscopy
- Cell culture work: culturing of various immortalised cell lines, primary isolated cells and primary isolated tumour cells
- SiRNA knockdown, Transformation, Transfection and Nucleofection

Languages

Mother tongue: English

Fluent: French

Basic knowledge: German

Additional interest

I enjoy sports (basketball, snowboarding, swimming, hiking), hands on technical work (automot repair), travelling, leisure and social times

Publications and Presentations

Refereed contributions

E.A. Bassett, **N.J. Tokarew**, E.A. Allemano, C. Mazerolle, K. Morin, A.J. Mears, B. McNeill, R. Ringuette, C. Campbell, S. Smiley, A.M. Dubuc, V. Ramaswamy, P.A. Northcott, M. Remke, Monnier, D. Potter, K. Paes, L.L. Kirkpatrick, K.J. Coker, D.S. Rice, C. Perez-Iratxeta, M Taylor, V.A. Wallace. Norrin/Frizzled4 signalling in the preneoplastic niche blo medulloblastoma initiation. eLife, (2016);5:e16764

Alvarez-Saavedra M, De Repentigny Y, Lagali PS, Raghu Ram EV, Yan K, Hashem E, Ivanochko D, Huh MS, Yang D, Mears AJ, Todd MA, Corcoran CP, Bassett EA, **Tokarew NJ**, Kokavec J, Majumder R, Ioshikhes I, Wallace VA, Kothary R, Meshorer E, Stopka T, Skoultchi AI, Picketts DJ. Snf2h-mediated chromatin organization and histone H1 dynamics govern cerebellar morphogenesis and neural maturation. Published in Nature Communication, 5 (2014), p. 4181

Conference contributions

Tokarew, N.J., Bassett, Erin A. Bassett, Ema A. Allemano, Brian McNeill, Chantal Mazerolle, Alan J. Mears, Carolina Perez-Iratxeta, Kim Paes, Dennis Rice, Adrian M. Dubuc, Paul A. Northcott, Marc Remke, Michael D. Taylor, Valerie A. Wallace. The Role of Norrie Disease Pseudoglioma (Ndp) in Cerebellar Development/Tumorigenesis and its Relationship with the Sonic Hedgehog Pathway. **Poster** Presentation (Canadian Cancer Research Conference (CCRC), Montreal, November 2015).

Tokarew, N.J., et al., The Role of Norrie Disease Pseudoglioma (Ndp) in Cerebellar Development/Tumorigenesis and its Relationship with the Sonic Hedgehog

Pathway. **Poster** Presentation (Hedgehog (HH) conference Puerto Montt, Chile, 2015).

Tokarew, N.J., et al., The Role of Norrie Disease Pseudoglioma (Ndp) in Cerebellar Development/Tumorigenesis and its Relationship with the Sonic Hedgehog Pathway. **Poster** Presentation (2014 HH conference Ann Arbor, 2014).

Tokarew, N.J., et al., The Role of Norrie Disease Pseudoglioma (Ndp) in Cerebellar Development/Tumorigenesis and its Relationship with the Sonic Hedgehog Pathway. **Poster** Presentation (First Healing consortium international meeting, Switzerland, 2013).

Tokarew, N.J., et al., The Role of Norrie Disease Pseudoglioma (Ndp) in Cerebellar Development/Tumorigenesis and its Relationship with the Sonic Hedgehog Pathway. **Poster** Presentation (4th annual Ottawa Brain Health Research day, 2013).

List of scholarships and awards

January 2013 – Present Ottawa University Ottawa Ont.

- Awarded travel grants for the conferences I have attended during my PhD.

January 2013 – Present Ottawa University Ottawa Ont.

- Awarded the Ph.D. Admission Scholarship

September 2011 – Present Ottawa University Ottawa Ont.

- Awarded the Queen Elizabeth II - Graduate Scholarship in Science and Technology (QEII - GSST)

September 2011 – April 2012 Ottawa University Ottawa Ont.

- Awarded the Masters Admission Scholarship

September 2010 – April 2011 Ottawa University Ottawa Ont.

- Awarded the Merit Scholarship